An Analysis of the NAD 83(NSRS2007) National Readjustment

Dennis Milbert, Ph.D.
Rockville, Md.

ABSTRACT

On February 6, 2007, the final fixed adjustment of the NAD 83(NSRS2007) National Readjustment was completed. GPS carrier phase data, reduced to correlated inter-station vectors observed from 1983 to November 2005, were processed in a simultaneous least-squares adjustment. A CORS coordinate set, epoch 2002.0, established the NAD 83 system; although crustal motion effects were applied to coordinates and vectors in California, Arizona, Nevada, Oregon, and Washington to realize an epoch of 2007.0. FGDC network accuracies (95% *a posteriori* statistics) show medians of 1.03 cm horizontal and 1.84 cm vertical. Analysis of the residuals shows insufficient outer rejection and the potential need to reweight four categories of projects. These problems lead to long tails in statistical distributions and inflation of the *a posteriori* statistics. Comparisons show that less than 1% of the residuals change horizontally by 1 cm or more between the free and fixed adjustments.

PREFACE

The formal name of the new readjustment of the GPS vectors conducted by the National Geodetic Survey (NGS), NOAA, is the NAD 83(NSRS2007) National Readjustment. Throughout this text and in the figures, the network or certain adjustment products are referred to as NSRS 2007 in the interests of concision.

As nomenclature, minimally constrained adjustments are referred to as *free* (or *float*) adjustments. Conversely, a *fixed* adjustment is one where conditions are imposed on a certain subset of coordinates. Such fixed adjustments and their associated control points are also referred to in this report as *constrained* or *rigid*. The numerical methods used to realize a fixed adjustment are such that any coordinate shifts at fixed points are negligible. If a coordinate equation is given an intermediate treatment such that its shift is non-negligible, that coordinate is considered *weighted*. An adjustment is only denoted as weighted if it is predominately controlled by coordinate equations that take non-negligible shifts.

This report is augmented by a variety of text files denoted as Electronic Support Material (ESM). This material documents the findings and recommendations, and it also supports subsequent analysis of the GPS vectors of the National Spatial Reference System (NSRS). However, such content is far too voluminous to reproduce in this report, even in an Appendix. It is anticipated that the ESM will be disseminated in conjunction with this report's distribution.

Finally, this report is an independent analysis of the NSRS 2007 readjustment. This report is not an expository composition of the background and methodology of the readjustment. It is assumed the reader has access to the readjustment final report (Pursell *et al*. 2008). However, as of this writing, the final report is still draft. To provide some context, the readjustment is summarized. GPS carrier phase data reduced to correlated inter-station vectors are stored in the NGS data base. Those vectors observed from 1983 to November 2005 were processed in a simultaneous least-squares adjustment. The first phase was progressive data cleansing (including observation rejection by downweighting) for the free adjustment. Then, CORS coordinates were imposed and occasionally downweighted throughout the computations of the fixed adjustment. No geodetic points were rejected in the free adjustment processing. And, no GPS vectors were rejected in the fixed adjustment processing. The *a priori* variance of unit weight was 1.0. And, *a posteriori* statistics were generated through linear error propagation. Crustal motion effects were applied to coordinates and vectors in California, Arizona, Nevada, Oregon, and Washington to realize an epoch of 2007.0.

INTRODUCTION

On February 6, 2007, the final fixed adjustment of the NAD 83(NSRS2007) National Readjustment was completed. Within a couple of days, the National Geodetic Survey (NGS), NOAA, had placed an unprecedented amount of material generated in the readjustment on the NGS web site. This included adjusted coordinates, residual components, plots, observational summaries, position shifts, and error propagation products.

NGS analysis of the GPS vector data occurred throughout the adjustment process, which can be considered to have begun in December 2005. In fact, the analysis of these data was conducted on a continual basis throughout the existence of GPS surveys. These studies were not merely the standard project quality control checks, but more involved investigations on how the projects fit into the network. For one example of network analysis, the NGS State Readjustment Program, see Milbert and Milbert (1994).

After completion of the NSRS 2007, NGS decided to contract for an independent analysis of the National Readjustment. This was to insure that NGS publishes the most accurate and reliable geodetic data to Federal, State, and local agencies, as well as the private sector. The analysis was to cover the traditional adjustment products, as well as the new network and local accuracies defined in FGDC (1998, parts 1 and 2).

The analysis in this report is comprehensive. It is broken into small sections to aid in the assimilation of the content. The initial sections cover key statistics of the adjustments, general exploratory perspectives on the National GPS geodetic network, and plots of the coordinate shifts. Analysis proceeds to the adjustment residuals in both their unweighted and standardized forms. A brief but critical section (Section 15) looks at the pre-adjustment computation of the horizontal and vertical project standard deviation scaling factors. Following this foundation, analysis then addresses the error propagation

products. This begins with the coordinate covariance matrix and the new FGDC network accuracies. Then, relative error relationships and the new FGDC local accuracies are analyzed. This study includes a comparison of network and local accuracy magnitudes. Next, the author conducts an extended analysis of variance (ANOVA) that includes consideration of the heterogeneous composition of the Nation's GPS network. The Continuously Operating Reference Station (CORS) coordinate fixed control is inspected, along with the CORS velocities and the Horizontal Time Dependent Positioning (HTDP) model of crustal motion. The NSRS 2007 variance of unit weight is considered in detail. Systematic errors associated with GPS vectors are discussed. And a section is devoted to consideration of user concerns. The report closes with findings and recommendations.

SECTIONS

1. Key statistics of the readjustment

Throughout the analysis, certain key statistics and measures of the readjustment were accumulated from the original adjustment files. The statistics in Table 1.1 can be considered authoritative, and supersede any other publication or web pages.

Table 1.1 – Key statistics of the NAD 83(NSRS2007) National Readjustment

```
57 initial level Helmert blocks (include DC, PR and VI, exclude HI)

3411 non-trashed projects
 170 trashed projects
 147 duplicate project ID's (due to splitting 5 state Helmert blocks)

 67693 points (includes 688 CORS)
203079 station parameters
236239 sessions
313477 vectors, total
283691 vectors, unrejected
 29786 vectors, rejected
851073 observations (non-constraint, non-rejected)
multiple network components

No vectors were rejected between free and fixed adjustments.
No auxiliary parameters were involved in either adjustment.

Free Adjustment
- - - - - - - - - - - -
0 auxiliary parameters
203079 unknowns
3 rigid constraints (10 micron)
0 weighted constraints (10 cm)
number of rank defects due to multiple components not clear
647997 degrees of freedom, approximate
1056077.7 variance sum (vᵗPv)
1.629757 variance of unit weight
1.276619 standard deviation of unit weight
```

```
Fixed Adjustment
- - - - - - - - - - - -
0 auxiliary parameters
203079 unknowns
673 CORS 3D constraints (10 micron)
5 CORS, 2D rigid constraints (10 micron/10 cm)
7 CORS, weighted constrained (10 cm)
3 CORS, never fixed or weighted at all (DF7065, AI9604, AH7473)
2055 constraints, total
2029 rigid constraints (10 micron)
  26 weighted constraints (10 cm)
650049 degrees of freedom, approximate
1229874.4 variance sum (vᵗpv)
1.8919718 variance of unit weight
1.375490 standard deviation of unit weight
```

The structure of Table 1.1 reflects the fact that no rejections of GPS vectors were made between the free and the fixed adjustments. Only the fixing of CORS coordinates and the selection of weighted CORS coordinates distinguish the two adjustments. As such, the increase of the standard deviation of unit weight from 1.276619 to 1.375490 solely reflects discrepancies between the CORS coordinates updated to 2007.0 (see NGS 2007) and the NSRS GPS vectors.

The approximate nature of the count of degrees of freedom for the free adjustment is due to the fact that the GPS network of unrejected vectors has multiple components. Ordinarily, one would remedy the resulting rank defects by fixing additional coordinates. The network singularities were masked, however, by the "rejection by downweighting" mechanic. That is, rejected GPS vectors were not excluded from the normal equations. Instead, the rejected GPS vectors were given large (100 m) standard deviations in each XYZ (Earth-Centered, Earth-Fixed) component. The free adjustment used rejected GPS vectors to resolve the rank defects caused by the multiple components.

The approximate nature of the count of degrees of freedom for the fixed adjustment is based on the fact that 26 of the constraints are weighted with a 10 cm standard deviation instead of being rigidly fixed or completely released. The fixed adjustment can be considered as having between 2029 and 2055 constraints when the 10 cm weighted constraints are included. The figure of 650049 degrees of freedom for the fixed adjustment is only true if the 10 cm constraints are counted as rigid. A more accurate value for the degrees of freedom of the fixed adjustment would have a fractional nature and be less than 650049. While a fractional value for the degrees of freedom of the fixed adjustment is available, it is perturbed by the "rejection by downweighting" mechanic causing uncertainty in selection of a tolerance to filter the redundancy numbers. For an example of how noninteger degrees of freedom arise in weighted control adjustments, see Table 2 of Bossler and Hanson (1980).

In addition, the approximate nature of the count of degrees of freedom for the fixed adjustment is due to the unknown number of components comprising the GPS network of unrejected vectors. For example, if the GPS network contained 2 components, then 6 of the 2055 CORS constraints would be used to satisfy the rank

defect of the second component, and not be counted as increasing the degrees of freedom. It can be reported, however, that the CORS constraints of the fixed adjustment *did* resolve all of the rank defects.

2. Detection of free adjustment singularities

Inspection of the coordinate standard deviations from the NSRS free adjustment shows an abrupt jump in magnitude from about 450 cm to 1250 cm. This identified 235 points that were associated with the free adjustment rank defects. The coordinate standard deviations from the fixed adjustment of these 235 points range from 0 to 28 cm, indicating satisfactory solution. (Refer to the end of sjoin1.s.txt in the Electronic Support Material.)

Multiple "weak" points can be created by a single rank defect. Thus, the count of 235 points represents an upper limit on the true rank defect of the free adjustment. For an example of how multiple points can be affected by a single "rejection by downweighting", consider a GPS vector set in project GPS1670:

AJ6946 --> DE5880
AJ6946 --> DE5881
AJ6946 --> HK0591 (rejected) .

The "historical" station is HK0591, found in GPS419/C and GPS1012. The trio (AJ6946, DE5880, DE5881) depend solely upon the connection of AJ6946 to HK0591. The trio forms a pendant (hanging) subgraph off the rest of the network. The subgraph is disjoint when the rejection is applied. In this example, one rejection creates an independent component containing three points. Also, in this example, the rank defect is remedied by fixing the CORS at AJ6946.

3. Portrayals of the NSRS 2007 network

Figure 3.1 displays the adjusted points in the NSRS 2007 in the conterminous United States. The figure is also provided as a full page plate, Plate 1. With the exception of 3 unweighted CORS, the points represent the passive (monumented) control of the three dimensional NSRS. The participation of various entities within the States is reflected in the coverage. Lineations in California, Colorado, Florida, Louisiana, and Minnesota are GPS points measured along highways and optical level lines. Figures for Alaska, Hawaii, and the Caribbean are in the Appendix.
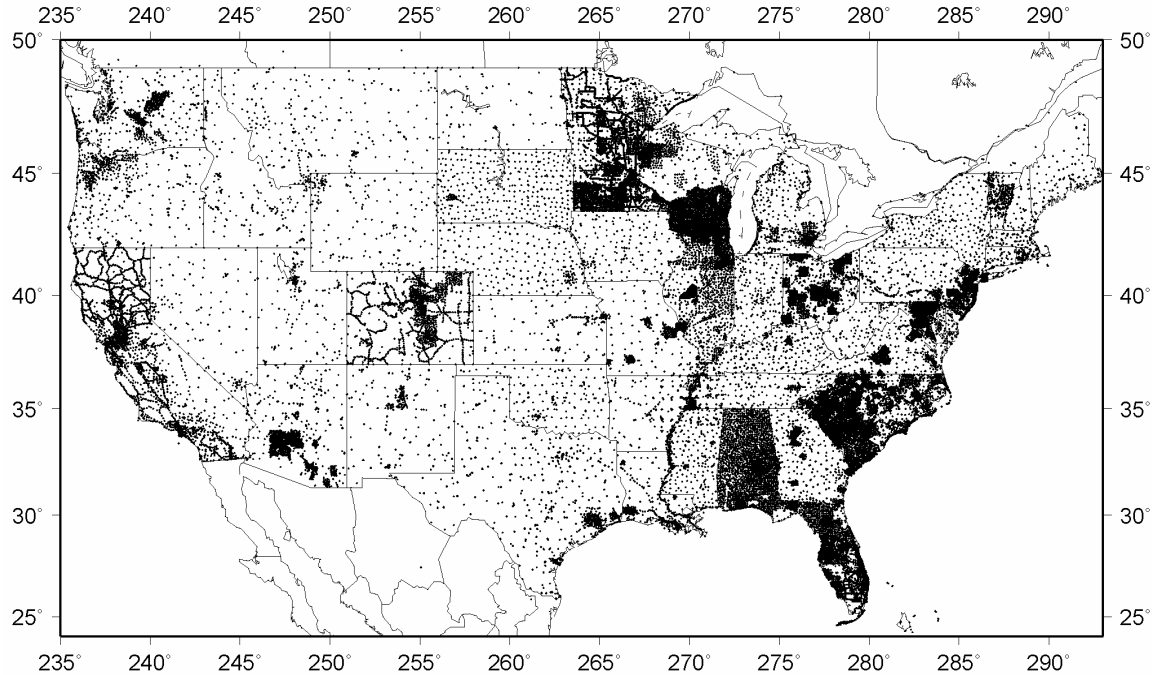
Figure 3.1. Monumented points of NSRS 2007, Conterminous U.S.

4. Age of the NSRS 2007 network

The NSRS network is built from GPS projects that date from 1983 to the cutoff date of November 15, 2005. All project GPS vector files (GFILE's) were processed to establish a mean date for each project. (Refer to proid3.txt in the Electronic Support Material.) The distribution of project activity is histogrammed in Figure 4.1. The increase in 1995 shows work supporting the FAA Airport Surveys program.
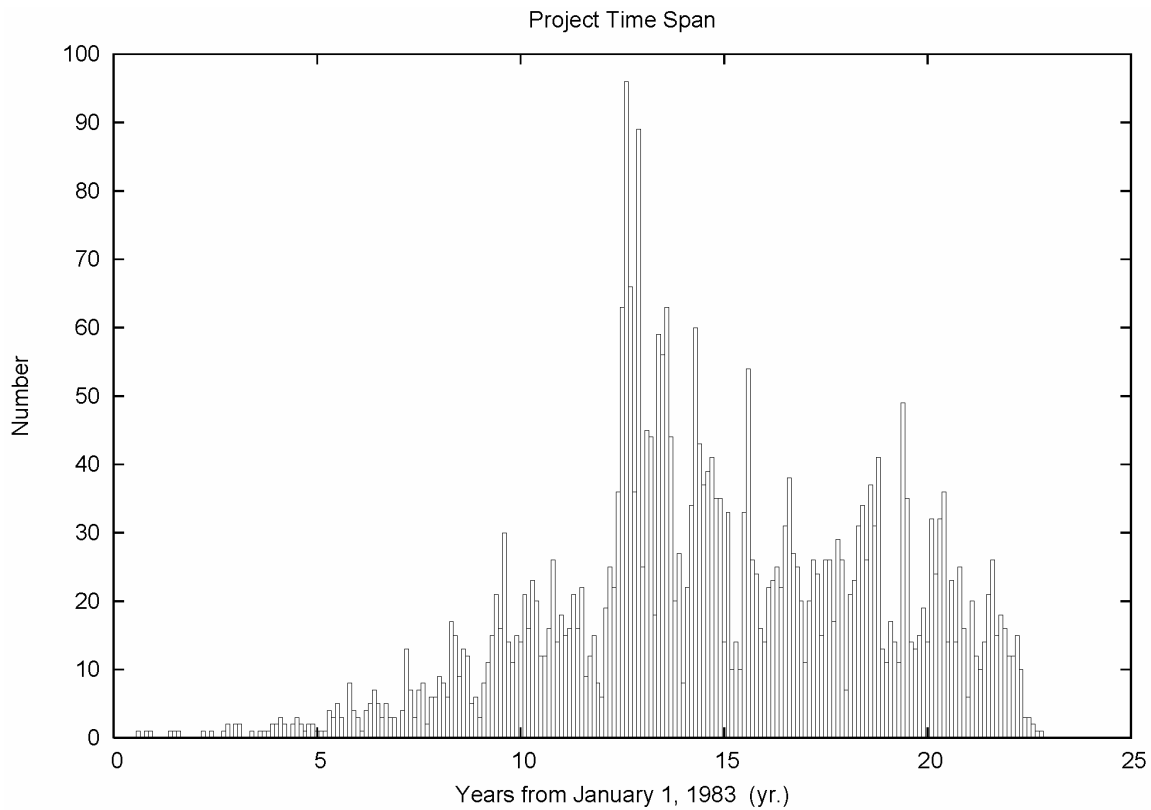
Figure 4.1. Temporal distribution of GPS projects in NSRS 2007.

For a somewhat different view of GPS survey activity, each adjusted point in the NSRS was assigned to a parent project, where that point was first observed. This allows assignment of an approximate "birth" date for each point. The distribution of the establishment of new points is histogrammed with a bin width of 0.1 year in Figure 4.2 and with a bin width of one year in Figure 4.3. Figure 4.2 shows the seasonal character of GPS survey work. And, Figure 4.3 show the level of annual activity. While there is a decrease in annual count in recent years, the 0.1 year counts continue to show significant recent spikes.
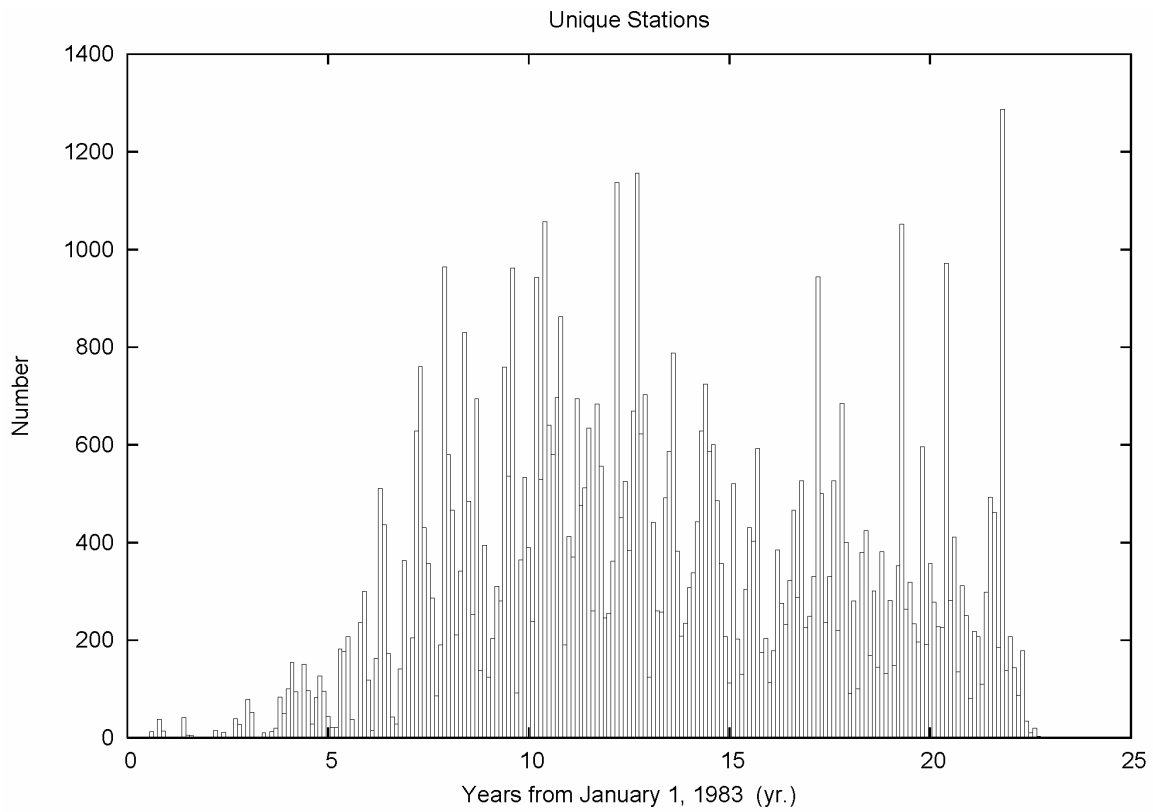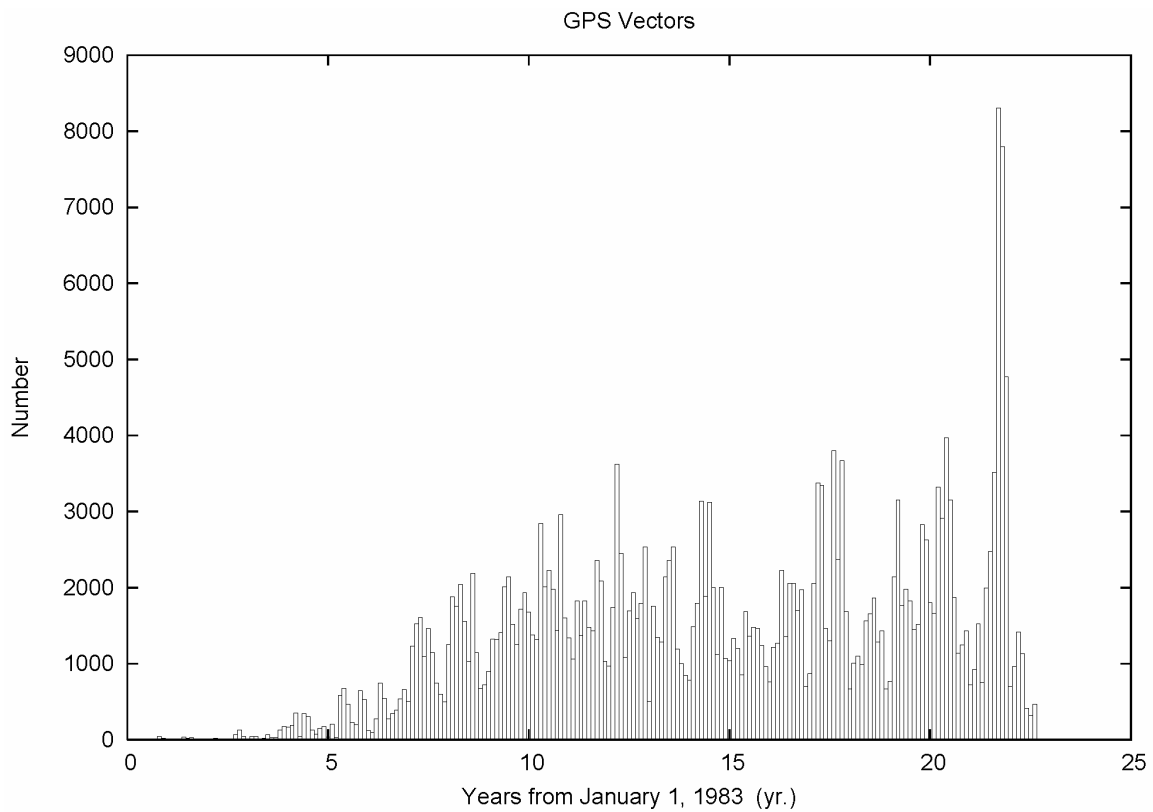
Figure 4.2. Temporal distribution of new GPS points. 0.1 year bin size.
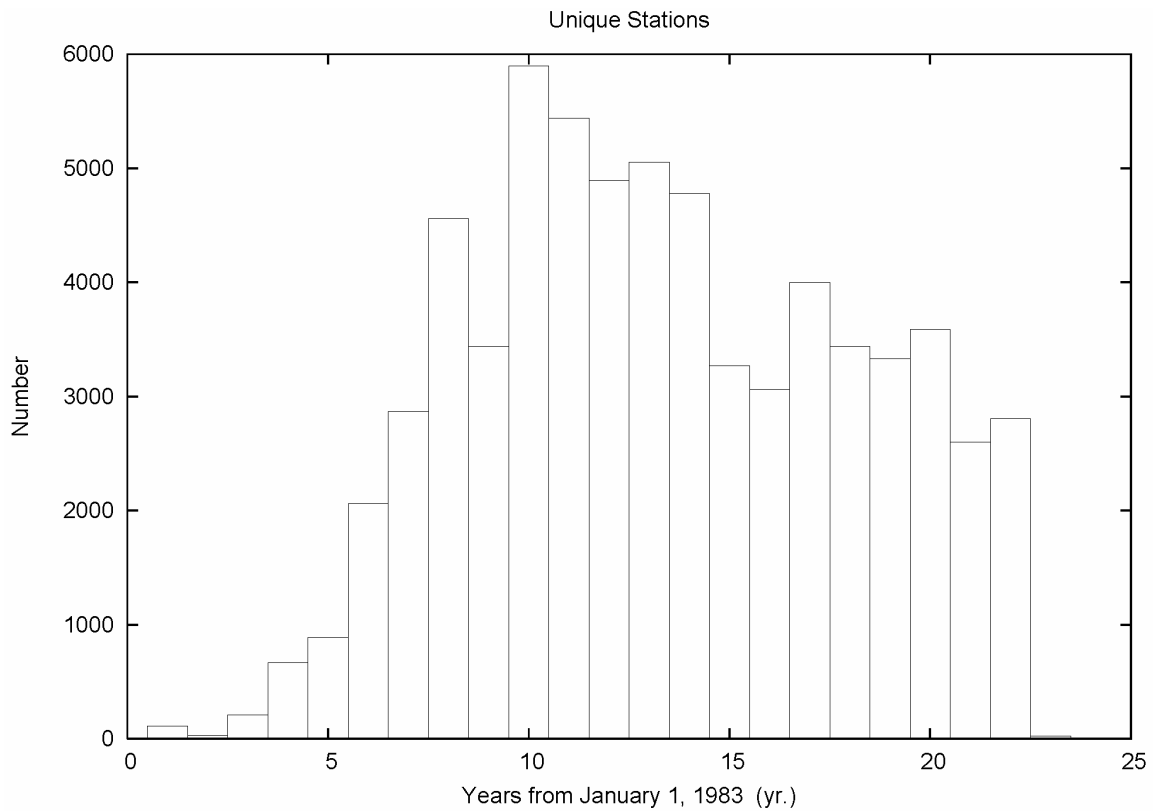
Figure 4.3. Temporal distribution of new GPS points. One year bin size.

A more complete perspective of GPS survey activity is seen when the observation dates of the GPS vectors are histogrammed. Figure 4.4 is plotted with a bin width of 0.1 year and Figure 4.5 is plotted with a bin width of one year, showing annual activity. Of interest, the number of vectors submitted to the NGS data base is uniform, if not actually increasing, in recent years. Taken in conjunction with the decrease in the annual rate of new points seen in Figure 4.3, one may conclude that the NSRS is becoming more robust through the inclusion of additional vectors. (Refer to filt18.txt in the Electronic Support Material.)

Figure 4.4. Temporal distribution of GPS vectors. 0.1 year bin size.
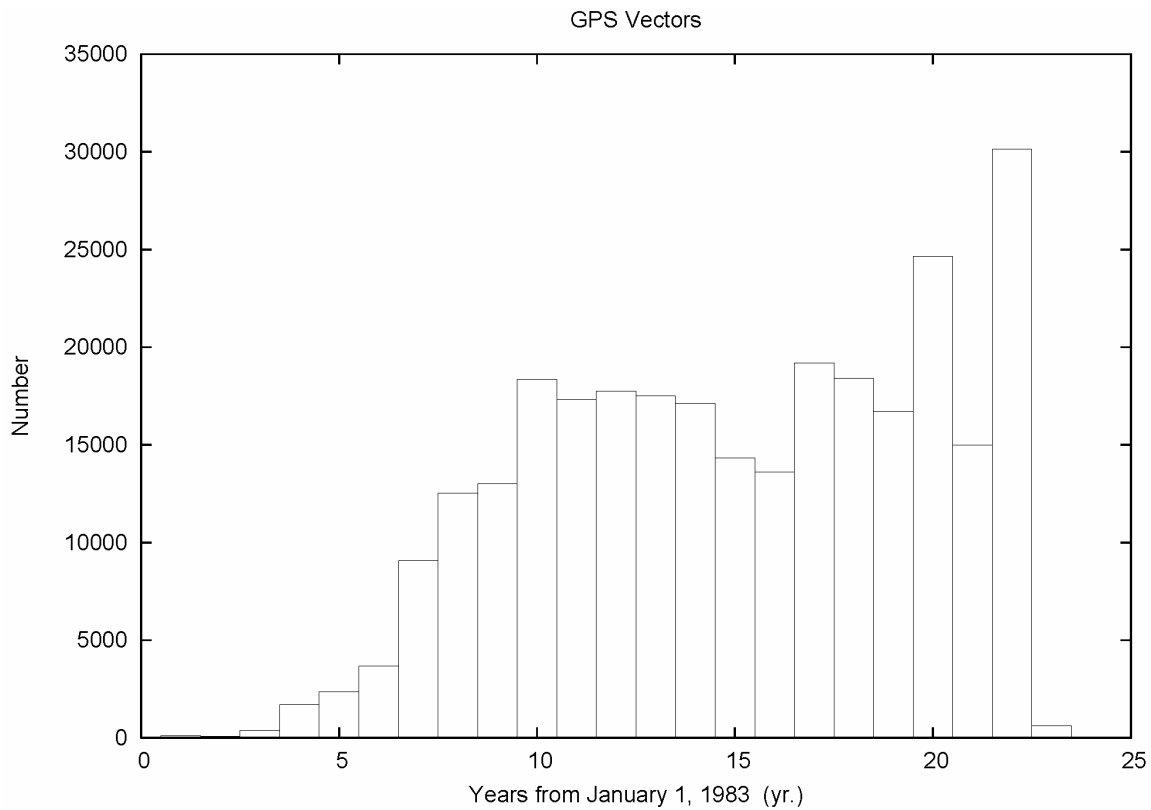
Figure 4.5. Temporal distribution of GPS vectors. One year bin size.

5. Connectivity of the NSRS 2007 network

While there are far too many vectors to show the connections within the network, some appreciation can be gained from inspecting the distributions of the lengths of the GPS vectors in the network. Figure 5.1 shows the vector lengths from 0 to 500 km with a 5 km bin size. Figure 5.1 is truncated, since the GPS vectors reach a maximum length of 5217 km.
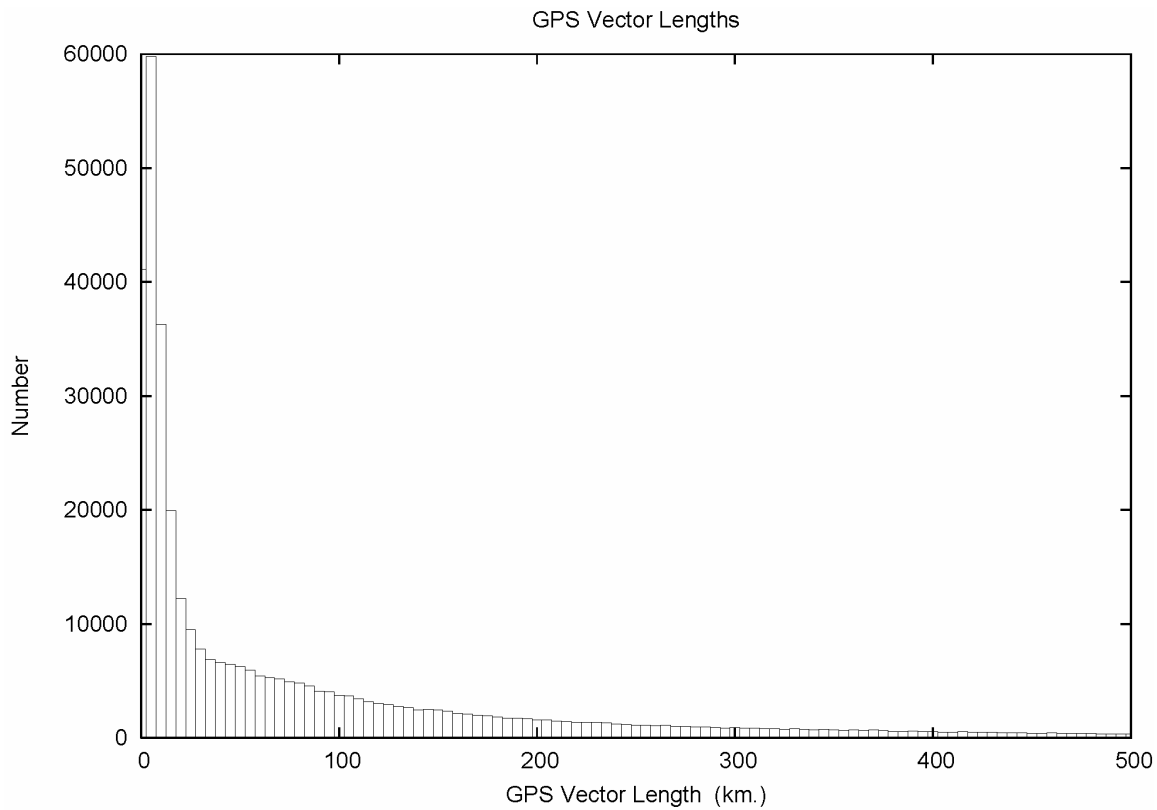
GPS Vector Lengths

Figure 5.1. Distribution of GPS vector lengths, 0 to 500 km. 5 km bin size.

The percentile distributions of the vector lengths are provided in Table 5.1

Table 5.1 – Percentiles of GPS vector lengths

Percentile	Length (km)
50%	31
68%	89
90%	297
95%	434
99%	770
99.9%	2259

The results are surprising. The median vector length is 31 km. The bulk of the work in the NSRS is of a rather local character. This work is tied together by a significant number of longer lines. Ten percent of the network consists of lines of 300 km or longer. To further inspect this phenomenon, detail plots are made with 200 km, Figure 5.2, and with 100 km, Figure 5.3. It is seen that over 18000 vectors range from 0.5 to 1.5 km. The "elbow" in the distribution curve is at about 20 km.
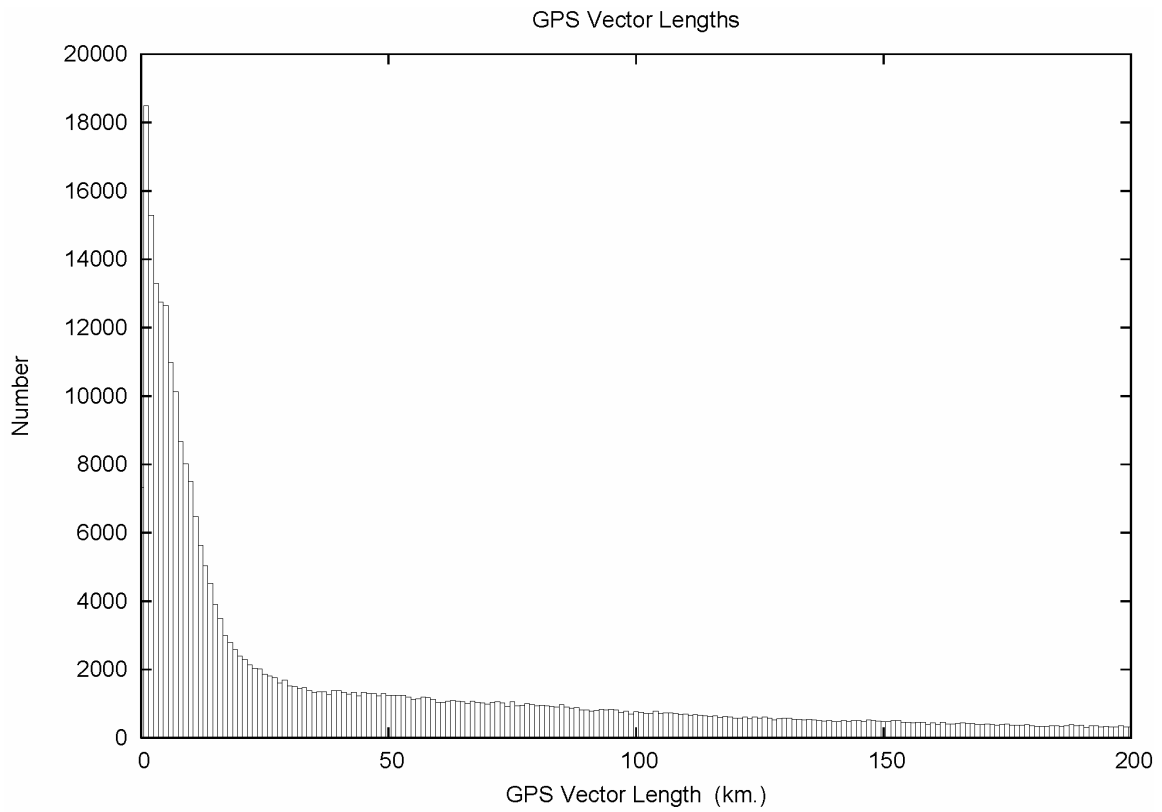
Figure 5.2. Distribution of GPS vector lengths, 0 to 200 km. One km bin size.
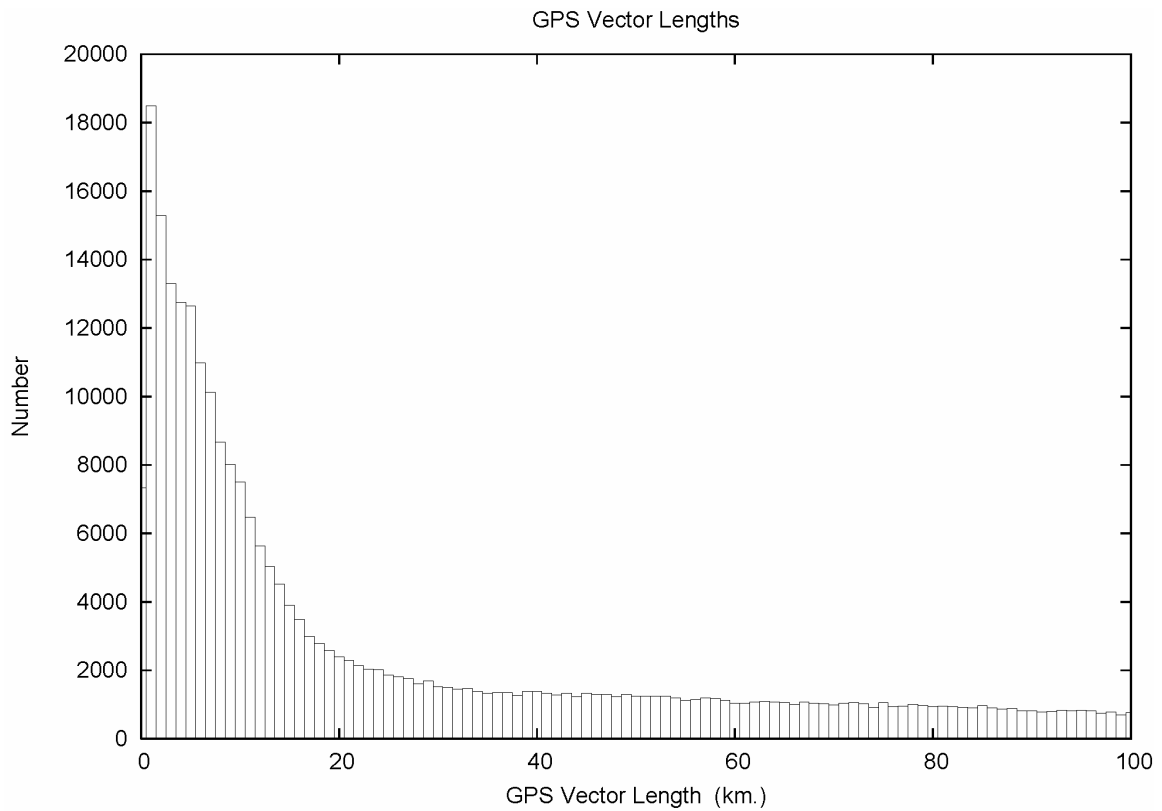

Figure 5.3. Distribution of GPS vector lengths, 0 to 100 km. One km bin size.

Three activities immediately spring to mind as sources of shorter vector baselines: urban surveying, airport surveys of runway ends, and GPS surveys along optical level lines. While not pursued in this analysis, additional data mining could establish activity levels in these categories, and, perhaps, uncover additional applications.

Figure 5.4 shows a scatter plot of the length and observation times of the unrejected GPS vectors. The figure depicts the historical nature of the very longest lines in the NSRS. Lines of 500 km or more are less prevalent than in the past. When considering vector lengths of 200 km or more, histogrammed in Figure 5.5, one sees a somewhat uniform temporal distribution of long lines. However, there is a profound decrease in long line survey activity in the annual bins for 2004 and 2005.
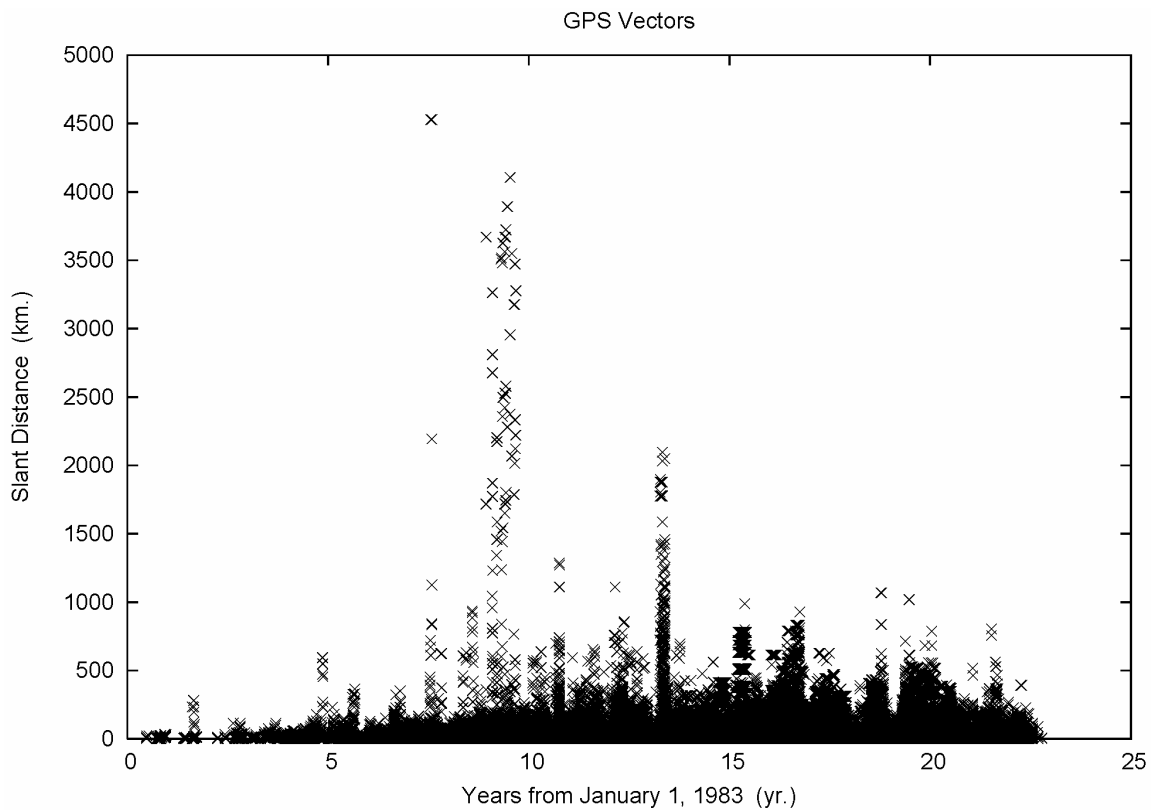

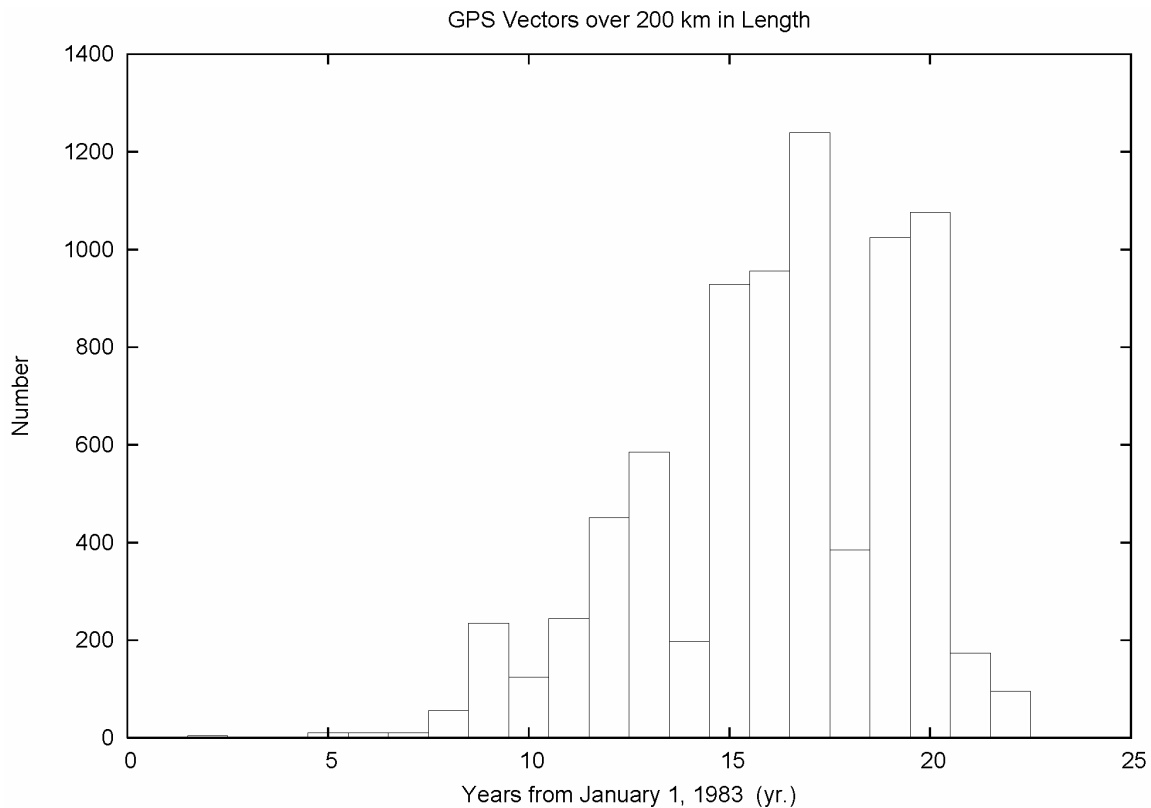Figure 5.4. Length and observation times of GPS vectors.

GPS Vectors over 200 km in Length

Figure 5.5. Temporal distribution of GPS vectors over 200 km. One year bin size.

6. Coordinate changes of the NSRS 2007 network

One of the key elements of the NSRS 2007 readjustment is the selection of an epoch of 2007.0. While this might be considered as significant only for the portion of California on the Pacific plate, the impact is much greater. This is due to the incorporation of the Horizontal Time Dependent Positioning (HTDP) models (Snay 1999) encompassing Oregon, Washington, Nevada, and Arizona, as well as California and Alaska.

Figure 6.1 displays horizontal position shifts from the older NAD 83 coordinates to the NAD 83(NSRS2007) set. As seen in Figure 3.1, the point distribution is too dense to show all position shifts. In Figure 6.1 the data set was thinned to an approximate one degree spacing.
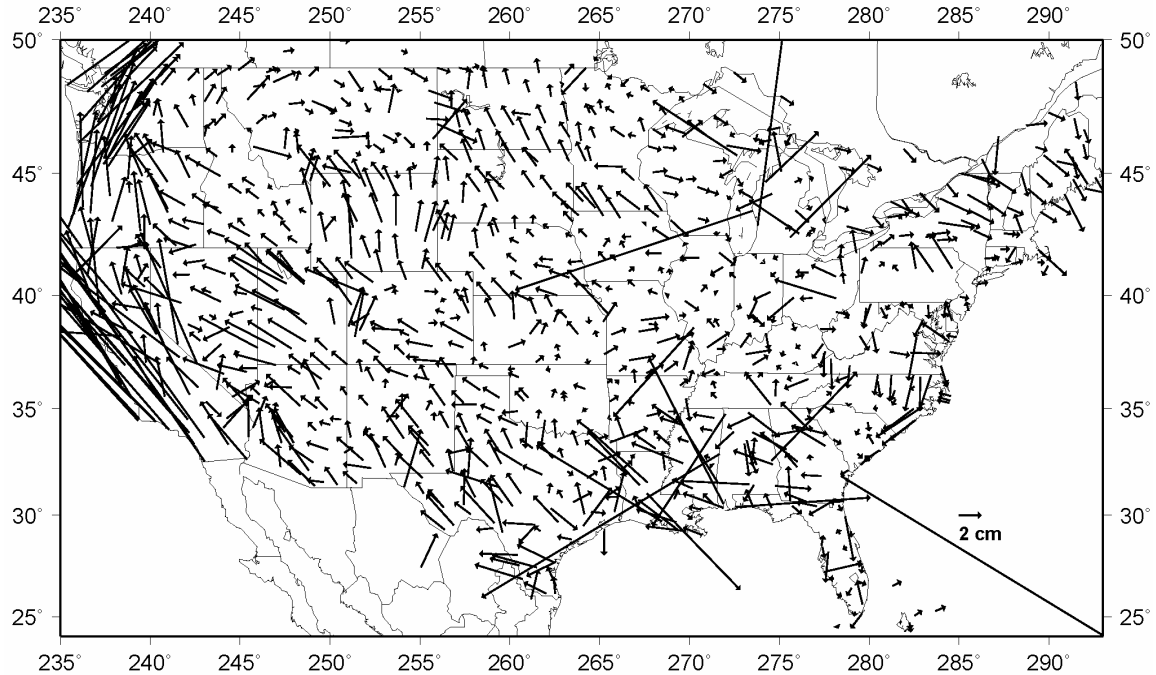
Figure 6.1. Horizontal position shifts of thinned point set, Conterminous U.S.

Aside from the systematic effects of tectonic plate and local crustal motion, the horizontal position shifts depict the residual errors in the statewide readjustments (Milbert and Milbert 1994). When one considers that the state readjustments were removing errors often exceeding 0.5 m and were performed to a nominal 5 cm criterion, the low levels of regional coordinate shifts is gratifying.

Also noticeable are some very large position shifts in the East. Such large, sporadic shifts can occur anywhere in the NSRS, and were retained in the plot of the thinned data set. These large shifts remind us that the data analysis associated with the readjustment will remove outliers that had significant effects on the coordinates.

Figure 6.2 shows vertical position shifts from the older NAD 83 coordinates to the NAD 83(NSRS2007) set. As with the horizontal position shifts, the data set was thinned to an approximate one degree spacing.
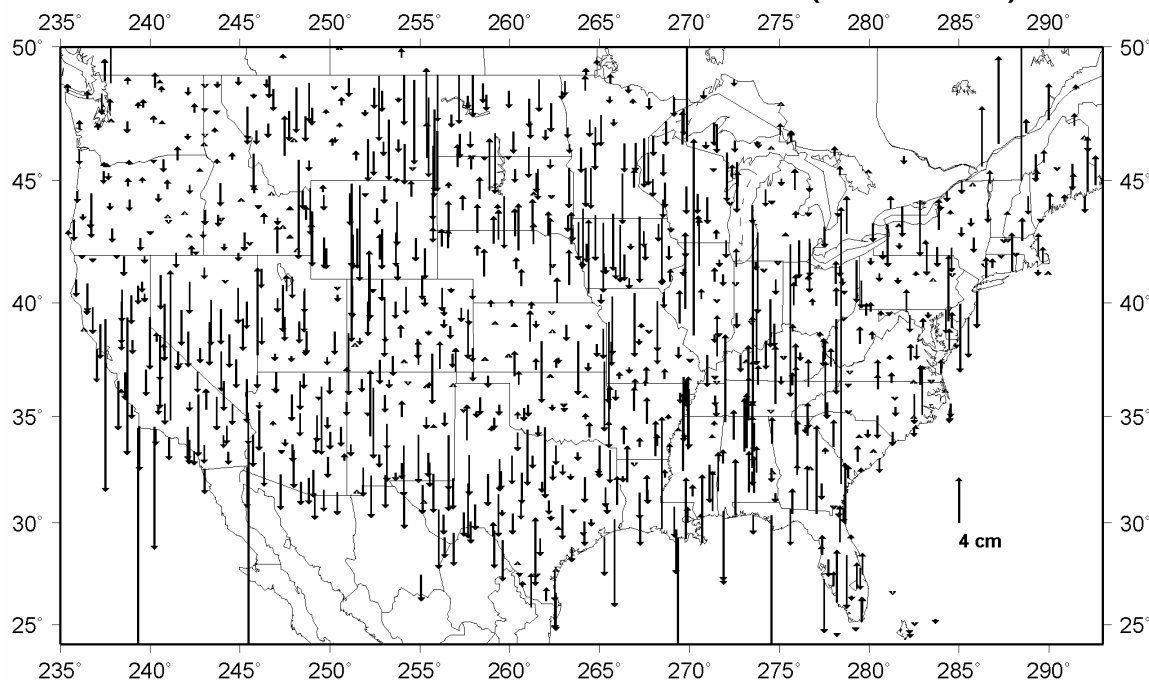
NSRS 2007 - Old NAD83 (thinned)

Figure 6.2. Vertical position shifts of thinned point set, Conterminous U.S.

While no vertical motion model treatment was applied to the NSRS 2007 as a whole, the inclusion of newer, more accurate GPS surveys will have an influence on the final NSRS coordinates. Note that the ellipsoidal heights along the Gulf Coast show a drop from the older NAD 83 heights. Even so, one must treat physical interpretations of these vertical coordinate shifts with caution. These shifts will also depict the residual errors of the statewide readjustments.

Note that the thinned data set shows a general lack of vertical shift in the Pacific Northwest. To further investigate this, Figure 6.3 displays vertical position shifts from the older NAD 83 coordinates to the NAD 83(NSRS2007) set. This is a detailed view, and the data set was not thinned. On the whole, the thinned data set depiction in Figure 6.2 is accurate. Figure 6.3 does show particular projects and individual points that have taken significant vertical shifts. Eastern Montana and Wyoming illustrate vertical shifts of a more regional character. (Refer to adiffnoc.txt in the Electronic Support Material.) Horizontal and vertical shifts for the unthinned data set in Alaska are plotted in the Appendix.
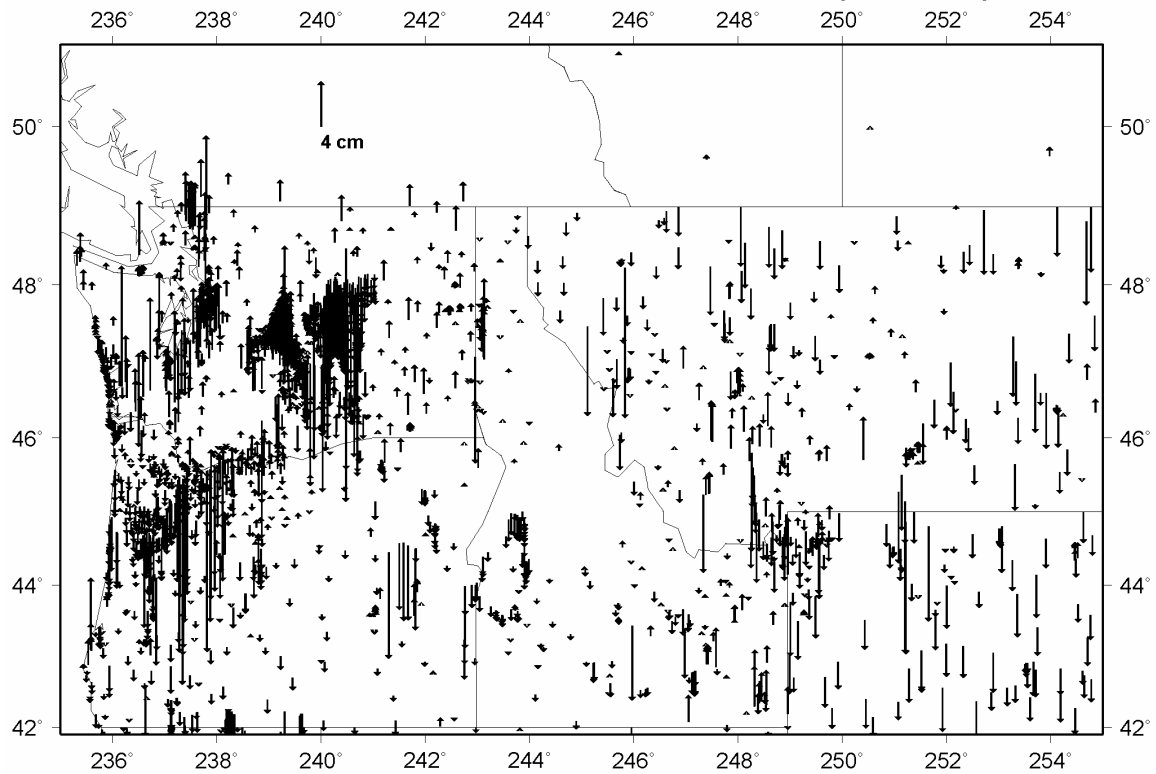
Figure 6.3. Vertical position shifts of NSRS 2007, Northwest U.S.

7. Horizontal residual errors of the GPS vectors

Figure 7.1 shows the histogram distribution of the horizontal (distance) component of the residuals from the free adjustment with a bin width of 1 mm. The residuals range to a maximum of 35 cm, as depicted in the figure. The sharp cutoff at 5 cm is due to the semiautomated rejection process that reported residuals exceeding 5 cm (Pursell *et al*. 2008).
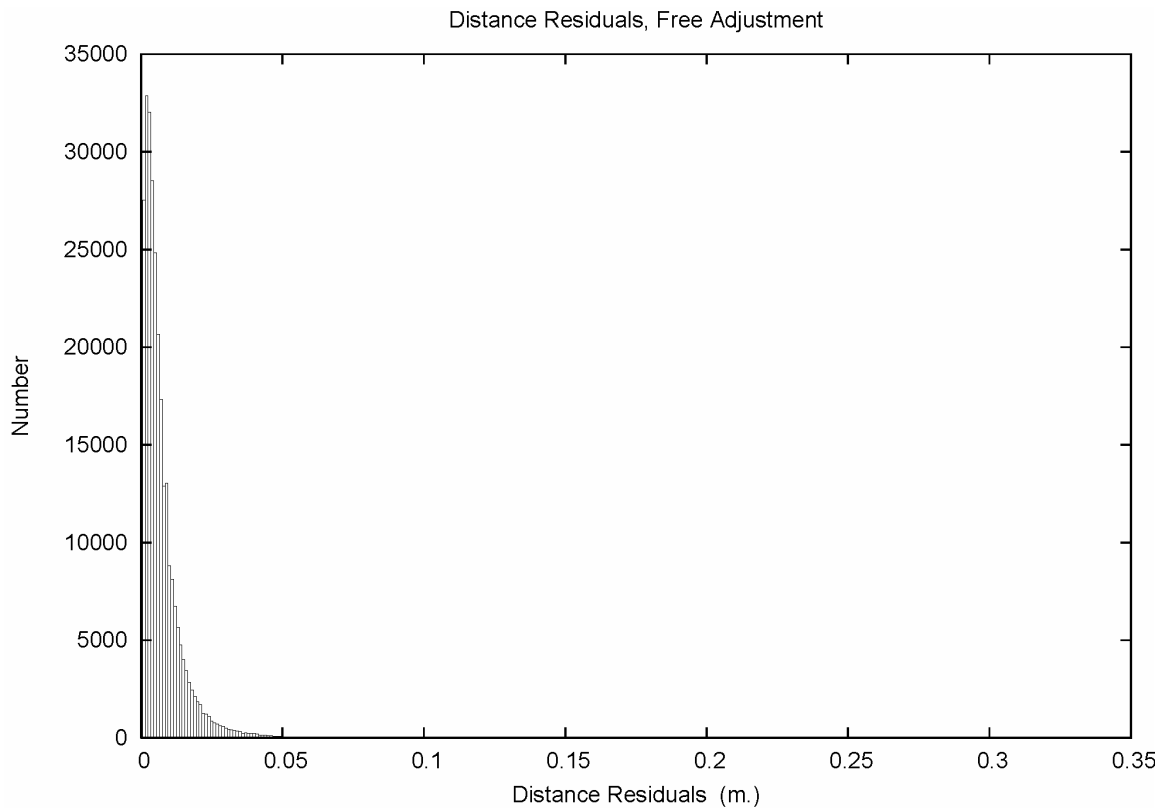
Figure 7.1. Distance residuals, free adjustment. One mm bin size.

To gain a better view, Figures 7.2 and 7.3 plot detailed views, left side and right side, of the residual distribution. Figure 7.2 and the percentiles in Table 7.1 show that the residuals seldom exceed 2 cm. Figure 7.3 depicts the occurrences of the largest, unrejected vectors. It is natural to second guess why these vectors were allowed to remain in the adjustment, and why a 5 cm inspection tolerance was selected.

Conversations (Maralyn Vorhauer, private communication, November 30, 2007) indicate that in certain circumstances rejections would lead to undetermined stations. However, after the data base pull, the analysts were locked into the station set through the interaction of the adjustment software and the station serial number (SSN) numbering. No stations were rejected after the data pull. That said, it was technically possible to reject observations and then carry undetermined stations with fixed "temporary coordinates". This option was not exercised due to a fear that such coordinates would be published inadvertently. Instead, this category of coordinates, stations determined from vectors with large residual errors, were retained and published.

On a related note, one can suggest that lines with large residuals would be prime candidates for reobservation. (Refer to allsresfrnor.txt in the Electronic Support Material.)
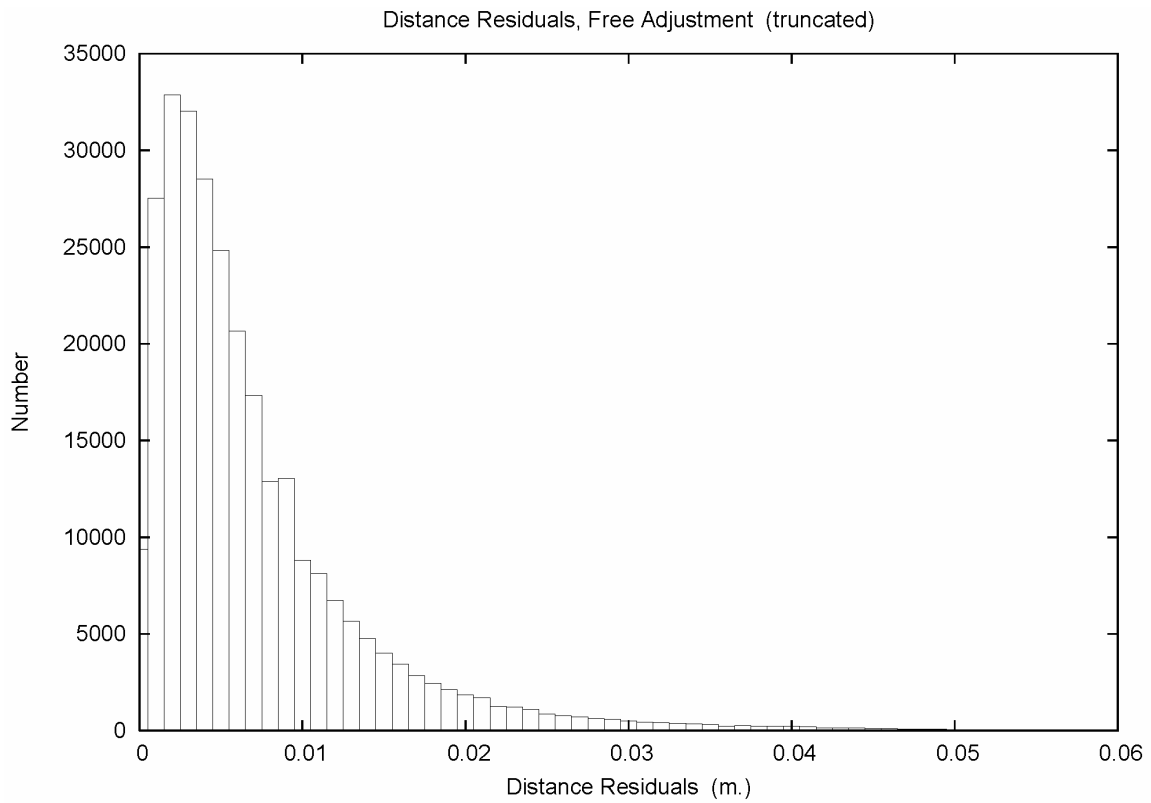
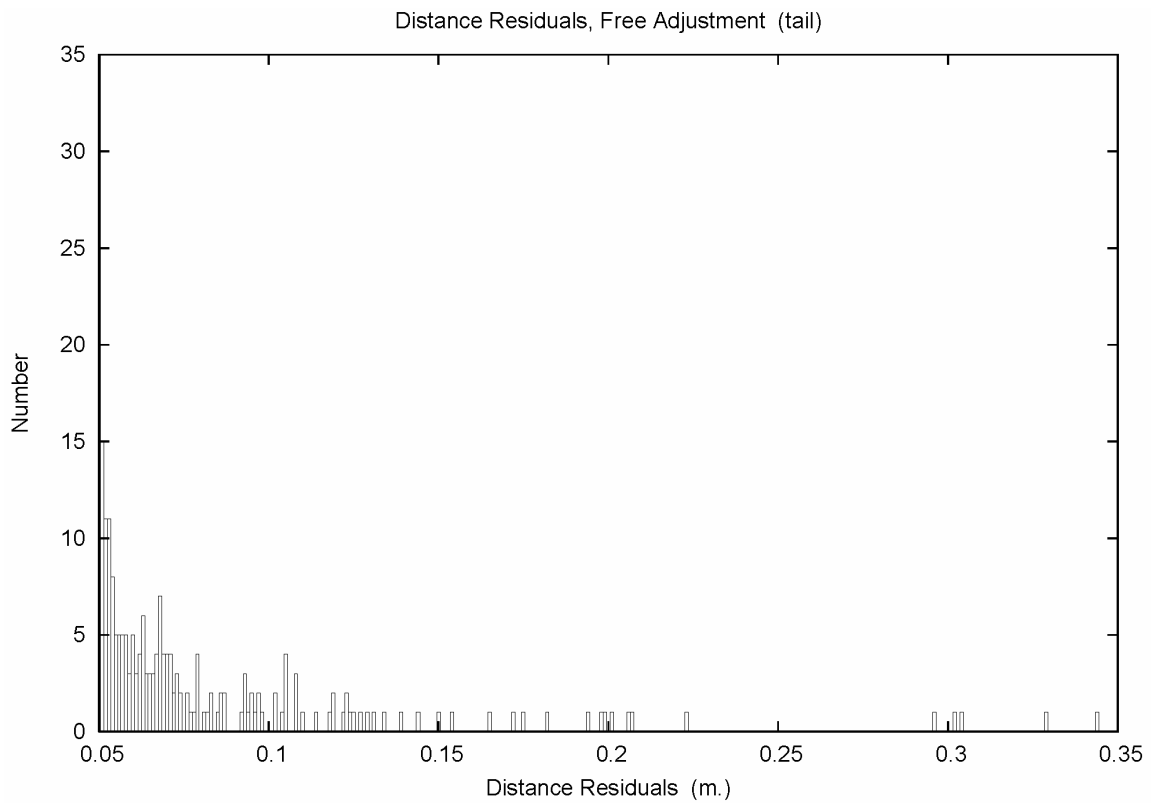Figure 7.2. Distance residuals, free adjustment, detail. One mm bin size.

Figure 7.3. Distance residuals, free adjustment, distribution tail. One mm bin size.

Table 7.1 – Percentiles of Distance Residuals, Free Adjustment

Percentile	Residual (cm)
50%	0.5
68%	0.7
90%	1.5
95%	2.0
99%	3.4
99.9%	4.9

Before closing this section, some comments must be made regarding the inspection of residuals in general. One should refer to a text on least squares adjustments, such as Mikhail (1976), for the detailed mathematics.

Residuals, v, in an adjustment always underestimate the full amount of random error. This is evident when inspecting the covariance (dispersion) matrix of the residuals, $\mathbf{D}_v$, and the covariance matrix of the observations, $\mathbf{D}_o$,

$$\mathbf{D}_v = \mathbf{D}_o - \mathbf{D}_{ao} \ , \tag{7-1}$$

where $\mathbf{D}_{ao}$ is the positive-definite covariance matrix of the adjusted observations. This is most evident when a point is uniquely determined (no check). Then, an uncorrelated observation will have a residual of zero, and a standard deviation of the residual of zero.

A population of residuals can contain contributions from high-accuracy, mid-accuracy, and low-accuracy surveys. And, those surveys can contain various amounts of redundancy; which, in turn, will vary the amount by which the residuals underestimate the true error. Of course, a 35 cm residual can safely be considered troublesome. But, outlier detection based only on inspection of residual magnitude, without considering underlying observation precision or redundancy, is problematic.

The answer is to standardize each residual by the standard deviation of that residual. This standard deviation of the residual would incorporate the effects of observation accuracy and network redundancy on the residual. In the early history of the National Geodetic Survey, such a statistic was computationally prohibitive. Outlier detection based on standardized residuals was routinely performed for classical surveys conducted with program ADJUST (Milbert and Kass 1987). The practice later fell into disuse at NGS due to the grossly overoptimistic dispersions generated by GPS reduction software, as well as concern regarding correct calibration of the vector covariance matrix to reflect the true ratio of horizontal-to-vertical accuracy.

As described in Pursell *et al*. (2008), NGS practice has been to scale the First Order (and lower order) GPS projects by the project *a posteriori* standard deviation of unit weight. As part of the readjustment analysis, distinct horizontal and vertical component dispersion scale factors were computed for all orders of GPS projects (Section 15). With this massive calibration effort it would be possible to finally place confidence

in the formal error estimates and postprocessing statistics generated by a GPS vector adjustment. However, despite this work, standardized residuals were not utilized in the NSRS 2007 readjustment.

8. GPS session redundancy

Redundancy can be globally quantified by the degrees of freedom. Redundancy numbers, q, can also be computed for uncorrelated observations, and range from 0 to 1 (El-Hakim 1981). A redundancy number in the vicinity of 0 indicates the error in an observation is being transferred to the adjusted parameters. A redundancy number in the vicinity of 1 indicates the error in an observation is being transferred to that observation's residual. The sum of all the redundancy numbers in an adjustment equals the degrees of freedom.

While redundancy numbers are problematic for correlated observations, they can be summed in sets, such as over GPS sessions (Milbert 1985, Milbert and Kass 1987). When considering a set of n correlated three-dimensional GPS vectors, the session redundancy sum will range from 0 to $3n$. Again, the numbers indicate a sliding scale that quantifies the transfer of observation error between the adjusted parameters and the residuals.

Analysis of the of the NSRS 2007 adjustment outputs shows the 283691 unrejected GPS vectors are grouped into 236239 sessions. This works out to about 1.2 vectors per session. In other words, the bulk of the GPS vectors in the NGS data base do not have correlation information between vectors. If most of the GPS vectors were, in fact, measured independently with only two receivers, this would be correct. However, it is known that certain GPS reduction softwares take computational shortcuts and do not issue the correct intervector correlation elements. NGS operating procedures recognize this failing and only allow certain software to be used for vector reduction of A and B Order GPS projects. Nonetheless, by accepting lower order work without the correct intervector correlation elements, a level of approximation will be inherent in any publication or interpretation of the formal error statistics. This level of approximation means methods of network maintenance that rely upon explicit promulgation of the network covariance matrix (Schwarz 2005) have questionable utility.

Figure 8.1 plots a histogram of the GPS session redundancy numbers. The session redundancy numbers range from 0 to 253.6. The left part of the figure is detailed in Figure 8.2.
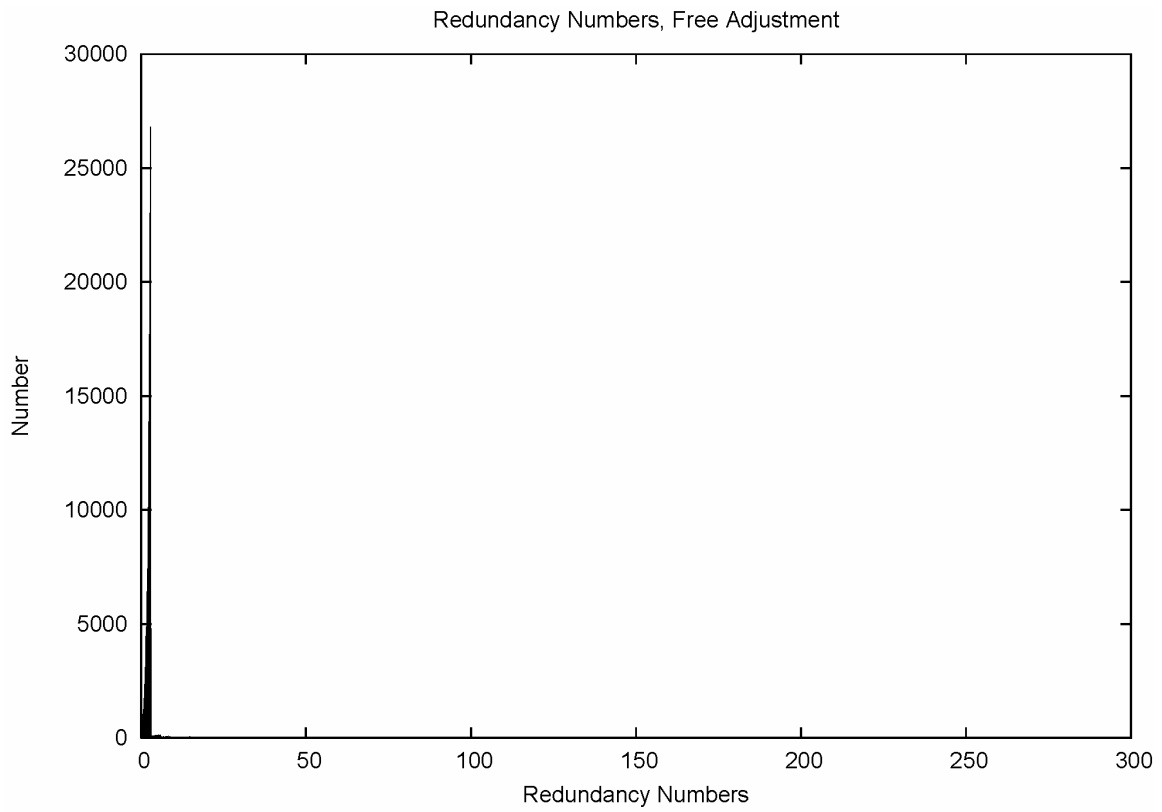
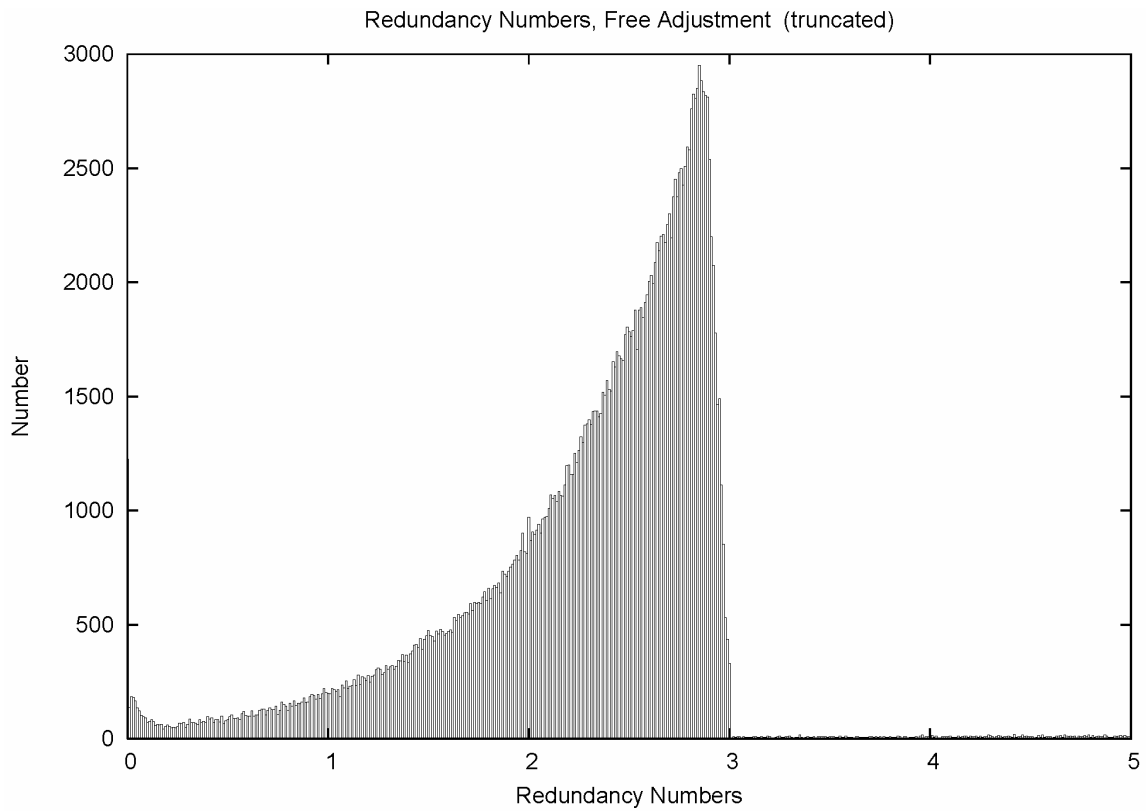Figure 8.1. GPS session redundancy. 0.01 bin width.

Figure 8.2. GPS session redundancy, low redundancy detail. 0.001 bin width.

Here the general absence of GPS intervector correlations is evident. Practically all of the GPS redundancy sums only range from 0 to 3. Of particular surprise is the skew of the redundancy sums towards 3. By virtue of the relative weights of the vectors, a large number of them are, in fact, redundant. While this property is useful for calibrating survey accuracy, and certainly provides a blunder check on other measurements, one can feel comfortable in rejecting such redundant observations if need arises, and if the underlying vector weight is accurate.

An additional detail view of the distribution of low redundancy vectors is provided in Figure 8.3. Most noticeable is the spike on the left hand side indicating 916 zeros, and 309 very tiny redundancy sums. Note that the count of 916 refers to the number of sessions that have a zero sum, and that some sessions do have multiple points observed. Hence the count of 916 sessions is not inconsistent with the report of 2605 non-check points in the NSRS 2007 readjustment.
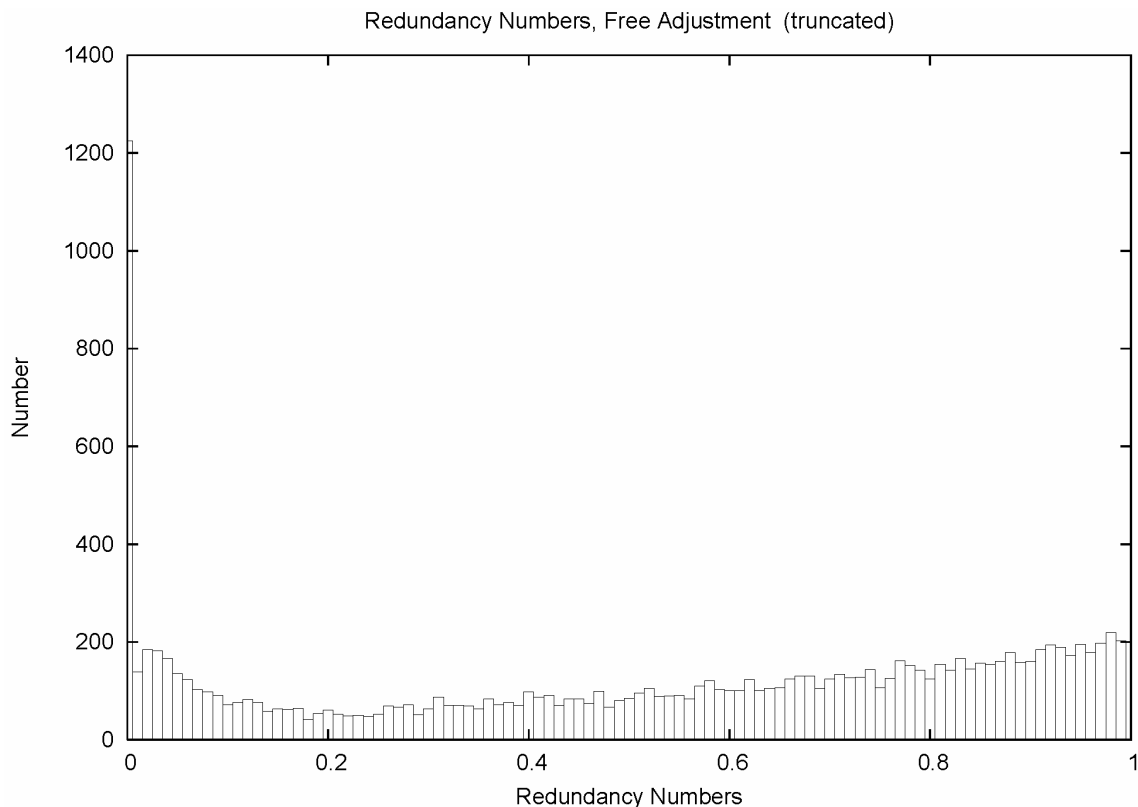

Figure 8.3. GPS session redundancy, very low redundancy detail. 0.001 bin width

9. Posteriori standard deviations of horizontal residuals

Since the standard deviations of the residuals are useful in standardizing the residuals for outlier detection and error diagnosis, they are now considered in this section. As described earlier in this report, and in Pursell *et al.* (2008) the dispersions of the survey observations have, in general, been scaled twice; once by a survey standard deviation factor for lower order projects, and again by separate survey standard deviation

factors for both the horizontal and vertical components. In addition, the standard deviations below are *a posteriori*. That is, they have been scaled by the *a posteriori* standard deviation of unit weight of the free adjustment of the NSRS, 1.276619. As such, they are corrected for covariance miscalibration due to inter-survey error sources.

Figure 9.1 plots a histogram distribution of the *a posteriori* standard deviations of the horizontal (distance) component of the residuals from the free adjustment. The standard deviations range from 0 to 15.469 m. The left part of the figure is detailed in Figure 9.2 with a bin width of 0.1 mm.

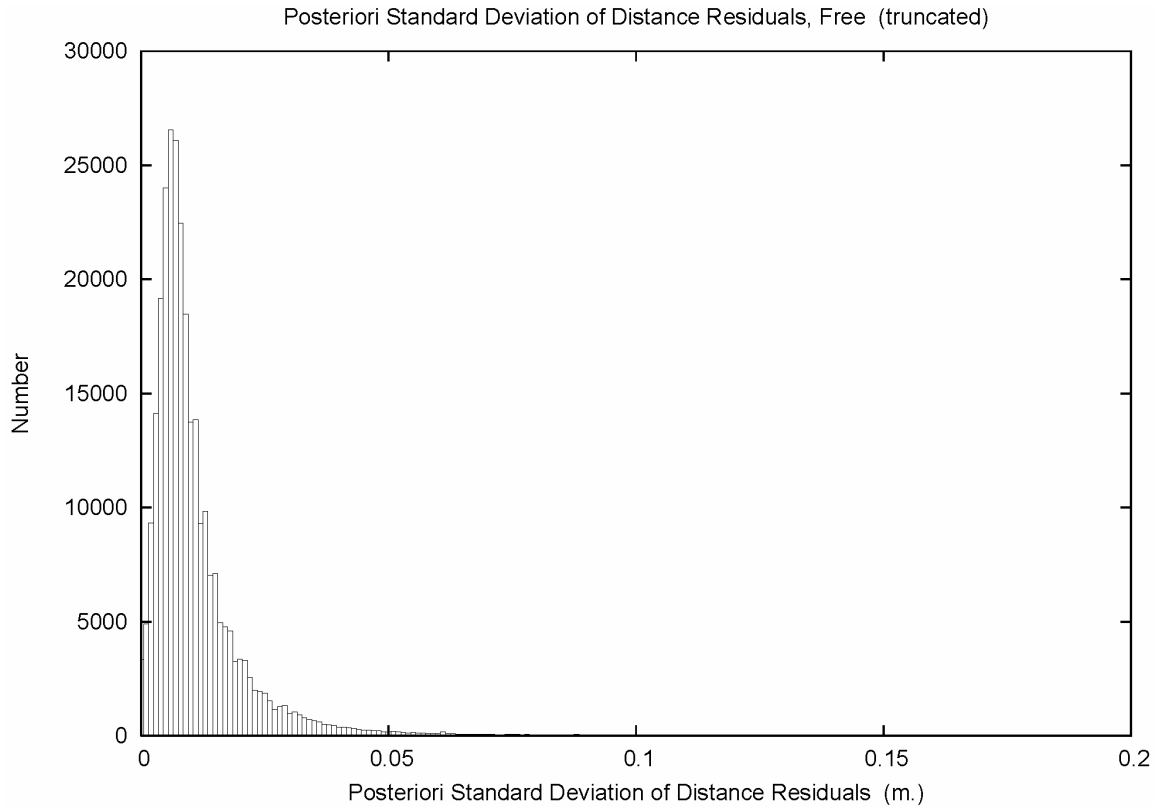Posteriori Standard Deviation of Distance Residuals, Free (truncated)

Figure 9.1. Standard deviation of distance residuals, free adjustment. 0.001 m bin width.
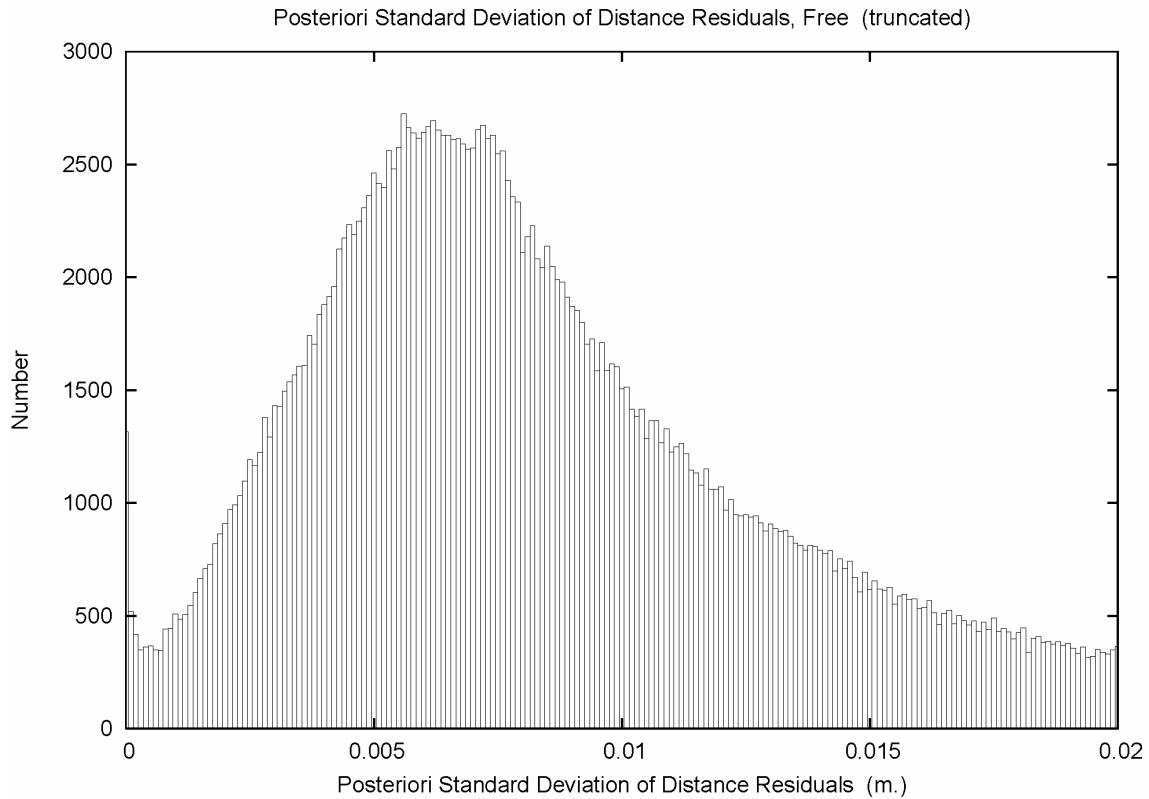
Figure 9.2. Standard deviation of distance residuals, free adjustment, detail. 0.1 mm bin.

Comparisons of Figure 7.2 with 9.1 and 9.2 show the same general distributions for the distance residuals and their standard deviations. This suggests that the weight calibration procedures were largely successful, and that the standardized residuals will be accurate in general.

10. Posteriori standardized horizontal residuals

As described in Section 7, standardized residuals are residuals divided by the standard deviation of that residual. And, that standardization process allows one to inspect residuals while accommodating the underlying variations in survey precision and network redundancy. Since the residuals were standardized using *a posteriori* standard deviations of residuals, they are *a posteriori* standardized horizontal residuals. And, as described in Section 9, they are thereby corrected for covariance miscalibration due to inter-survey error sources. Standardized horizontal residuals can be expected to approximate a Rayleigh distribution (assuming the horizontal component variates are of equal averge magnitudes and uncorrelated). Figure 10.1 plots a histogram distribution of the *a posteriori* standardized horizontal residuals from the free adjustment. The standardized residuals (unitless) range from 0 to 26.857.
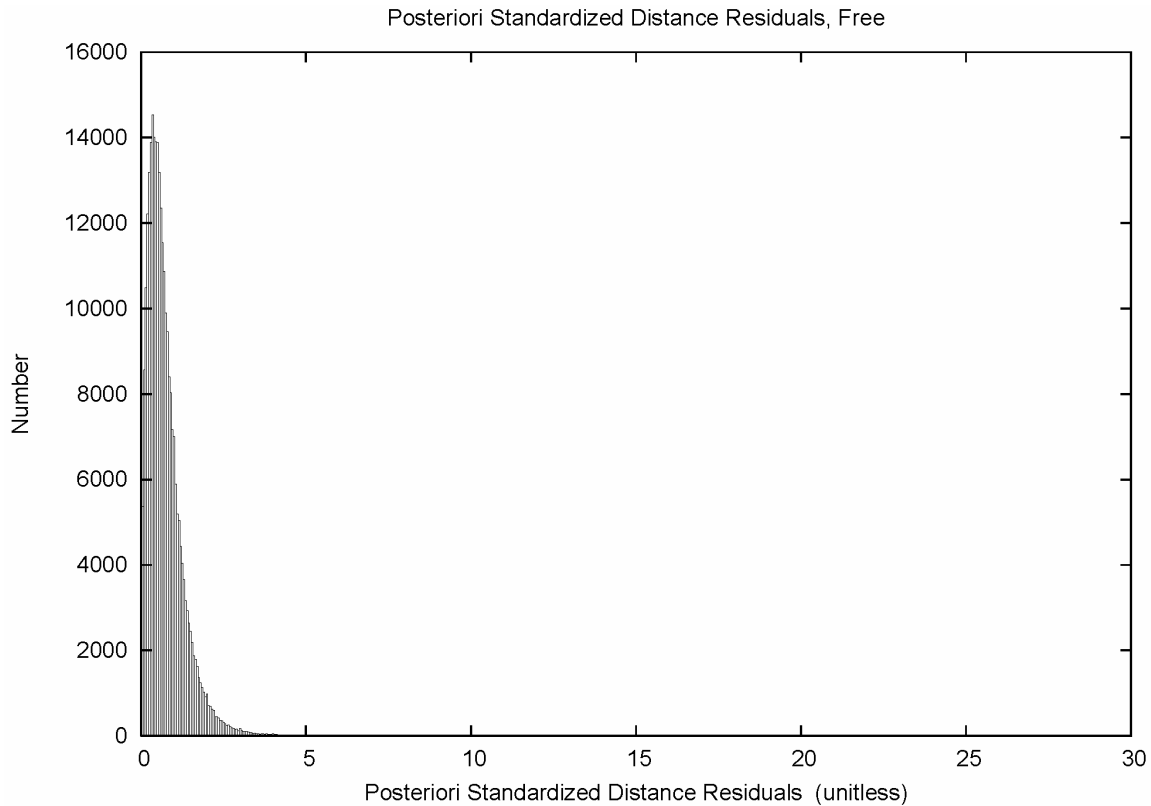
Figure 10.1. Standardized distance residuals, free adjustment.

       Figure 10.2 displays a detail view of the left hand side of Figure 10.1. This serves to emphasize the distribution of the standardized horizontal residuals. Outlying residuals in the tail of the distribution are plotted in Figure 10.3. These are residuals that should be considered for rejection. (Refer to allsresfrnor.txt in the Electronic Support Material.)

      Inspection of the statistics file (allsresfrnor.txt) for the large standardized residuals shows non-standardized residual magnitudes of 4 to 5 cm as well as 4 to 5 mm. Large standardized residuals appear due to a large residual and/or a small standard deviation of the residual. A small standard deviation of the residual occurs for a combination of two reasons. The underlying observation is very precise, or, the underlying observation has little or no redundancy. In either case, the residual of the measurement is far larger than what is expected. Of course, as part of the process of inspecting the standardized residuals, the variance scaling of the project and its components should also be considered (Section 15). There may be cases where new project standard deviation factors need to be assigned by the analyst.
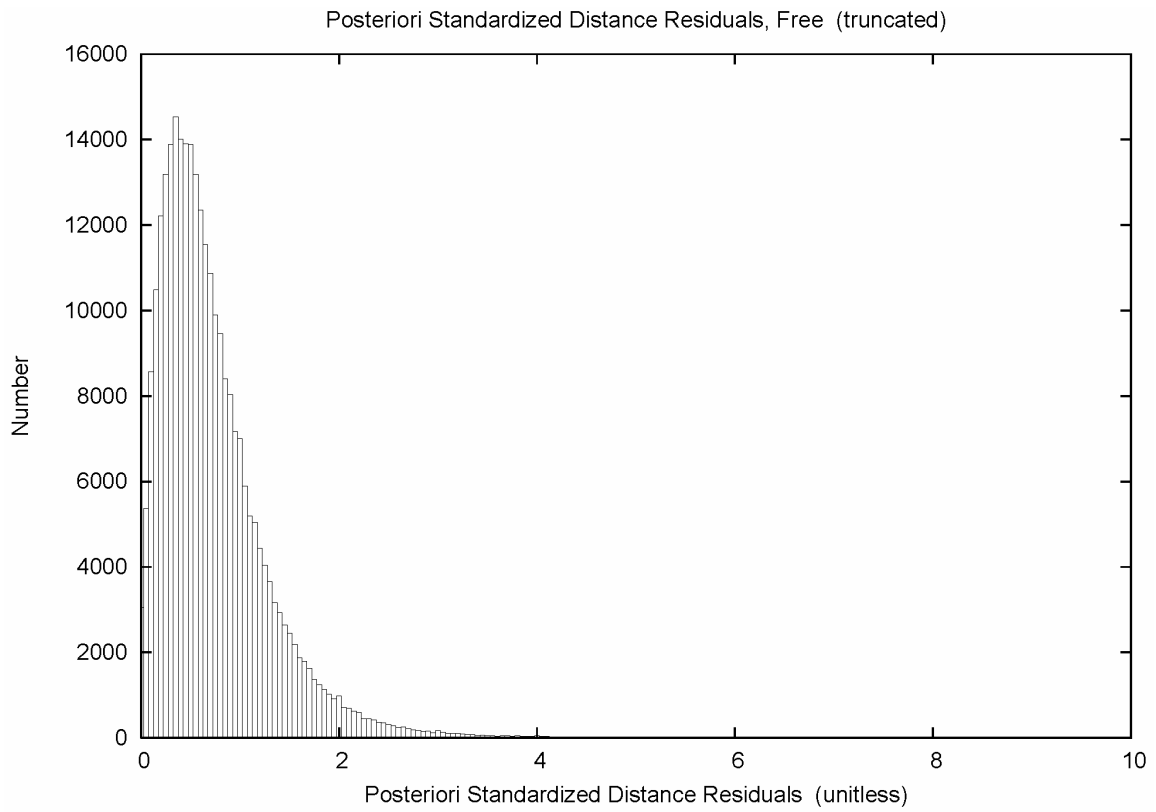
Figure 10.2. Standardized distance residuals, free adjustment, detail.
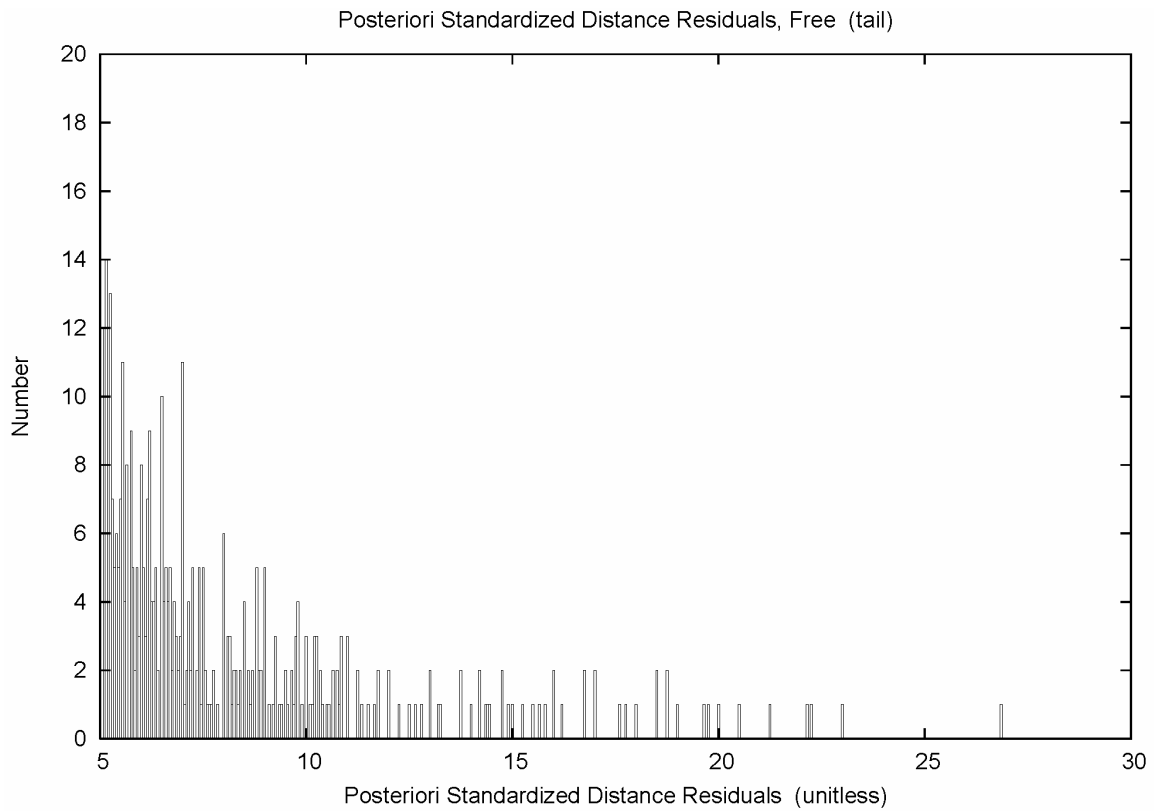

Figure 10.3. Standardized distance residuals, free adjustment, distribution tail.

Table 10.1 collects the percentiles of the distributions displayed in Sections 7, 9 and 10. It is seen that the standardized residuals are remarkably small. This tends to suggest that the presence of sizable residuals caused the project weight scaling procedures to assign larger standard deviation factors to all observations in troublesome projects. This in turn, would tend to underestimate sets of standardized residuals.

Table 10.1 – Percentiles of Distance Residual Statistics, Free Adjustment

Percentile	Residual (cm)	Std. Dev. (cm)	Standardized (unitless)
50%	0.50	0.82	0.5667
68%	0.75	1.13	0.7826
90%	1.50	2.22	1.2234
95%	2.02	3.17	1.4154
99%	3.44	10.31	1.6546
99.9%	4.88	50.05	1.7273

11. Height residual errors of the GPS vectors

Figure 11.1 shows the histogram distribution of the vertical (height) component of the residuals from the free adjustment with a bin width of 1 mm. The residuals range from -24.66 to 42.01 cm, as depicted in the figure. The sharp cutoffs at +/-5 cm are due to the semiautomated rejection process (Pursell *et al*. 2008).
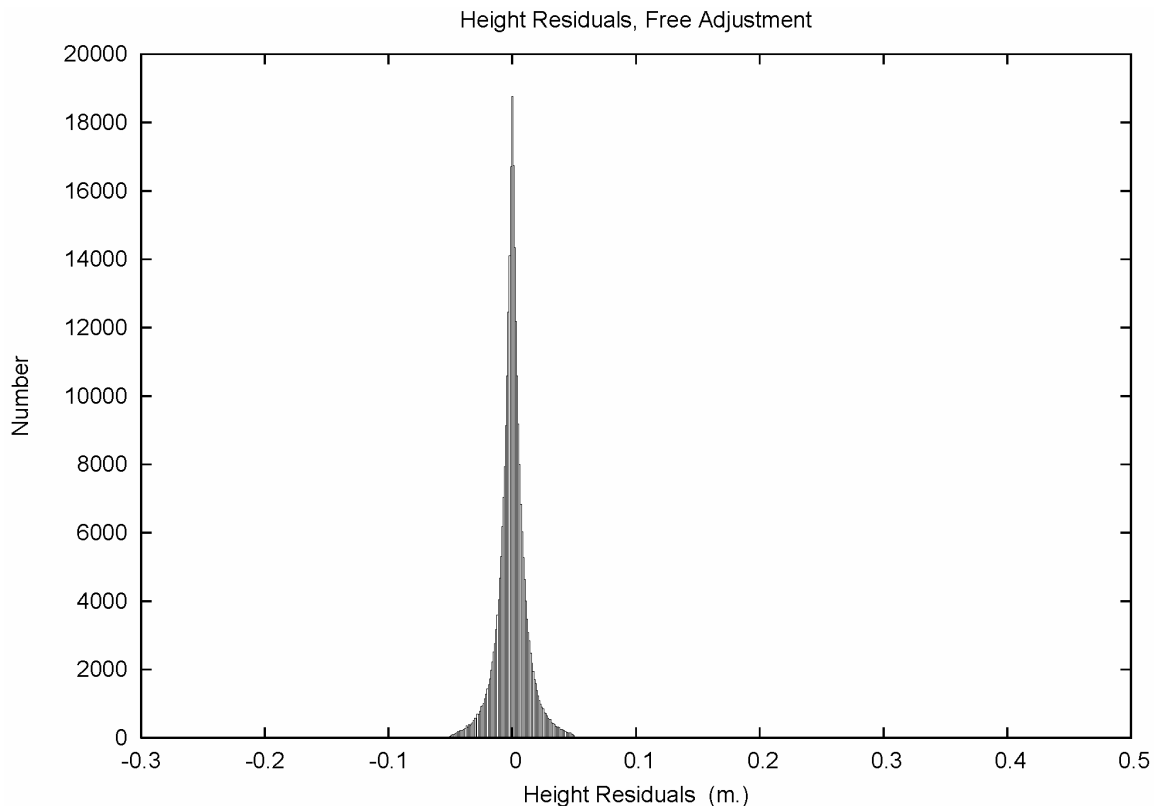

Figure 11.1. Height residuals, free adjustment.

Figure 11.2 plots the detail of the height residual distribution. What is immediately noticeable is that the residuals do not follow a Gaussian normal distribution. This emphasizes the discussion in Section 7. Residuals come from numerous parent populations that whose individual dispersions vary with measurement accuracy and network redundancy. By pooling the residuals, one obtains a distribution that is heteroscedastic. As such, the residuals show high kurtosis, with a sharp peak and long flat tails. The distance residuals of Figures 7.1 and 7.2 were similarly kurtotic, but were not recognized as such due to having a parent Rayleigh distribution.
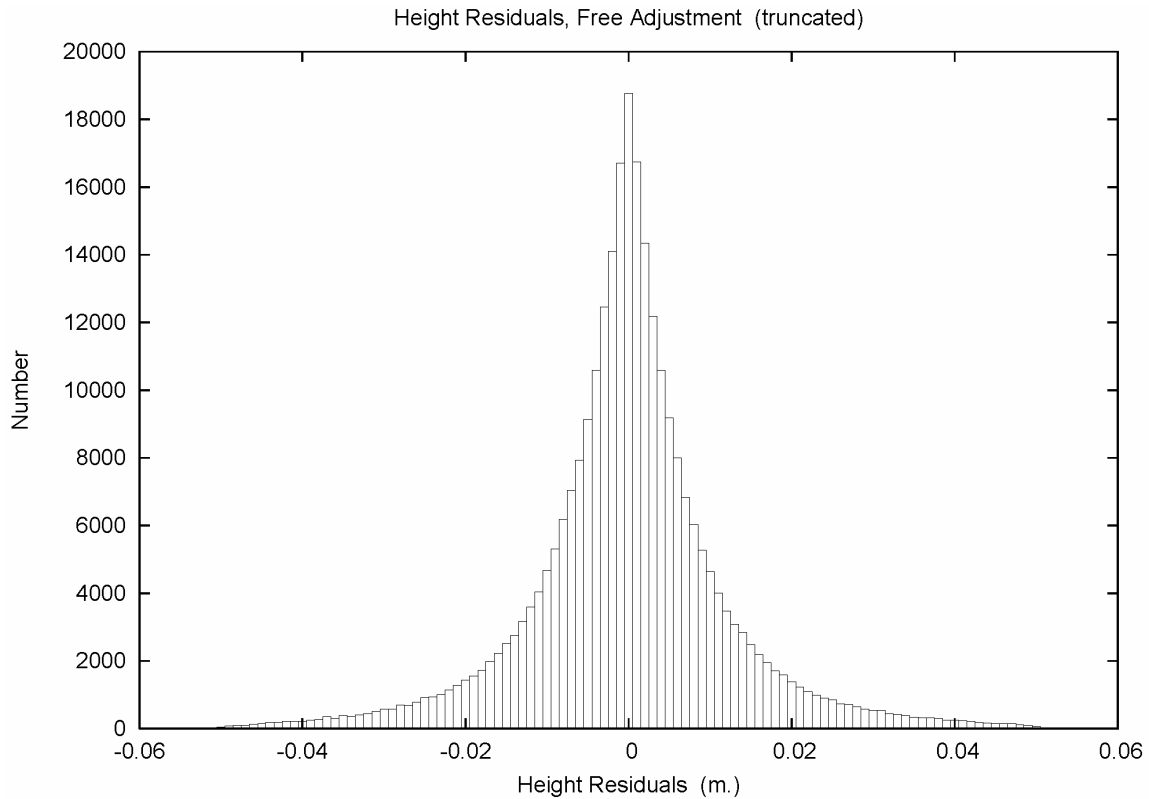

Figure 11.2. Height residuals, free adjustment, detail.

Figures 11.3 and 11.4 display the right and left tails, respectively, of the height residual distribution. It is seen that some residuals were retained, even when they had large magnitudes.
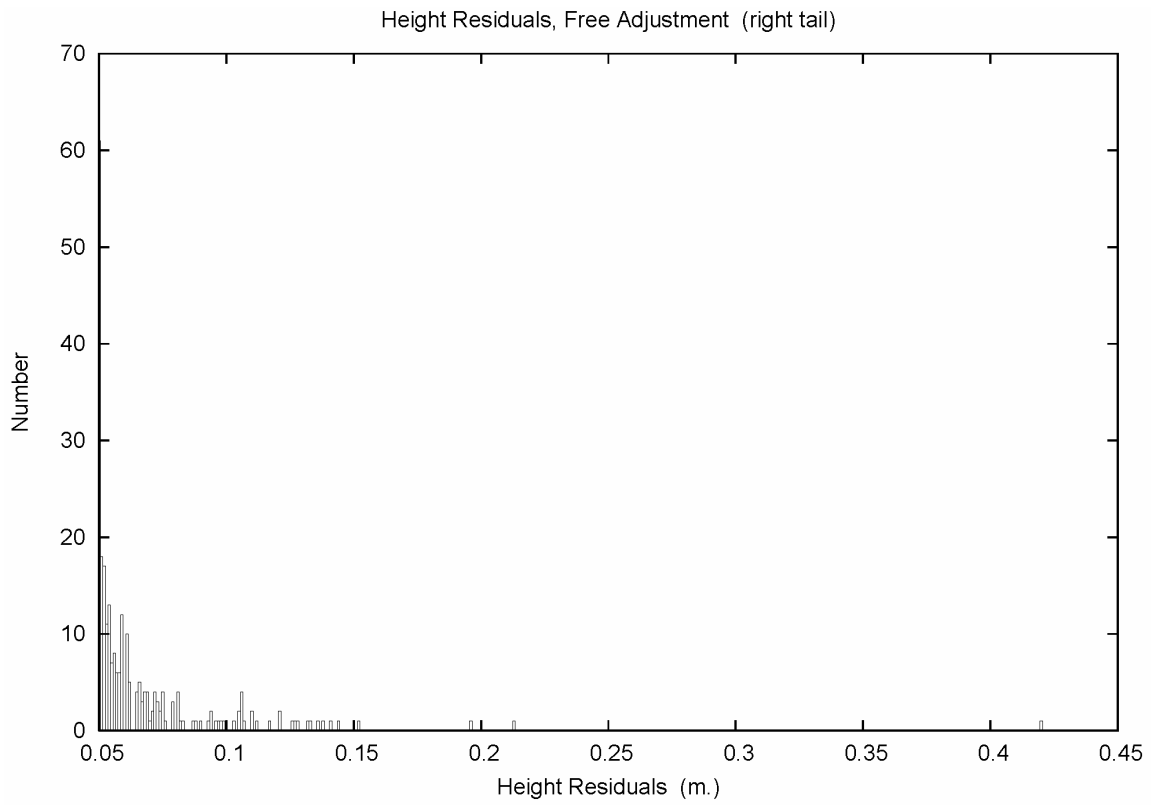
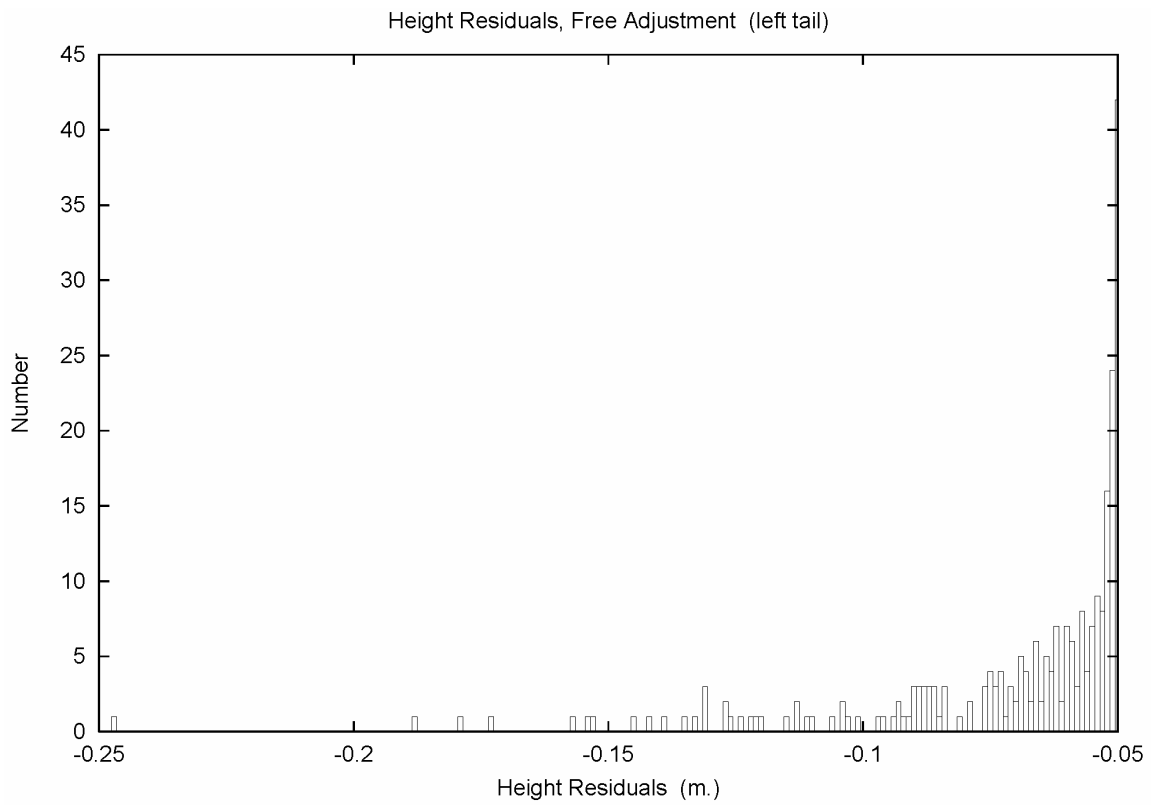Figure 11.3. Height residuals, free adjustment, right tail.

Figure 11.4. Height residuals, free adjustment, left tail.

12. Posteriori standard deviations of vertical residuals

Inspection of the leptokurtotic height residual distribution of Figures 11.1 and 11.2 reinforces the need to consider standardization by the standard deviations of the height residuals. As described in Section 9, they have been scaled by the *a posteriori* standard deviation of unit weight of the free adjustment of the NSRS, 1.276619.

Figure 12.1 plots a histogram distribution of the *a posteriori* standard deviations of the vertical (height) component of the residuals from the free adjustment. The standard deviations range from 0 to 13.551 m. The left part of the figure is detailed in Figure 12.2 with a bin width of 0.1 mm.
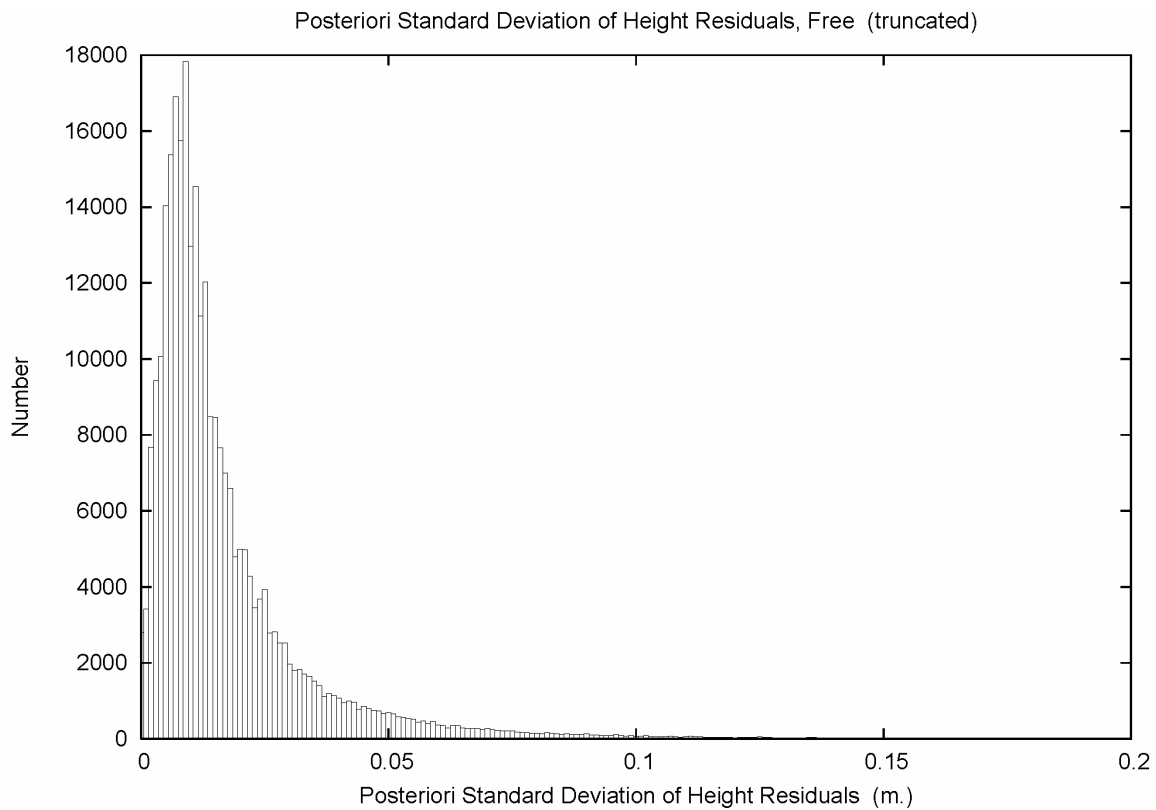

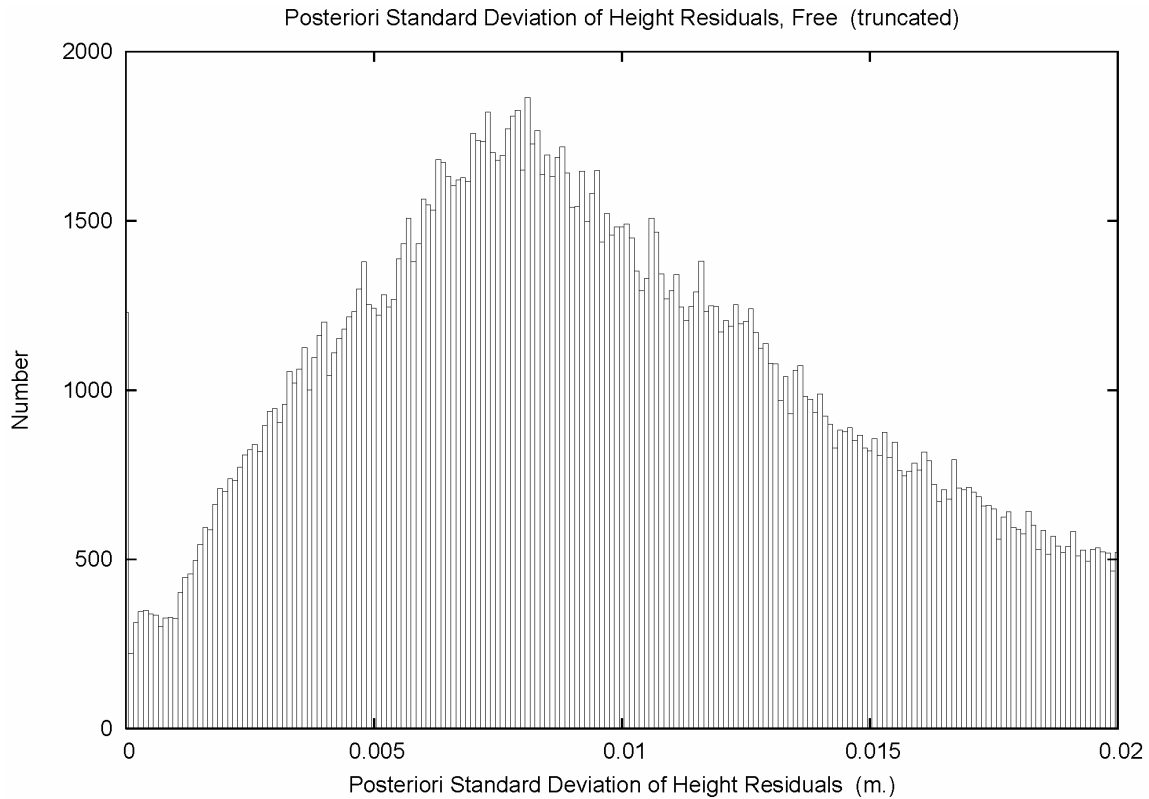Figure 12.1. Standard deviation of height residuals, free adjustment.

Figure 12.2. Standard deviation of height residuals, free adjustment, detail.

The figures show a somewhat broader distribution of the standard deviations of the height residuals when compared to the distance residuals. Even so, there are marked similarities in the horizontal and vertical residual standard deviation plots.

13. Posteriori standardized vertical residuals

The height residuals are standardized using *a posteriori* standard deviations, and, thus, are *a posteriori* standardized height residuals. Standardized height residuals can be expected to follow a Gaussian distribution. Figure 13.1 plots the histogram of the *a posteriori* standardized height residuals from the free adjustment. The standardized residuals (unitless) range from -53.137 to 24.226.

Figure 13.2 displays a detail view of the central portion of Figure 13.1. This serves to emphasize the distribution of the standardized height residuals. While the distribution seems less kurtotic than that of the height residuals (Figure 13.1), it is not Gaussian. We may infer that the project reweighting procedures (Pursell *et al*. 2008) were not a complete remedy for the problem of GPS survey weight calibration.
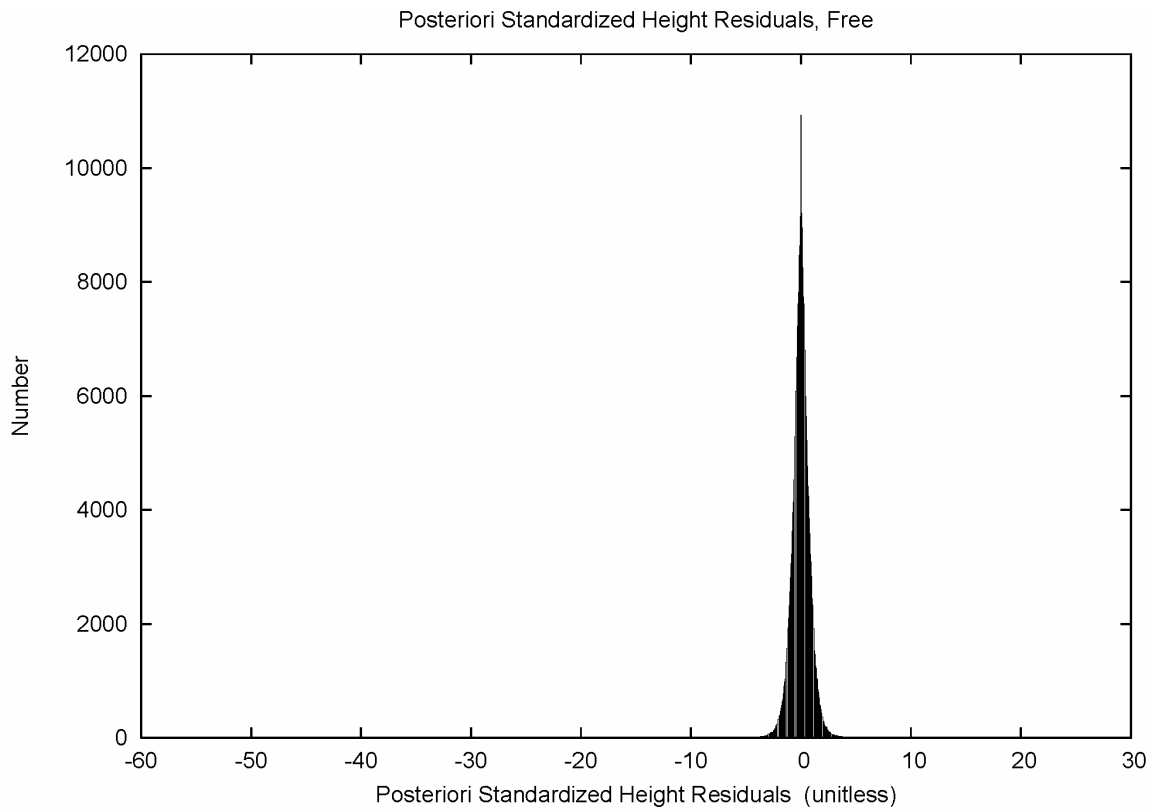
Figure 13.1. Standardized height residuals, free adjustment.
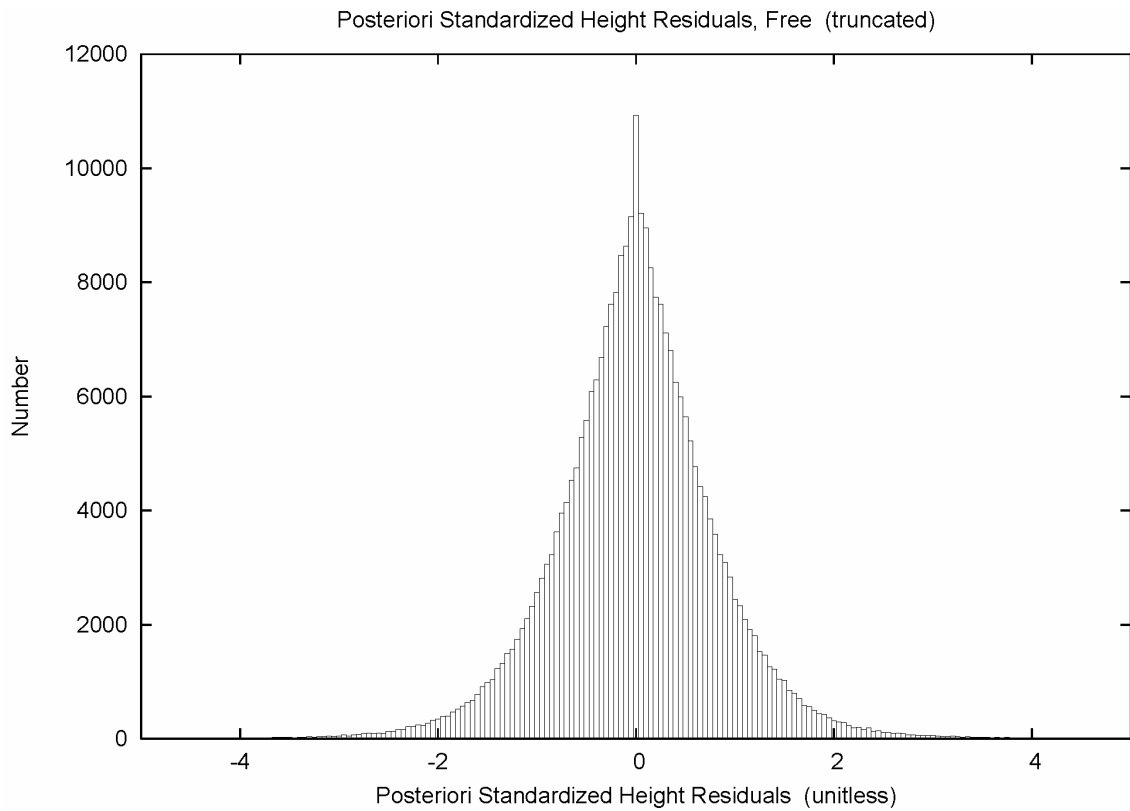

Figure 13.2. Standardized height residuals, free adjustment, detail.

Outlying residuals in the right and left tails of the distribution are plotted in Figures 13.3 and 13.4 respectively. These are residuals that should be considered for rejection. (Refer to allsresfrnor.txt in the Electronic Support Material.)

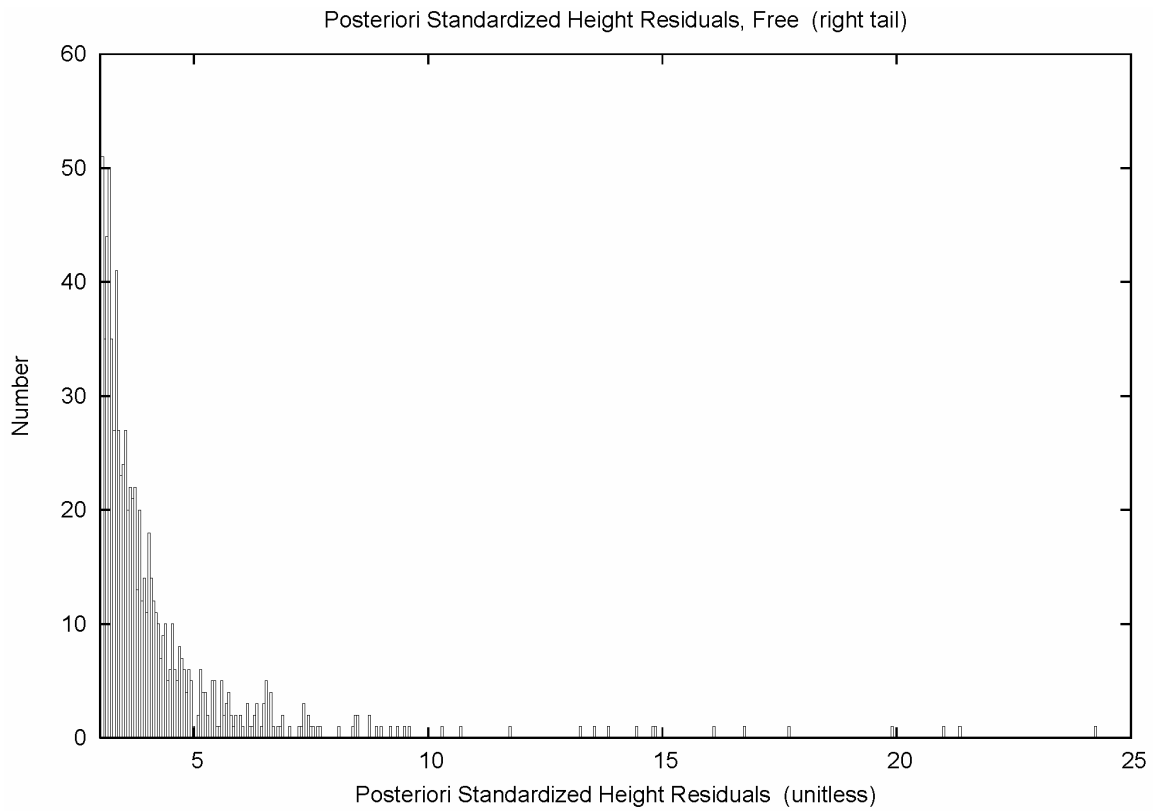Posteriori Standardized Height Residuals, Free (right tail)

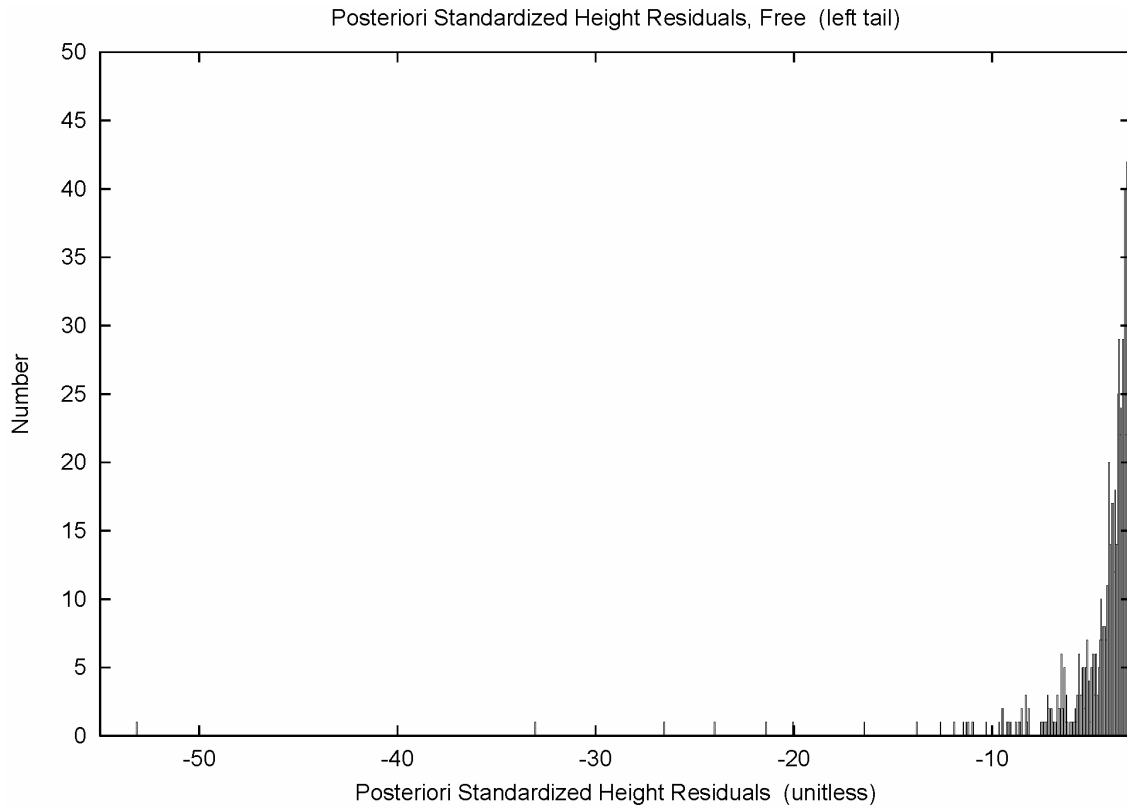Figure 13.3. Standardized height residuals, free adjustment, right tail.

Figure 13.4. Standardized height residuals, free adjustment, left tail.

Table 13.1 displays the percentiles of the distributions shown in Sections 11, 12 and 13. Note that the percentiles for height residual and standardized height residual are accumulated symmetrically about a zero mean.

It is seen that the standardized height residuals are larger in magnitude than the standardized distance residuals of Table 10.1. However, the standardized height residuals are still smaller than expected by a Gaussian distribution. This, as for the distance residuals, suggests that sizable residuals caused the project weight scaling procedures to assign over-large standard deviation factors that, in turn, underestimated the standardized residuals.

Table 13.1 – Percentiles of Height Residual Statistics, Free Adjustment

Percentile	Residual (cm)	Std. Dev. (cm)	Standardized (unitless)
50%	0.53	1.16	0.454
68%	0.90	1.70	0.709
90%	2.01	3.69	1.311
95%	2.73	5.36	1.657
99%	4.15	12.28	2.595
99.9%	5.46	51.88	4.749

14. Residual statistics from the fixed adjustment

In the interests of concision, only summary remarks will be made regarding the residuals from the fixed adjustment. Eighteen distribution figures were generated, however, and are provided in the Appendix. Tables 14.1 and 14.2 display percentiles for various fixed adjustment statistics for the distance and height residuals, respectively. In addition, one may refer to allsresfxnor.txt in the Electronic Support Material. All standardized statistics are scaled by the *a posteriori* standard deviation of unit weight of the fixed adjustment of the NSRS, 1.37549.

Table 14.1 – Percentiles of Distance Residual Statistics, Fixed Adjustment

Percentile	Residual (cm)	Std. Dev. (cm)	Standardized (unitless)
50%	0.52	0.88	0.5455
68%	0.79	1.22	0.7556
90%	1.56	2.40	1.1897
95%	2.09	3.42	1.3837
99%	3.53	11.10	1.6299
99.9%	4.99	53.69	1.7101
Extrema	36.57	1666.70	29.5000

Table 14.2 – Percentiles of Height Residual Statistics, Fixed Adjustment

Percentile	Residual (cm)	Std. Dev. (cm)	Standardized (unitless)
50%	0.54	1.25	0.432
68%	0.93	1.84	0.676
90%	2.06	3.98	1.259
95%	2.80	5.78	1.600
99%	4.25	13.22	2.511
99.9%	6.32	54.41	4.814
Extrema	-46.74 to 41.26	1460.04	-49.363 to 22.580

Little difference is seen between the free and fixed residual statistics. Inspection of the figures and tables do show a slight broadening of the distributions. As expected, one sees an increase in the standard deviations of the residuals. This behavior is due to a decrease in the standard deviation of the adjusted observations (as seen in Equation 7-1).

The fixed adjustment standardized residuals, both distance and height, show slight decreases when compared to the free adjustment. But, as described earlier, the height standardized residuals are smaller than what one would expect from a standard Gaussian distribution. It is believed that insufficient outlier rejection lead to large factors applied to project dispersions. This effect is intensified slightly in the fixed adjustment.

15. Pre-adjustment project standard deviations

At this point, the NSRS 2007 adjustment analysis shifts focus towards the predicted errors of the coordinates. Such predictions use formal methods of error propagation, and rely upon the validity of the assumed weights of the GPS vectors. For a variety of reasons, GPS reduction software is notorious for the optimistic weights assigned to vectors. For this reason (Pursell *et al*. 2008) NGS practice has been to scale the First Order (and lower order) GPS projects by the project *a posteriori* standard deviation of unit weight.

However, GPS physical models have known shortcomings that behave differently between horizontal and vertical. For example, carrier phase error is treated as uncorrelated. However, phase multipath shows distinct time correlation and its magnitude is also correlated with vertical angle to the satellite. Tropospheric models are neglected, or generally rely on self-calibration under an assumption of azimuthal symmetry. Recovery of troposphere becomes problematic at short time scales. And, multipath error, correlated with vertical angle, maps into a self-calibrating tropospheric model. All of these issues can cause systematic, common mode errors that mask as receiver clock error and become mapped into the vertical component.

In an unprecedented effort, distinct horizontal and vertical component standard deviation scale factors were computed for all orders of GPS projects. This component scaling was critical in supporting the FGDC accuracy standards, which require valid weight estimates in both horizontal and vertical. At the direction of the author, component scaling was performed for 3314 non-trashed projects. The method involved accumulation of the weighted variance sums, $v^t \mathbf{D}_o^{-1} v$, in both the horizontal and vertical components, on a project-by-project basis. The vertical degrees of freedom, *df*, was simply the number of unrejected GPS vectors. And the horizontal *df* was twice the vertical *df*. This allowed computation of pre-adjustment project variances and standard deviation scaling factors for both the horizontal and vertical. Figure 15.1 shows the histogram of the project horizontal standard deviation factors with a bin width of 0.01. (Refer to proid3.txt in the Electronic Support Material.) The maximum horizontal factor was 51.48. Figure 15.2 shows the histogram of the project vertical standard deviation factors with a bin width of 0.05. The maximum vertical factor was 43.44.
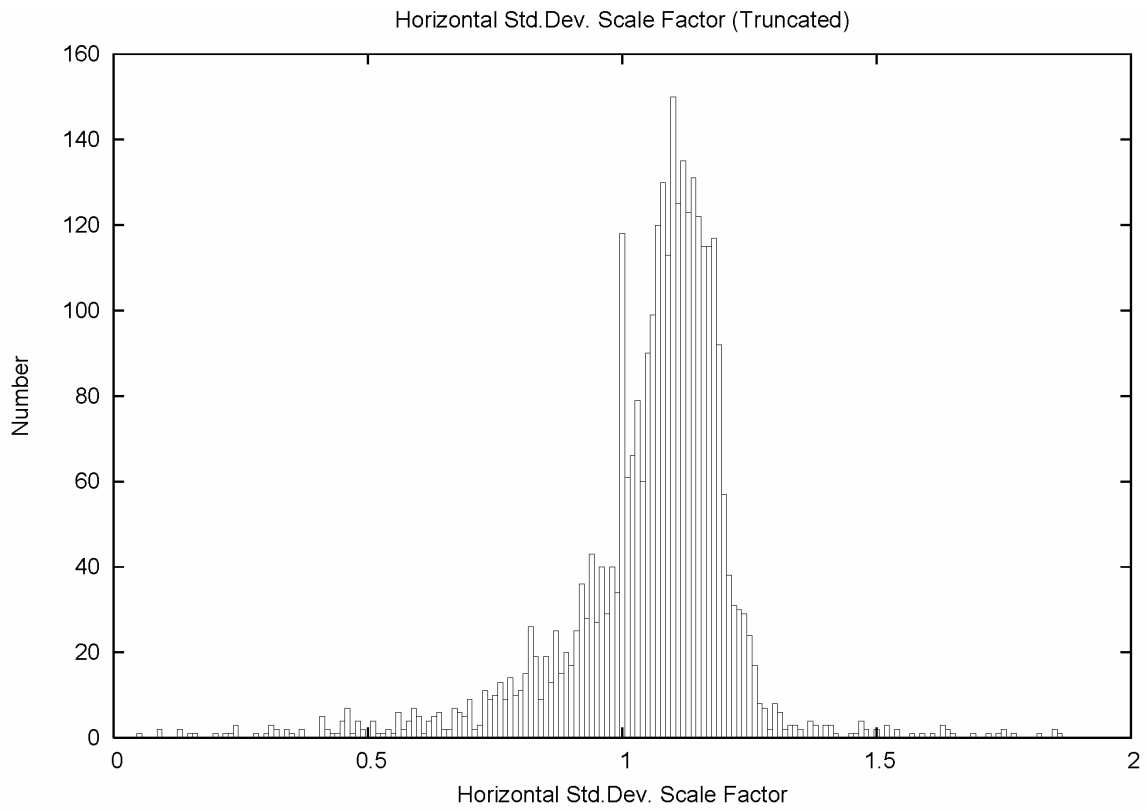
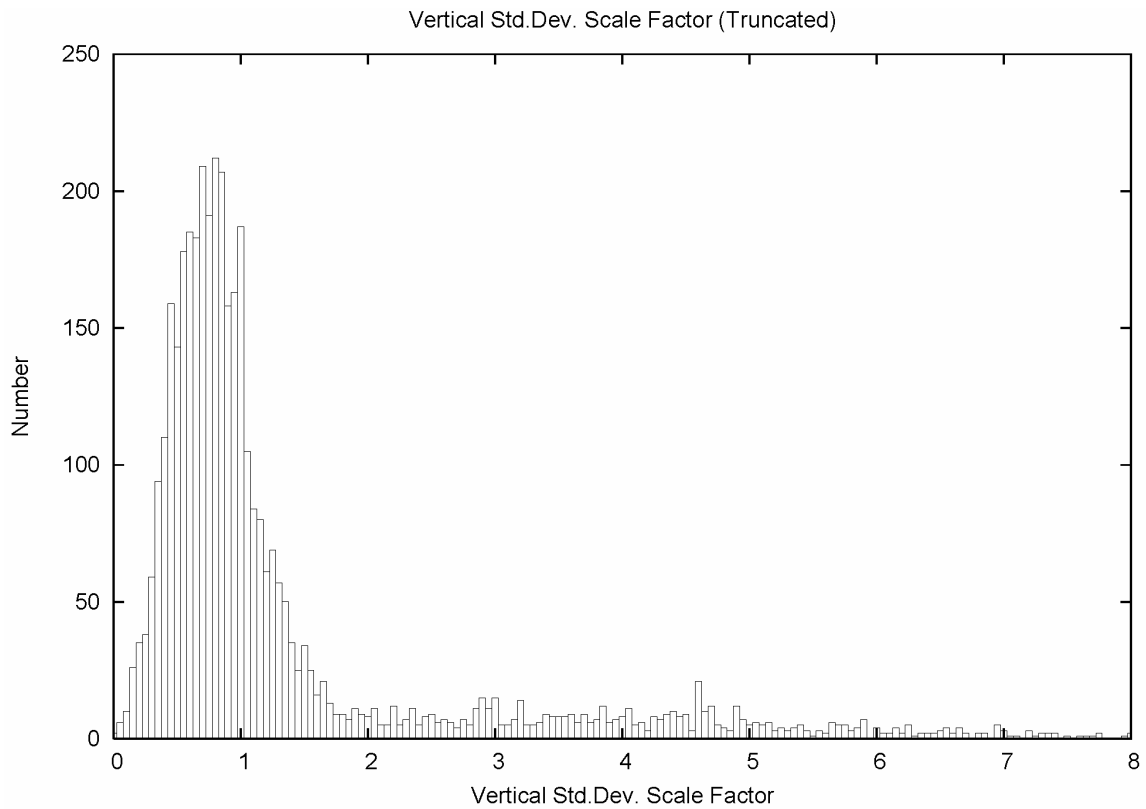Figure 15.1. Pre-adjustment project standard deviation factors, horizontal.

Figure 15.2. Pre-adjustment project standard deviation factors, vertical.

Interpretation of Figures 15.1 and 15.2 relies on the fact that most surveys in the NSRS 2007 adjustment had already been scaled by their respective project standard deviations of unit weight. One would naturally expect the horizontal and vertical factors to be 1.0. The spike at the 1.0 bin in Figure 15.1 shows that for some projects no significant change occurred between the scaling by the project standard deviation of unit weight and the subsequent horizontal standard deviation factor estimation. Thirty eight of the projects have a 1.0 factor for both horizontal and vertical. In general, though, Figure 15.1 shows a median value of 1.12. That is, the horizontal weights obtained from simple project scaling were too optimistic. Figure 15.2 shows the reverse case, with a median value of 0.87. Here, the vertical weights from simple project scaling were too pessimistic.

Ratios of horizontal/vertical standard deviation scale factors were computed and are presented in Figure 15.3 with a bin width of 0.05. The maximum ratio was 159.0. It is seen that the median value is 1.50. In other words, the horizontal standard deviations from simple project scaling were too optimistic relative to the vertical standard deviations by 50%. This result validates the effort by NGS personnel, by Mrs. Jane Hobson in particular, in the pre-adjustment weight rescaling.
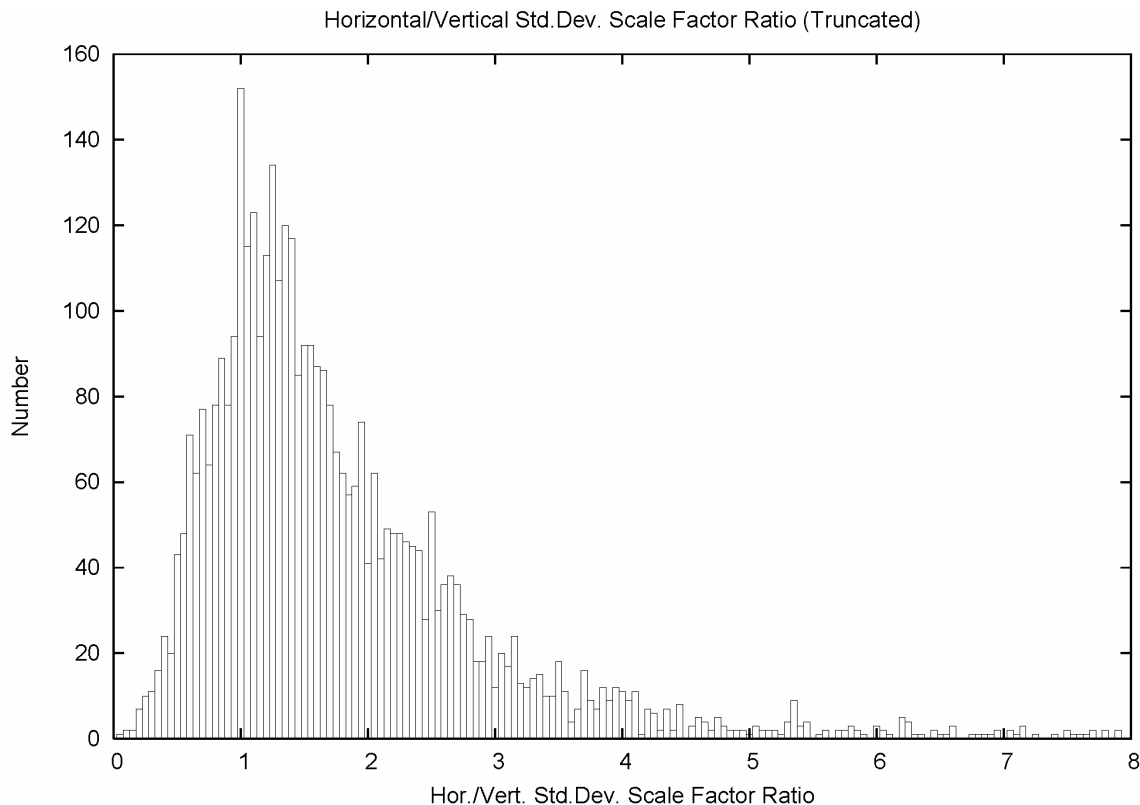

Figure 15.3. Pre-adjustment project standard deviation factor ratios, horizontal/vertical.

It must be cautioned that the horizontal and vertical component standard deviation scale factors were, in some cases, computed for projects with very few degrees of freedom (*e.g.* only two GPS vectors to establish a single new point). This will cause

considerable scatter in the standard deviation factor estimates. The remedy would be to pool the statistics from projects that have a similar character prior to computation of the factors.

Also, it is imperative that outliers be cleared from projects prior to performing standard deviation factor estimation. Just as outliers will grossly inflate a variance of unit weight, they will inflate these factors. The small standardized residuals seen in Tables 13.1 and 14.2 are likely being caused by inflated standard deviations of the residuals. The inflation occurred through these factors. One should note the long tails on the right of Figures 15.1 and 15.2, and recall that the maximum horizontal and vertical standard deviation factors were 51.48 and 43.44, respectively. It might be appropriate to establish suitable ranges for GPS weights and review the project factor estimation to insure it remains within certain limits.

Finally, these project standard deviation factors should be updated as an inherent part of any outlier rejection or data deweighting process. While it is certainly helpful to the adjustment to reject an outlier that caused a very large standard deviation factor to be issued, those project standard deviations won't be correctly included in the adjustment until the standard deviation factor is re-estimated. Unfortunately, the pre-adjustment factors were not updated after the NSRS 2007 free adjustment rejection process.

16. Posteriori position standard deviations

This section displays results for the *a posteriori* standard deviations of the coordinates from the fixed adjustment of the NSRS 2007. It must be emphasized that the numbers in this section are *not*, repeat, *not* network accuracies. Network accuracies will be reported in Section 20.

The standard deviations here have been scaled by the *a posteriori* standard deviation of unit weight of the NSRS, 1.37549. Figure 16.1 displays the histogram distribution of the latitude standard deviations with a 0.01 cm bin width. The maximum latitude standard deviation is 4.86 meters. The latitude standard deviations show remarkable precision, with a median of 0.44 cm. It is notable that these standard deviation statistics are in general agreement with the horizontal (distance) residual statistics reported in Section 7. This is to be expected given the extensive pre-adjustment weight scaling and use of *a posteriori* statistics. The details of the latitude standard deviations are shown in Figure 16.2. The spike in the zero bin of Figure 16.2 is predominantly comprised of the fixed CORS control points.
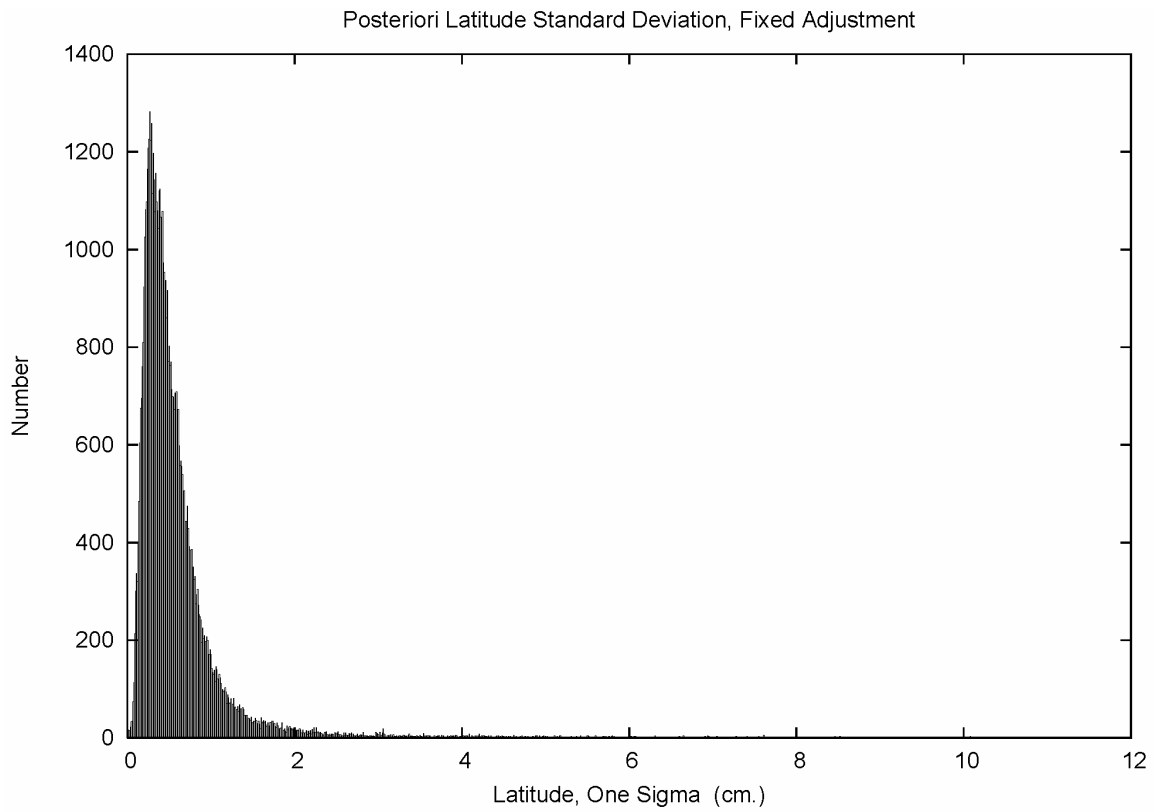
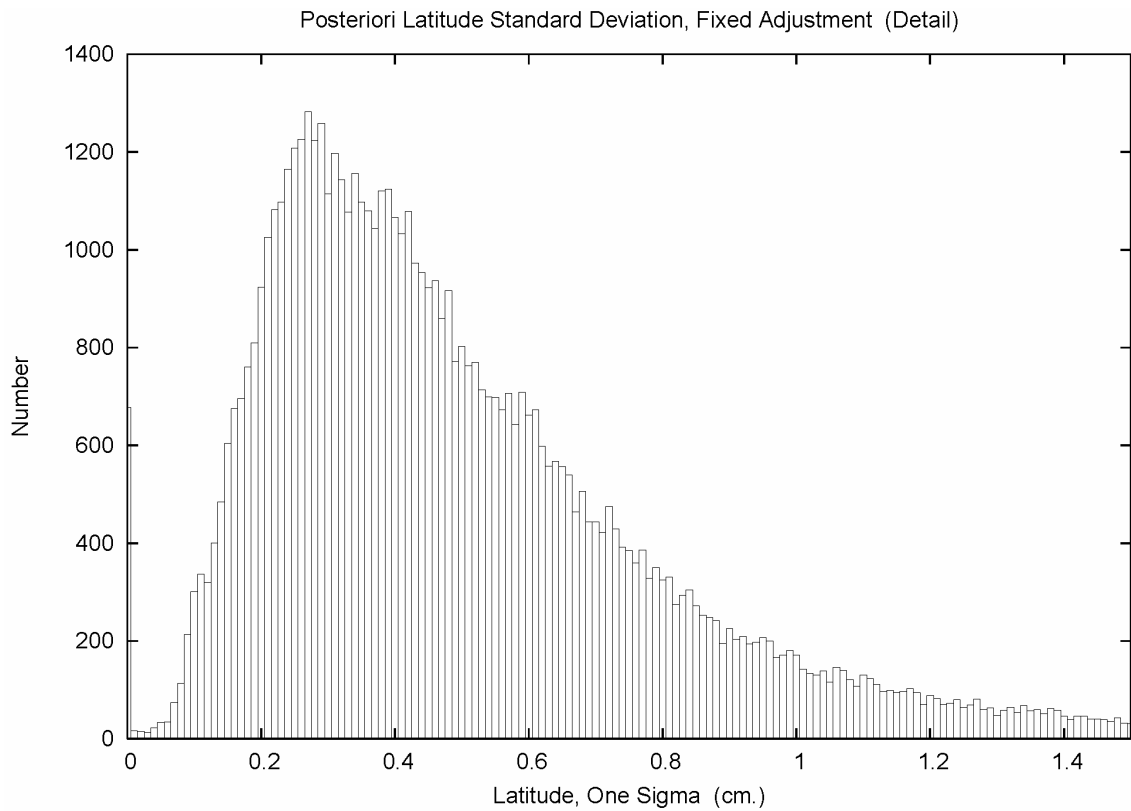Figure 16.1. Latitude standard deviation distribution. 0.01 cm bin size.

Figure 16.2. Latitude standard deviation distribution, detail. 0.01 cm bin size.

Figure 16.3 displays the histogram distribution of the longitude standard deviations with a 0.01 cm bin width. The maximum longitude standard deviation is 4.91 meters. The longitude standard deviations show a slightly smaller precision, with a median of 0.38 cm. The details of the longitude standard deviations are shown in Figure 16.4. The distributions are generally the same, with a slight broadening of latitude standard deviations in Figure 16.2 compared to 16.4.
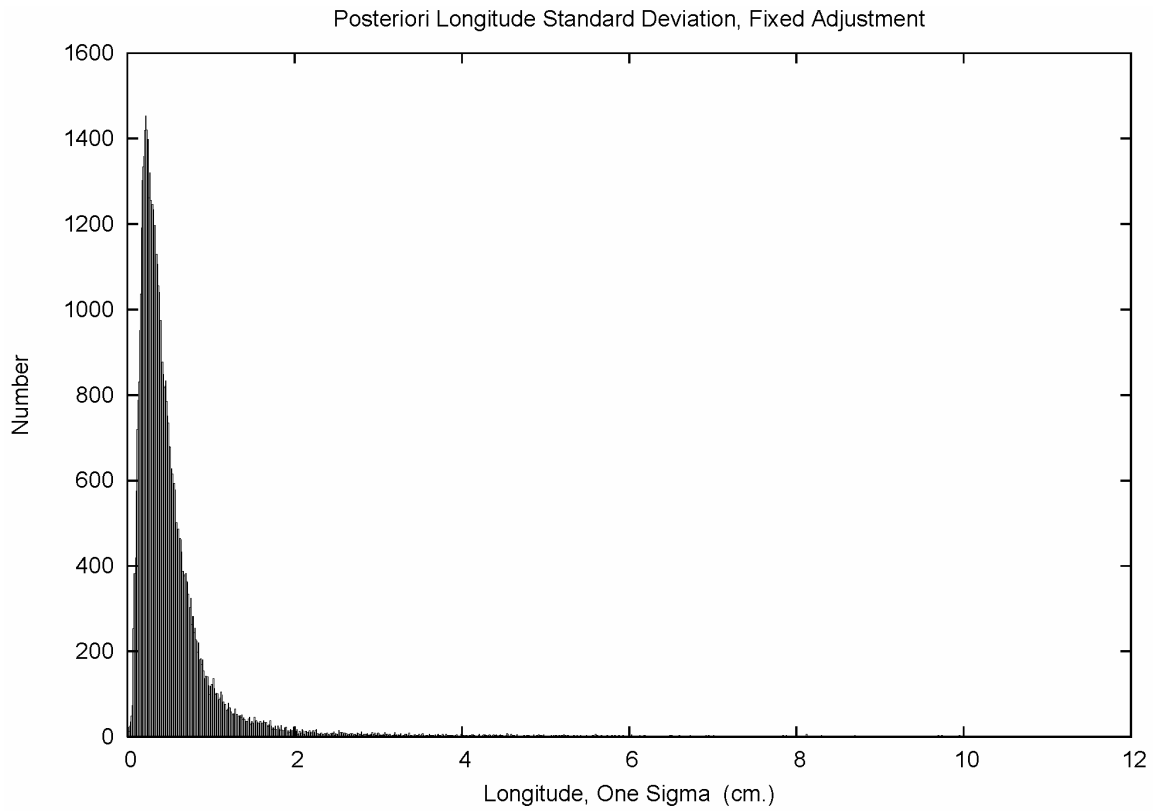

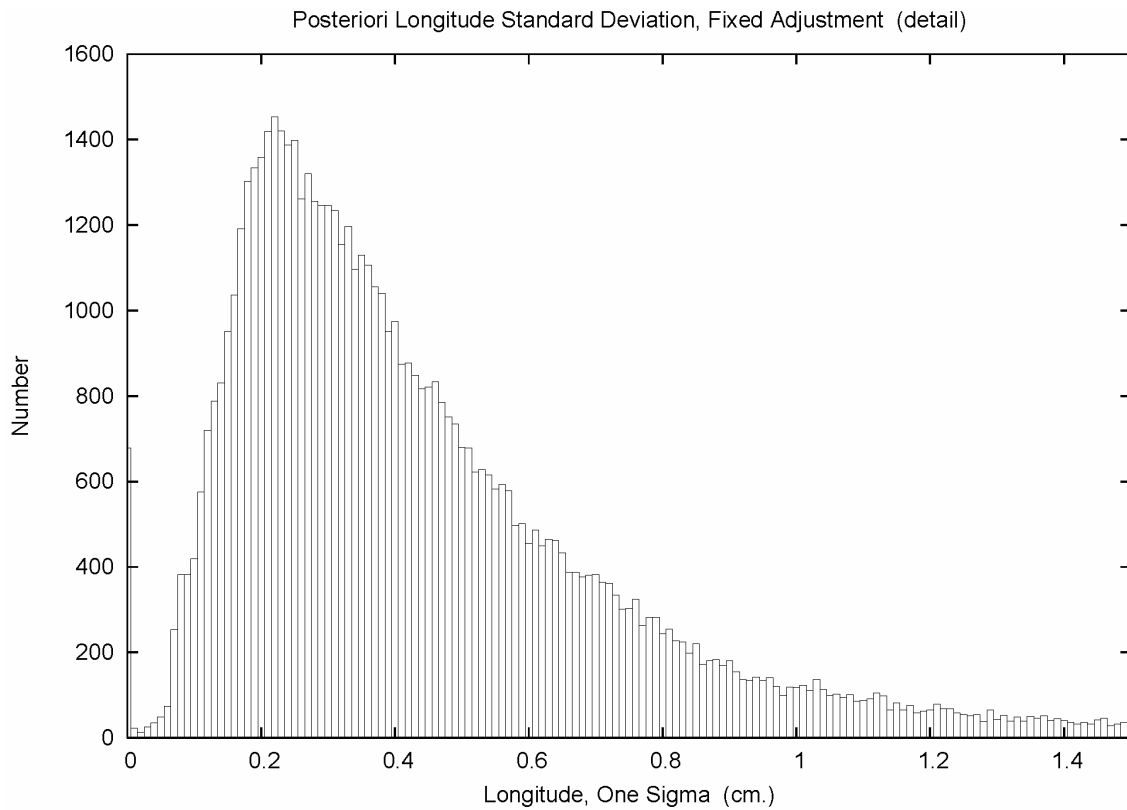Figure 16.3. Longitude standard deviation distribution. 0.01 cm bin size.

Figure 16.4. Longitude standard deviation distribution, detail. 0.01 cm bin size.

Figure 16.5 displays the histogram distribution of the height standard deviations with a 0.01 cm bin width. The maximum height standard deviation is 2.50 meters. The height standard deviations show a larger precision, with a median of 0.93 cm. This confirms behaviors often seen in geodetic analyses, where the height precision is double that of the horizontal. The details of the height standard deviations are shown in Figure 16.6.
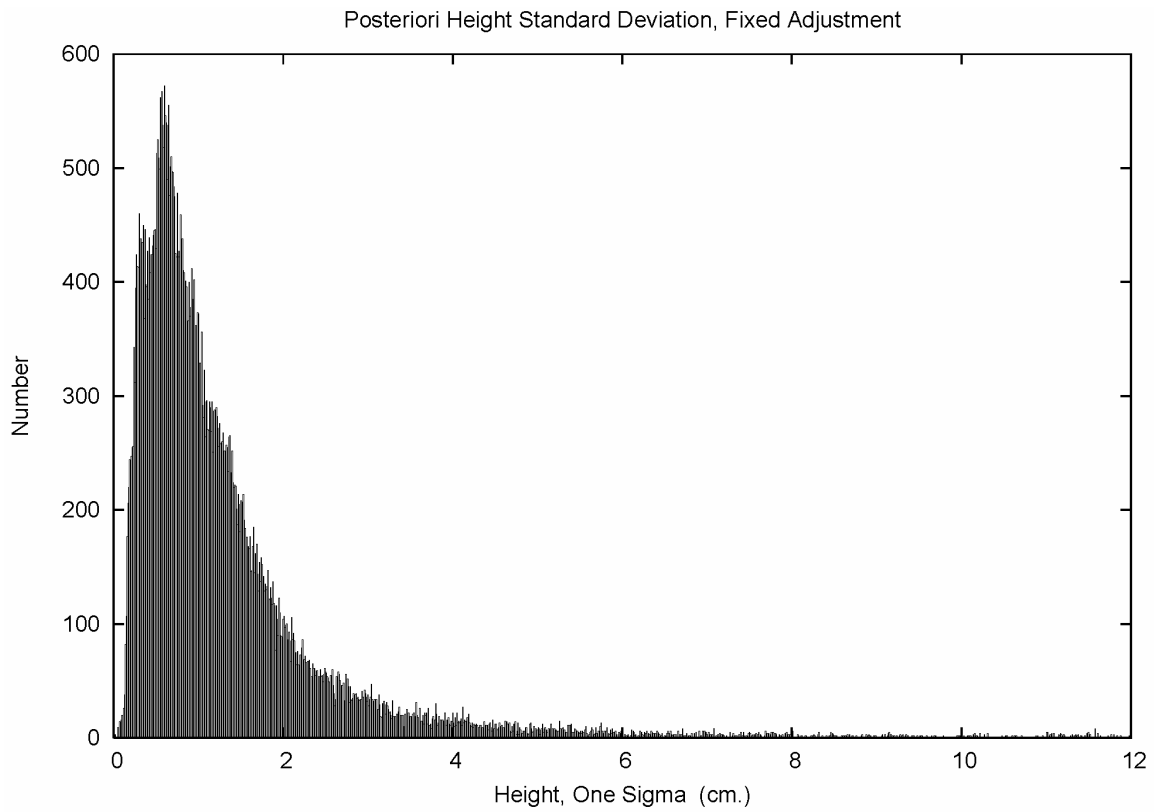
Figure 16.5. Height standard deviation distribution. 0.01 cm bin size.
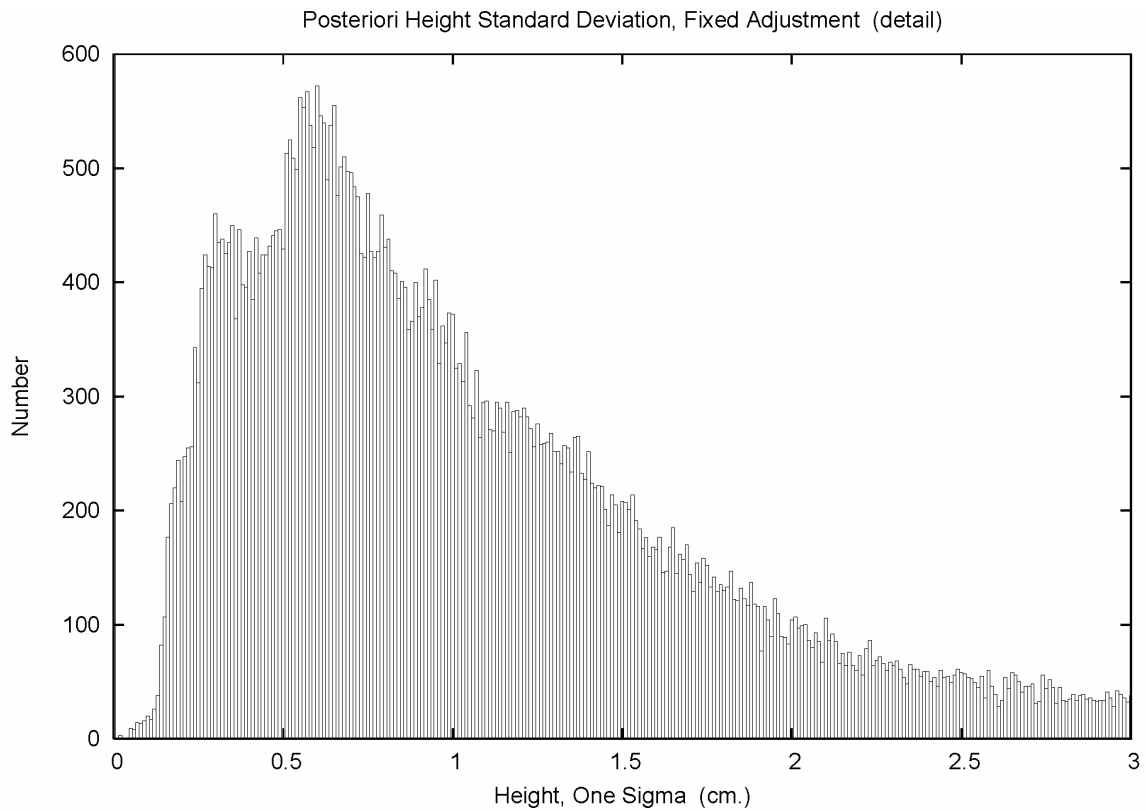

Figure 16.6. Height standard deviation distribution, detail. 0.01 cm bin size.

A very remarkable feature of the height standard deviations is that the distribution appears to be bimodal. That is, a secondary peak occurs in the distribution at about 0.3 cm. In general, positional standard deviations, as well as point error ellipses, are rather uniform (when compared to relative error statistics). So, it is surprising to see network structure in any of the coordinate standard deviation distributions. This feature is explored in Section 23.

In closing this section, the percentiles of the distributions are collected into Table 16.1. This emphasizes the marked similarities of latitude and longitude, and the larger magnitudes of the height dispersions. (Refer to allpos.txt in the Electronic Support Material.)

Table 16.1 – Percentiles of Posteriori Position Standard Deviations, Fixed Adjustment

Percentile	Latitude (cm)	Longitude (cm)	Height (cm)
50%	0.44	0.38	0.93
68%	0.60	0.52	1.34
90%	1.05	0.99	2.62
95%	1.51	1.49	3.86
99%	5.00	5.27	11.02
99.9%	31.97	37.00	32.74
Extrema	486.34	491.47	249.76

17. Posteriori position horizontal correlation

Despite the notable similarity in the distributions of the positional latitude and longitude standard deviations, questions naturally arise regarding the level of correlation of these components. Figure 17.1 plots the horizontal component correlations from the fixed adjustment with a 0.05 bin width.
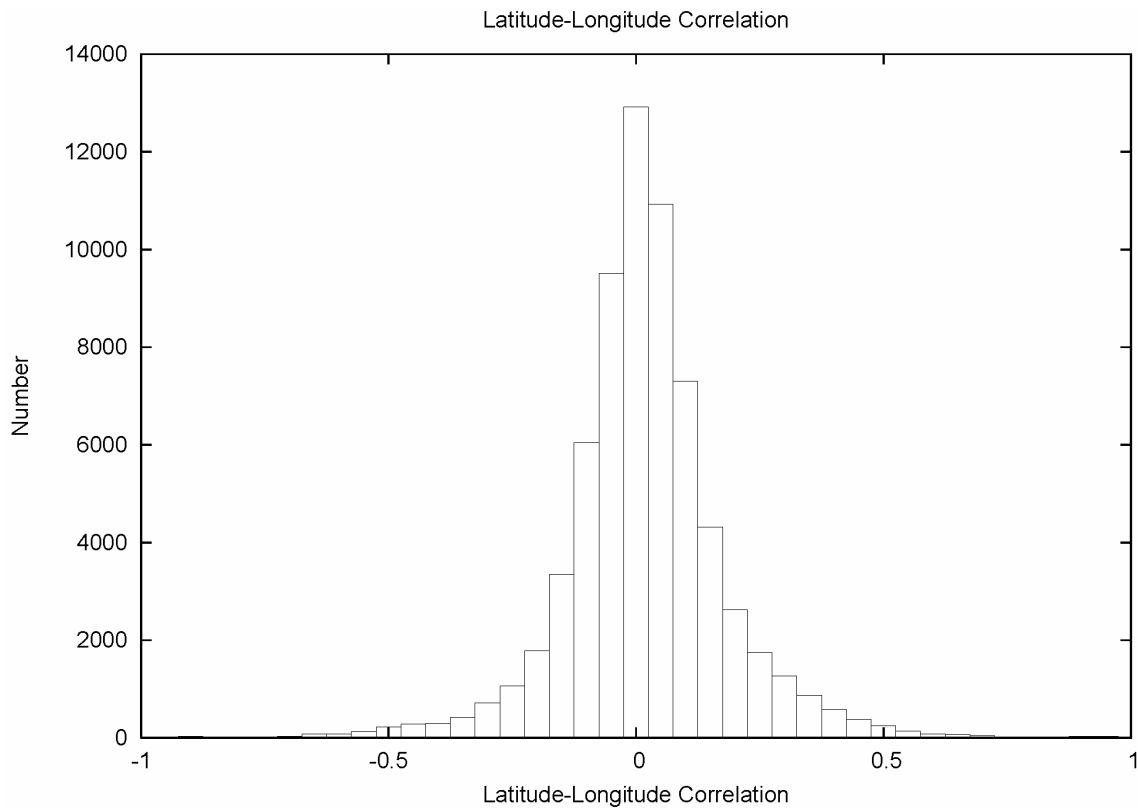
Figure 17.1. Latitude-longitude correlation, fixed adjustment. 0.05 bin size.

The general absence of correlation in Figure 17.1, coupled with the similar magnitudes of the standard deviations of latitude and longitude seen in Section 16, suggests that horizontal error ellipses would tend to be circular. Horizontal error ellipses were computed and the ratios of the semiminor/semimajor axes are histogrammed in Figure 17.2 with a bin width of 0.01. The ratio ranges from 0 to 1, where 1 indicates perfect circularity.
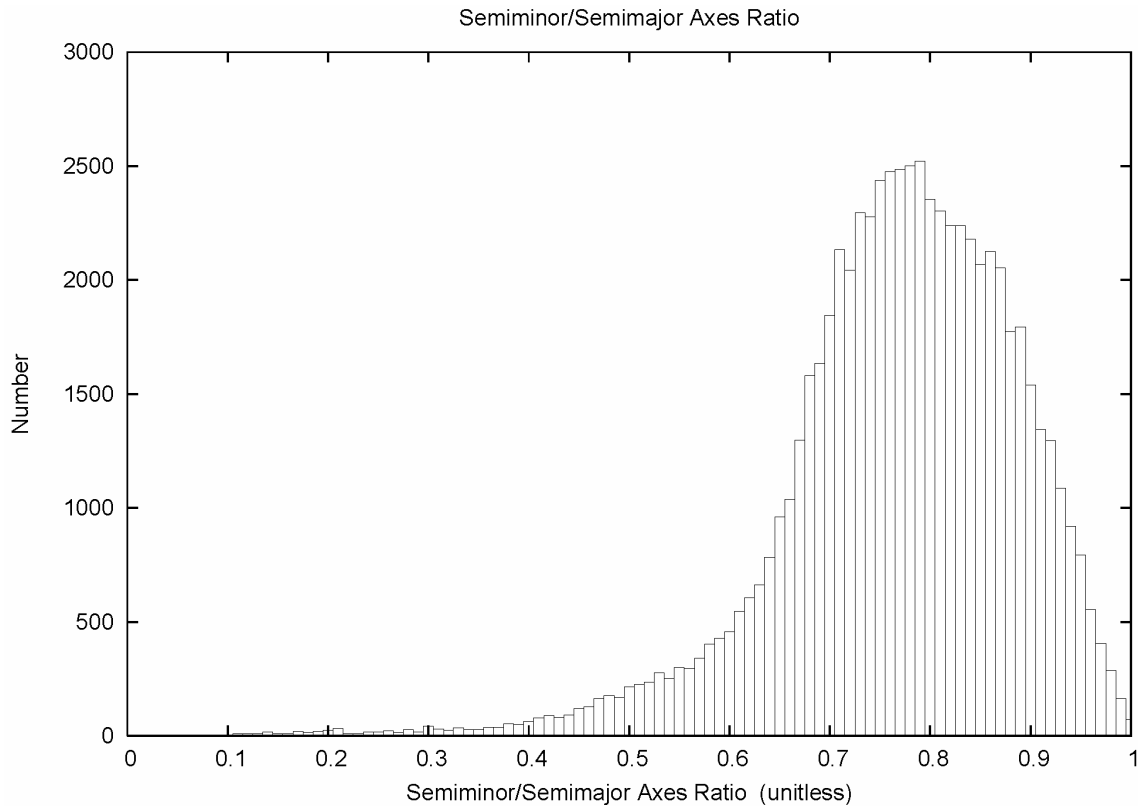
Figure 17.2. Ratio of semiminor/semimajor axes of horizontal error ellipse.

As seen in Figure 17.2, the semiminor axis is in the vicinity of 80% of the semimajor axis. While not perfectly circular, the point error ellipses are near circular. This result seems to validate the choice of a single number to represent horizontal network accuracy (FGDC 1998).

Since the horizontal error ellipses are not perfectly circular, the semimajor axis will possess an orientation. The distribution of the azimuth of the semimajor axis is plotted in Figure 17.3. The interesting result is that the distribution is not flat, the orientation is not random. The semimajor axis is aligned in a North-South direction. This can be explained by the inclination of the GPS satellites, about 55°. One may expect a general balance of GPS satellites to the East and West of a given mid-latitude point. However, there will tend to be a GPS "hole" in the sky coverage to the North. This average distribution of GPS satellites is reflected in the error ellipse orientation.
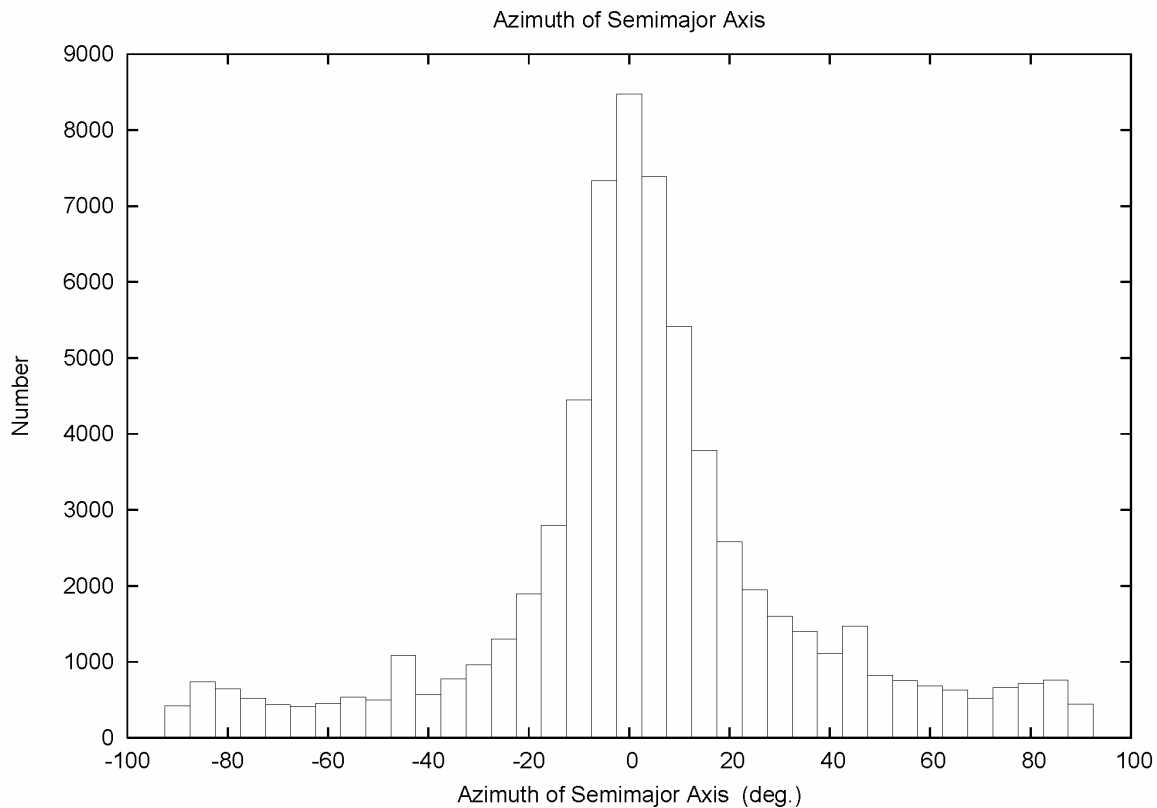
Figure 17.3. Azimuth of semimajor axis of horizontal error ellipse.

18. Posteriori position dispersion component ratios

To gain a slightly different view of the position error components, ratios are computed using the *a posteriori* standard deviations from the final free adjustment.

The ratio of height to latitude dispersion is plotted in Figure 18.1, with a detail view in Figure 18.2. The detail of the height to longitude dispersion is given in Figure 18.3. And, the detail of latitude to longitude dispersion is given in Figure 18.4. The percentiles of the dispersion ratios from the free adjustment are collected in Table 18.1.

Table 18.1 – Percentiles of Position Standard Deviation Ratios, Free Adjustment

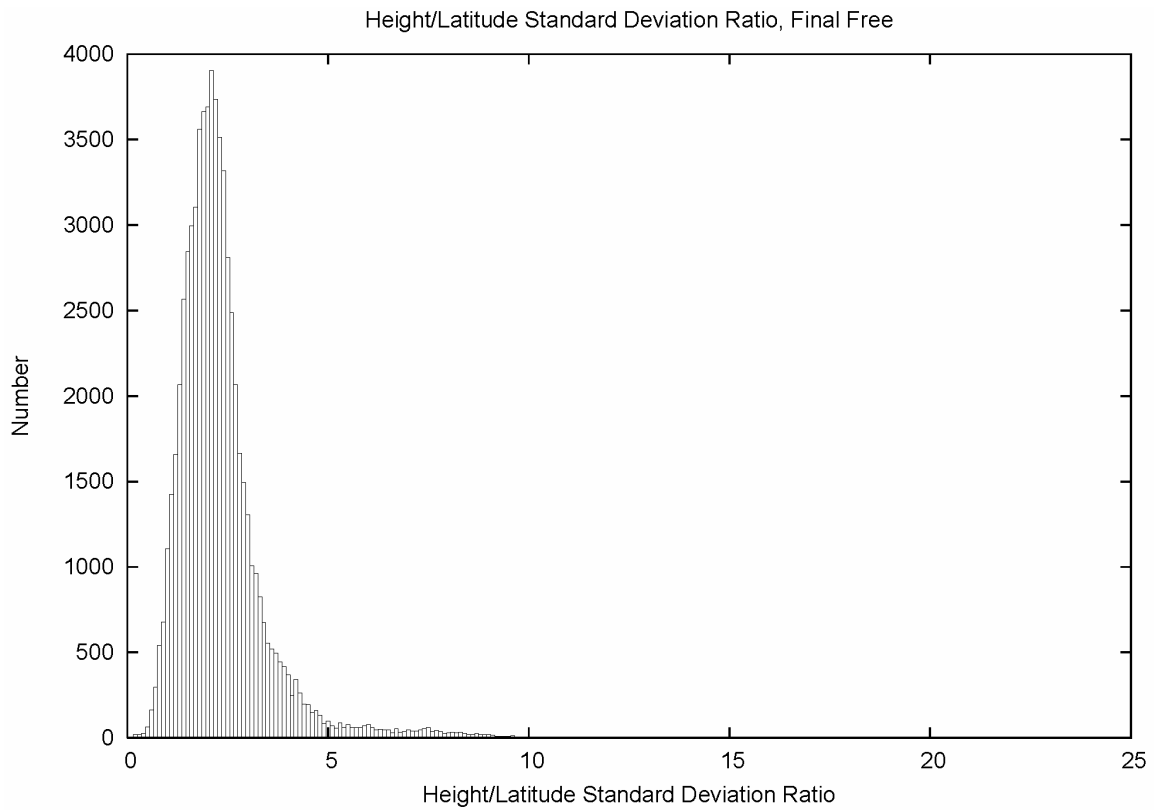| Percentile	Ht./Lat.	Ht./Lon.	Lat./Lon.
50%	2.13	2.42	1.17
68%	2.48	2.80	1.25
90%	3.46	3.79	1.40
95%	4.26	4.44	1.48
99%	7.65	6.27	1.78
99.9%	13.86	15.58	2.55

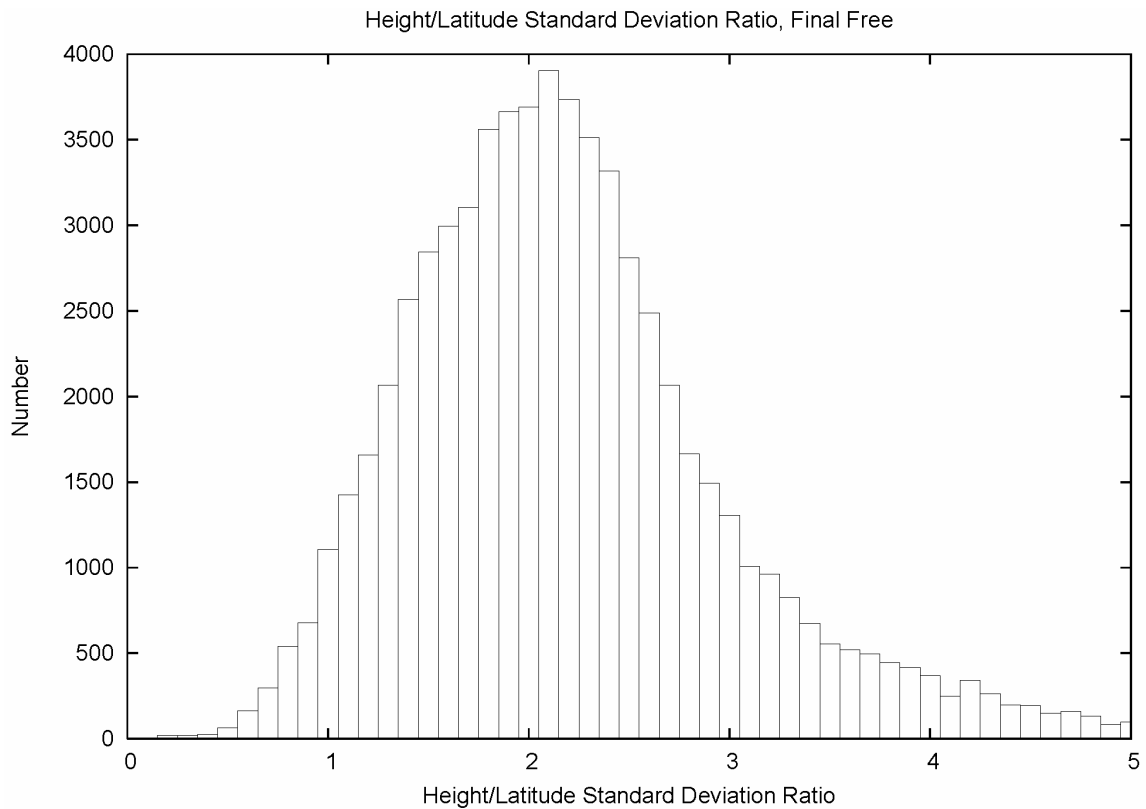Figure 18.1. Ratio of height/latitude standard deviations.

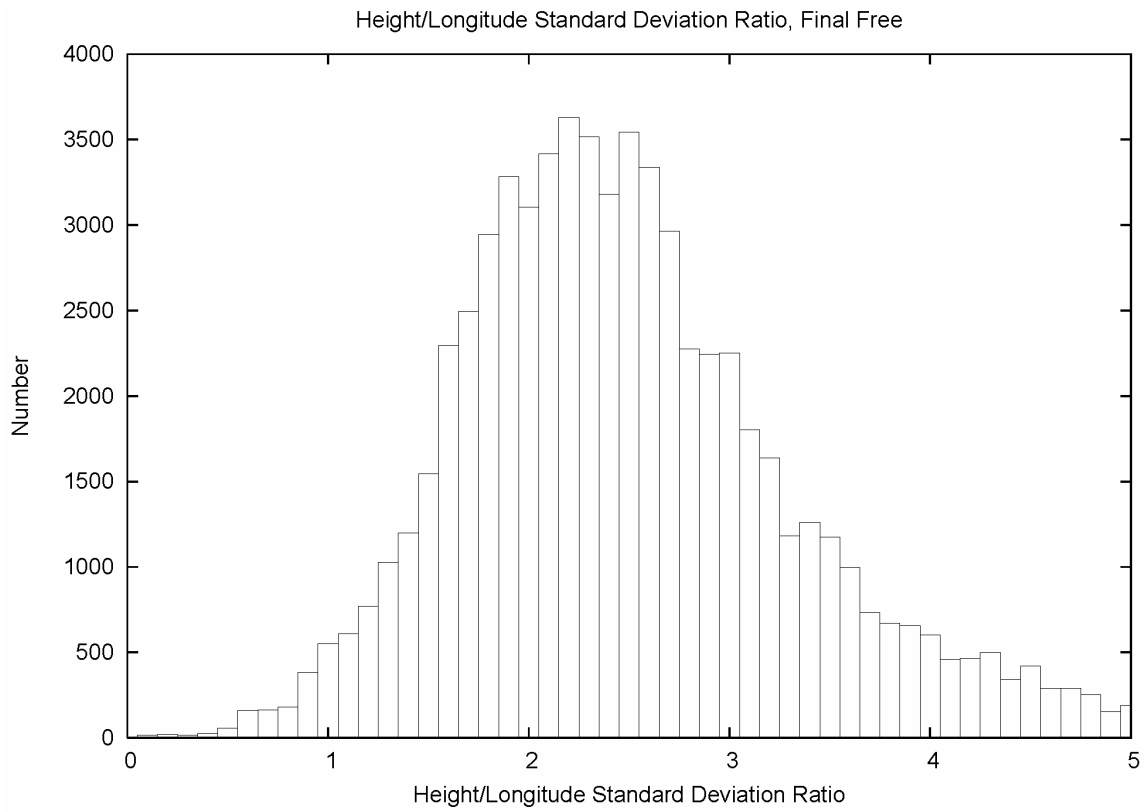Figure 18.2. Ratio of height/latitude standard deviations, detail.

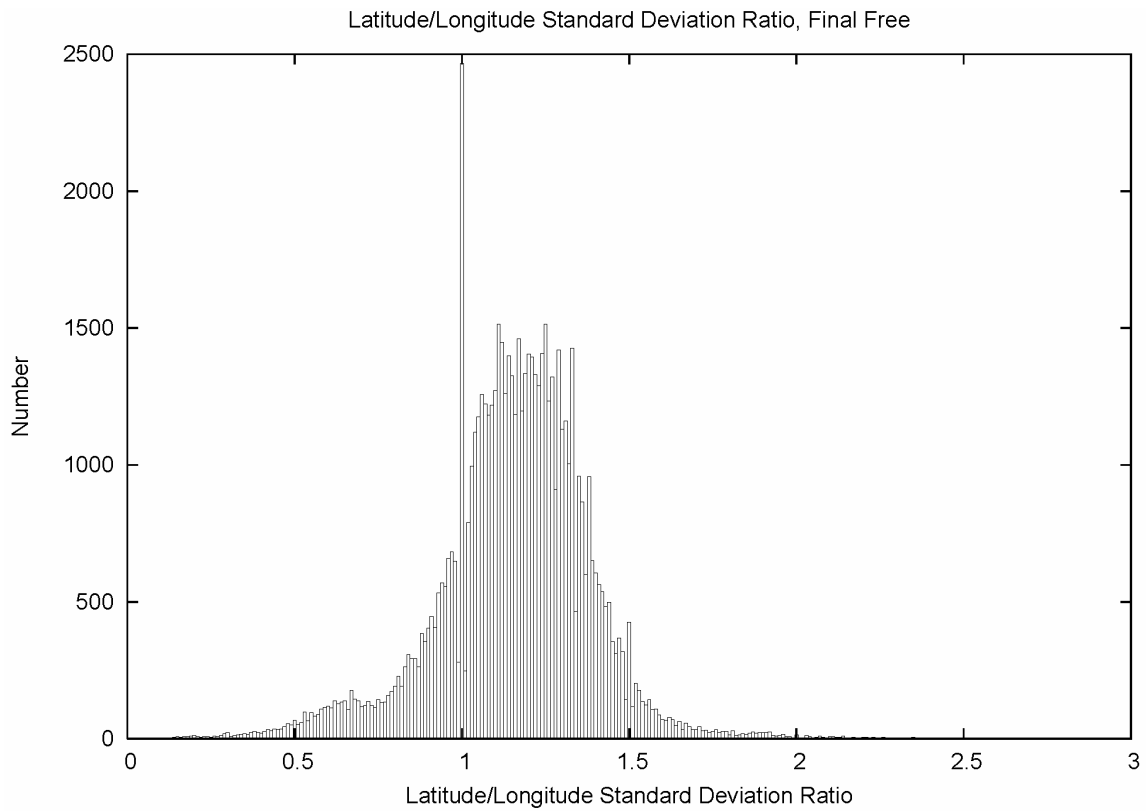Figure 18.3. Ratio of height/longitude standard deviations, detail.

Figure 18.4. Ratio of latitude/longitude standard deviations, free adjustment detail.

The medians of the height standard deviation to latitude and longitude are seen to somewhat greater than 2. The median ratio of 1.17 for the latitude/longitude shows a 17% differential. This is in good agreement with the 0.8 figure for the ratio of semiminor to semimajor axes of the horizontal error ellipse in Section 17. The spike at the 1.0 bin in Figure 18.4 is an artifact related to the fixed number of digits carried in the working file. As the standard deviation magnitudes get smaller, more of them get rounded up and down. This, in turn, creates more instances where the latitude and longitude standard deviations appear to match exactly.

Another aspect of the height ratio figures is that they display a number of cases where the heights are more precise than the horizontal components (ratios < 1.0). Although not done so in this report, deeper analysis of this set would be interesting.

Finally, to foreshadow the next section, the latitude/longitude ratios from the final fixed adjustment are provided in Figure 18.5. The similarities allow one to conclude that one may use either the free or fixed adjustments when analyzing the standard deviation ratios.
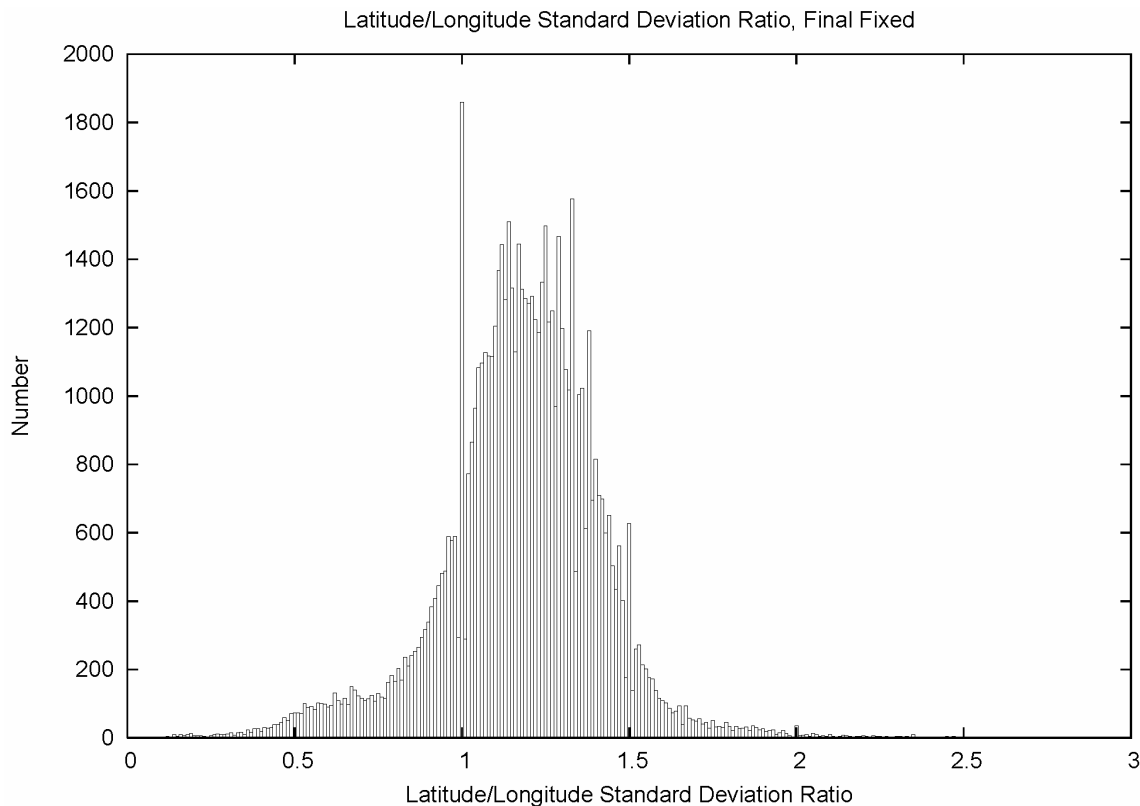

Figure 18.5. Ratio of latitude/longitude standard deviations, fixed adjustment, detail.

19. Free-to-fixed adjustment ratios

A natural avenue in exploring the structure of the NSRS is to examine how much strength comes from the GPS vectors in the network and how much strength comes from

the fixed control points. This is done by computing the ratios of standard deviations of the free/fixed adjustments. In general, one would expect ratios in excess of 1.0, indicating greater dispersion of the free adjustment coordinates when compared to the fixed adjustment. Note that the ratio comparisons use *a posteriori* statistics. The *a posteriori* standard deviation of unit weight for the free adjustment was 1.276619, and for the fixed adjustment was 1.37549. The relative ratio is 0.928.

The distribution of the ratios of the free/fixed *a posteriori* latitude standard deviations are shown in Figure 19.1 with a 0.01 bin width. One sees the bulk of the points with ratios less than 1.0, indicating smaller dispersion of the free adjustment coordinates compared to the fixed. The mode of the distribution is, indeed, in the 0.93 bin. The distribution skew to the right does show strengthening due to the fixed control. However, error between the GPS network and the GPS CORS fixed control inflated the fixed adjustment *a posteriori* variance of unit weight to such an extent that one loses any strengthening through fixing.
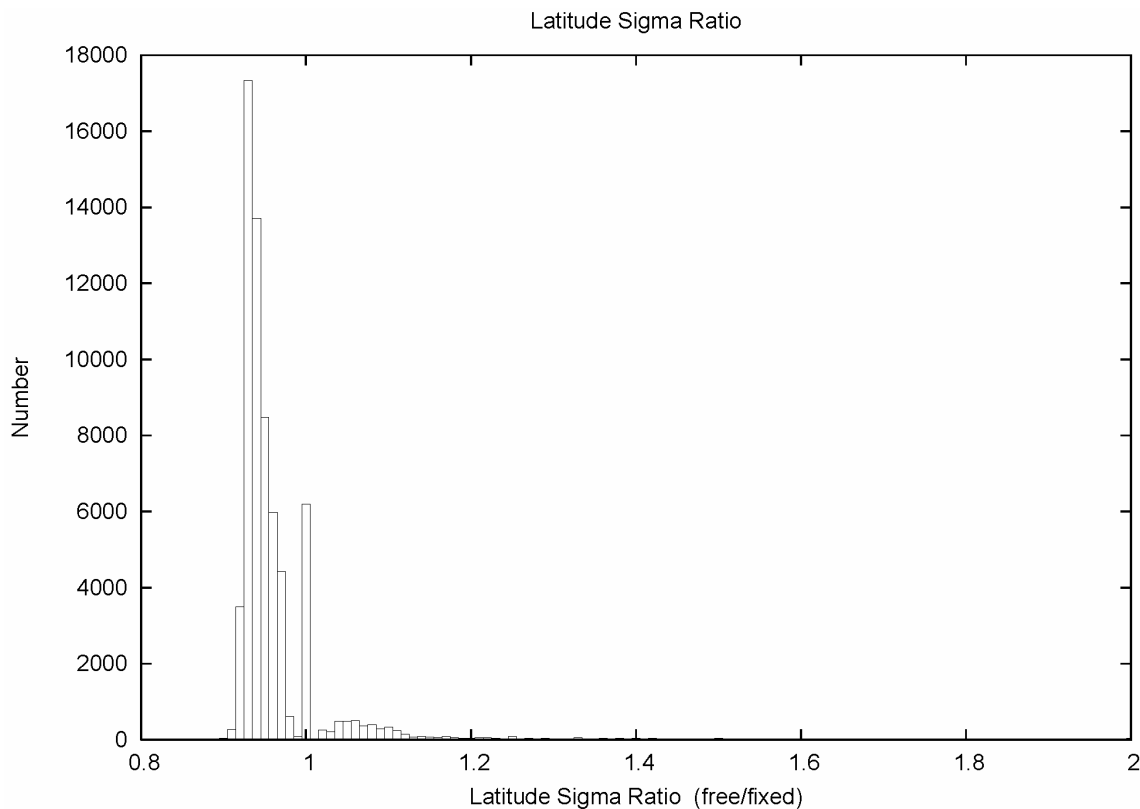

Figure 19.1. Ratio of free/fixed latitude standard deviations, detail.

The spike in the 1.0 bin is an artifact related to the fixed number of digits carried in the working file. As the standard deviation magnitudes get smaller, more of them get rounded up and down. This, in turn, creates more instances where the free and fixed standard deviations appear to match exactly.

Figure 19.2 plots the distribution of the ratios of the free/fixed *a posteriori* longitude standard deviations with a 0.01 bin width. And, Figure 19.3 shows the ratios of

the free/fixed *a posteriori* height standard deviations with a 0.01 bin width. One sees similar behaviors. Some small levels of network strengthening occur when imposing the fixed control. But the levels of misfit between the network and the control lead to an overall increase in the dispersions of the fixed coordinates.
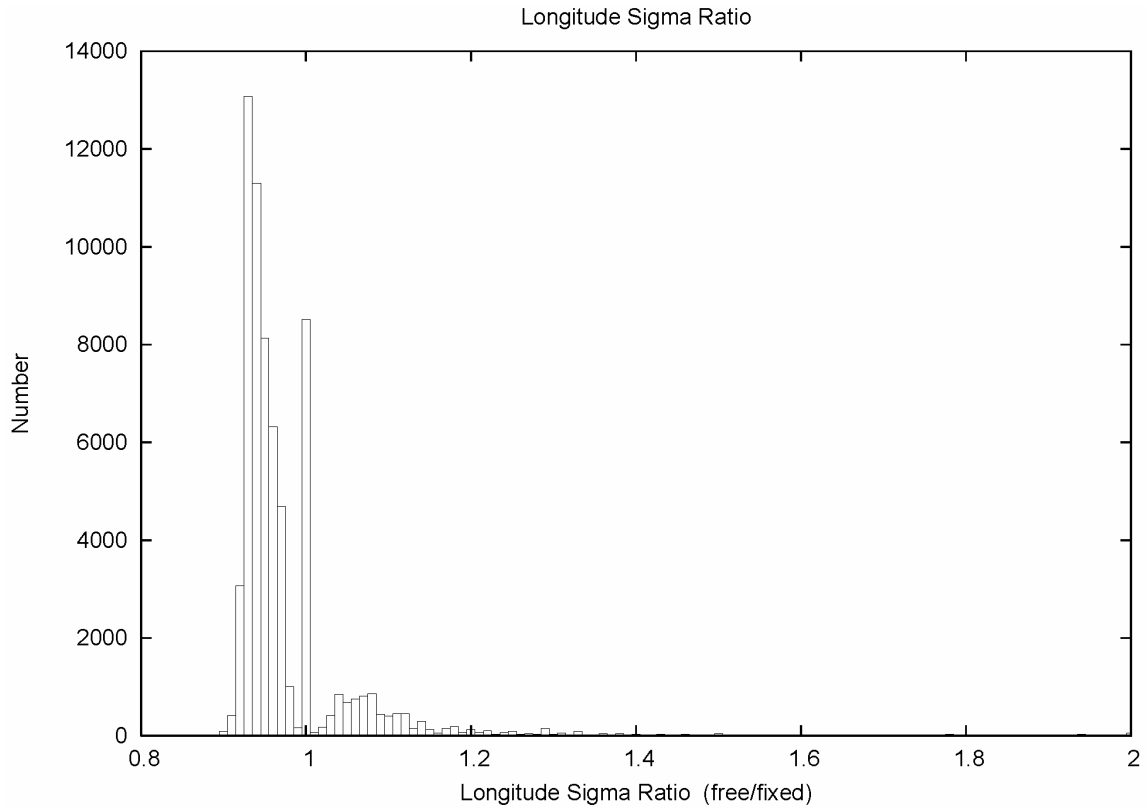

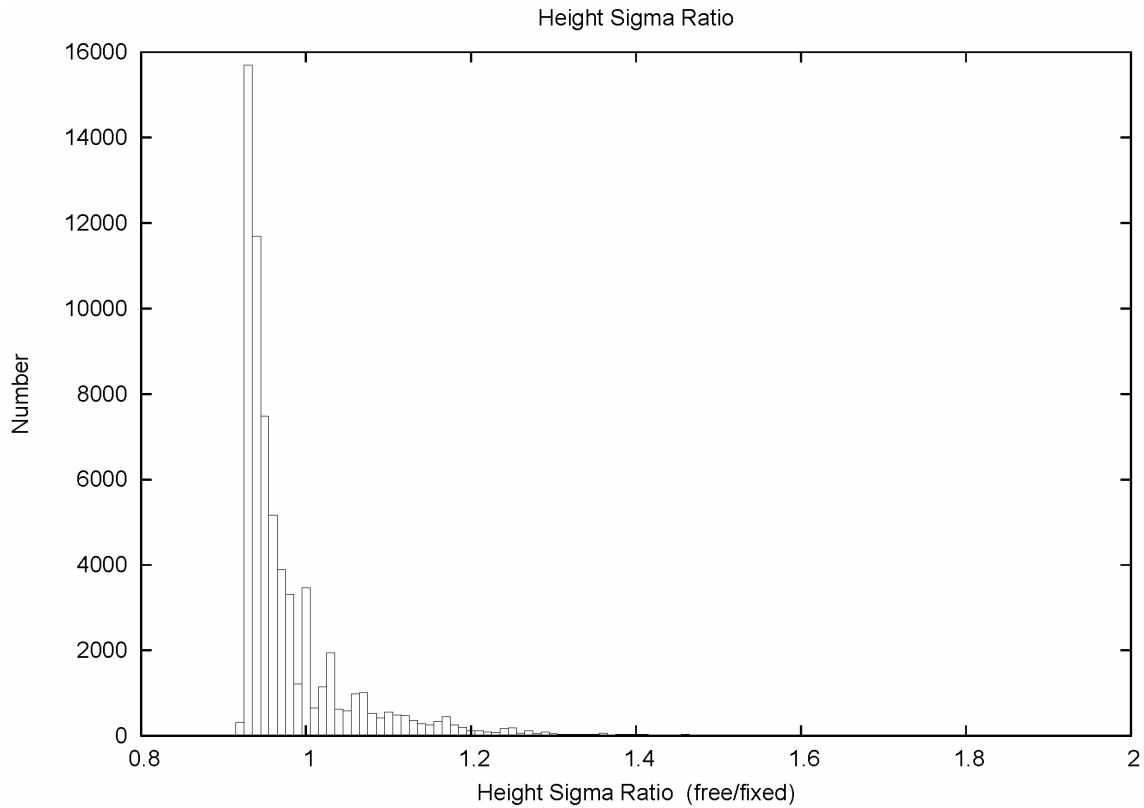Figure 19.2. Ratio of free/fixed longitude standard deviations, detail.

Figure 19.3. Ratio of free/fixed height standard deviations, detail.

20. Network accuracies of the NSRS 2007

The horizontal network accuracy is the radius of a circle of uncertainty, such that the reported coordinate is within the radius 95% of the time (FGDC 1998, Part 1, pg. 1-5).

Naturally, one may develop information from formal error propagation processes that indicate one has a bi-normal Gaussian error distribution. Even in the case of bi-normality, it is possible to establish a radius that encompasses 95% of the bi-normal probability distribution. Leenhouts (1985) provides a simple cubic equation that relates the radius of the error circle, r, to the horizontal error ellipse semimajor and semiminor axes, a and b, respectively. For the 95% probability level:

$$r = a \, (1.960790 + 0.004071 \, C + 0.114276 \, C^2 + 0.371625 \, C^3) \qquad (20\text{-}1)$$

where

$$C = b/a \qquad\qquad (20\text{-}2)$$

One immediately can see the pleasing result that when the error ellipse elongates to a one-dimensional distribution, then C approaches 0 and the radius approaches 1.96 a. Also, when the error ellipse approaches circularity, then C approaches 1.0 and the radius approaches 2.45 a.

The approximation involved in Equation 20-1 is utterly negligible. Leenhouts (1985) reports better than 6 cm for a 16 meter semimajor axis. Since the NSRS horizontal standard deviations are on the order of 0.4 cm, the approximation would be smaller than 15 microns (1 micron = 10^{-6} meter). A human hair is about 50 to 100 microns wide.

The use of Leenhouts for computation of the horizontal network accuracy (radius of the 95% error circle) was in the first NGS draft to FGDC (FGCS 1995). It was also adopted by Canada (GSD 1996). And, it has been briefed by National Geodetic Survey in survey workshops (e.g. McKay 2001). It is regrettable if there has been confusion on the facts listed above. The horizontal network accuracy for a point is a single number, it is at a 95% confidence level, it possesses azimuthal symmetry, and it is computed from horizontal error ellipse components by Equations 20-1 and 20-2.

Figure 20.1 displays the distribution of the horizontal network accuracies of the NAD 83(NSRS2007) National Readjustment. Figure 20.2 shows the detail on the left. The maximum horizontal network accuracy is 13.45 meters.
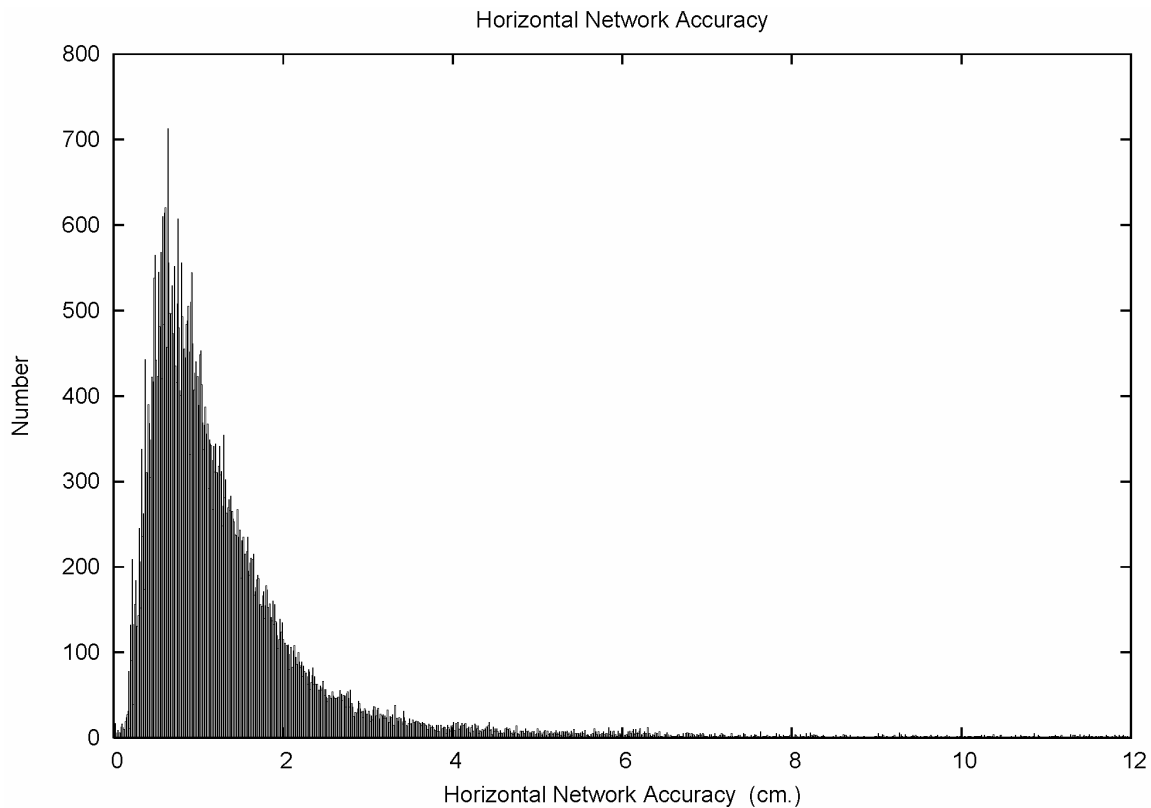

Figure 20.1. Distribution of horizontal network accuracies. 0.01 cm bin size.
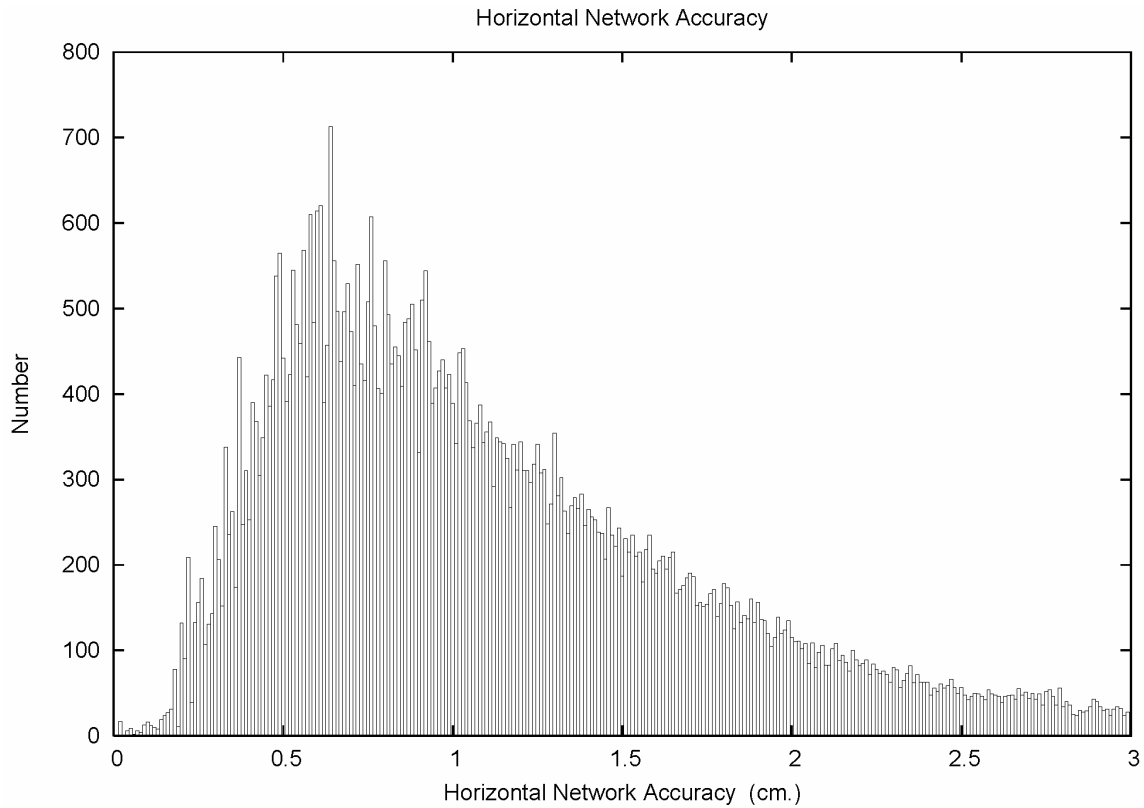
Figure 20.2. Distribution of horizontal network accuracies, detail. 0.01 cm bin size.

The distribution of horizontal network accuracies show the behavior seen in the latitude standard deviations of Figure 16.2, albeit converted to a 95% error circle by Equations 20-1 and 20-2. The somewhat spiky nature of the distribution is an artifact of the bin size aliasing against the least count of the standard deviations output by the adjustment software.

Vertical network accuracy is a single number representing the 95% probability limits of a one-dimensional distribution. Figure 20.3 displays the distribution of the vertical network accuracies of the NAD 83(NSRS2007) National Readjustment. Figure 20.4 shows the detail on the left. The maximum vertical network accuracy is 4.90 m.
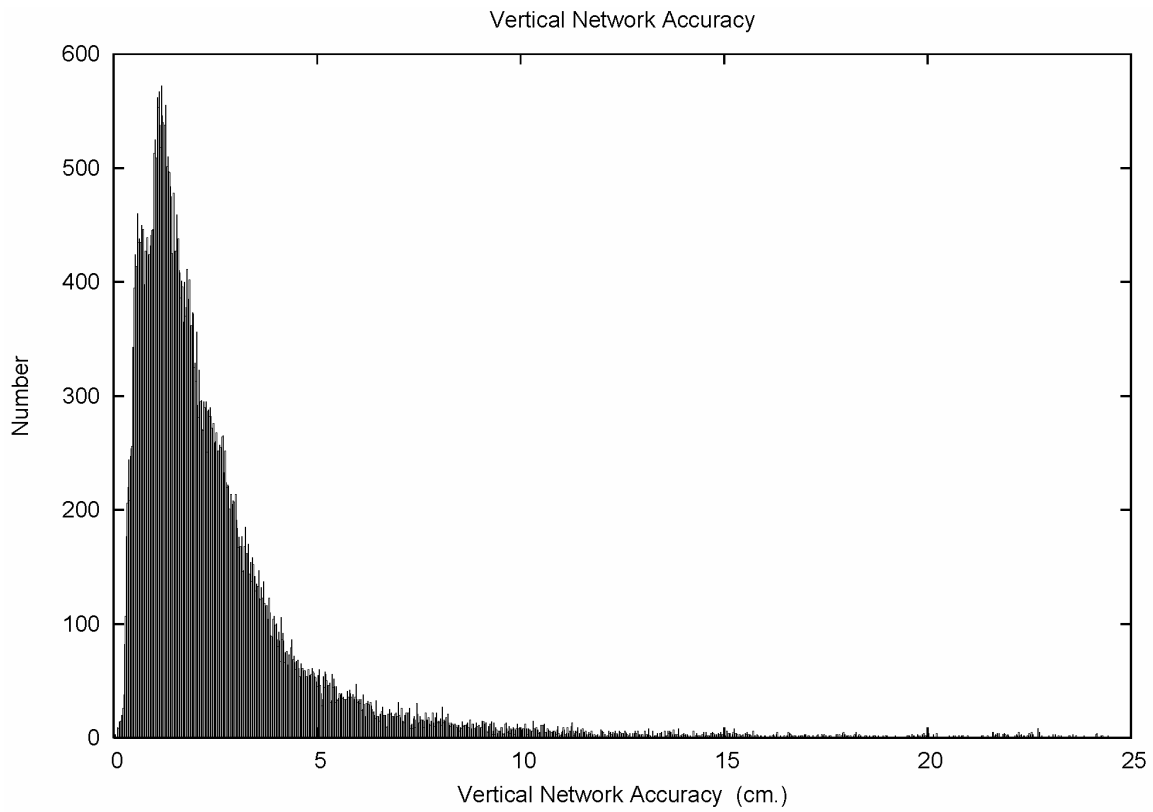
Figure 20.3. Distribution of vertical network accuracies. 0.0196 cm bin size.
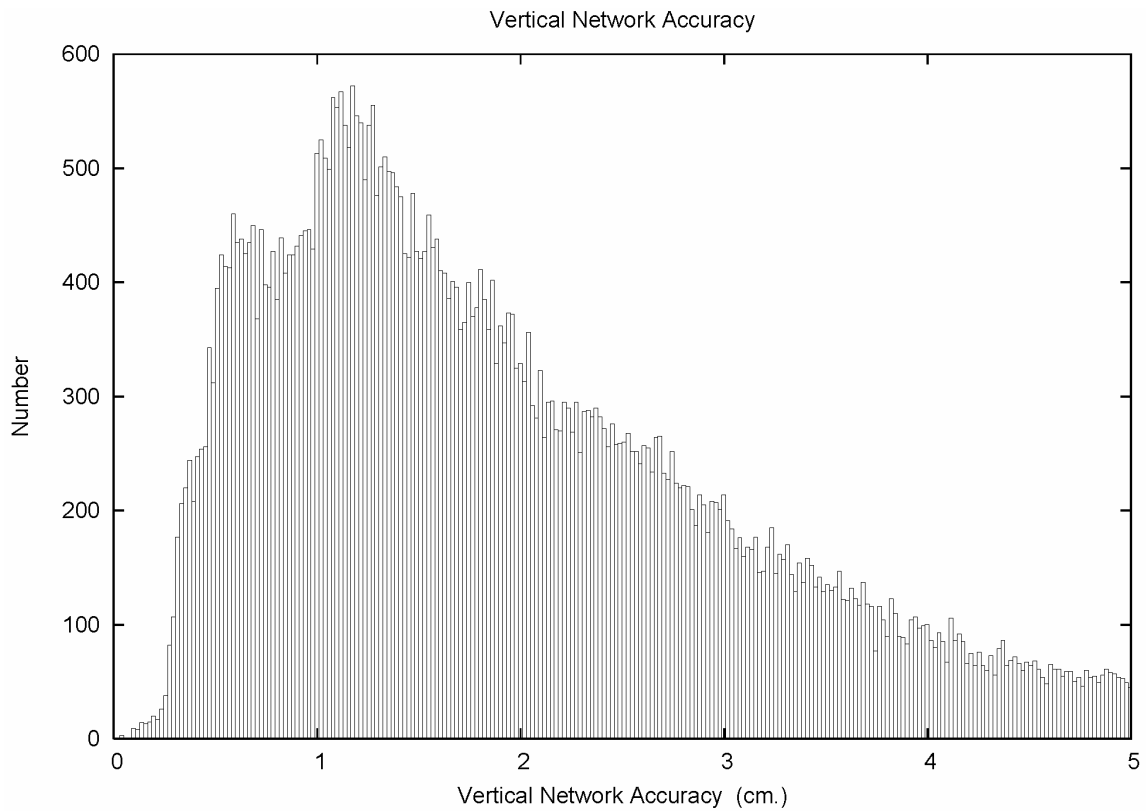

Figure 20.4. Distribution of vertical network accuracies, detail. 0.0196 cm bin size.

The distribution of vertical network accuracy seen in Figures 20.3 and 20.4 is a simple rescaling of the height standard deviations displayed by Figures 16.5 and 16.6. The choice of the 0.0196 cm bin size is to suppress spikes in the histogram that would otherwise arise from a 0.02 cm bin size aliasing against the least count of the standard deviations output by the adjustment software. (Refer to allcirc2.txt in the Electronic Support Material.)

The percentiles of the distributions of the network accuracies are collected in Table 20.1. The median 95% accuracy of the NSRS network is 1 cm horizontal and 2 cm vertical. The distributions contain long tails. However, the 95% network accuracies seldom exceed 4 cm horizontal and 8 cm vertical.

Table 20.1 – Percentiles of Network Accuracies of the NAD 83(NSRS2007)

Percentile	Horizontal (cm)	Vertical (cm)
50%	1.03	1.84
68%	1.41	2.63
90%	2.57	5.17
95%	3.81	7.60
99%	12.80	21.66
99.9%	73.85	64.25

21. Spatial distribution of network accuracies of the NSRS 2007

This section analyzes the spatial distribution of the network accuracies of the NSRS 2007. The approach is to develop gridded versions of the network accuracies that could be plotted on a color scale. Due to the lack of coverage in Alaska, Hawaii, and the Caribbean (Figures A.3.2, A.3.3, and A.3.4), the gridding was only performed for the conterminous U. S.

A land mask was extracted from the GMT (Generic Mapping Tools) software suite (Wessel and Smith 1995) and represented on a 2' x 2' grid from 24° to 50° N and 235° to 294° E. The points over water were extracted as a synthetic data set with values of 0.0 to stabilize the subsequent gridding process.

Horizontal network accuracies were thinned with a GMT 2' x 2' block median algorithm and mixed with the synthetic data over water. The data were then gridded with a GMT splines in tension method (Smith and Wessels 1990) with a tension of T=0.4. Finally, the color image of the grid was rendered with GMT mapping software. Figure 21.1 displays the spatial distribution of the horizontal network accuracies of the NAD 83(NSRS2007) National Readjustment. The figure is also provided as a full page color plate, Plate 2.
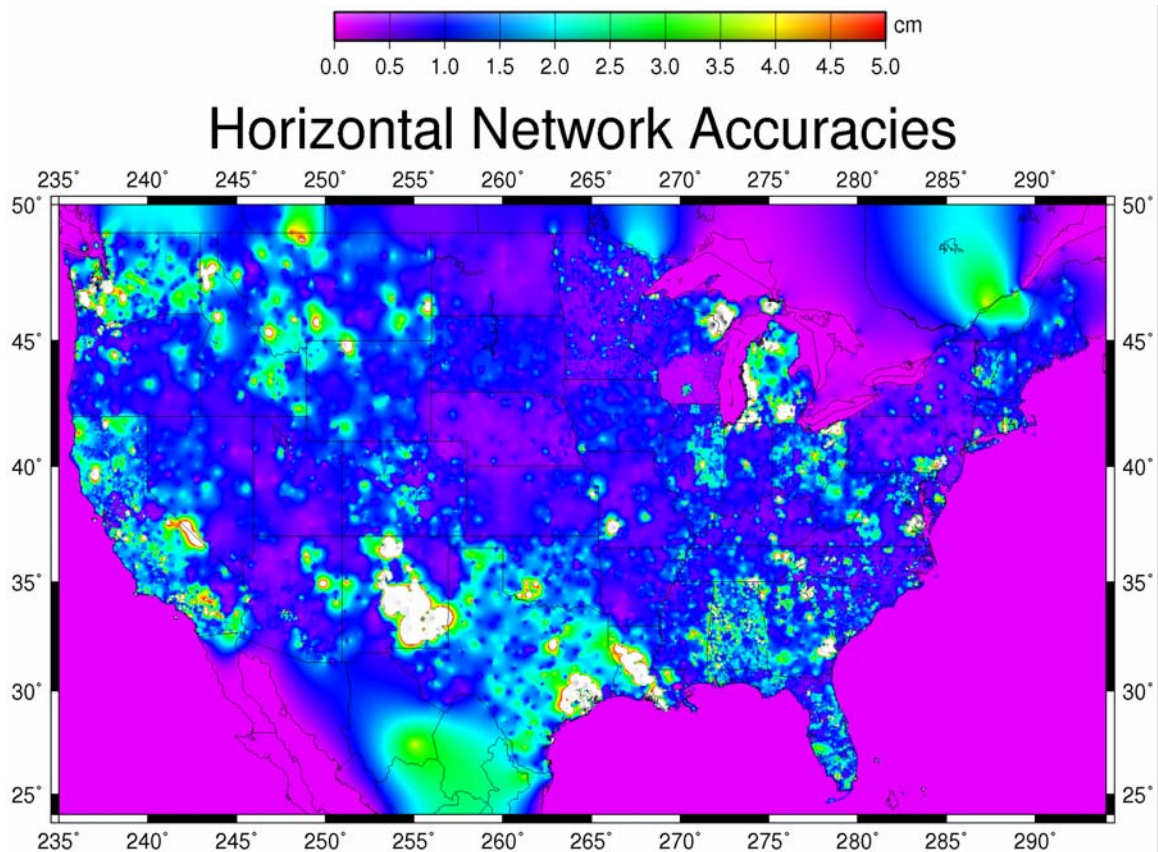
Figure 21.1. Gridded horizontal network accuracies. White exceeds 5 cm.

The general impression is a blue color, which matches the 1 cm median horizontal network accuracy of Section 20. Sizable regions, such as Southern Wisconsin, New York, Pennsylvania, Nebraska, and North Dakota have even better accuracies. However, patches of poorer accuracy are present, such as New Mexico, Southeast Texas, Southwest Louisiana, and in the Northwest. It is remarkable that the grouping of larger horizontal accuracies on the West Coast coincides with the California state boundaries. This is due in part to the special California weighting scheme, which is inspected in detail in Section 33.

An identical gridding process was applied to the vertical network accuracies. Figure 21.2 displays the spatial distribution of the vertical network accuracies of the NAD 83(NSRS2007) National Readjustment. The color scale is expanded to double the range of the horizontal network accuracies to provide easy comparisons. The figure is also provided as a full page color plate, Plate 3.
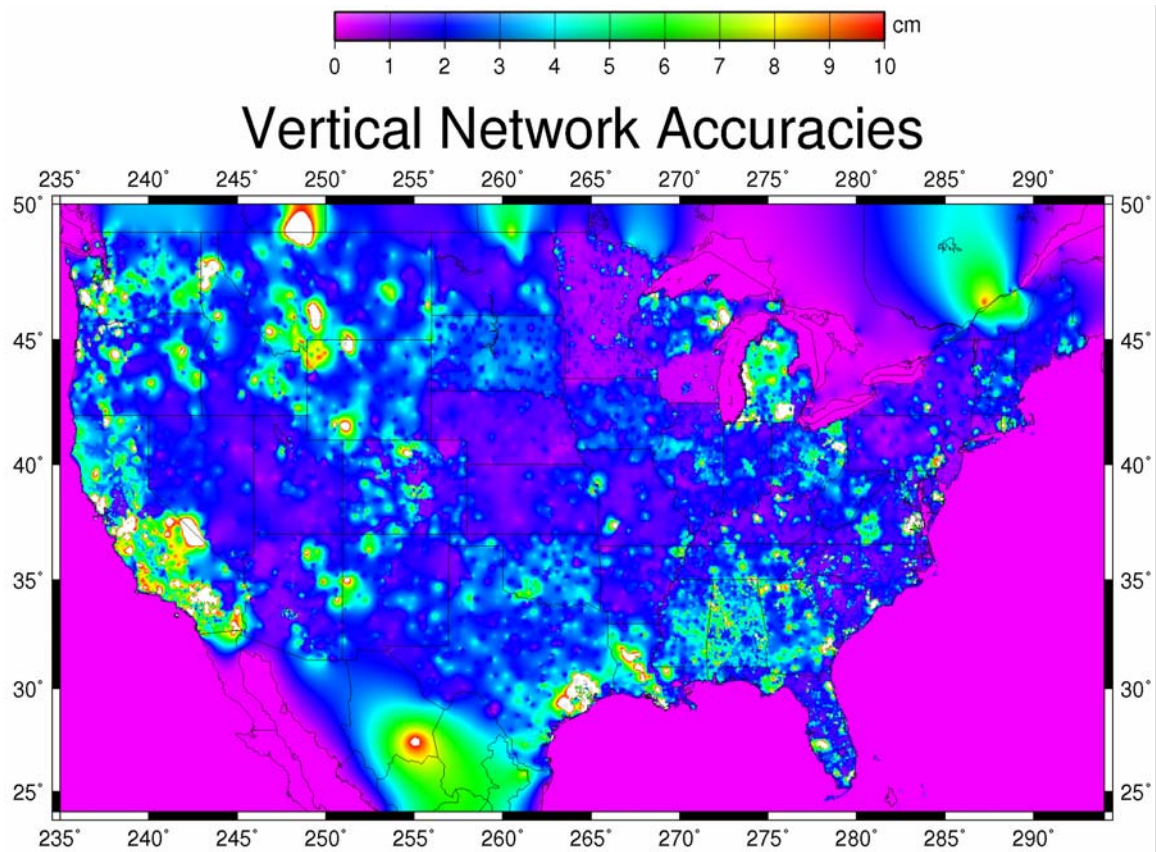
Figure 21.2. Gridded vertical network accuracies. White exceeds 10 cm.

Once again, the general impression is a blue color, which matches the 2 cm median vertical network accuracy of Section 20. Sizable regions have even better accuracies, now including most of Minnesota. Patches of poorer vertical accuracy are similar to those seen for the horizontal network accuracies. The larger vertical accuracies on the West Coast are due in part to the special California weighting scheme (Section 33). However, the source of the increase in Southern California is not clear.

22. Temporal distribution of network accuracies of the NSRS 2007

This section analyzes the temporal distribution of the network accuracies of the NSRS 2007. The approach is in two parts. All project GPS vector files (GFILE's) were processed to establish a mean date for each GPS project (Section 4). Then all observations were processed to identify the first project where each point was first observed. (Refer to allcirc2.txt in the Electronic Support Material.)

Figure 22.1 shows a scatter plot of the horizontal network accuracies with the times of point establishment indexed from January 1983. Little can be seen, although the figure highlights the very inaccurate points of 20 cm or more. More detail is provided in Figure 22.2
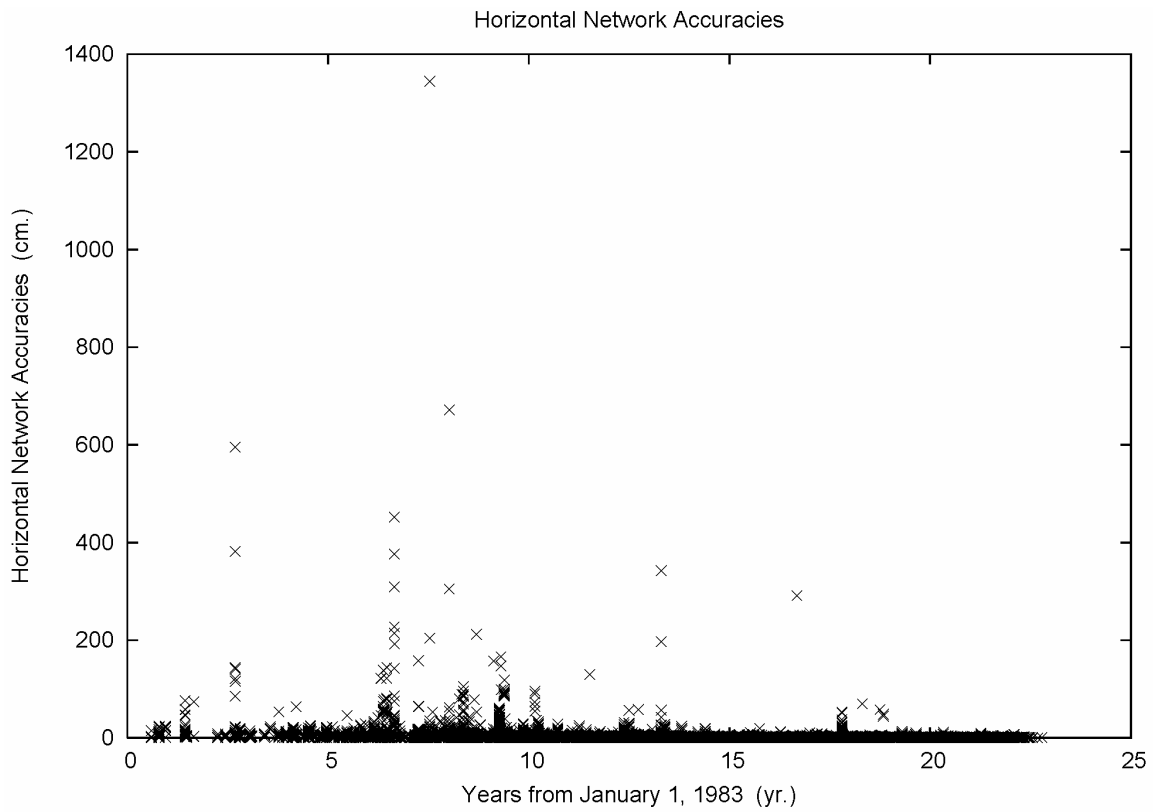
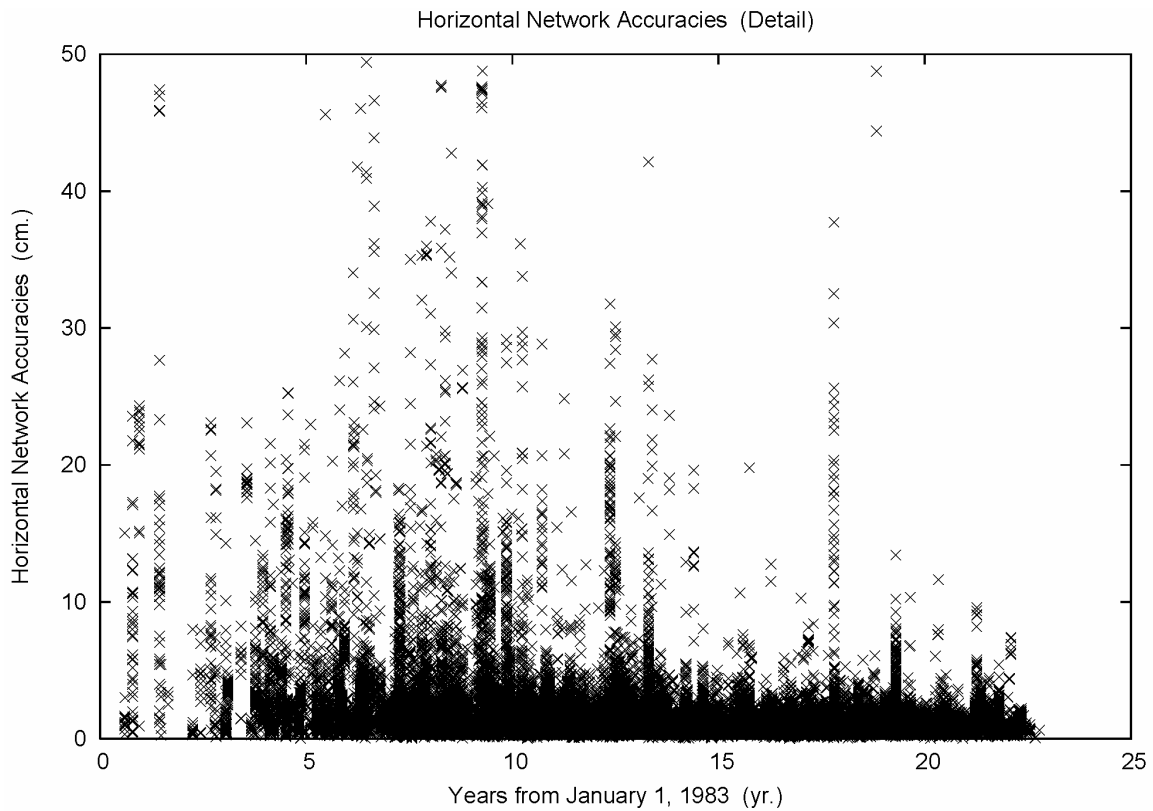Figure 22.1. Temporal distribution of horizontal network accuracies.

Figure 22.2. Temporal distribution of horizontal network accuracies, detail.

The vertical structures reflect the aggregation of points into parent projects, followed by the assignment of a mean date to each project. Of note, a trend of improving accuracy is evident in Figure 22.2, and is most notable since 2000. To highlight this, a high detail scatter plot is generated in Figure 22.3.
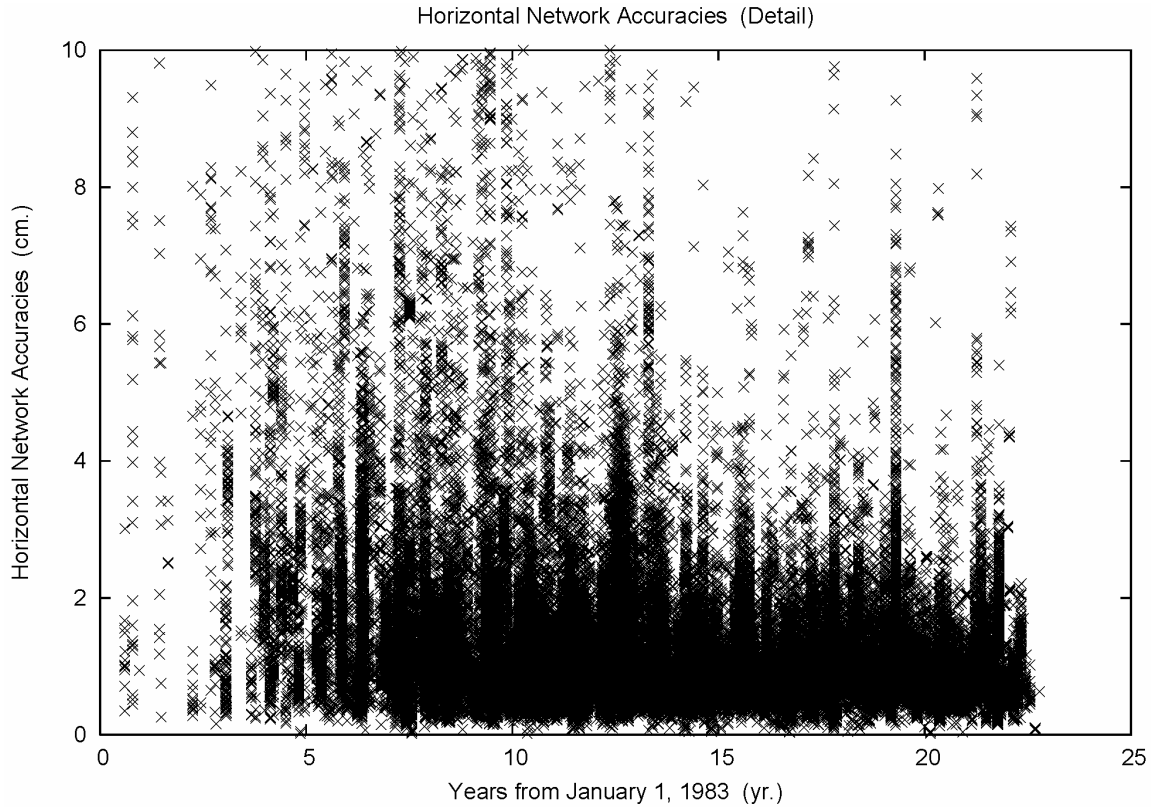
Figure 22.3. Temporal distribution of horizontal network accuracies, high detail.

Figure 22.3 displays the improved horizontal network accuracies over time. Likely causes are improved hardware (fewer cycle slips) and better data editing (leading to successful cycle slip repairs).

Figure 22.4 shows a scatter plot of the vertical network accuracies against time. As with the horizontal network accuracies, little can be seen beyond the inaccurate points. More detail is provided in Figure 22.5
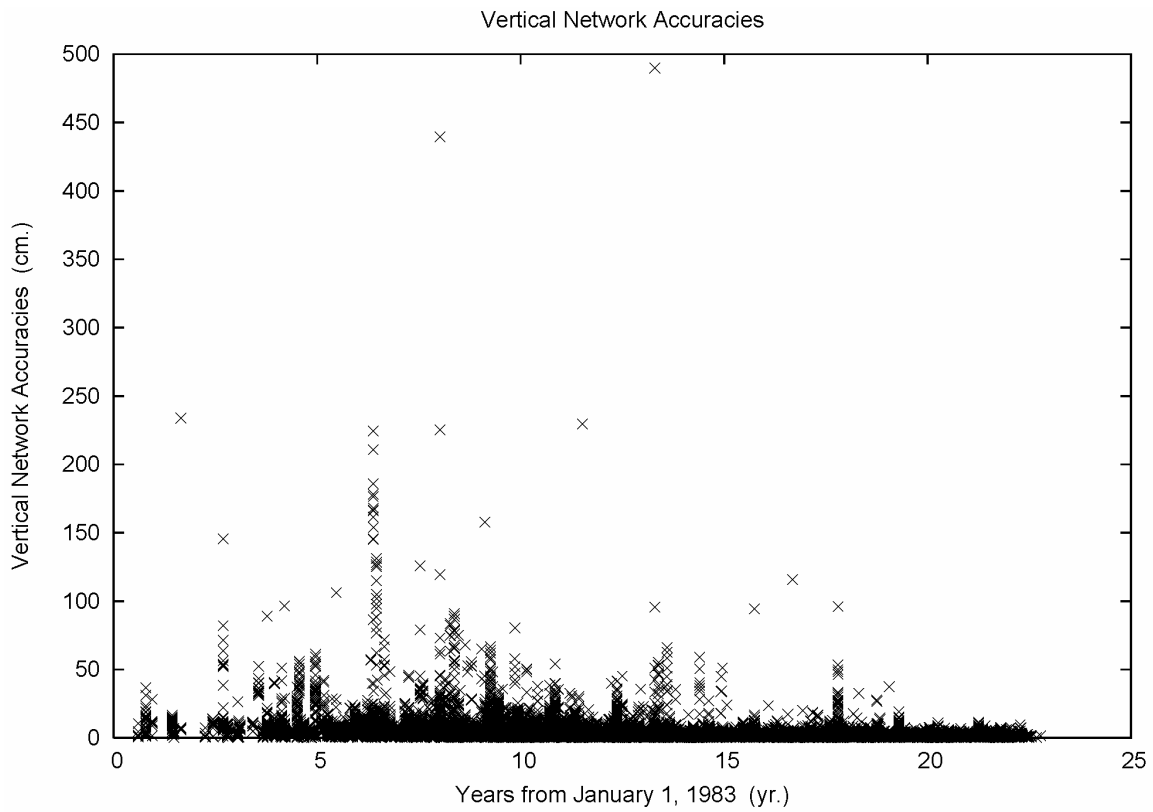
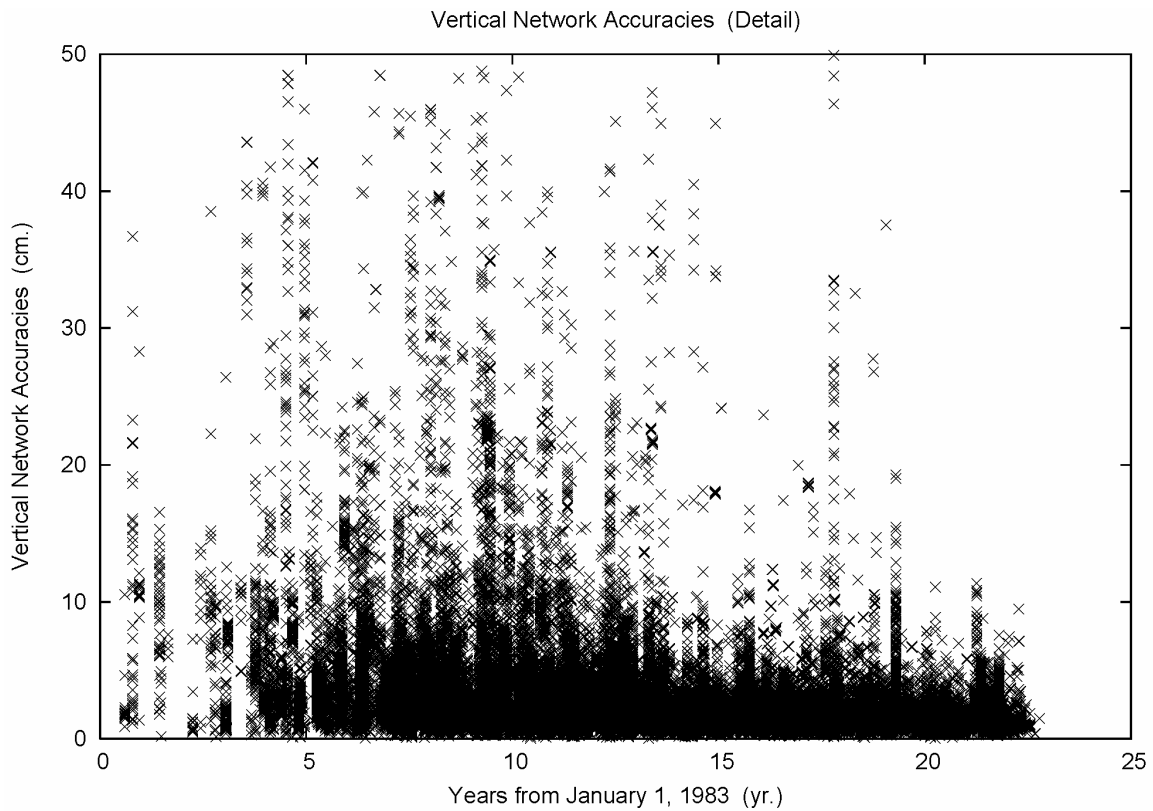Figure 22.4. Temporal distribution of vertical network accuracies.

Figure 22.5. Temporal distribution of vertical network accuracies, detail.

The improvement vertical accuracy in time is evident in Figure 22.5. In fact, better vertical accuracies were being observed by 1996. To emphasize this, a high detail scatter plot is generated in Figure 22.6.
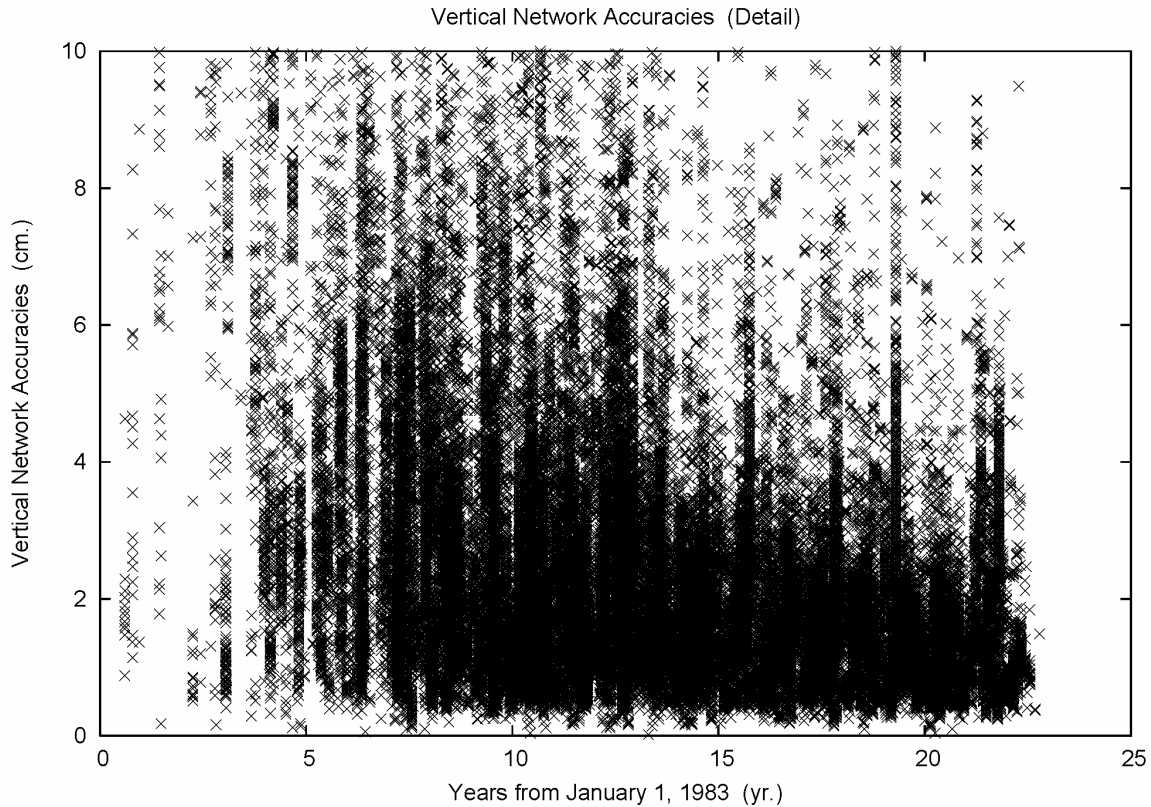

Figure 22.6. Temporal distribution of vertical network accuracies, high detail.

An interesting feature of Feature 22.6 is that the improvement in vertical network accuracy has not yet leveled off. In other words, the noise floor for GPS vertical accuracy has not yet been reached. Given the numerous physical factors that affect GPS vertical, this is heartening. While it is not clear (aside from elements discussed above) why the vertical improvement continues, the adoption of high accuracy GPS vertical guidelines (Zilkoski *et al.*, 1997) deserves some credit.

23. Superior vertical network accuracies of the NSRS 2007

Two very remarkable aspects were seen in the network accuracies. The first was the excellent level of accuracy of 1 cm horizontal and 2 cm vertical. And, the second fascinating element was the bimodal structure of the vertical network accuracies seen in Figures 20.3 and 20.4. To pursue this, the vertical network accuracies of 1 cm or better were extracted from the full set. This 1 cm value roughly corresponds to the local minima between the two peaks of Figure 20.4. These points are plotted in Figure 23.1.
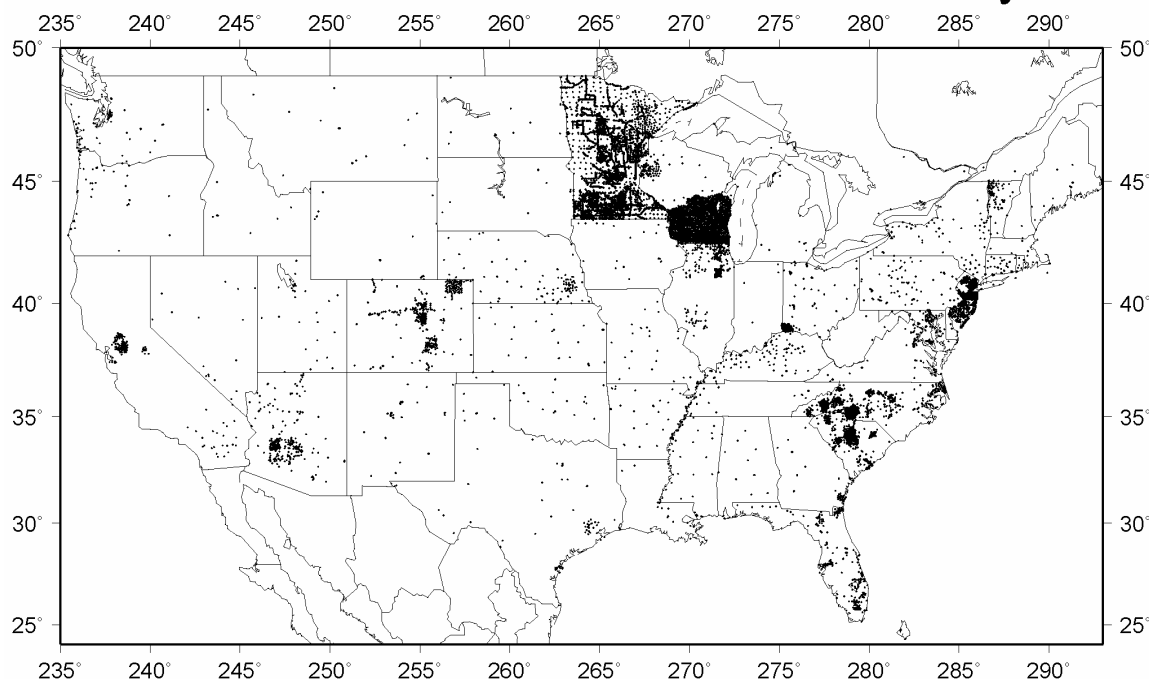
One-CM Vertical Network Accuracy

Figure 23.1. Points with one cm vertical network accuracy, conterminous U.S.

The figure shows the points with superior vertical network accuracy. One immediately sees the clustering, indicating the accuracy is deliberate, and associated with specific surveys and states. Minnesota, New Jersey, Southern Wisconsin, parts of the Carolinas, and the Upper Mississippi River are evident in the figure. The coverage plot above shows good agreement with the magenta colored areas in Figure 21.3.

A survey program dedicated to accurate heights is the NGS National Height Modernization Program (c.f. www.ngs.noaa.gov/heightmod/). These points are established with special codes in the NGS data base, and so, can be cross referenced against various adjustment products.

The height modernization points were indexed against the monumented points of the NSRS National Readjustment. The resulting points are plotted in Figure 23.2. (Refer to hmcirc.txt in the Electronic Support Material.) Figures 23.1 and 23.2 are quite similar, with concentrations in Southern Minnesota, Wisconsin, New Mexico, the Carolinas, and along the Mississippi River. Not all of the Height Modernization points are seen to possess 1 cm vertical network accuracy. It must be remembered, the intended accuracy of Height Modernization points are 2 and 5 cm vertical network accuracy. Given that fact, the degree of correspondence is remarkable. And, of course, New Jersey serves as an example that points need not be coded as Height Modernization, yet may still deliver superior vertical network accuracy.

Height Modernization
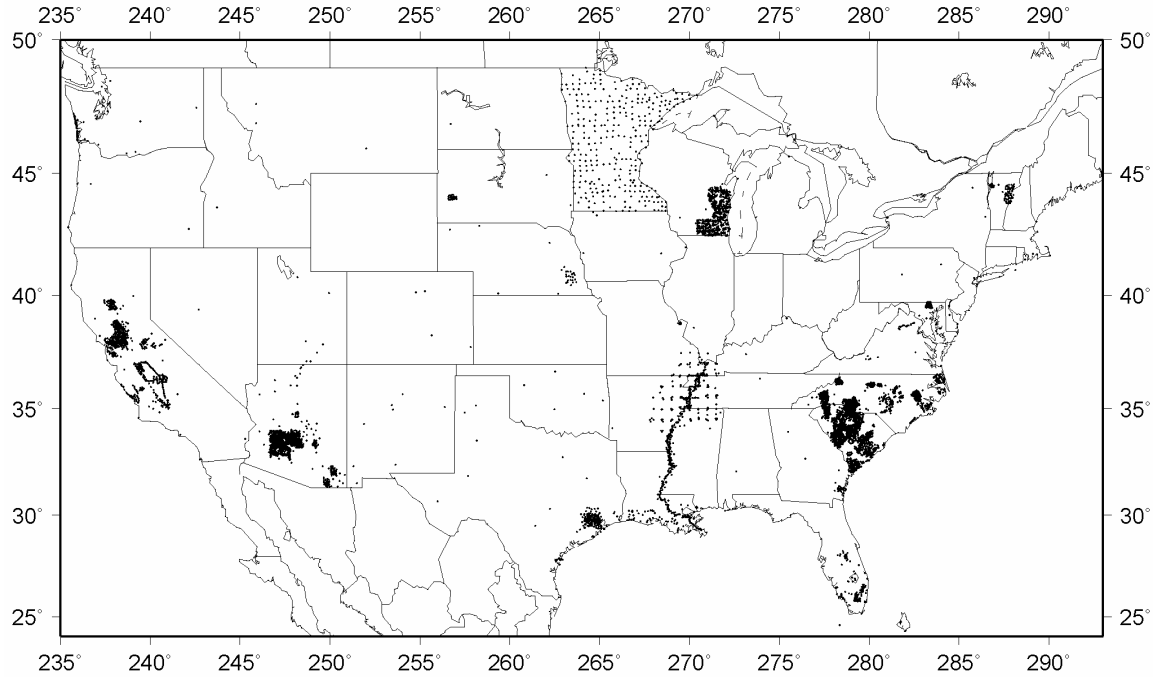
Figure 23.2. Height modernization points, conterminous U.S.

As an additional view of the Height Modernization project, histogram distributions of the horizontal network accuracy of this station subset are plotted in Figure 23.4. Vertical network accuracy is histogrammed in Figure 23.5. And, the percentile statistics are collected into Table 23.1.

Table 23.1 – Percentiles of Network Accuracies of Height Modernization Points

Percentile	Horizontal (cm)	Vertical (cm)
50%	0.88	1.20
68%	1.16	1.59
90%	1.93	2.78
95%	2.48	3.76
99%	13.54	16.31
99.9%	27.42	41.45

Figure 23.3. Height modernization horizontal network accuracies.

Figure 23.4. Height modernization vertical network accuracies.

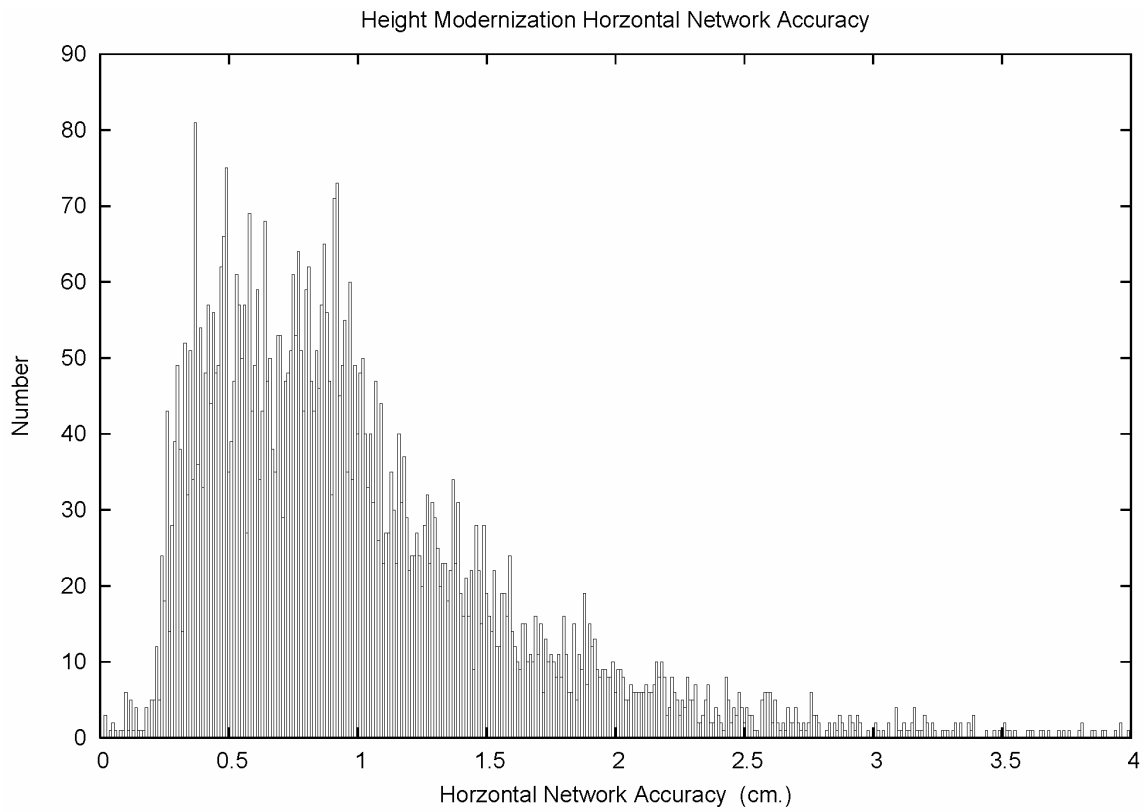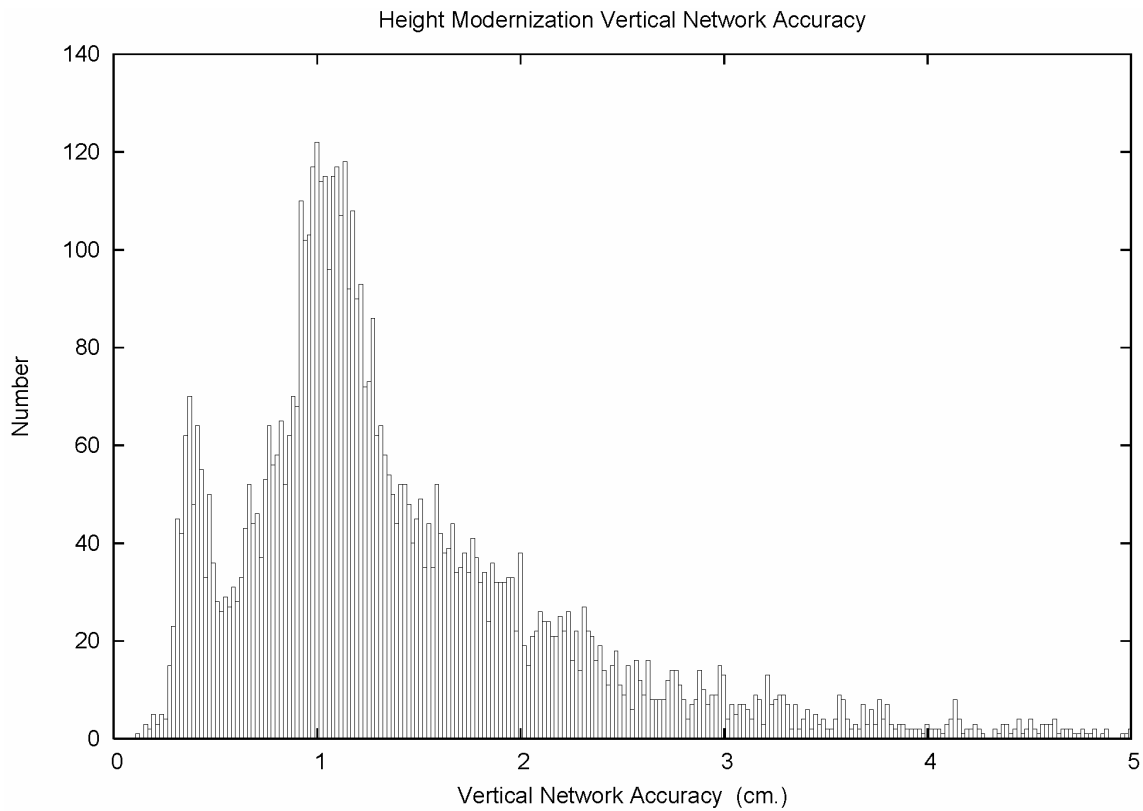One sees that the median 95% vertical network accuracy of the Height Modernization points is 1.2 cm. This is markedly better than the 1.84 cm vertical network accuracy of NSRS as a whole. The distributions still possess sizable tails. While not done so in this report, the survey design and data reduction issues that relate to these tails may be a fruitful avenue to explore. And, somewhat surprisingly, the vertical network accuracy distribution is distinctly bimodal. It had been thought that Height Modernization was the source of the bimodality in Figures 20.3 and 20.4. But, now it is seen that there is another source.

To track down the source of the left hand peak in Figure 23.4, the vertical network accuracies of 0.55 cm or better were extracted from the NSRS set. This value roughly corresponds to the local minima between the two peaks of Figure 23.4. These points are plotted in Figure 23.5.

Half-CM Vertical Network Accuracy

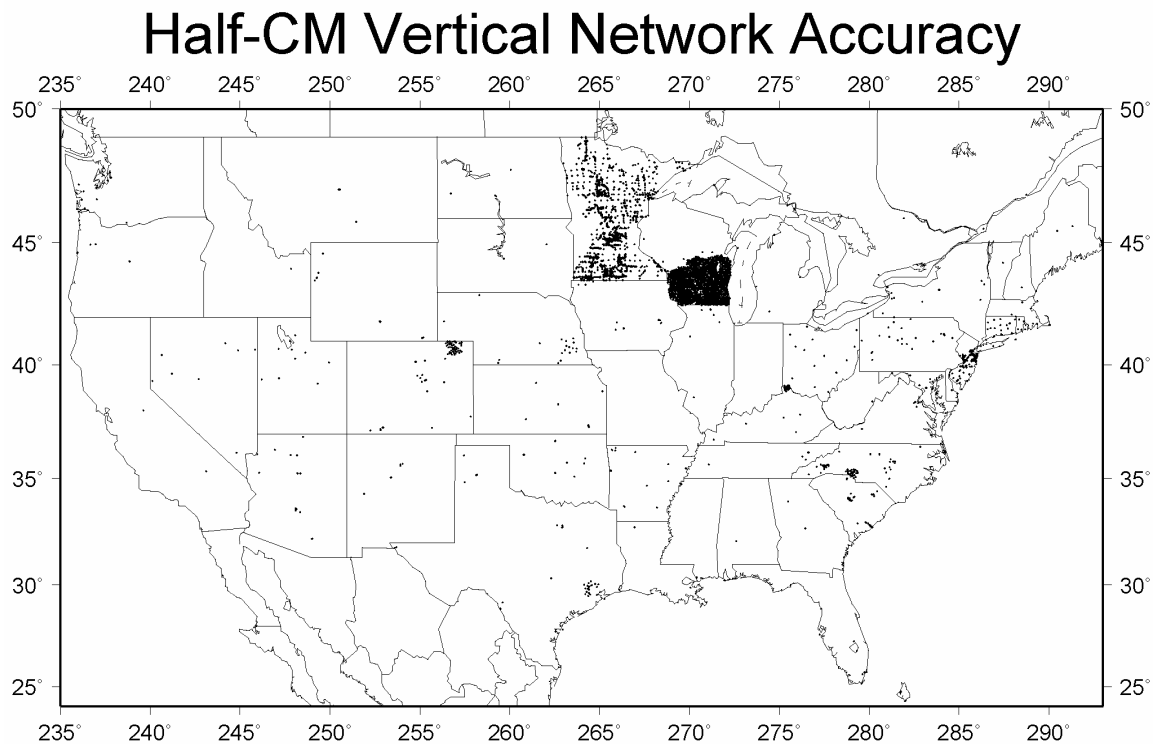Figure 23.5. Points with 0.55 cm vertical network accuracy, conterminous U.S.

The points in Figure 23.5 represent the "Diamond Level" of vertical network accuracy quality. With a few local exceptions, these are the surveys of Minnesota and Southern Wisconsin.

Later in this report (Section 32), an issue regarding a survey project in Southern Wisconsin will be addressed that conceivably could alter Figure 23.5.

24. Posteriori relative position standard deviations

Focus changes at this point to the *a posteriori* relative position standard deviations from the fixed adjustment of the NSRS 2007. It must be emphasized that the numbers in this section are *not*, repeat, *not* local accuracies. Local accuracies will be reported in Section 27.

The standard deviations in this section have been scaled by the *a posteriori* standard deviation of unit weight of the NSRS, 1.37549. Figure 16.1 displays the histogram distribution of the relative latitude standard deviation with a 0.01 bin width. The maximum relative latitude standard deviation is 4.86 meters. The relative latitude standard deviations also show a remarkable precision, with a median of 0.34 cm. The details of the relative latitude standard deviations are shown in Figure 24.2. These standard deviation statistics are in general agreement with the horizontal (distance) residual statistics reported in Section 7. This is expected given the extensive pre-adjustment weight scaling and the use of *a posteriori* statistics. And, as expected, the relative latitude standard deviations are somewhat smaller than the latitude standard deviations plotted in Figures 16.1 and 16.2.

Figure 24.1. Relative latitude standard deviation distribution. 0.01 cm bin size.

Figure 24.2. Relative latitude standard deviation distribution, detail. 0.01 cm bin size.

Figure 24.3 plots the histogram distribution of the relative longitude standard deviations with a 0.01 cm bin width. The maximum relative longitude standard deviation is 4.95 meters. The details of the relative longitude standard deviations are shown in Figure 24.4. The relative longitude standard deviations show a slightly tighter precision, compared to the relative latitude standard deviations of Figure 24.3. And, as noted for the relative latitude standard deviations above, the relative longitude standard deviations are smaller than the longitude standard deviations of Figures 16.3 and 16.4.
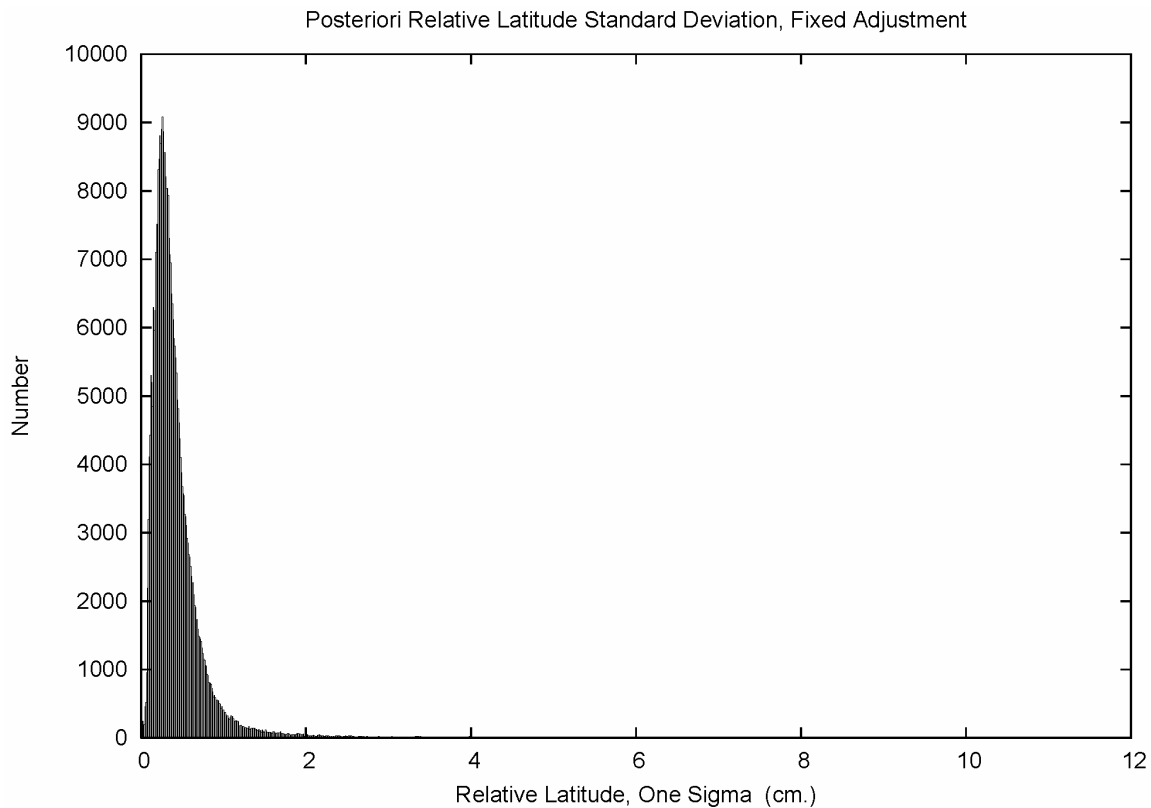
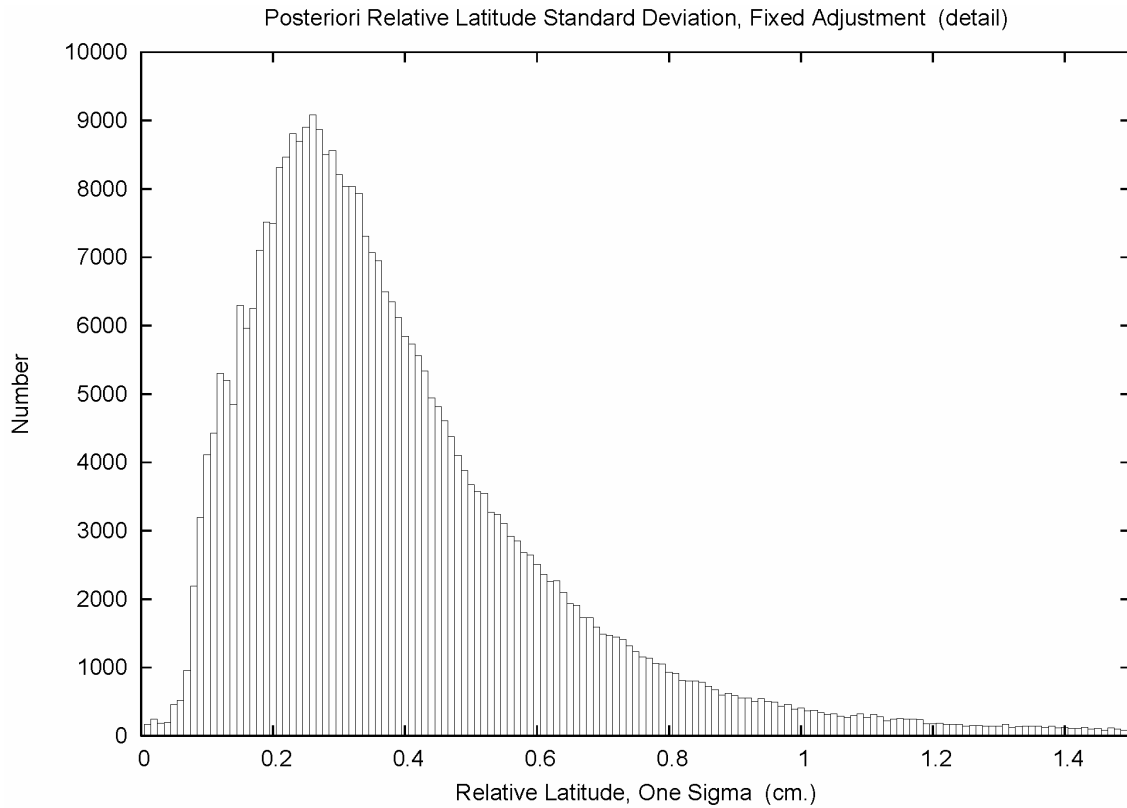Figure 24.3. Relative longitude standard deviation distribution. 0.01 cm bin size.
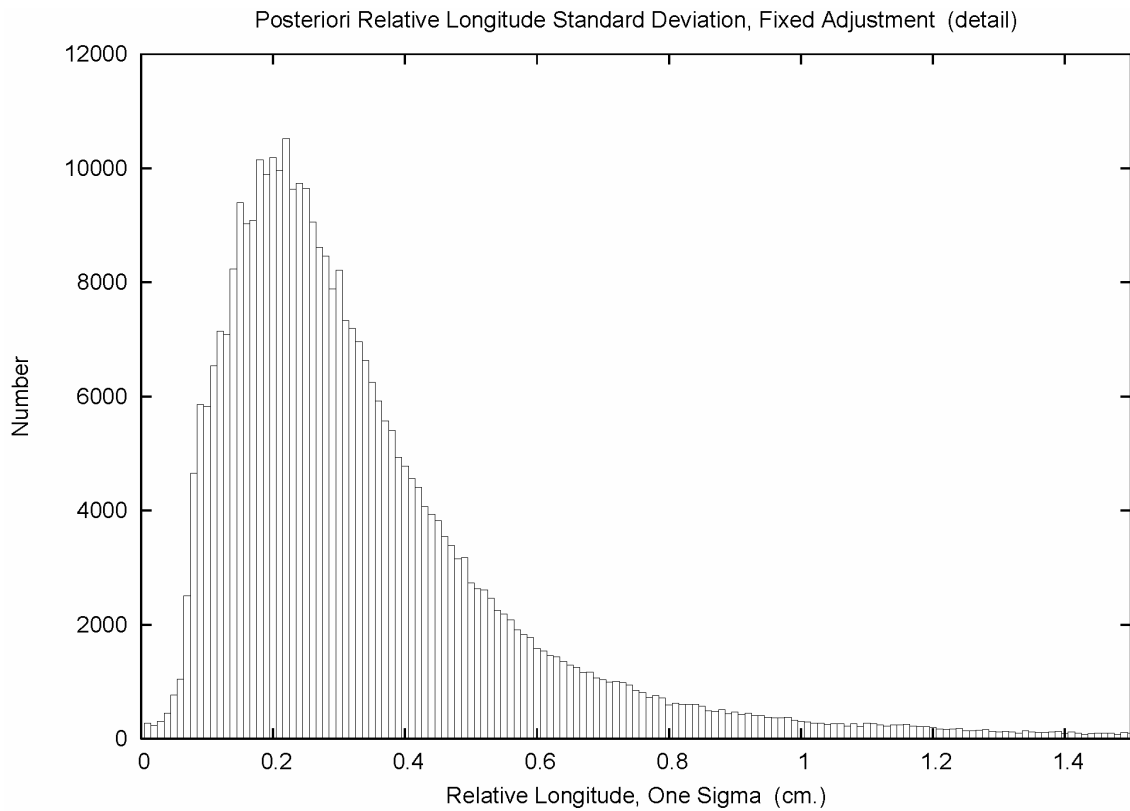
Figure 24.4. Relative longitude standard deviation distribution. 0.01 cm bin size.

Figure 24.5 portrays the histogram distribution of the relative height standard deviations with a 0.01 bin width. The maximum relative height standard deviation is 2.49 cm. The details of the relative height standard deviations are shown in Figure 24.6. The relative height standard deviations show a larger precision than their horizontal counterparts, with a median of 0.79 cm. This confirms behaviors often seen in geodetic analyses, where height precision is double that of the horizontal. And, once again, the relative height standard deviations in Figure 24.6 are seen to be smaller than the height standard deviations depicted in Figure 16.6.
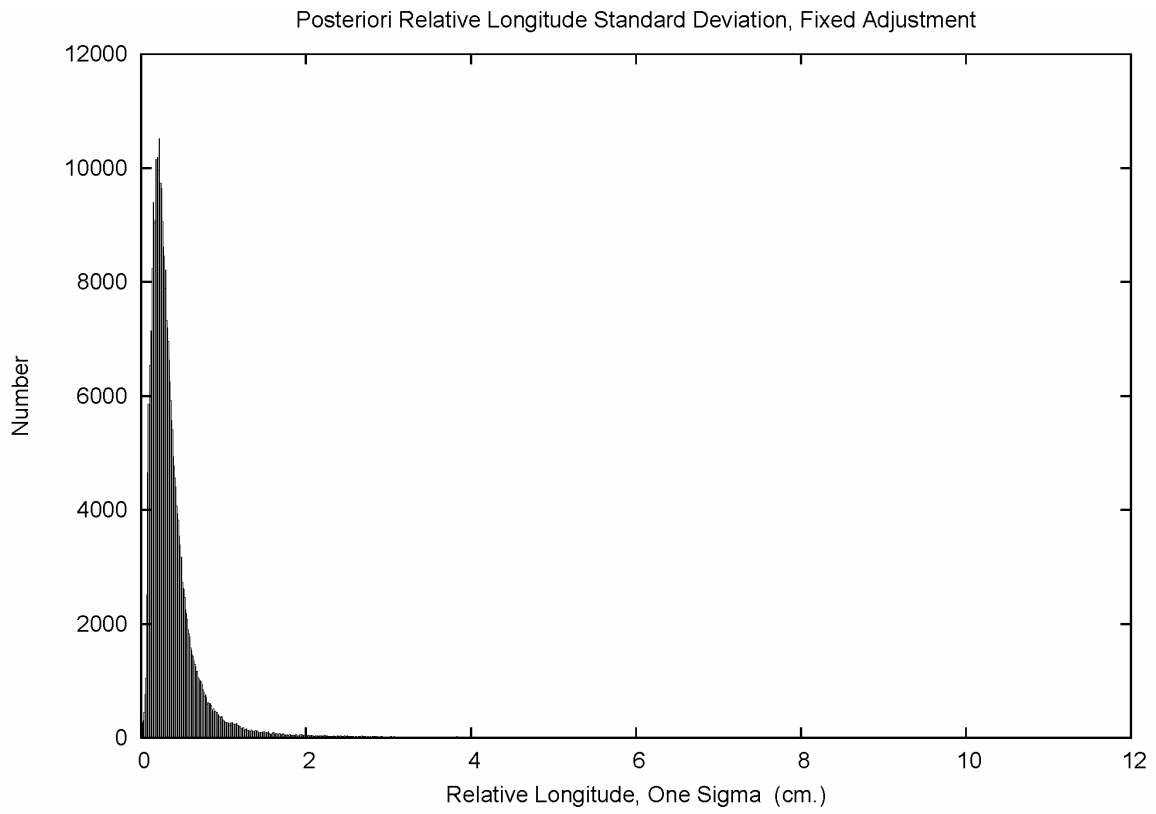

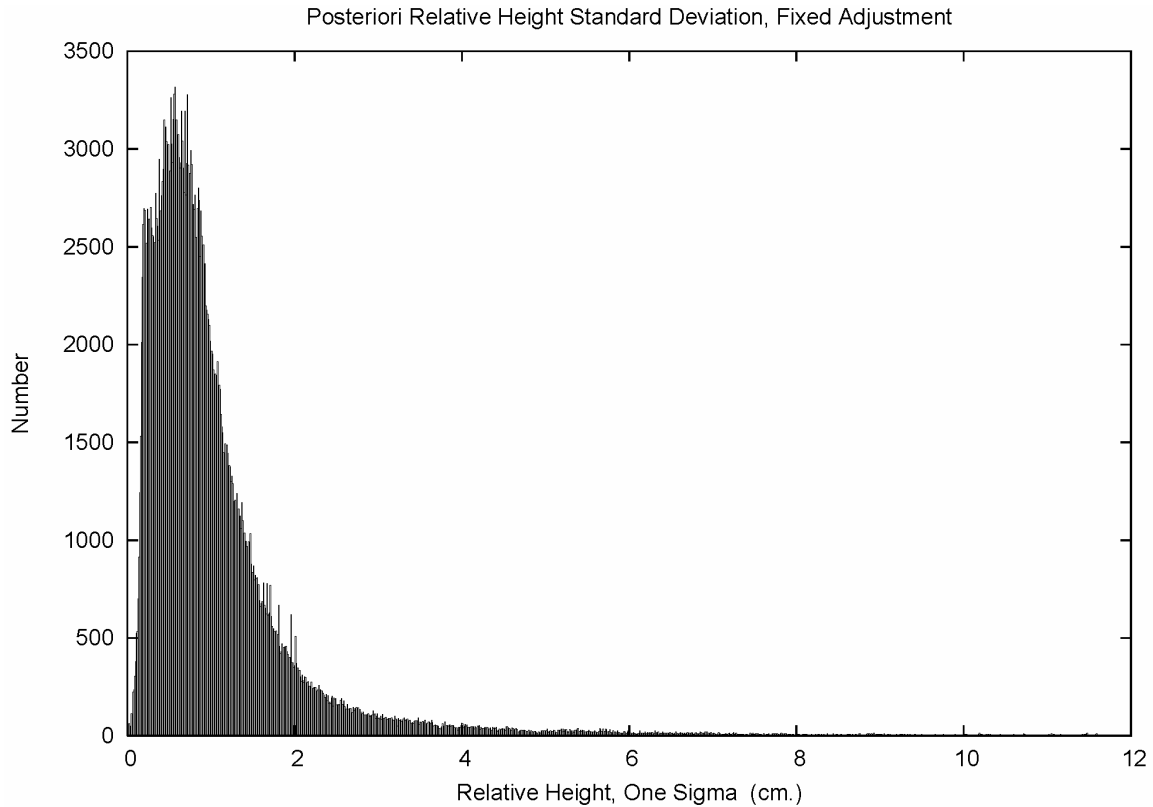Figure 24.5. Relative height standard deviation distribution. 0.01 cm bin size.
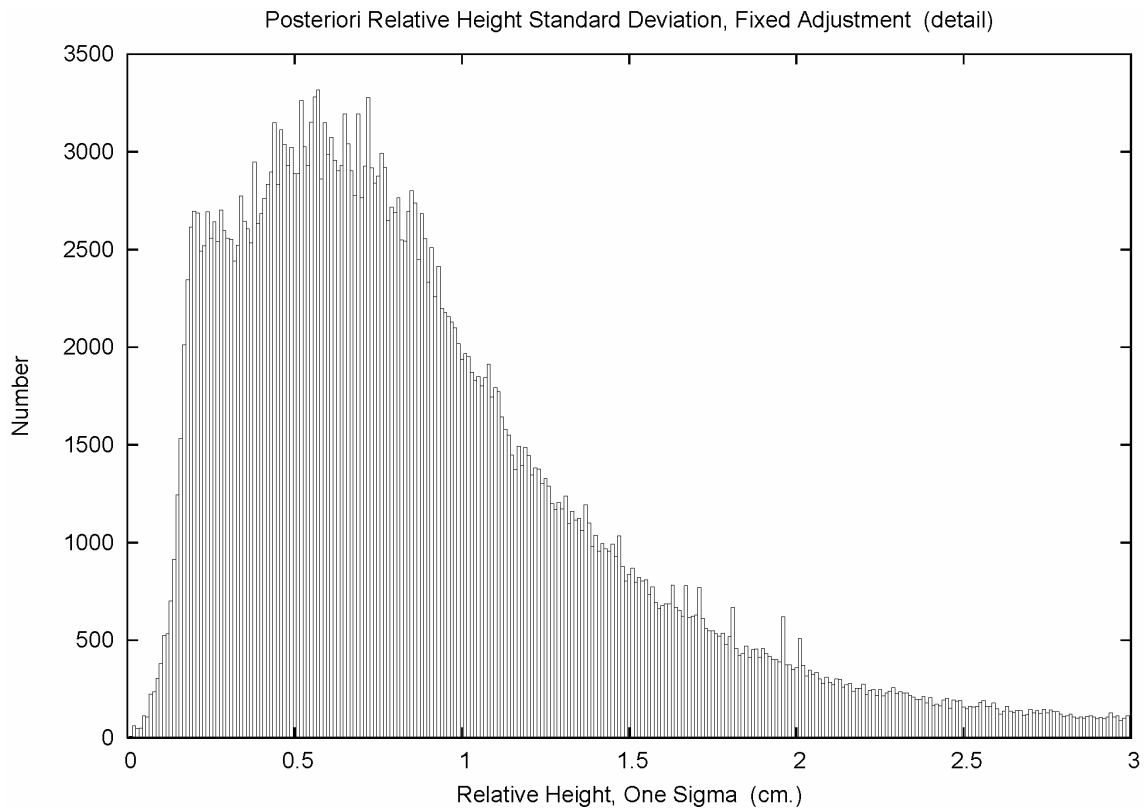
Figure 24.6. Relative height standard deviation distribution, detail. 0.01 cm bin size.

As a footnote, not all possible combinations of relative positions were computed in the NSRS 2007 adjustments. In general, the 368,163 relative relations collected above were computed between points that were connected by a GPS vector. Such a connection could be direct, or indirect through the presence of intervector correlations that arise from the rigorous reduction of GPS sessions of three or more receivers. However, certain relative relations were inadvertently generated as a result of the "rejection by downweighting" mechanic. This did not have a large impact on the statistics above. However, this issue is examined in more detail in Section 29.

In closing this section, the percentiles of the distributions are collected into Table 24.1. This emphasizes the marked similarities of latitude and longitude, and the larger magnitudes of the height dispersions. (Refer to laccfix.txt in the Electronic Support Material.) Comparison to the companion Table 16.1 for the position standard deviations shows the smaller values of the relative standard deviations. This reflects positive correlations in the position covariance matrix generated by the GPS vectors themselves.

Table 24.1 – Percentiles of Posteriori Relative Position Standard Deviations, Fixed Adj.

Percentile	Latitude (cm)	Longitude (cm)	Height (cm)
50%	0.34	0.28	0.79
68%	0.44	0.38	1.08
90%	0.74	0.70	2.00
95%	0.99	1.00	2.94
99%	2.52	3.15	7.48
99.9%	11.56	15.96	24.43
Extrema	485.54	495.05	249.00

25. Posteriori relative position horizontal correlation

This section addresses the correlation aspects of the relative latitude and relative longitude standard deviations. Figure 25.1 plots the relative horizontal correlations from the fixed adjustment with a bin width of 0.01.
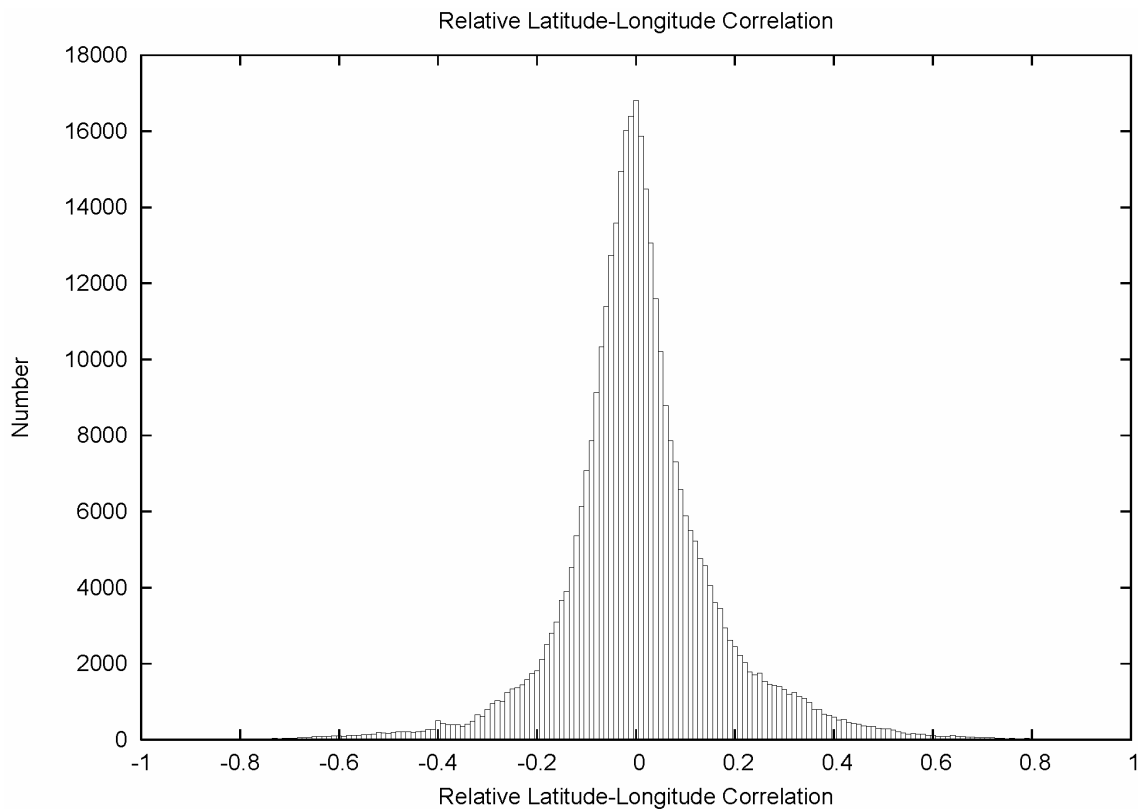
Figure 25.1. Relative latitude-longitude correlation distribution. 0.01 bin size.

One sees the same behavior in Figure 25.1 as for the horizontal positional correlation in Figure 17.1. Once again, the similarity of standard deviations in relative latitude and relative longitude coupled with the low magnitudes of correlation suggest that the horizontal relative error ellipses tend to be circular. The horizontal relative error ellipses were computed and the ratios of the semiminor/semimajor axes are

histogrammed in Figure 25.2 with a bin width of 0.01. The ratio ranges from 0 to 1, where 1 indicates perfect circularity.

Relative Semiminor/Semimajor Axes Ratio
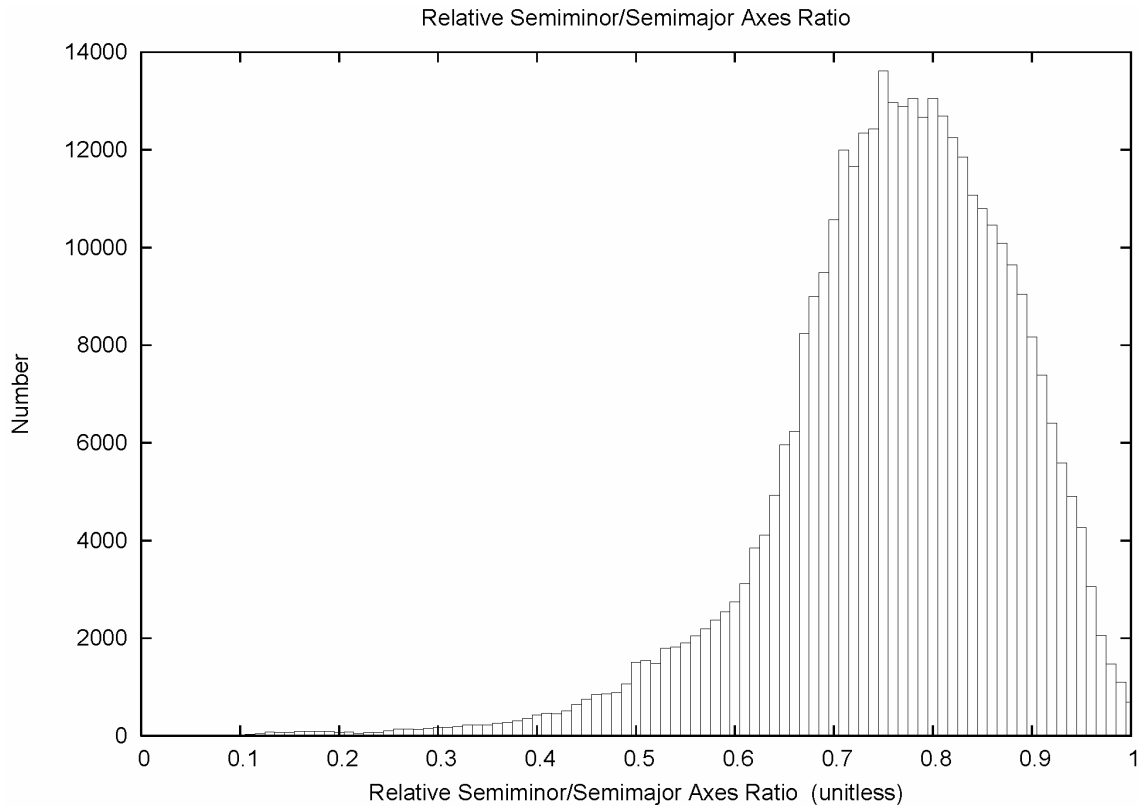
Figure 25.2. Ratio of semiminor/semimajor axes of horizontal relative error ellipse.

As seen in Figure 25.2, the magnitudes of the semiminor axes are in the vicinity of 80% of the semimajor axis. It is somewhat surprising that the distribution of circularity in Figure 25.2 so closely tracks the distribution of horizontal positional circularity plotted in Figure 17.2.

As performed for the horizontal error ellipses in Section 17, the distribution of azimuth of the semimajor axis of the horizontal relative error ellipses is displayed in Figure 25.3. The semimajor axis is aligned in a North-South direction. This is due to the GPS "hole" in the sky coverage to the North, as described in Section 17.
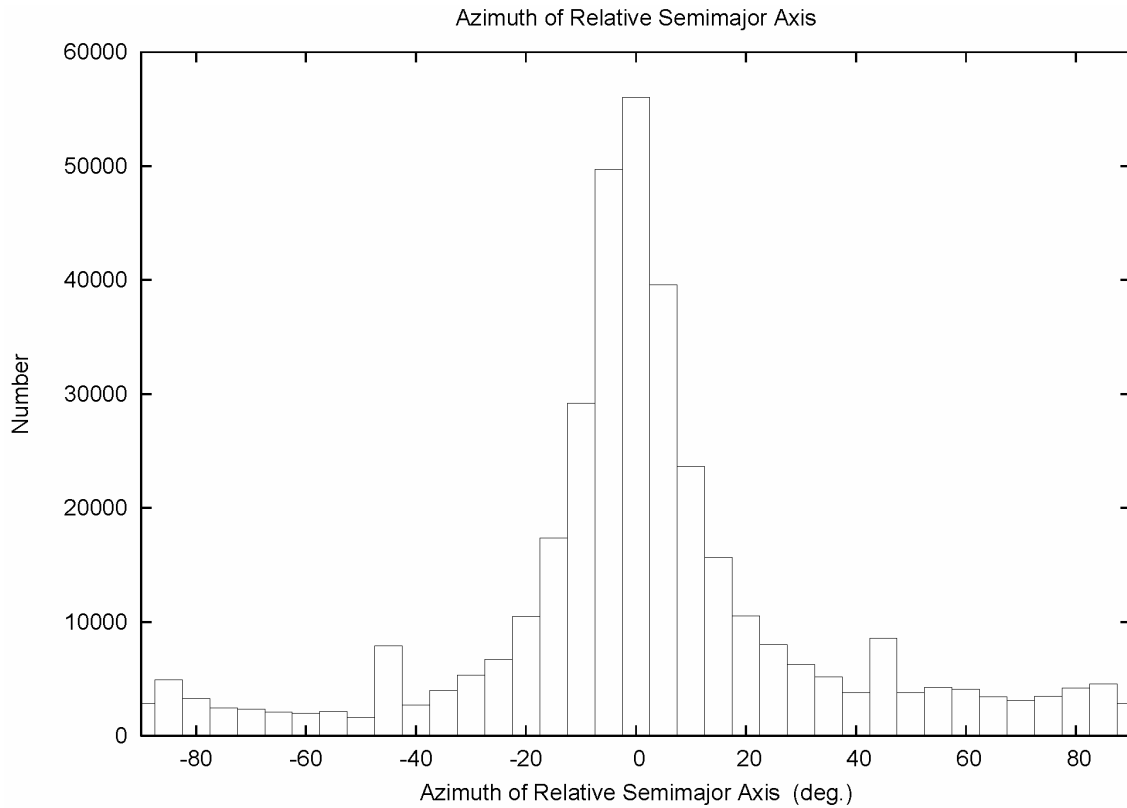
Figure 25.3. Azimuth of semimajor axis of horizontal relative error ellipse. 5 deg. bin.

One might notice slight peaks at +/- 45° in Figure 25.3. These are artifacts of the rounding associated with the fixed precision format used in the working files. The detailed description of this artifact may be found in the Appendix in Section A.25.

26. Posteriori relative position dispersion component ratios

The ratios of the *a posteriori* relative standard deviations from the final fixed adjustment are provided in this section. Note that when comparing these results to those of Section 18, the Section 18 ratios are from the final free adjustment. However, as seen the ratio comparison between free and fixed in Section 19, the fixed control caused only slight strengthening (skew to the right).

The ratio of relative height to relative latitude dispersion is plotted in Figure 26.1, with a detail view in Figure 26.2. The detail of the relative height to relative longitude dispersion is given in Figure 26.3. And the detail of relative latitude to relative longitude dispersion is given in Figure 26.4. The percentiles of the relative dispersion ratios from the fixed adjustment are collected in Table 26.1. (Refer to rats.txt in the Electronic Support Material.)

Figure 26.1. Ratio of relative height/latitude standard deviations.

Figure 26.2. Ratio of relative height/latitude standard deviations, detail.
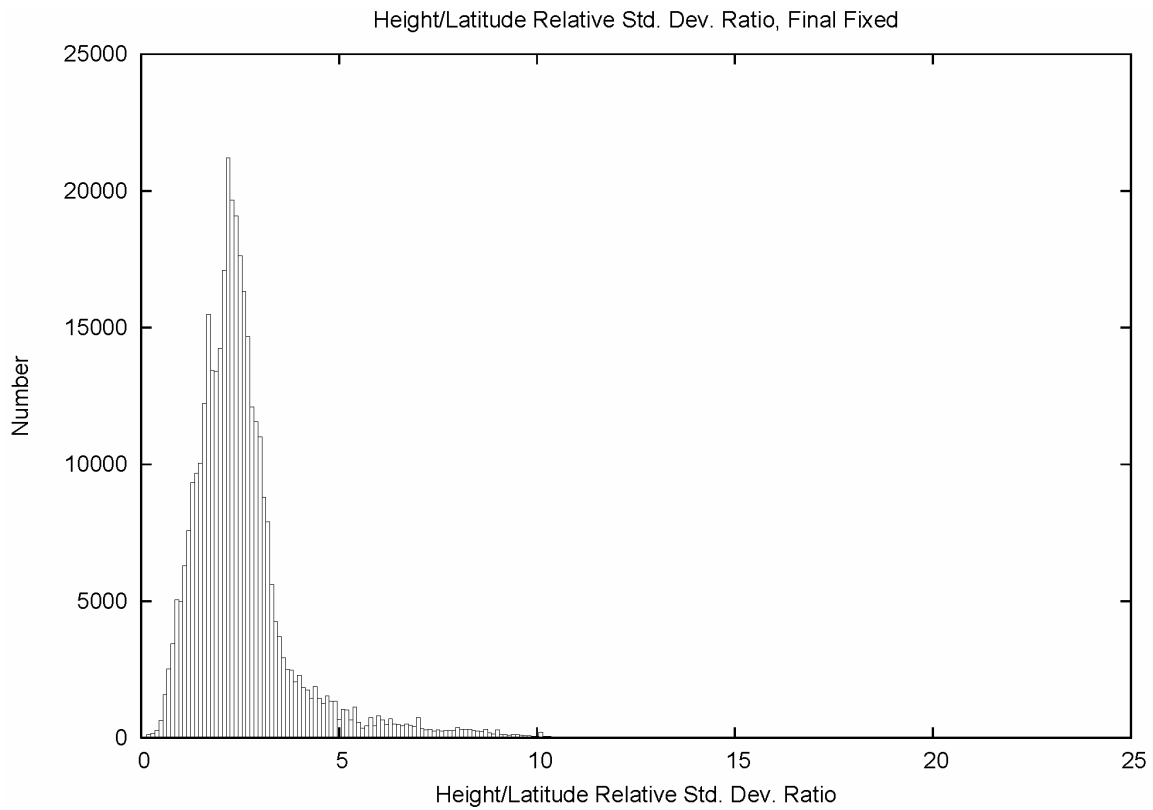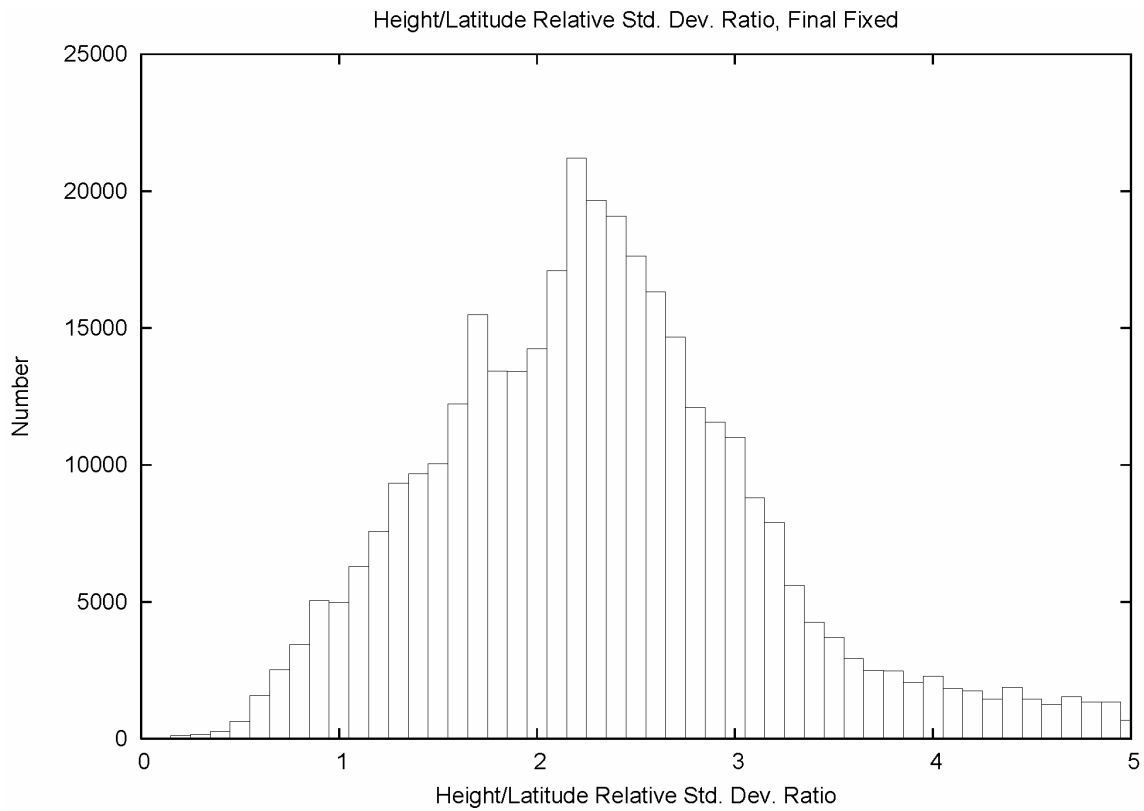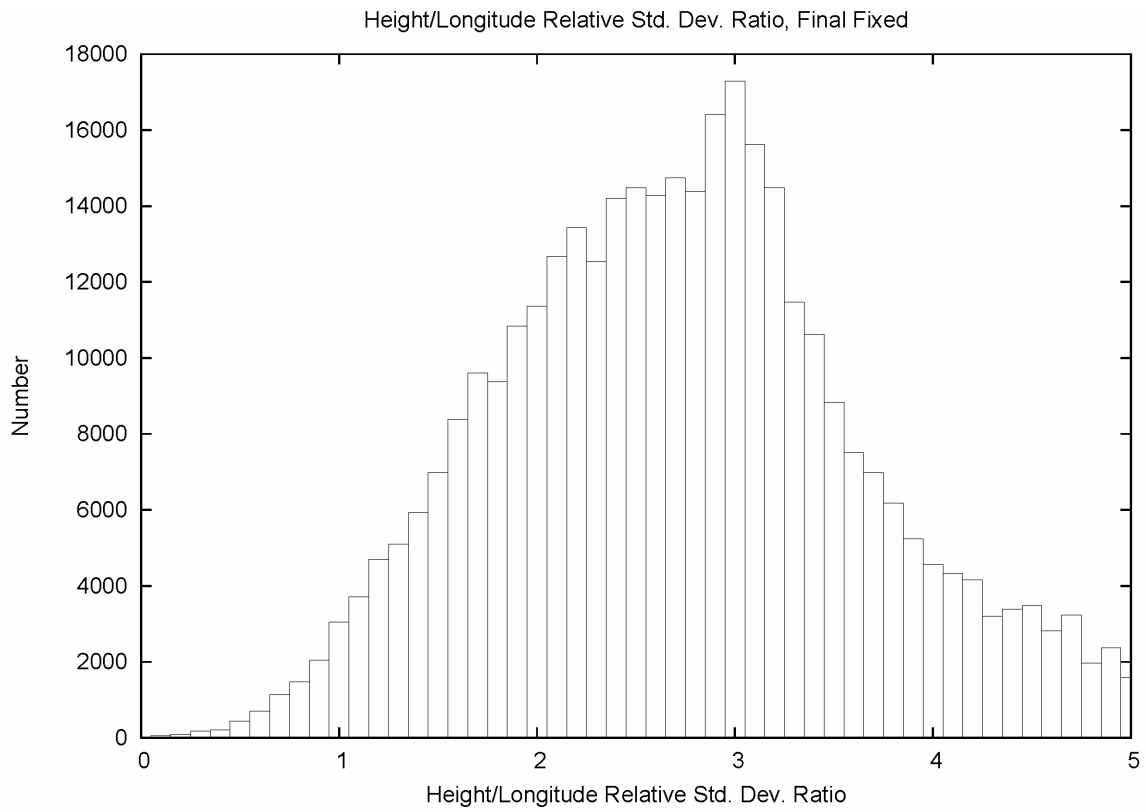
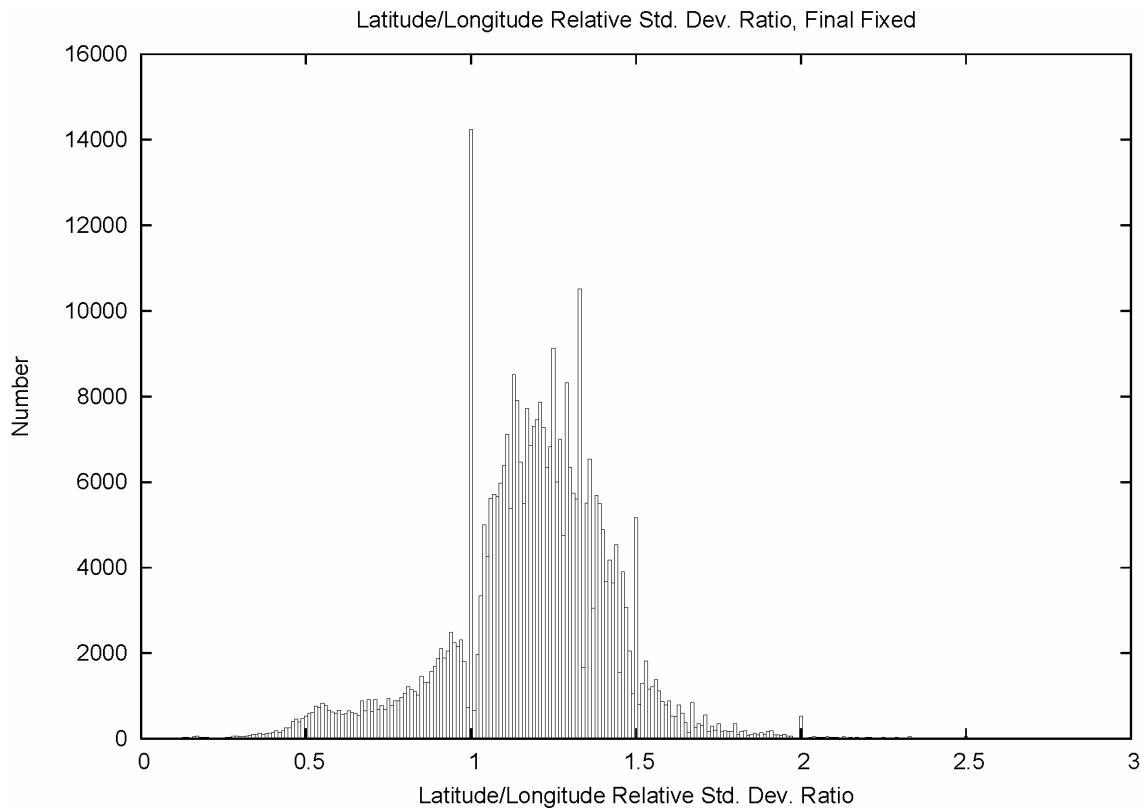Figure 26.3. Ratio of relative height/longitude standard deviations, detail.

Figure 26.4. Ratio of relative latitude/longitude standard deviations, detail.

Table 26.1 – Percentiles of Relative Position Standard Deviation Ratios, Fixed Adjust.

Percentile	Ht./Lat.	Ht./Lon.	Lat./Lon.
50%	2.33	2.77	1.20
68%	2.71	3.18	1.29
90%	3.96	4.30	1.46
95%	5.22	4.92	1.54
99%	8.35	7.31	1.86
99.9%	12.38	14.40	2.91

The medians of the relative height standard deviation to relative latitude and longitude are seen to be greater than 2, and greater than the associated position standard deviation ratios in Table 18.1. This would be expected due to the smoother character of positional error propagation statistics compared to relative error statistics.

The median ratio of 1.20 for the relative latitude/longitude shows a 20% differential. This is in good agreement with the 0.8 figure for the ratio of semiminor axis to semimajor axes of the horizontal relative error ellipse in Section 25. The relative latitude/longitude ratios of Table 26.1 very closely track the position latitude/longitude ratios of Table 18.1. And, as described in Section 18, the spike at the 1.0 bin of Figure 26.4 is an artifact related to the fixed number of digits carried in the working file.

27. Local accuracies of the NSRS 2007

Local accuracies represent uncertainty in the coordinates of a control point relative to the coordinates of other directly connected, adjacent control points at the 95% confidence level (FGDC 1998, Part 1, pg. 1-9).

Such relative error relationships are typically developed from formal error propagation processes.   These express horizontal relations through bi-normal Gaussian error distribution parameters. Leenhouts (1985) describes how to simply compute the radius of an error circle that encompasses 95% of the bi-normal probability distribution. Refer to the description in Section 20, and use horizontal relative error ellipse components in place of horizontal positional error ellipse components.

Figure 27.1 displays the distribution of the horizontal local accuracies of the NAD 83(NSRS2007) National Readjustment. Figure 27.2 shows the detail on the left. The maximum horizontal local accuracy is 13.48 meters.

Figure 27.1. Distribution of horizontal local accuracies. 0.01 cm bin size.

Figure 27.2. Distribution of horizontal local accuracies, detail. 0.01 cm bin size.

The distribution of horizontal local accuracies reflects the behavior seen in the relative latitude and longitude standard deviations of Figures 24.2 and 24.4. The spiky nature of the distribution is an artifact of bin size aliasing against the least count.

Vertical local accuracy is a single number representing the 95% probability distribution of a one-dimensional distribution. Figure 27.3 portrays the distribution of the vertical local accuracies of the NAD 83(NSRS2007) National Readjustment. Figure 27.4 shows the detail on the left. The maximum vertical local accuracy is 4.88 meters.
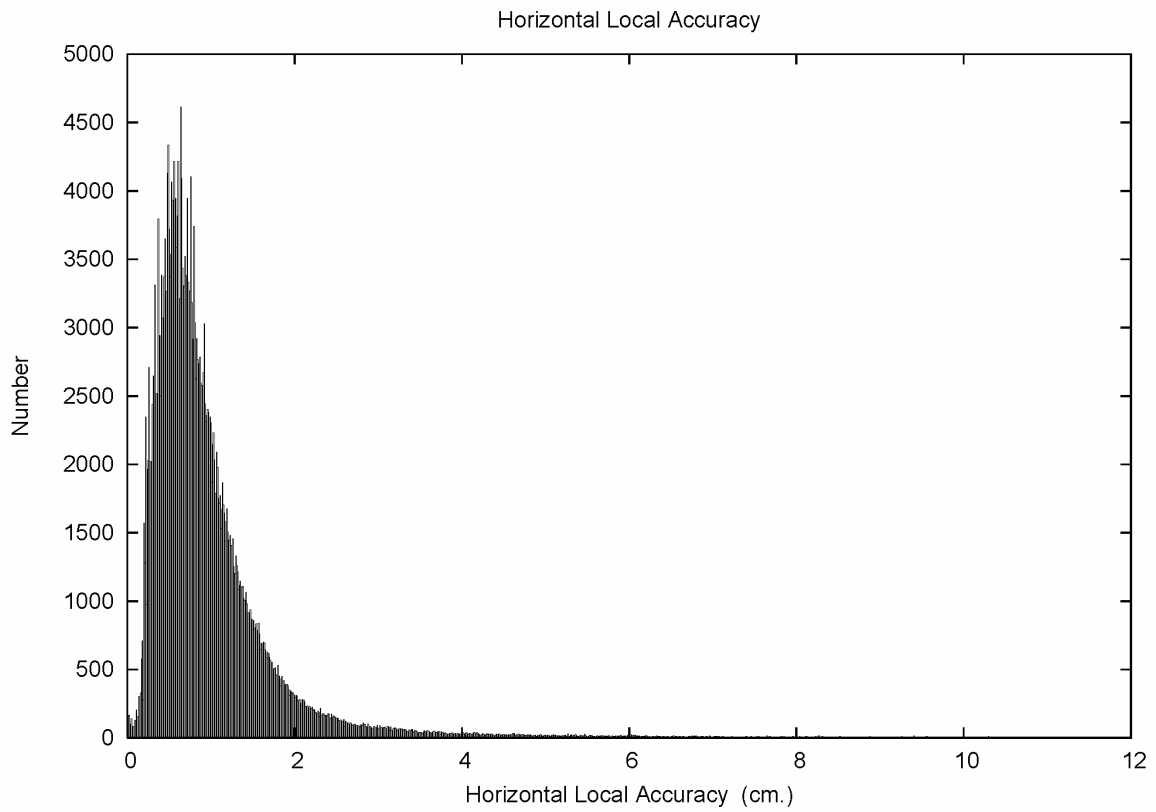

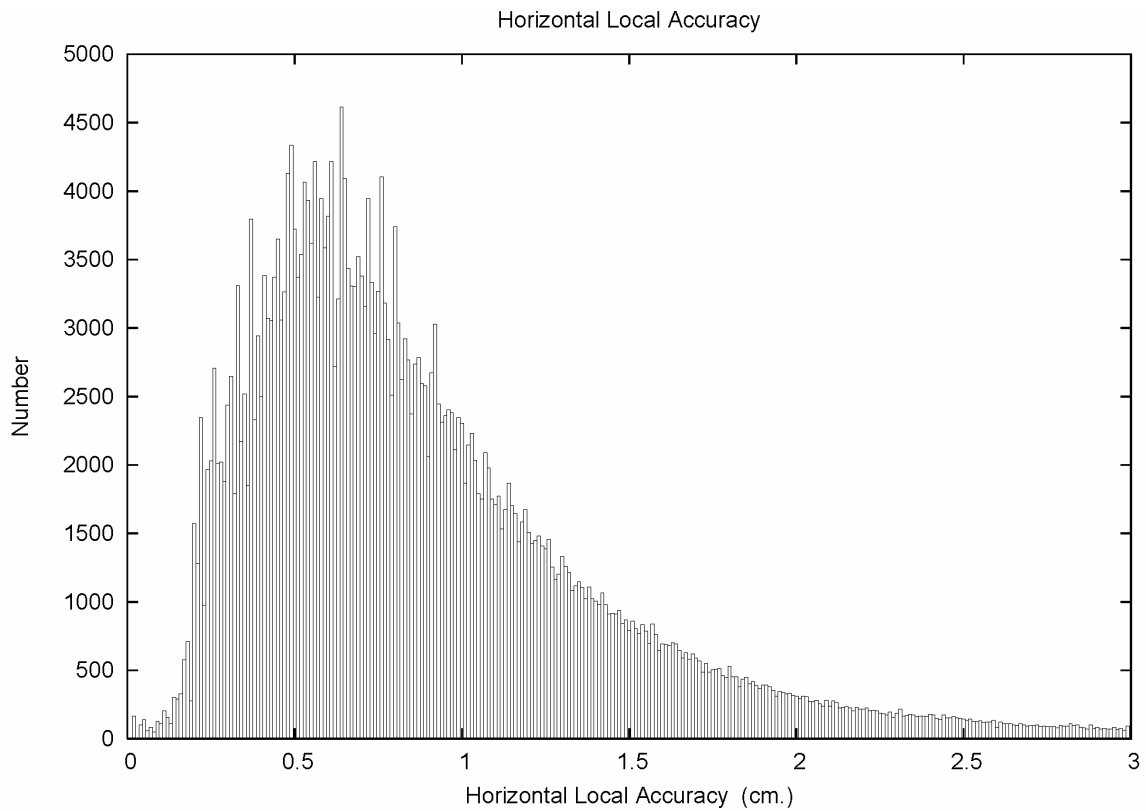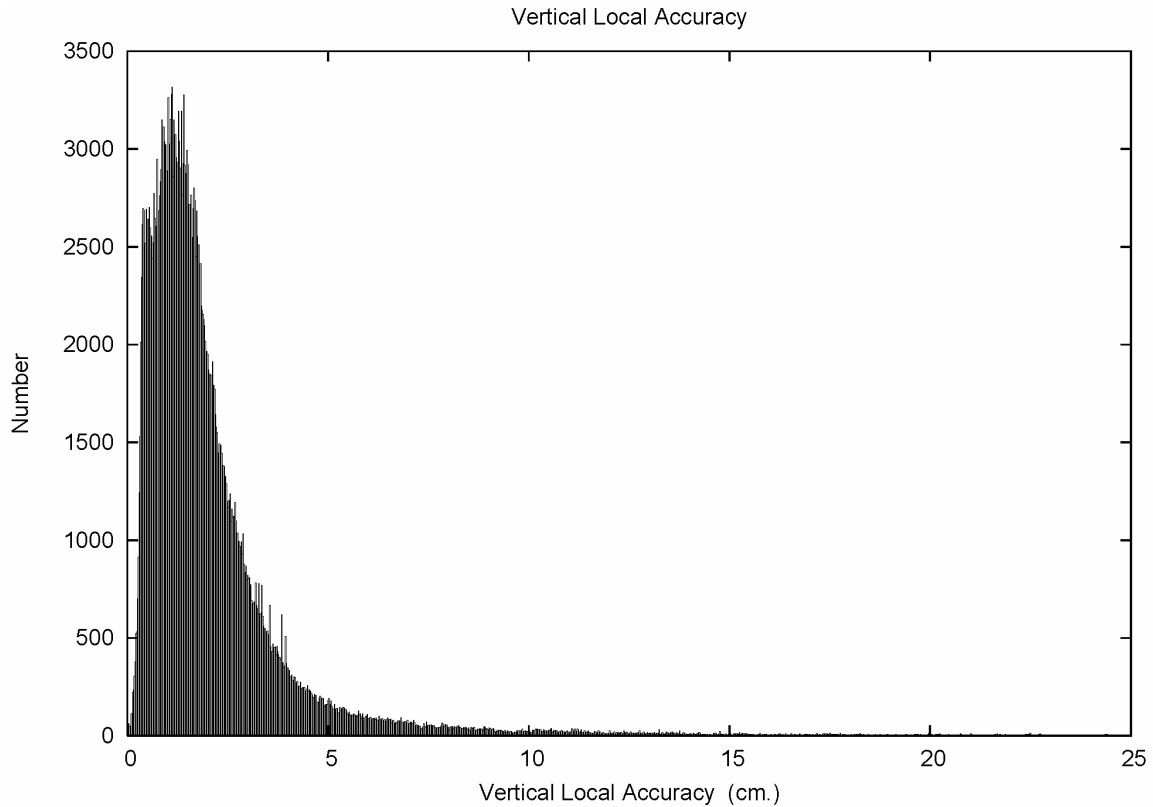Figure 27.3. Distribution of vertical local accuracies. 0.0196 cm bin size.
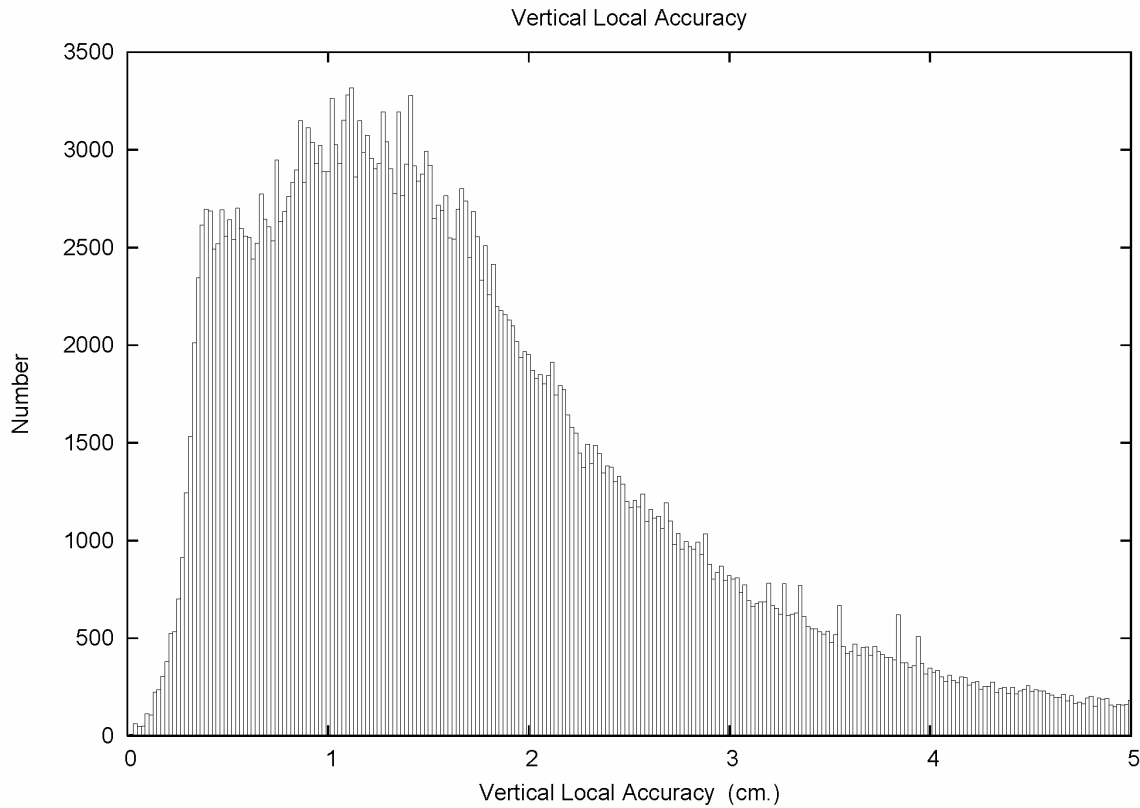
Figure 27.4. Distribution of vertical local accuracies, detail. 0.0196 cm bin size.

The distribution of vertical local accuracy seen in Figures 27.3 and 27.4 is a simple rescaling of the relative height standard deviations displayed by Figures 24.5 and 24.6. The 0.0196 cm bin size suppresses spikes in the histogram that would arise from a 0.02 cm bin size aliasing against the least count of the standard deviations output by the adjustment software. (Refer to laccfix.txt in the Electronic Support Material.)

The percentiles of the distributions of the local accuracies are collected in Table 27.1. The median 95% local accuracy of the NSRS is 0.8 cm horizontal and 1.6 cm vertical. The distributions contain long tails. However, the local accuracy tails are shorter than those seen for network accuracy in Table 20.1. This is expected, since the network will display error propagation of observational error. The 95% local accuracies seldom exceed 2.5 cm horizontal and 6 cm vertical.

Table 27.1 – Percentiles of Local Accuracies of the NAD 83(NSRS2007)

Percentile	Horizontal (cm)	Vertical (cm)
50%	0.78	1.55
68%	1.04	2.12
90%	1.80	3.92
95%	2.51	5.76
99%	7.33	14.66
99.9%	32.94	47.90

28. Length distributions of local accuracies of the NSRS 2007

This section analyzes local accuracies of the NSRS relative to vector length. This is a natural comparison. In the past, horizontal geodetic survey work accuracy was categorized by proportional measures (e.g. 1:10,000). Even the first draft GPS specifications (never adopted by the Federal Geodetic Control Committee) contained a proportional accuracy component (FGCS 1988).

Figure 28.1 shows a scatter plot of horizontal local accuracy relative to the vector length for each individual accuracy. The ranges of the plot reflect the maximum horizontal local accuracy of 13.48 meters, and the maximum vector length of 5217 km.
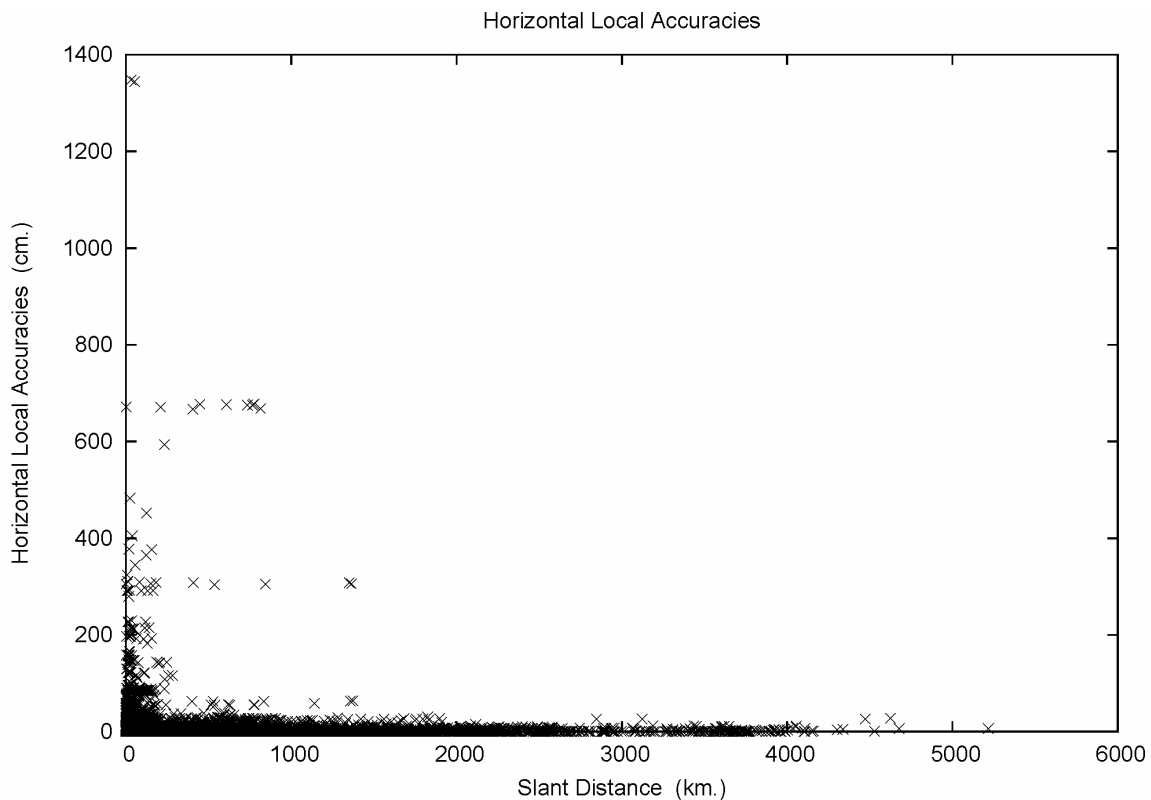
Figure 28.1. Length distribution of horizontal local accuracies.

No obvious length dependence is present in Figure 28.1. Outliers are evident, some as horizontal lineations. The lineations appear related to particularly weak projects with long lines. To gain a better view, detail is presented in Figure 28.2.
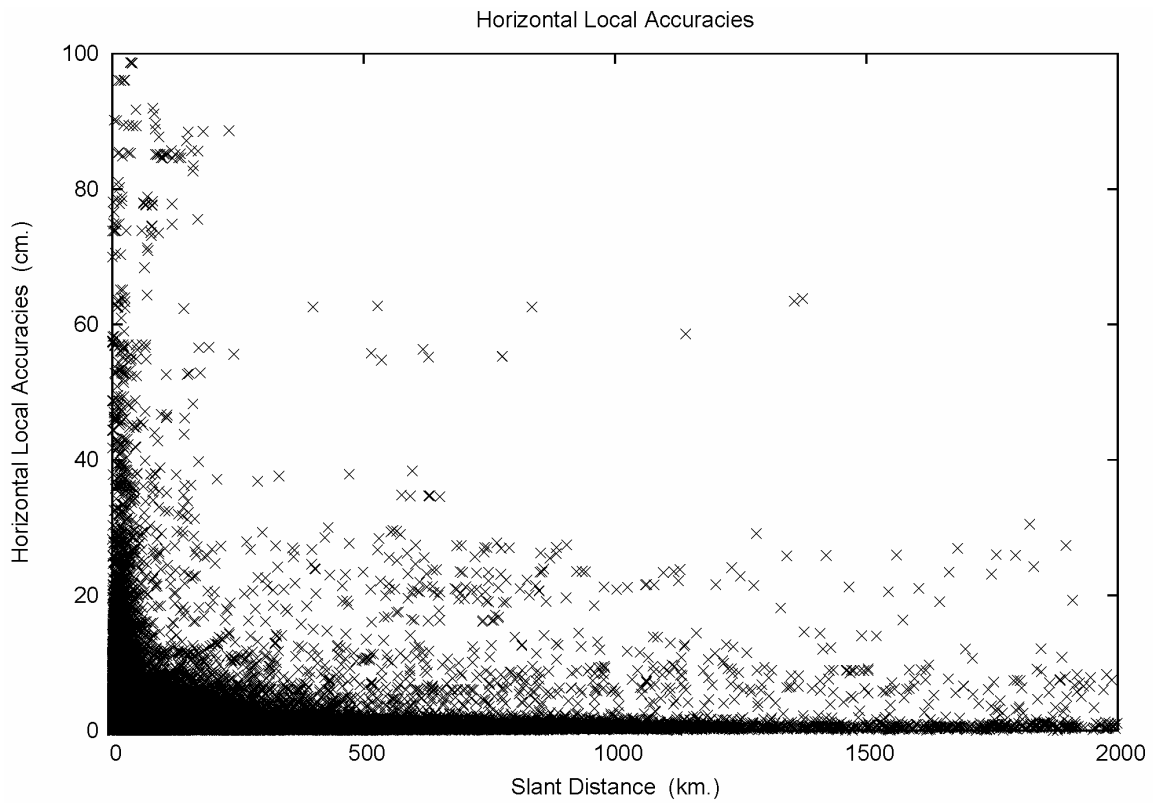
Figure 28.2. Length distribution of horizontal local accuracies, detail.

Even at the detail view of Figure 28.2, no proportional error is discernable. Of interest, it does seem that good local accuracies can be obtained from very long lines. To further pursue this point, additional detail views are presented in Figures 28.3 and 28.4.
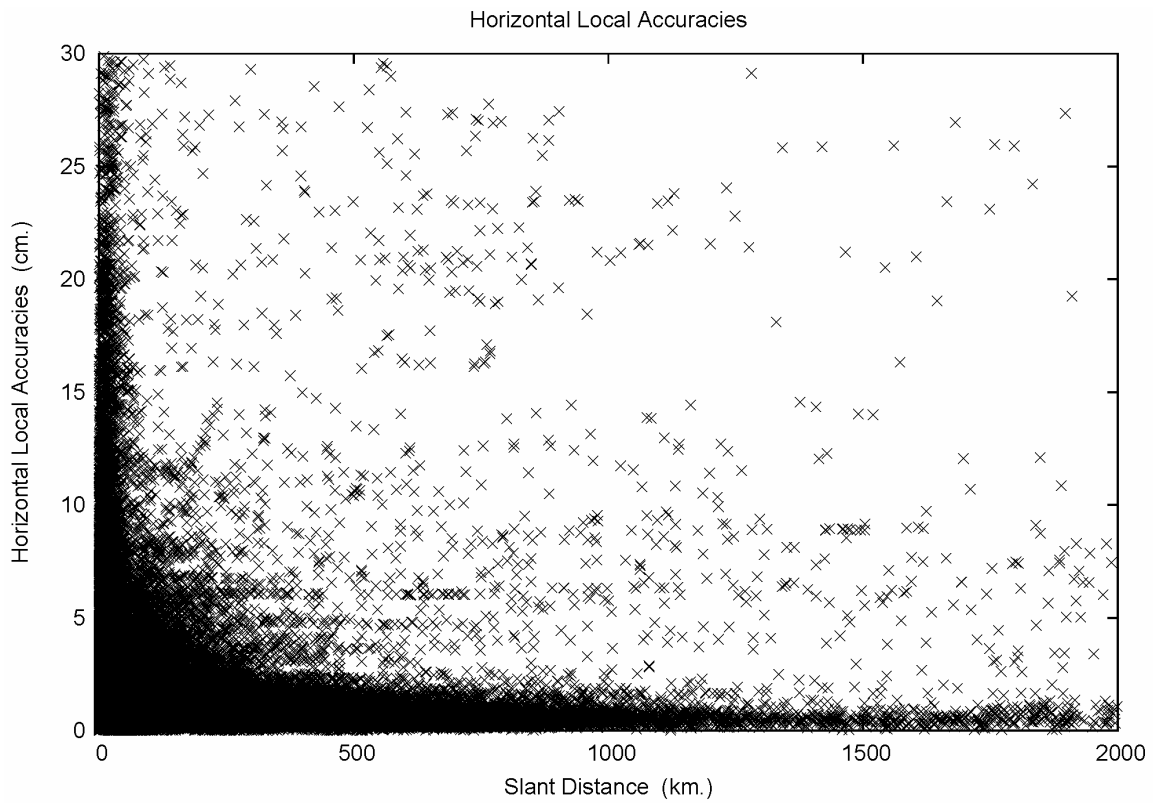
Figure 28.3. Length distribution of horizontal local accuracies, detail 2.
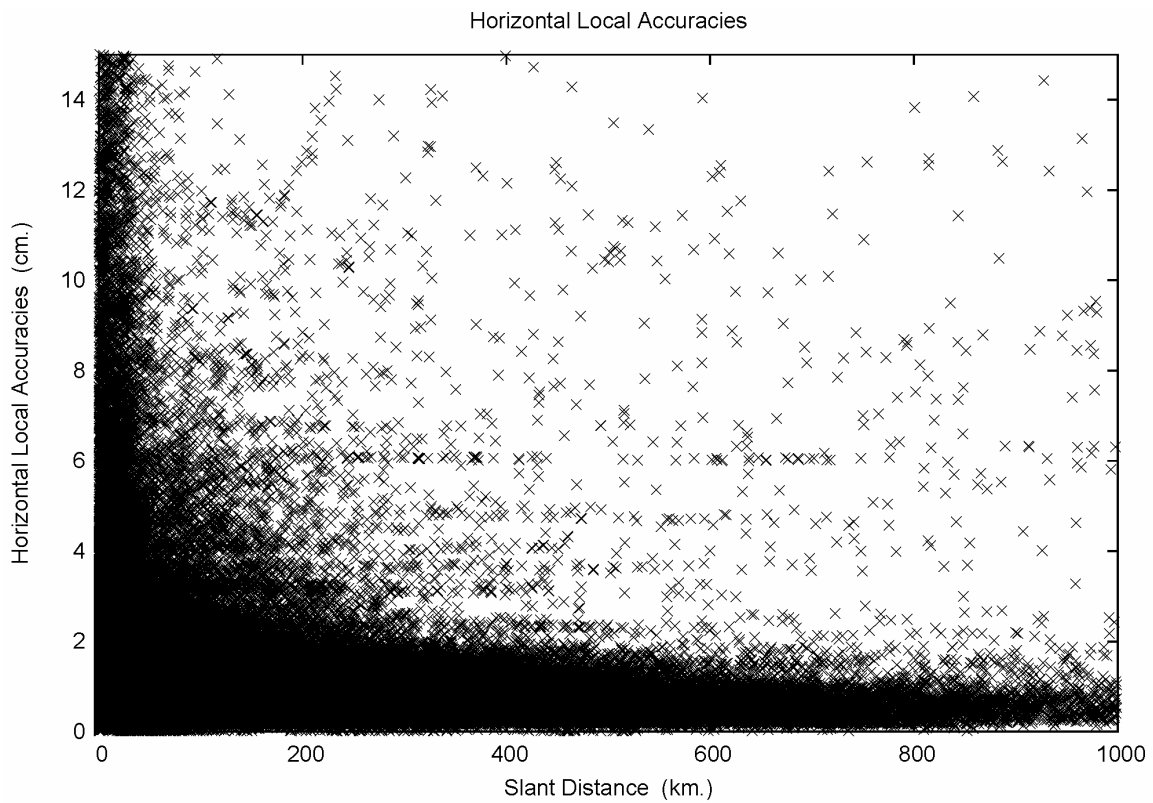
Figure 28.4. Length distribution of horizontal local accuracies, detail 3.

Some horizontal lineations appear in Figure 28.3 and 28.4. As with the outliers of Figure 28.1, they appear associated with particular projects that have a number of long lines. Once again, it must be emphasized, there is no proportional error behavior. Inspect Figure 28.4, and recall that 10 cm over 1000 km is 1 part in 10,000,000. Such an "A Order" error behavior would be clearly evident on the plot.

The quasi-hyperbolic appearance of the scatter plots of horizontal local accuracy is principally due to the very large number of small local accuracies over a variety of line lengths. And, there are fewer local accuracies with larger magnitudes. In essence, the scatter plot is showing a histogram-like view of local accuracies as seen in Figure 27.2, but with the X and Y axes reversed. This only further emphasizes the absence of length dependence. A final level of detail is provided in Figure 28.5.
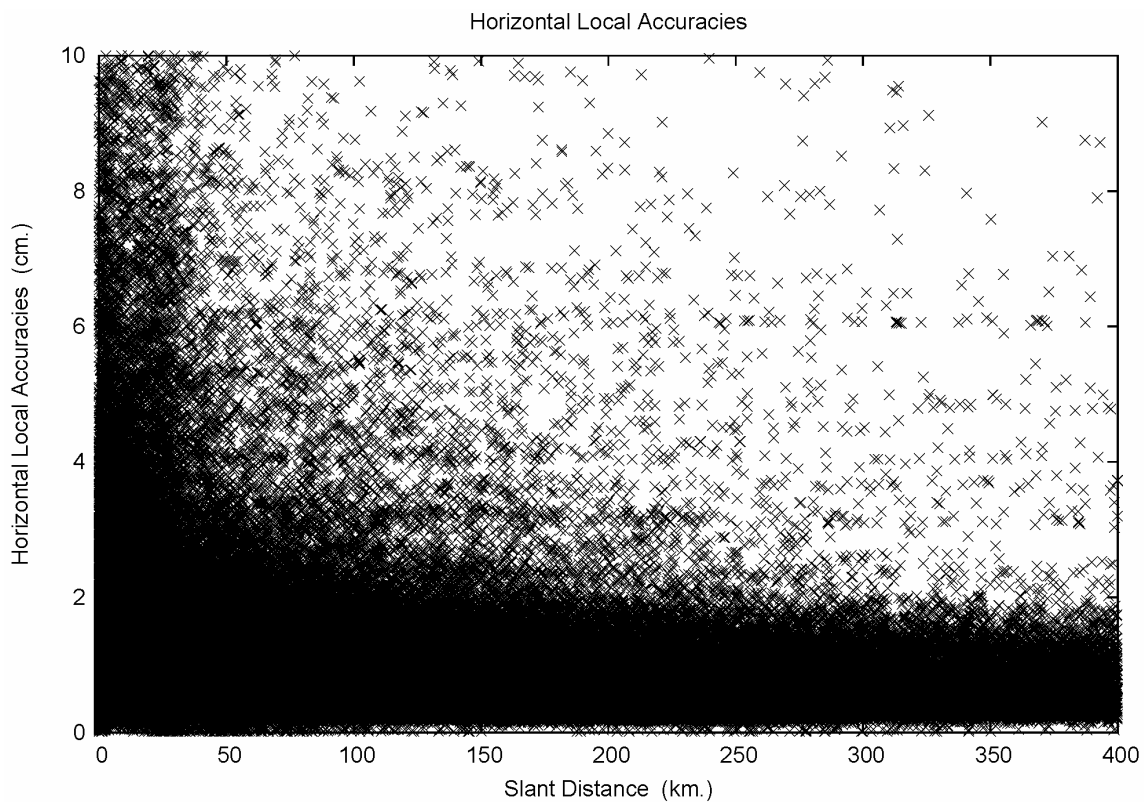
Figure 28.5. Length distribution of horizontal local accuracies, detail 4.

In the interests of concision, Figures A.28.6-A.28.10, portraying length distributions of vertical local accuracies, can be found in the Appendix. The character of these vertical local accuracy scatter plots is identical to the horizontal local accuracy plots depicted above. No length dependence can be seen.

The absence of length dependent error in GPS vectors at the length scales depicted above has been known for some time, and can be traced to use of GPS orbits of comparable accuracy, dual frequency receivers to remove ionosphere, and long-line carrier phase ambiguity resolution (Blewitt 1989). The length invariance of GPS

positioning, coupled with the smoothing seen in local accuracies when combined into a geodetic network, lead to the recommendation (FGCS 1995) of length-free accuracy measures in the current standards (FGDC 1998).

29. Diagnostic tests of local accuracy magnitudes

By special request, additional analysis was performed on the behavior of the local accuracies and of the *92* relative error records described in Pursell *et al*. (2008).

The general magnitudes of the local accuracies in Section 27 compare well with the network accuracies in Section 20. The contents of Table 20.1 and Table 27.1 are joined to form Table 29.1.

Table 29.1 – Percentiles of Network and Local Accuracies of the NAD 83(NSRS2007)

Percentile	Network Horizontal (cm)	Network Vertical (cm)	Local Horizontal (cm)	Local Vertical (cm)
50%	1.03	1.84	0.78	1.55
68%	1.41	2.63	1.04	2.12
90%	2.57	5.17	1.80	3.92
95%	3.81	7.60	2.51	5.76
99%	12.80	21.66	7.33	14.66
99.9%	73.85	64.25	32.94	47.90

One naturally may expect smaller local accuracies when compared to network accuracies. This is because the local accuracies capture the correlations created by observations between points (i.e. "directly connected"); whereas network accuracies quantify the positional accuracy, and relative relationships between a given point and the fixed control.

To inspect these magnitudes at a point level is more difficult. Local accuracies are relative accuracies, and express a binary relationship (between two points). Network accuracies are relative to a point and the fixed control. But, since one side of that relationship is invariant (identically zero), the network accuracies are unary. Because of the relational character of local accuracies, one may see very large and very small values in a list at a given station. These would reflect very loose and very precise measurements to or from that given station.

However, limits of local accuracy magnitudes can be detailed. Without loss of generality, only consider height standard deviations, σ, and the height component, h:

$$\Delta h = h_2 - h_1 \tag{29-1}$$

$$\sigma_{\Delta h} = (\sigma_{h1}^2 + \sigma_{h2}^2 - 2\, \sigma_{h12})^{1/2} \tag{29-2}$$

Assume a measurement will induce a positive correlation between points 1 and 2. So that

$$\sigma_{h12} \geq 0.0 \tag{29-3}$$

The assumption produces a bound

$$\sigma_{\Delta h} \leq (\sigma_{h1}{}^2 + \sigma_{h2}{}^2)^{1/2} \tag{29-4}$$

or, in ratio form

$$\sigma_{\Delta h} / (\sigma_{h1}{}^2 + \sigma_{h2}{}^2)^{1/2} \leq 1.0 \tag{29-5}$$

So, for local and network vertical accuracy, la_h and na_h, respectively:

$$la_{\Delta h} / (na_{h1}{}^2 + na_{h2}{}^2)^{1/2} \leq 1.0 \tag{29-6}$$

Then, 368158 local accuracies were extracted and the size ratio on the left hand side of Equation 29-6 was computed for both horizontal and vertical. (Refer to lasize2.txt in the Electronic Support Material.) A limit tolerance of 0.05 cm was imposed on the elements of the ratio computation to suppress the artifacts caused by rounding when using working files with a fixed precision format. The histogram distribution of the size ratios is portrayed in Figure 29.1. The maximum size ratio is 2.11. The horizontal local accuracy size ratios are detailed in Figure 29.2.

Figure 29.1. Horizontal local accuracy size test ratios.
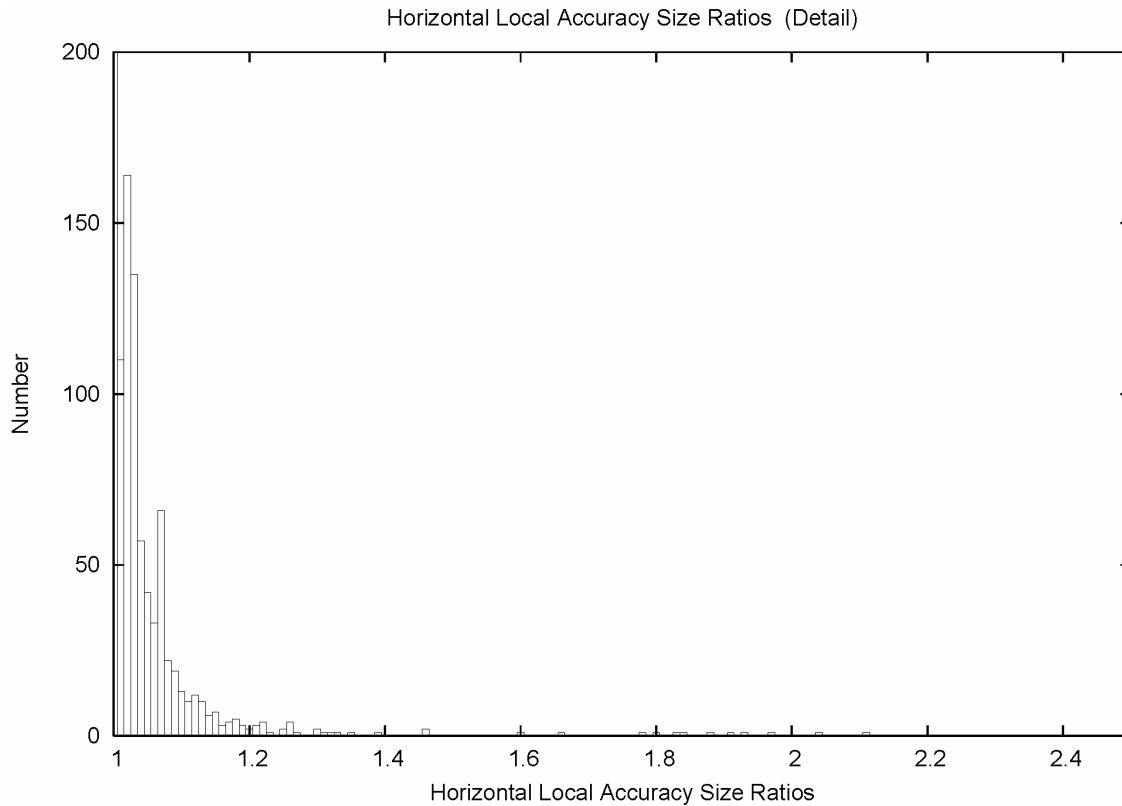
Figure 29.2. Horizontal local accuracy size test ratios, detail.

The figures show that the magnitudes of individual local accuracies do correspond to their parent network accuracies. Of interest, is that a large number of measured point relations do not have a high correlation. In fact, over a quarter of the measured network lines have essentially no correlation whatsoever. This validates a number of aspects of the network and local accuracy computation procedure for geodetic surveys that is specified in the FGDC standards (FGDC 1998, Part 2, pg. 2-4).

The outliers to the right of the 1.0 bin in Figure 29.2 represent 759 instances where the local accuracy is expressing a negative correlation along a connected line. Further discussion of these outliers will be provided shortly.

Size ratios for the vertical local accuracies were computed analogously to the horizontal local accuracy size ratios. The histogram distribution of the vertical size ratios is portrayed in Figure 29.3. The maximum vertical size ratio is 1.21. The vertical local accuracy size ratios are detailed in Figure 29.4. That figure depicts 270 excessive ratios.
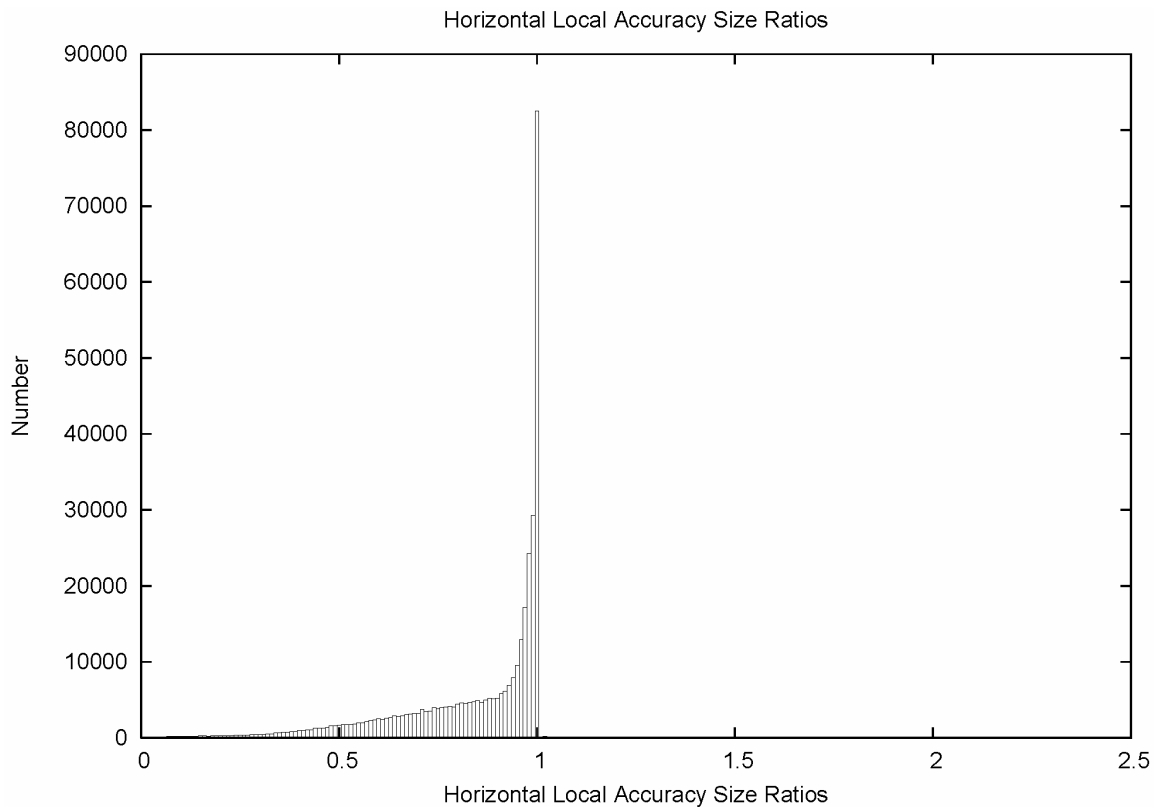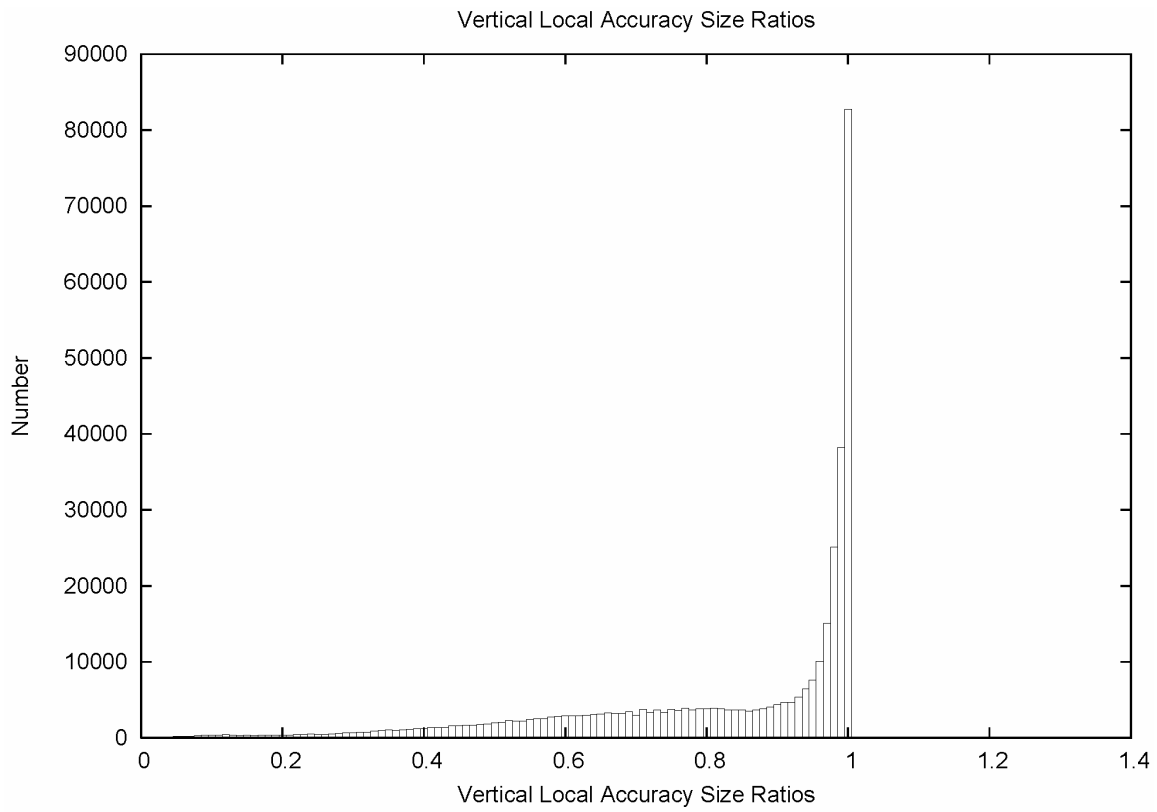
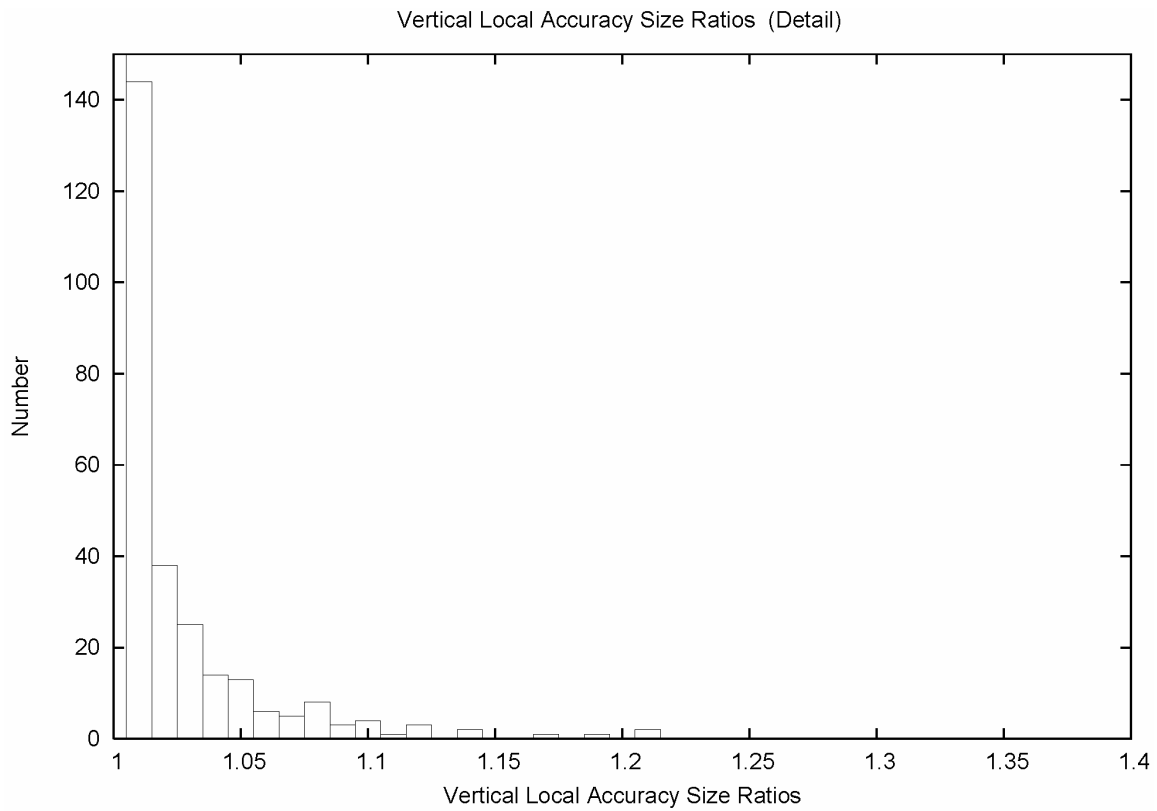Figure 29.3. Vertical local accuracy size test ratios.

Figure 29.4. Vertical local accuracy size test ratios, detail.

Deeper investigation of the local accuracy size ratios found that the offending lines either had a rejected observation between them, or the line endpoints were participants in a correlated GPS session that contained a rejected observation within it. Recall that a "rejection by downweighting" mechanic was used in the NSRS 2007 adjustment software. It is anticipated that if rigorous treatment of rejections is implemented, then the only local accuracy bound violations will be due to rounding caused by fixed precision formats.

30. Survey project dispersion scale factors

This section marks a transition from considering certain products of formal error propagation to the detailed inspection of categories of residuals. Such inspection is frequently called Analysis of Variance (ANOVA). While this analysis can be used to develop refined weighting models, it is used in this report for basic exploratory and diagnostic investigation. In this report, variance factors, and their square roots, are computed for survey projects. It will be seen that these statistics can be examined on a project basis, as well as collected into larger sets for analysis. Large values of these statistics can indicate problems at a group level, just as a large *a posteriori* variance of unit weight can indicate problems for the entire adjustment.

The methodology is to consider the general mixed model, where not only unknown parameters, x, are estimated, but where multiple variance components (variance factors), f_i, are also estimated. The observations can be partitioned into k groups, where each group has a variance factor,

$$\mathbf{D}_o = f_1 \mathbf{D}_1{}^0 + f_2 \mathbf{D}_2{}^0 + \ldots + f_k \mathbf{D}_k{}^0 \qquad (30\text{-}1)$$

Where $\mathbf{D}_o$ is the symmetric covariance (dispersion) matrix of the observations.

Due, in part, to computational feasibility, the Iterated Almost Unbiased Estimator (IAUE) is selected to compute the variance factors (Förstner 1979a, Förstner 1979b, Lucas 1985). The IAUE estimator for the k-th variance factor is

$$f_k = (v^t \mathbf{D}_o{}^{-1} v)_k / \text{tr}(\mathbf{Q}_k) \qquad (30\text{-}2)$$

where $\mathbf{Q}$ is the redundancy matrix (El-Hakim 1981, Förstner 1979c), and

$$\mathbf{Q} = \mathbf{D}_v \mathbf{D}_o{}^{-1} \qquad (30\text{-}3)$$

where for the full redundancy matrix, $\text{tr}(\mathbf{Q}) = n - u = df$, the degrees of freedom. For the purposes of this report, we define dispersion scale factors, d_k, as

$$d_k = (f_k)^{1/2} \qquad . \qquad (30\text{-}4)$$

Despite the forbidding character of the formal definition of the redundancy matrix (Eq. 30-3), Lucas (1985) shows that the diagonal elements of **Q** can be computed in a sparse matrix context, and Milbert (1985) provides an alternative form of the redundancy matrix (central redundancy) that is efficient for correlated observations. And, IAUE estimation is a standard option available in program ADJUST (Milbert and Kass 1987).

Other, more elaborate estimators exist for variance component estimation. However, it has been shown that IAUE, at convergence, is identical to the iterated forms of other estimators, such as MINQUE. Hence, one may speak of IAUE as being unbiased at convergence. This makes IAUE particularly alluring due to its low computational load. For a recent study of variance component estimation, the report (Amiri-Simkooei 2007) is recommended.

One immediately notes that the IAUE variance factor estimate, f_k, (Eq. 30-2) is identical to the *a posteriori* variance of unit weight, when k equals 1. That is, the *a posteriori* variance of unit weight can be considered a global variance factor. And, when multiple variance factors are estimated, they could be considered local variances of unit weight. By the same token, the dispersion scale factors, d_k, (Eq. 30-4) may be considered local standard deviations of unit weight. Thus, just as one can use the standard deviation of unit weight to diagnose the overall quality of an adjustment, one may also use local statistics, such as the dispersion scale factor, d_k, to gain a finer look.

The operation of the adjustment program used for NSRS 2007 differs from ADJUST in a number of ways. One detail is that the NSRS 2007 adjustment formed the weighted variance sums, $(v^t \mathbf{D}_o^{-1} v)_k$, with an *a posteriori* observation covariance matrix. Because of this detail, a global variance factor will not match the *a posteriori* variance of unit weight of the adjustment. Instead, such a global variance factor will be 1.0. And, sets of local variance factors (local variances of unit weight) will also tend towards 1.0, instead of tending towards the *a posteriori* variance of unit weight of the adjustment. In essence, if one uses weighted variance sums with an *a posteriori* observation covariance matrix to form variance factor estimates, f_k, then one obtains posteriori-posteriori variance factors. This behavior was evident in the NGS National Readjustment web page that collected summary statistics for free and fixed adjustment (www.ngs.noaa.gov/NationalReadjustment/StatusReports/Statistics.final/readjustment%2 0statistics%20final.html). One found "Variance" statistics for each Helmert block that tended to cluster around 1.0, while the "Total" reported values of the *a posteriori* variances of unit weight of the free and fixed adjustments, 1.63 and 1.89 respectively. It is hoped that the summary statistics web page will be updated someday.

When interpreting the dispersion scale factors, d_k, it should be remembered that most First Order or lower projects were rescaled by the variance of unit weight and that most (3315 of 3558) of the projects went through horizontal and vertical weight rescaling prior to the National Readjustment (Pursell *et al.* 2008). The rescaling was done on a project-by-project basis (Section 15). The principal effect to be expected, when looking at the dispersion scale factors, is to highlight errors that appear when projects are joined

into networks. This expectation must be tempered by the fact that outliers were not completely cleared in the free adjustment analysis (Sections 7, 10, 11, and 13).

The numerators and denominators of Equation 30-2 were accumulated for the horizontal, vertical, and three-dimensional (total) components as a post-processing step for all 3558 projects in the NSRS 2007 final free adjustment. Then, by Equations 30-2 and 30-4, 3550 project dispersion scale factors, d_k, were computed. (Refer to proid3.txt and nproid3.txt in the Electronic Support Material. Eight projects are no-check projects.) In 147 cases, projects were split in the creation of Helmert blocks. In these sections, the project counts treat these cases as distinct projects. Note that the expected value of the dispersion scale factors will be 1.0, per the discussion above. The histogram of the project dispersion scale factors is plotted in Figure 30.1. The maximum d_k is 10.649. The detail of the project dispersion scale factors is shown in Figure 30.2 with a 0.01 bin width.
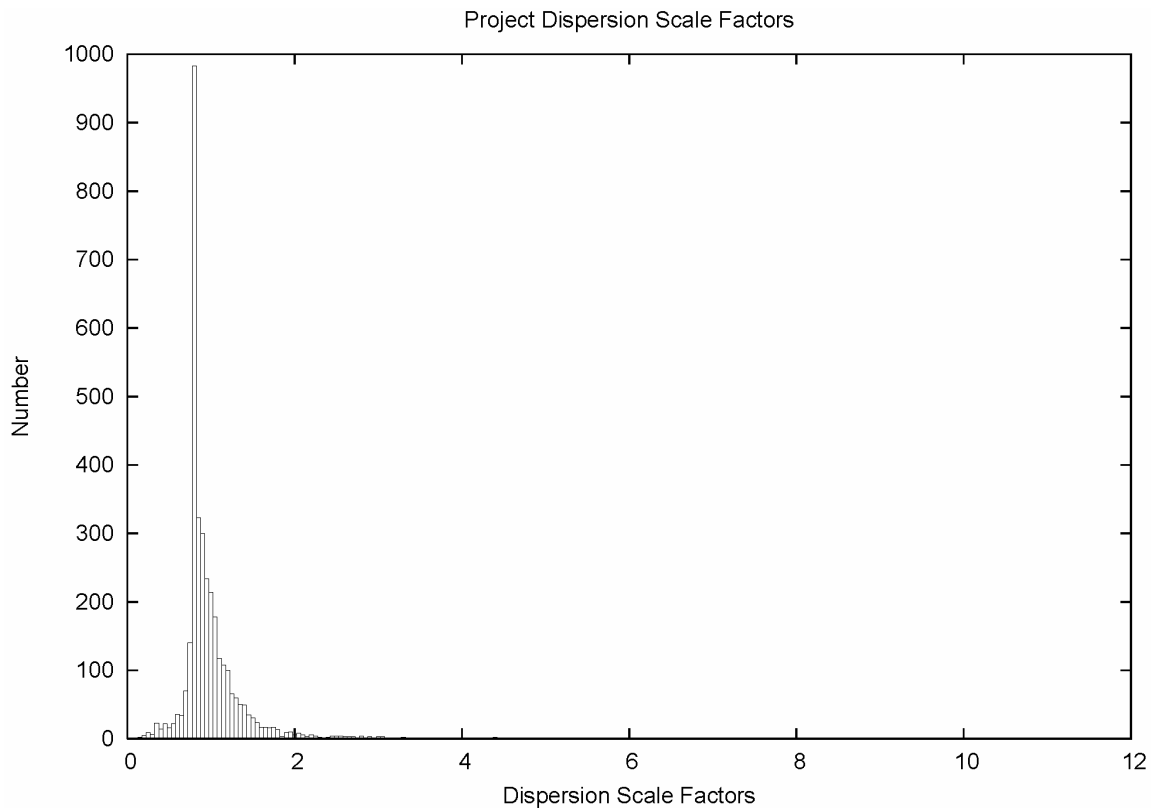
Figure 30.1. Project dispersion scale factors.

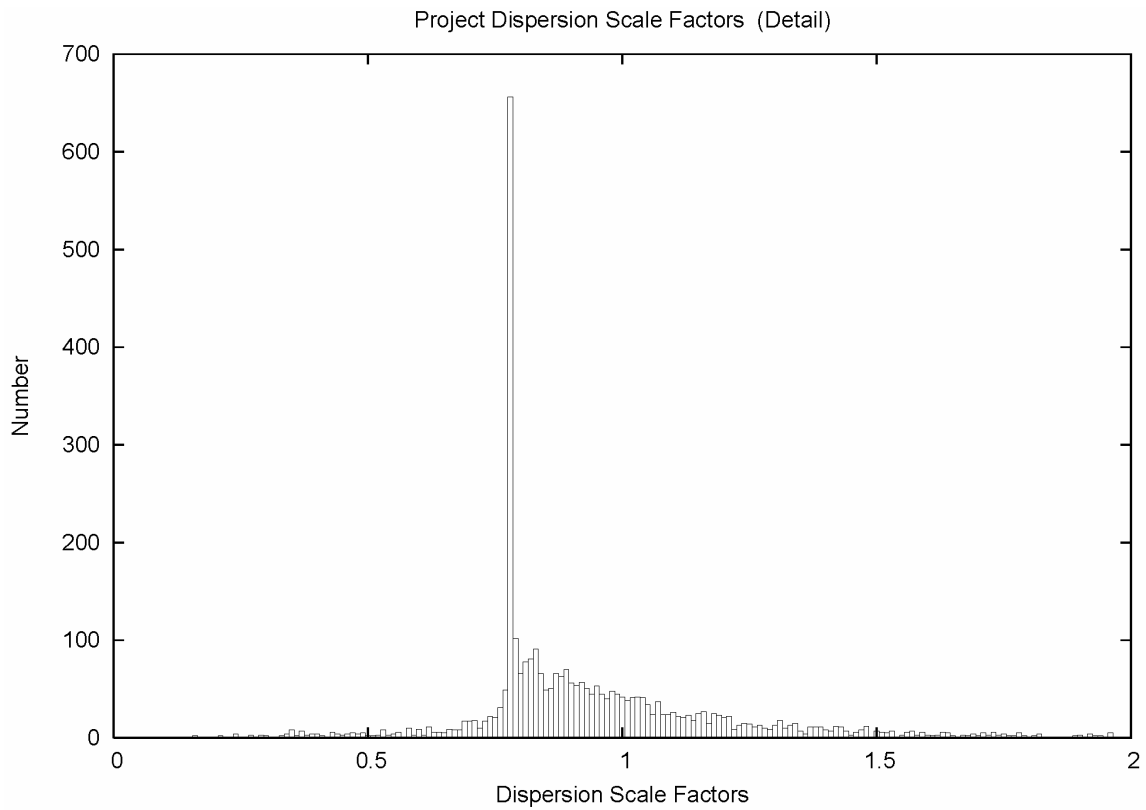Figure 30.2. Project dispersion scale factors, detail. 0.01 bin size.

One notes in Figure 30.1 that the general dispersion factor is around 1. However, the detail view in Figure 30.2 shows a large spike at the 0.78 bin. The spike is so large that it is still difficult to see the remaining distribution. To gain a better view of the remainder, the spike is truncated in the high detail view of Figure 30.3.
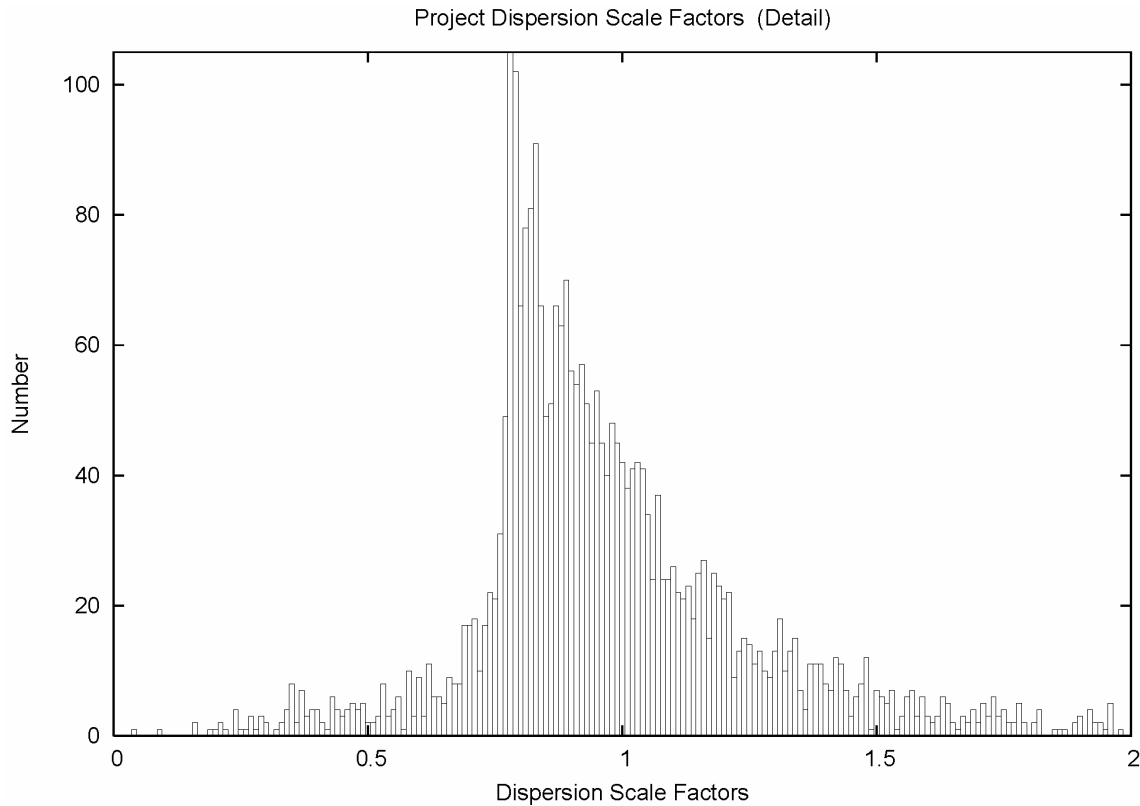
Figure 30.3. Project dispersion scale factors, high detail.

The nature of the spike has a rather involved explanation that is deferred to the next section. It can be noted here that the distribution does have a skew to the left, towards the spike. However, there is a long tail to the right, so that the general estimate is still 1.0. As a check, all the numerators of Equation 30-2 were summed (and all the denominators) to form an estimate of the global dispersion scale factor, d:

$$d = (648209.57/648460.50)^{1/2} = 0.9998065 \tag{30-5}$$

The scatter seen in Figure 30.3 has a principal source. The pre-adjustment project standard deviations (Section 15) were estimated project-by-project. So, as was discussed above, the project dispersion scale factors, d_k, reflect how each project fits in the network.

As an additional test on the overall horizontal and vertical reweighting described in Section 15, global horizontal and vertical dispersion scale factors, d_h and d_v, were computed from the 3315 projects that did get pre-adjustment scaling. These are collected into Table 30.1.

Table 30.1 – Dispersion Scale Factors, Global for 3315 Scaled Projects

Component	Value
Horizontal	0.964727
Vertical	0.861102
V/H ratio	0.892586

As seen above, the vertical component of the standard deviations of the observations could be tightened up by 14%. This small correction confirms the general validity of the NSRS 2007 weights and that the vertical network accuracies are, indeed, generally twice as large as the horizontal network accuracies.

31. Temporal distribution of survey project dispersion scale factors

This section studies if there is any time-related signal in the estimates of dispersion factors for the projects of the NSRS 2007. The scatter plot of d_k relative to time is shown in Figure 31.1.
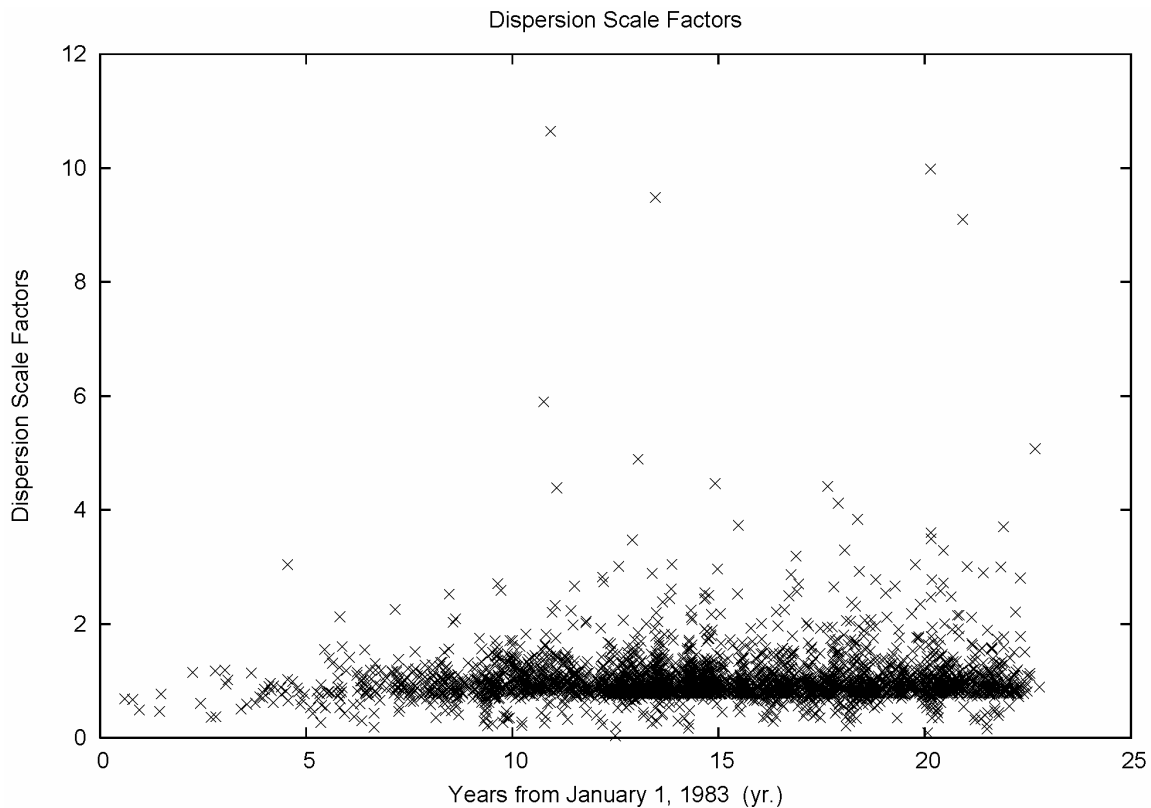
Figure 31.1. Temporal distribution of project dispersion factors.

Figure 31.1 shows the general cluster of factors around 1. Outliers are evident in the figure and show a different view of the tail of the histogram in Figure 30.1. The outliers in Figure 31.1 are projects whose covariance estimates require revision. However, as a general principle, one should *always* clear the residual outliers first, prior to performing ANOVA. As has been seen in Figures 7.3, 10.3, 11.3, 11.4, 13.3 and 13.4, a significant number of GPS vector outliers are still present in the NSRS 2007.

A detail scatter plot is now presented in Figure 31.2.
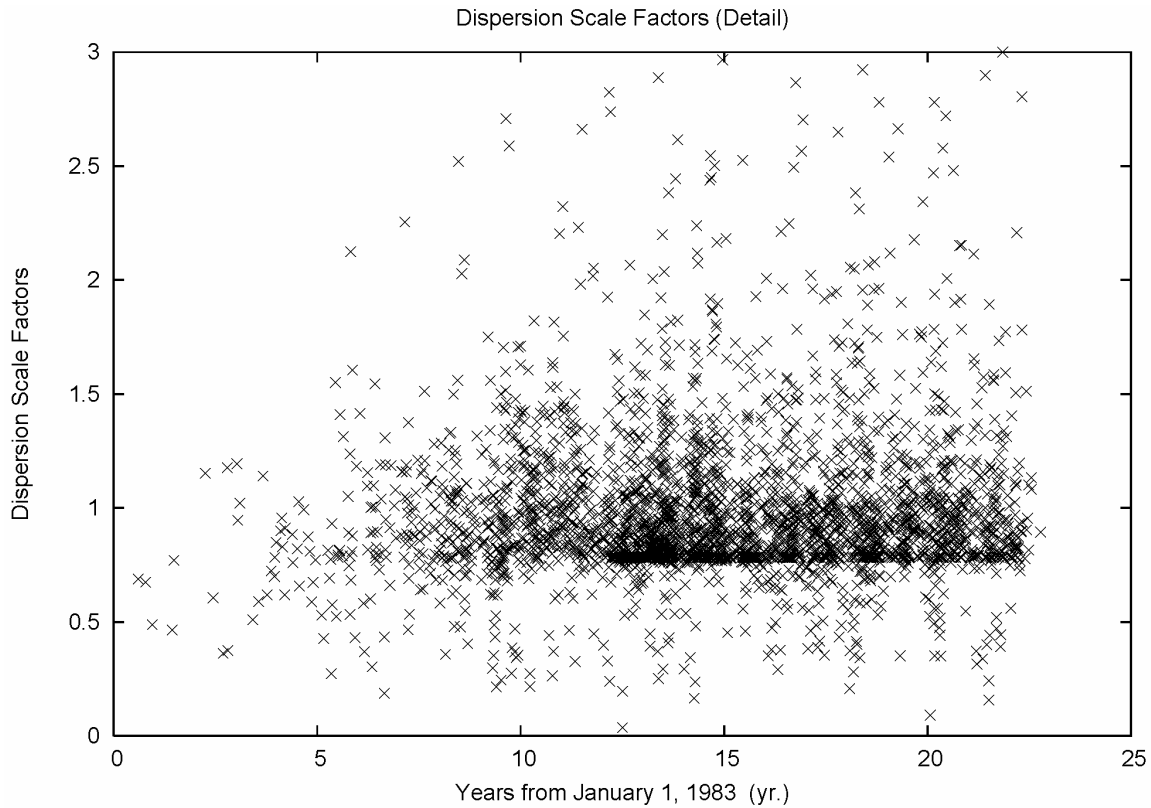
Figure 31.2. Temporal distribution of project dispersion factors, detail.

One immediately notices that there is no obvious time dependence of the dispersion scale factor estimates. However, there is a suggestion in Figure 31.2 of slightly greater scatter as time advances. This would indicate that later projects are relying more on the network to provide redundant checks, or, that there are more network connections being made. The effect is minor.

Also evident in Figure 31.2 is a horizontal lineation beginning in 1995. To gain a better view of this, a high detail scatter plot is presented in Figure 31.3.
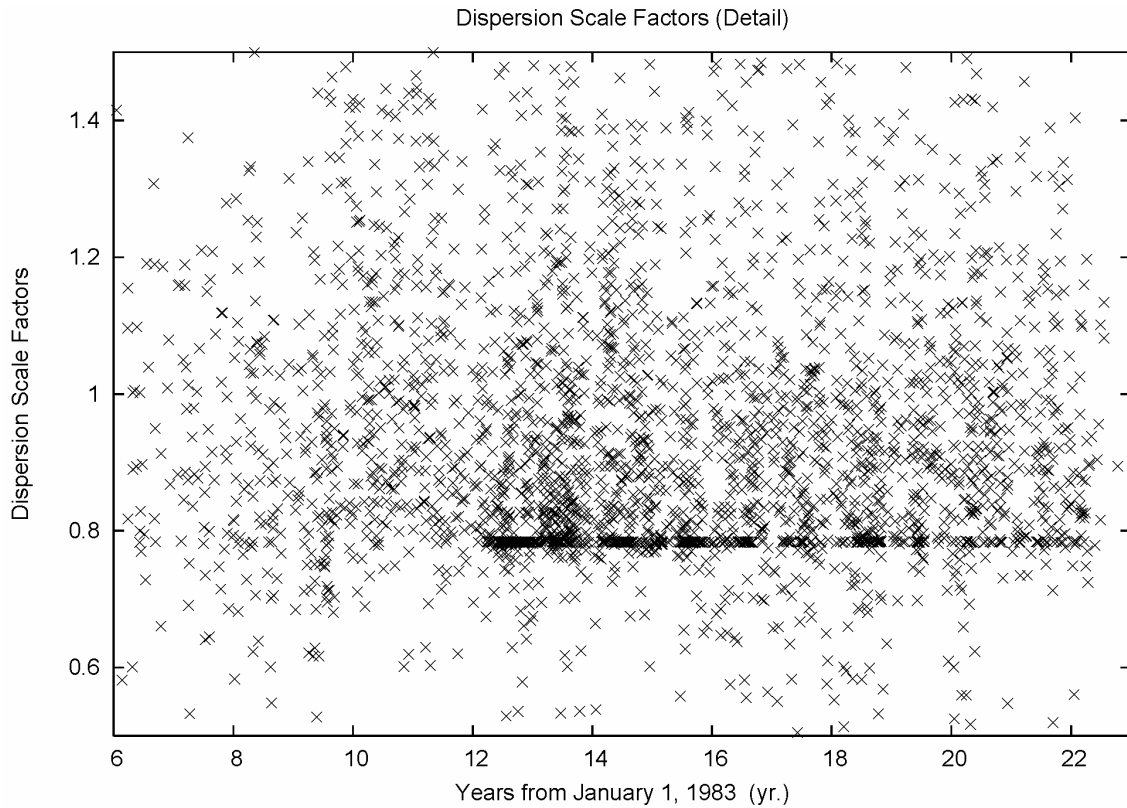
Figure 31.3. Temporal distribution of project dispersion factors, high detail.

The horizontal lineation is now quite evident in Figure 31.3, and is seen to correspond to the spike in the 0.78 bin found in the Figure 30.1 and 30.2 histograms. Detail inspection of the working files found a curious pattern in the variance sums that constitute the numerator of Equation 30-2. The histogram distribution was computed for all the variance sums. An initial segment of that variance sum histogram is plotted in Figure 31.4. Sequential views can be found in the Appendix in Figures A.31.5 and A.31.6.
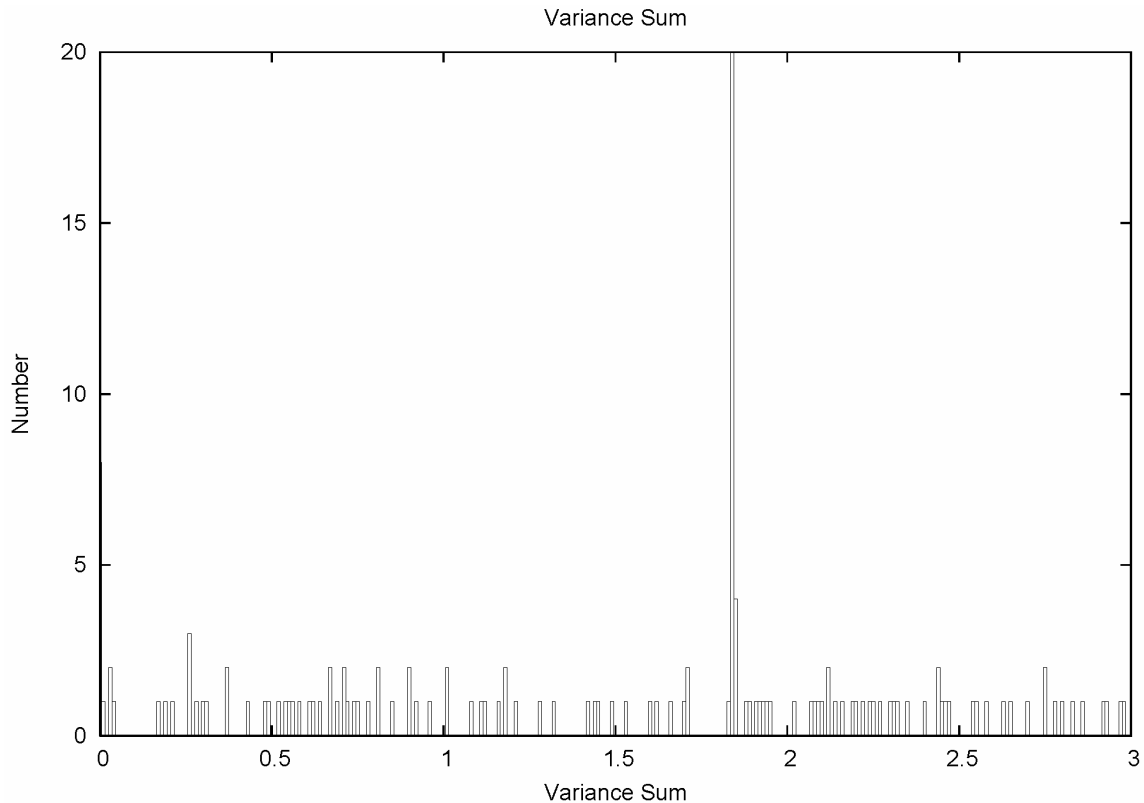
Figure 31.4. Irregular distribution of project variance sums, detail 1.

The periodic pattern in Figures 31.4, A.31.5, and A.31.6 are explained by a category of projects known as "runway end" surveys. These are part of a much broader collection of survey work under the NGS Aeronautical Survey Program (ASP), performed through funding by the Federal Aviation Administration. In short, a GPS vector is measured twice from a local airport reference point, A, to a given runway end, B. Since the baseline AB is measured twice, the relations are check. But, the line AB to a given runway end, B, is spur (or pendant).

The pre-adjustment estimate of standard deviation (Section 15) calibrates the horizontal and vertical error for a project. Thus, when the pre-adjustment calibrations are applied, and one repeats the calibration process, then one will exactly obtain 1.0 standard deviation factors from that point onward. This changes when the project is combined with all the other projects in the network. Then, the new calibration numbers (project dispersion scale factors) will reflect the adjustment of the observational error through the network.

But, when a project consists solely of spur lines, or spur (pendant) figures, then the estimates of that project's observational error will never change from what was obtained in the free adjustment of that project. One may certainly gain a new estimate of point A in the network adjustment, and that change in A will propagate directly into a new estimate of point B. But the relative relationship AB of a spur line will not change from that of a project free adjustment. And, it will never change until a connection is made between B and some other existing network point, C. Any observational error in

the network can not contaminate the observational error in a spur line (or spur figure). And the observational error in the spur line (or figure) can not influence the network. In essence, spur lines do not participate in the geodetic network; they are "along for the ride".

The spike in Figure 31.4 represents 20 projects that consist of a pair of repeated GPS vectors. The standard error factors for each of those projects were exactly computed in the pre-adjustment calibration. Because those lines are spur, the free adjustment error calibration will not change in the National Readjustment. But, because the NSRS 2007 adjustment program formed the weighted variance sums, $(v^t \mathbf{D}_o^{-1} v)_k$, with an *a posteriori* observation covariance matrix (Section 30), instead of recovering the runway end projects with project dispersion scale factors of 1.0, they are recovered with the reciprocal of the *a posteriori* standard deviation of unit weight of the free adjustment, $0.783319 = 1/1.276619$.

The spike in the 0.78 bin in Figures 30.1 and 30.2, the horizontal lineation in Figures 31.2 and 31.3, and the periodic spikes in Figures 31.4, A.31.5, and A.31.6, are due to projects consisting solely of spur lines and figures that previously passed through a pre-adjustment calibration process. Their dispersion factors will always be 1.0 if the variance sums use *a priori* observation weights, and will be the reciprocal of the *a posteriori* standard deviation of unit weight if the variance sums use *a posteriori* weights.

One could make a case, in fact, that the variance sum and the degrees of freedom from projects only containing spur lines should be withheld from the estimate of the variance of unit weight of a network adjustment. This question is pursued in Section 32.

This spike created by the spur lines and figures in Figure 30.2 makes the left leaning skew of the distribution in Figure 30.3 particularly interesting. It could be caused, in part, by projects that are composed partly of spur lines and figures, and partly by vectors that are redundant with the network. It does suggest that a significant number of the projects are comprised of local or "breakdown" surveys. This is consistent with the median GPS vector length of 31 km found in Table 5.1.

To gain some alternative views of the scatter plot against time, some subsets of the dispersion scale factors were created. In Figure 31.5, 3232 projects that had passed through the pre-adjustment rescaling (Section 15) and contain more than one degree of freedom are shown. (Refer to propullb.txt in the Electronic Support Material.) In Figure 31.6, low redundancy/tiny projects with less than 27.0 degrees of freedom are also withheld. Figure 31.6 depicts 1717 projects. (Refer to propullc.txt in the Electronic Support Material.)
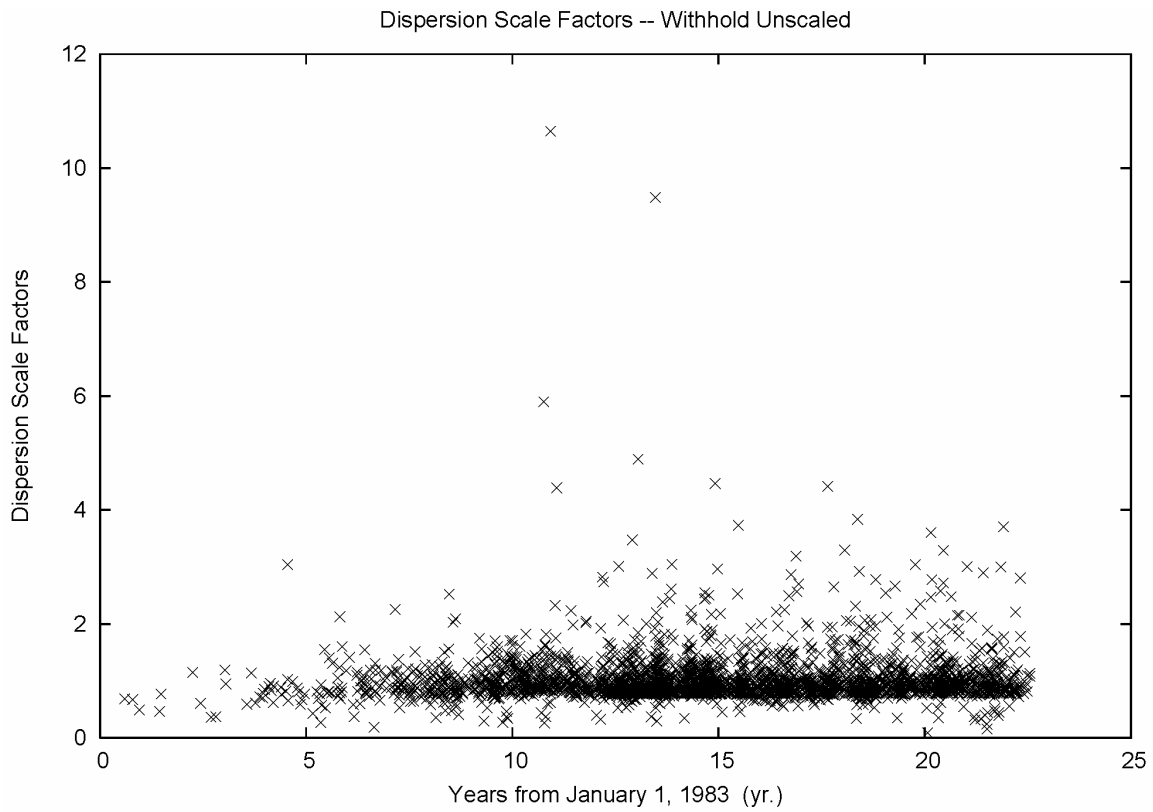
Figure 31.5. Temporal distribution of project dispersion factors, scaled projects.
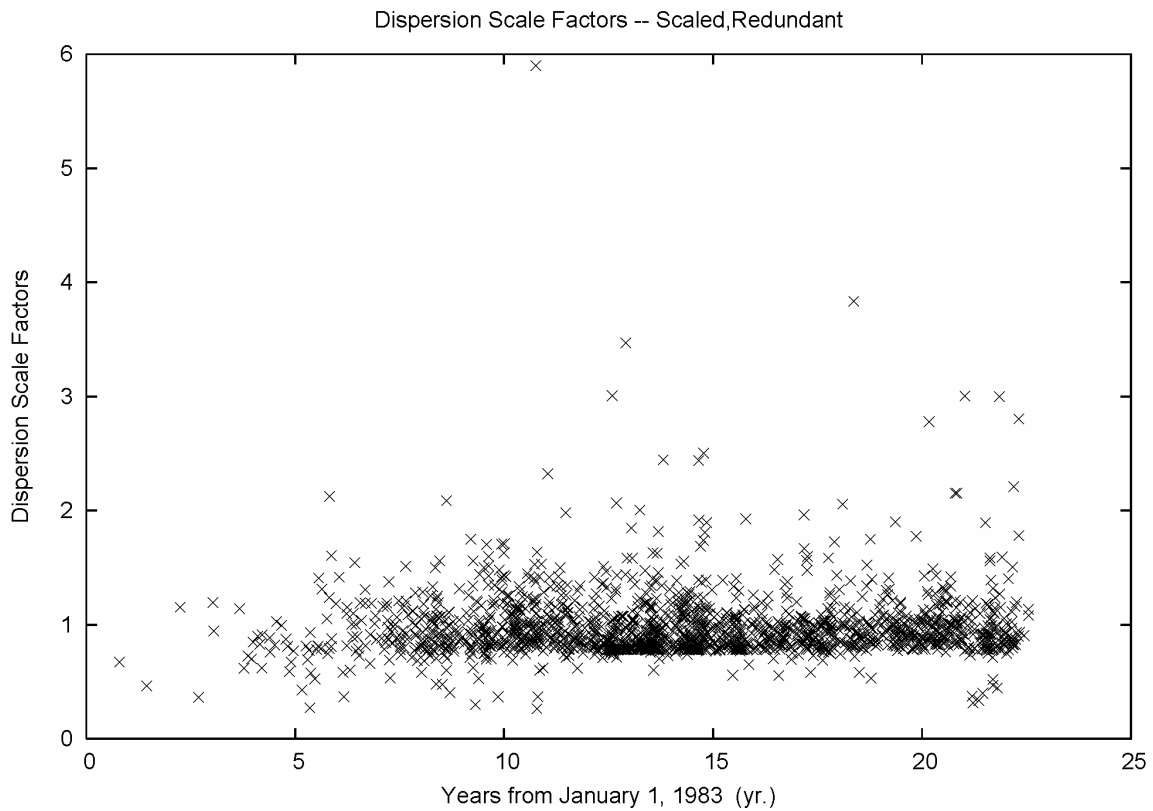

Figure 31.6. Temporal distribution of project disp. factors, scaled, redundant projects.

101

Figure 31.5 looks very much like Figure 31.1. Some of the outlying dispersion factors are missing, which indicates that either they were not scaled or they have extremely low redundancy. Also, there are fewer of the low magnitude dispersion scale factors.

Figure 31.6 depicts the distribution when low redundancy/tiny projects are dropped. Outliers are still present, although fewer in number. The distribution is thinned, but no qualitative change becomes evident.

32. The accuracy layers of NSRS 2007

As has become evident from the collection of material presented to the reader at this point, the NSRS 2007 network is not homogenous. GPS vectors date back to 1983. Surveys are conducted to a variety of intended accuracies. Different receivers and vector reduction softwares were used. The vector line lengths range from a few meters to over 5000 km. And the purposes of the GPS surveys, themselves, would greatly vary. The surveys establish fundamental geodetic control as well as set runway end points.

Because of the heterogeneous nature of the network, and the analytic experience gathered from the decades of work that adjusted the Eastern Strain Network, the High Precision Network, the High Precision Geodetic Network, the High Accuracy Reference Network (HARN), and the HARN reobservation (Federal Base Network Vertical Component), as well as the myriad surveys conducted in support of the Cooperative Base Network and User Densification Network, it was recognized that GPS carrier phase ambiguities are not always correctly resolved, and that GPS precise orbits and reduction software have evolved over time. Outliers, such as those retained in Sections 7 and 11, were known. Redundancy and network connectivity varied greatly. Reweighting efforts were needed, but they would not necessarily cure underlying systematic issues. It is known from the Gauss-Markov theorem that simultaneous least-squares adjustments are the best choices only in the absence of systematic error (Liebelt 1967).

The then-current National Readjustment Project Manager, Mrs. Kathryn Milbert, recognized the heterogeneous character of the network and recommended a layered approach to the readjustment. To quote from the Concept of Operation of the National Readjustment Plan of October 2003 (Milbert 2003):

"*Using adjustment layers has the advantage of allowing us to separate projects into categories and thus reduce systematic errors by keeping the more accurately observed data separate from less accurately observed data.*"

While a simultaneous adjustment was ultimately selected for the National Readjustment, the heterogeneity of the network is a fact. The analysis performed by Mrs. Milbert, who assigned GPS projects to various adjustment layers, can be used to group the project dispersion scale factors into categories that reflect NSRS survey components.

The file master.projects.all.txt is an index, summary count, and annotated log of the GPS projects that also contains assignment to a historic adjustment layer. While the process of layer assignment was suspended in 2004, 2759 of the 3201 projects in the file did have a layer assignment. In addition, the author completed the assignment of seven FBN-Vertical Component projects to the N1 layer. The summary of the network accuracy layers for those projects that were part of the NSRS 2007 adjustment is given in Table 32.1. (Refer to proid3.txt in the Electronic Support Material.)

Table 32.1 – NSRS 2007 Network Accuracy Layers

Code	ID	Content	Projects
0	N0	The National CORS coordinate set	
1	N1	The FBN/CBN projects	50
2	N2	A & B Order projects with CORS ties	285
3	FAACORS	FAA projects with CORS ties	100
4	N3	A Order projects without CORS ties	29
5	N4	B Order projects without CORS ties	135
6	N5	B+1st O. combo & 1st O. with CORS ties	189
7	AIR	Lower order FAA projects, no CORS ties	1273
8	R1	Recent (post-1992), residuals under 7 cm	688
9	R2	Residuals under 15 cm	166
10	R3	Large residuals or few ties	90
11	TRASH		1

The layer assignment summary of Table 32.1 helps to provide insight on the heterogeneous character of the network. The variance sums and fractional degrees of freedom (Eq. 30-2) are accumulated, and the accuracy layer dispersion scale factors are presented in Table 32.2. Since pre-adjustment weight scaling was performed and since the variance sums are *a posteriori*, the expected factor magnitude is 1.0.

Table 32.2 – NSRS 2007 Accuracy Layer Dispersion Scale Factors

Code	ID	Projects	D.S.F.	
1	N1	50	0.936	
2	N2	285	1.021	
3	FAACORS	100	1.227	*
4	N3	29	1.113	*
5	N4	135	1.109	*
6	N5	189	0.980	
7	AIR	1273	0.991	
8	R1	688	0.977	
9	R2	166	0.949	
10	R3	90	0.877	
11	TRASH	1	1.178	
	UNSCALED	243	1.774	**

Table 32.2 shows that additional error appears in the projects of the FAACORS, the N3, and the N4 layers, when those surveys are combined into the final free

adjustment. These projects have error increases of 11 to 23% when they are combined in the network. Also, as a separate grouping, the projects that did not get distinct horizontal and vertical pre-adjustment standard deviation factors show a very large dispersion scale factor. They will be examined later in detail.

Next scatter plots of the individual project dispersion scale factors vs. time of observation are show for each of the accuracy layers. Figure 32.1 shows the N1 layer. (Refer to p-1.txt in the Electronic Support Material.)
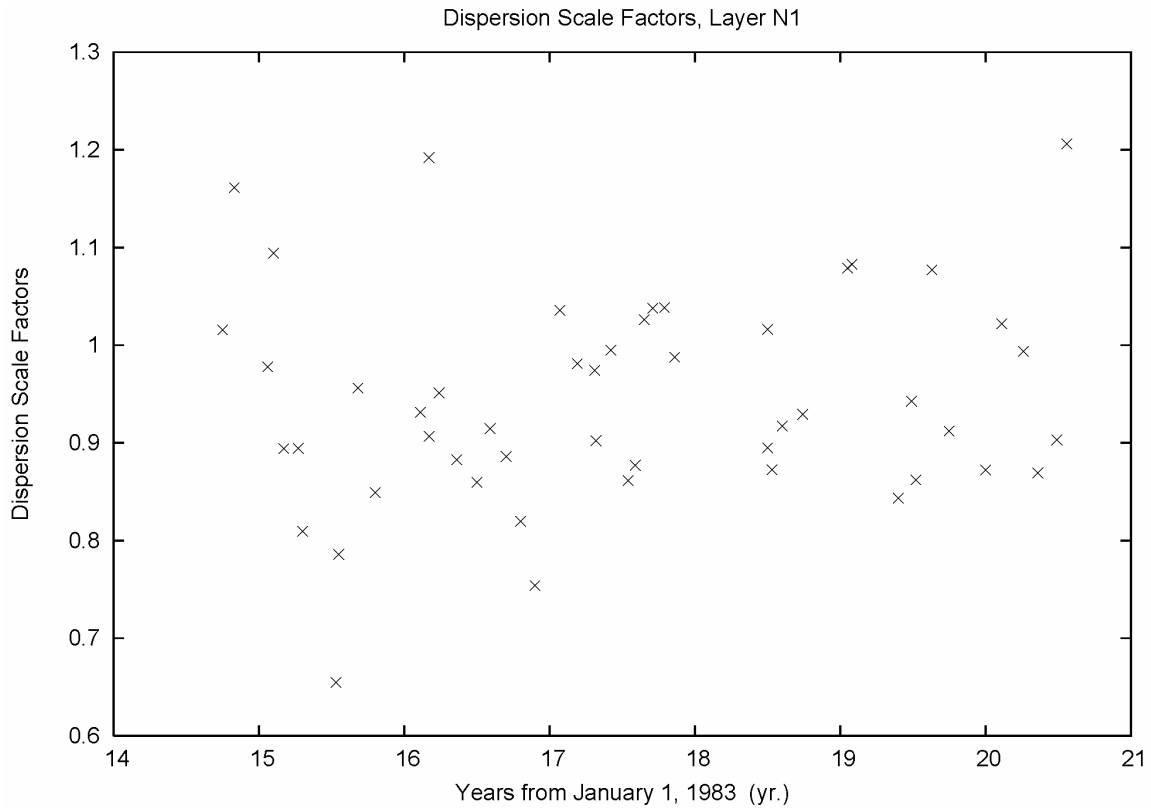
Figure 32.1. Dispersion scale factors, layer N1 projects.

This layer represents the highest accuracy. A tight clustering around 1.0 is evident. This figure provides a baseline for expected scatter of project dispersion factors.

Next, Figures 32.2 through 32.10 are shown as a group. (Refer to p-2.txt through p-10.txt in the Electronic Support Material.) Comments will follow the figures.

Figure 32.2. Dispersion scale factors, layer N2 projects.

Figure 32.3. Dispersion scale factors, layer FAACORS projects.

Dispersion Scale Factors, Layer N3

Figure 32.4. Dispersion scale factors, layer N3 projects.

Dispersion Scale Factors, Layer N4

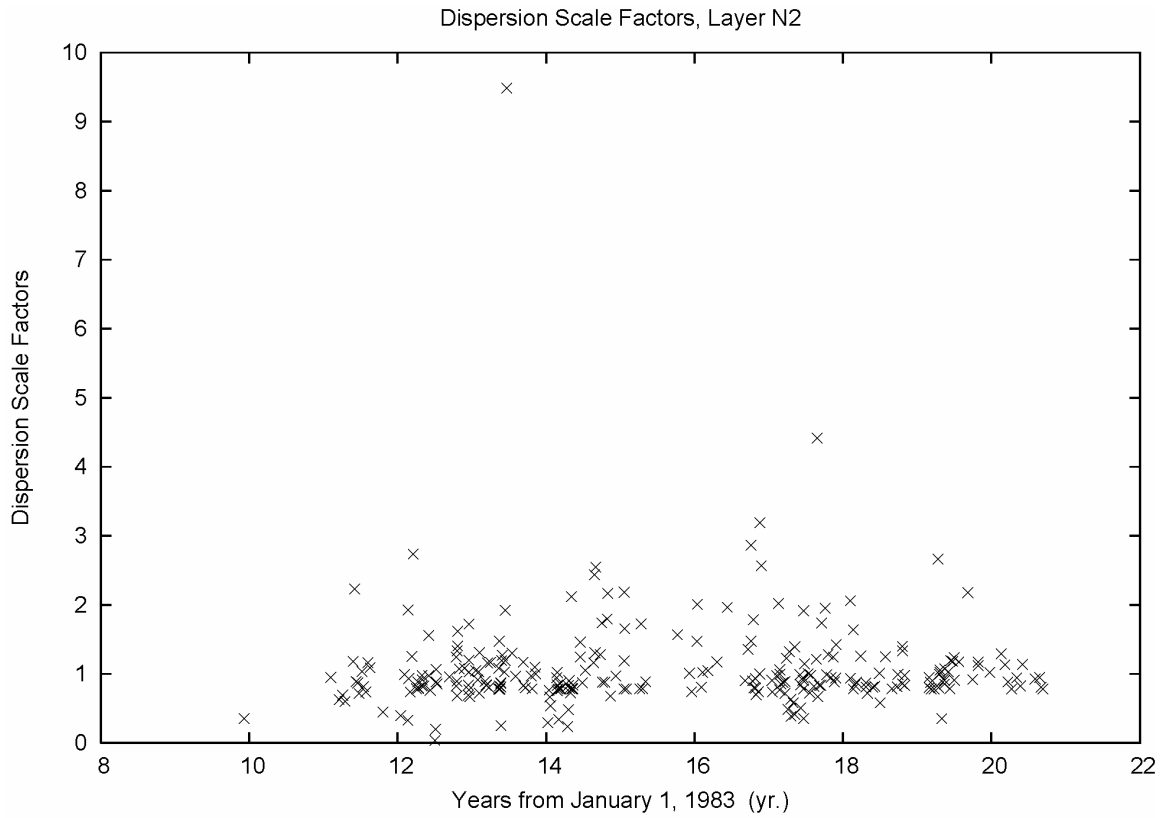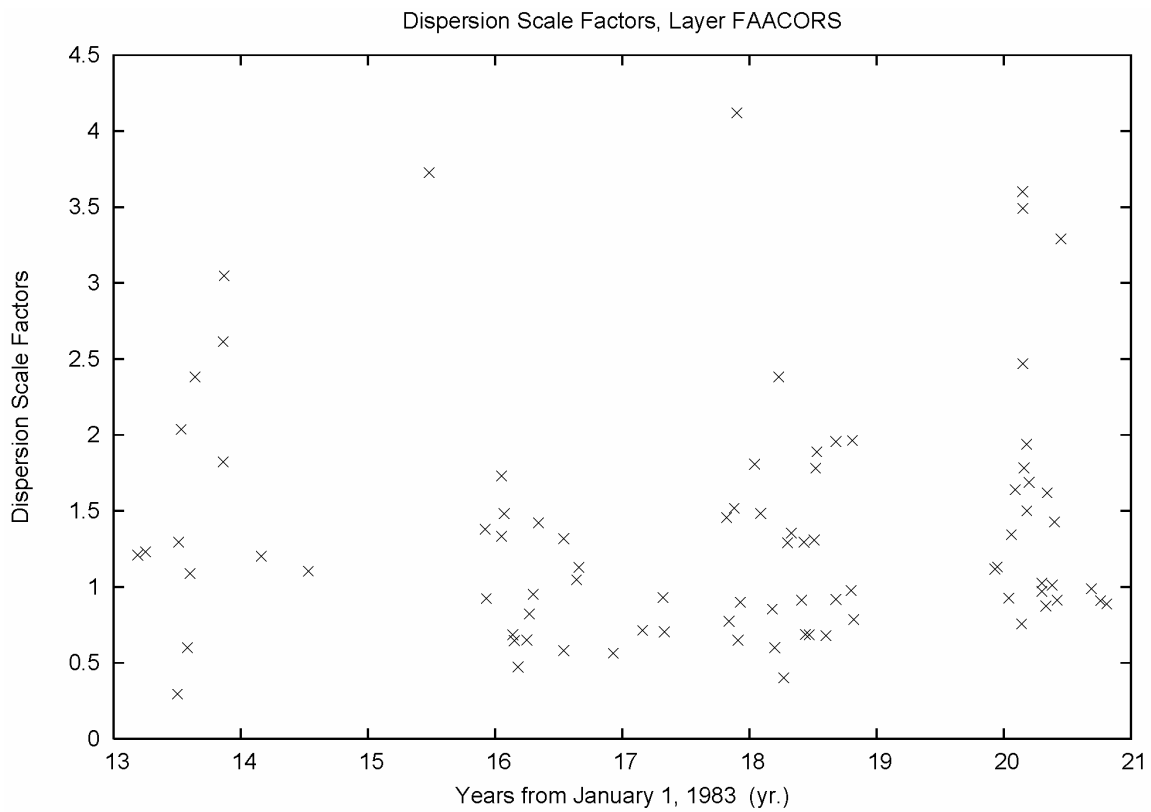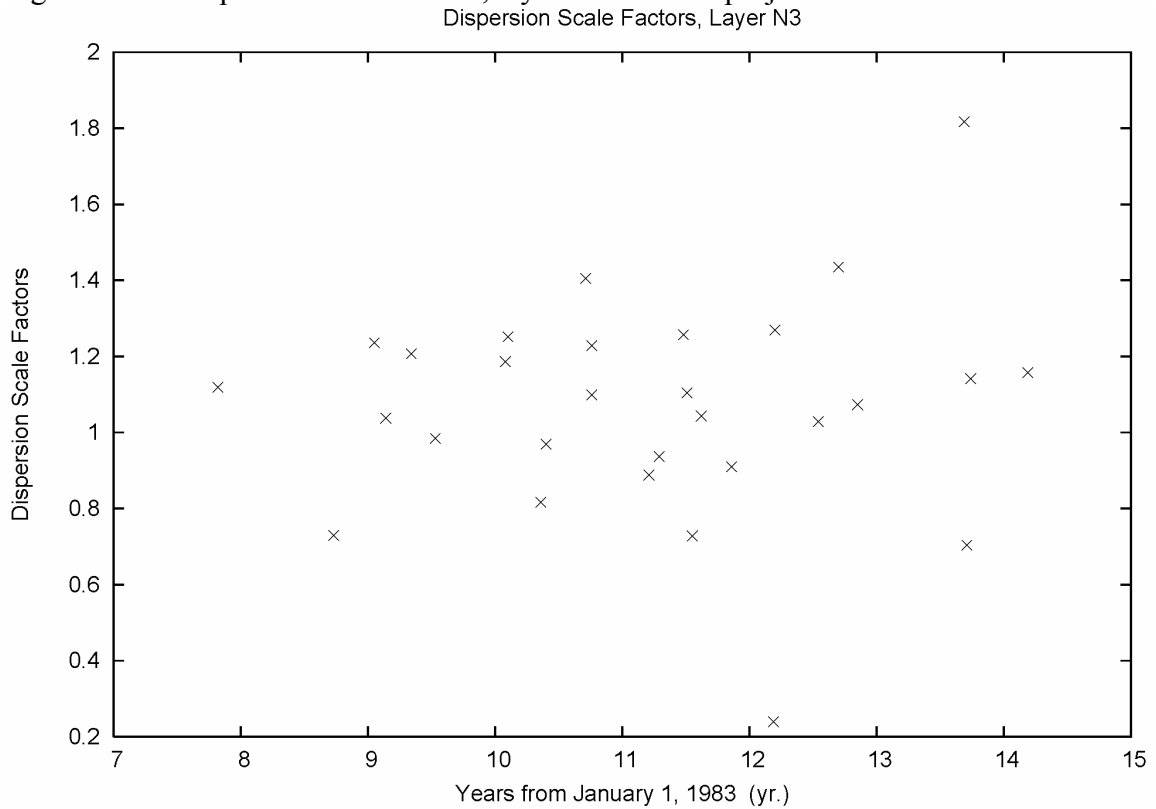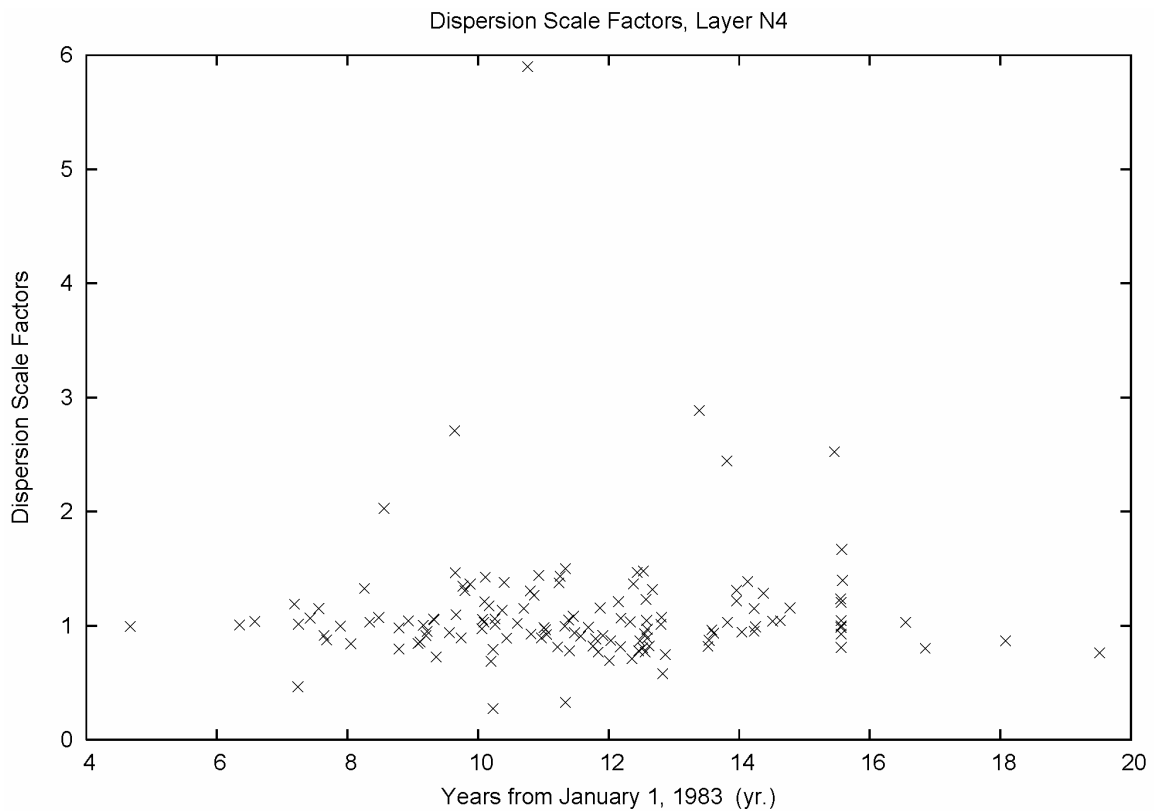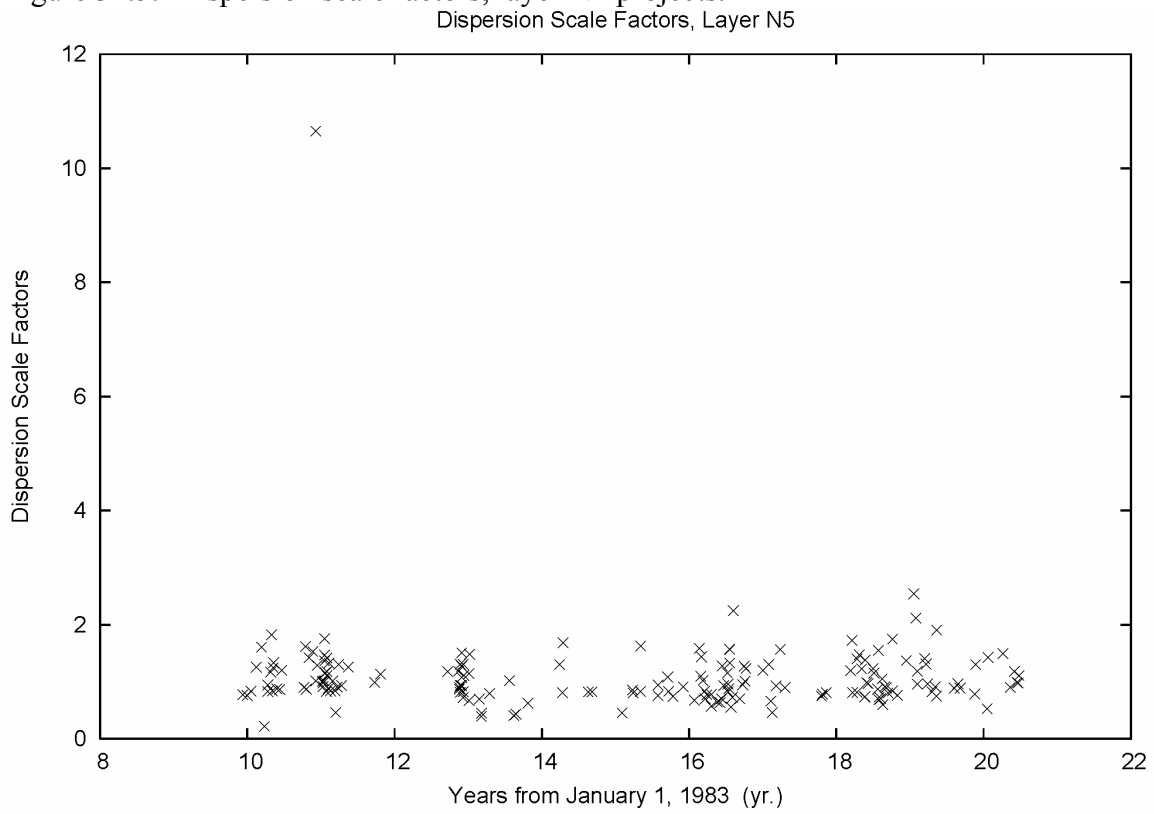Figure 32.5. Dispersion scale factors, layer N4 projects.

Figure 32.6. Dispersion scale factors, layer N5 projects.

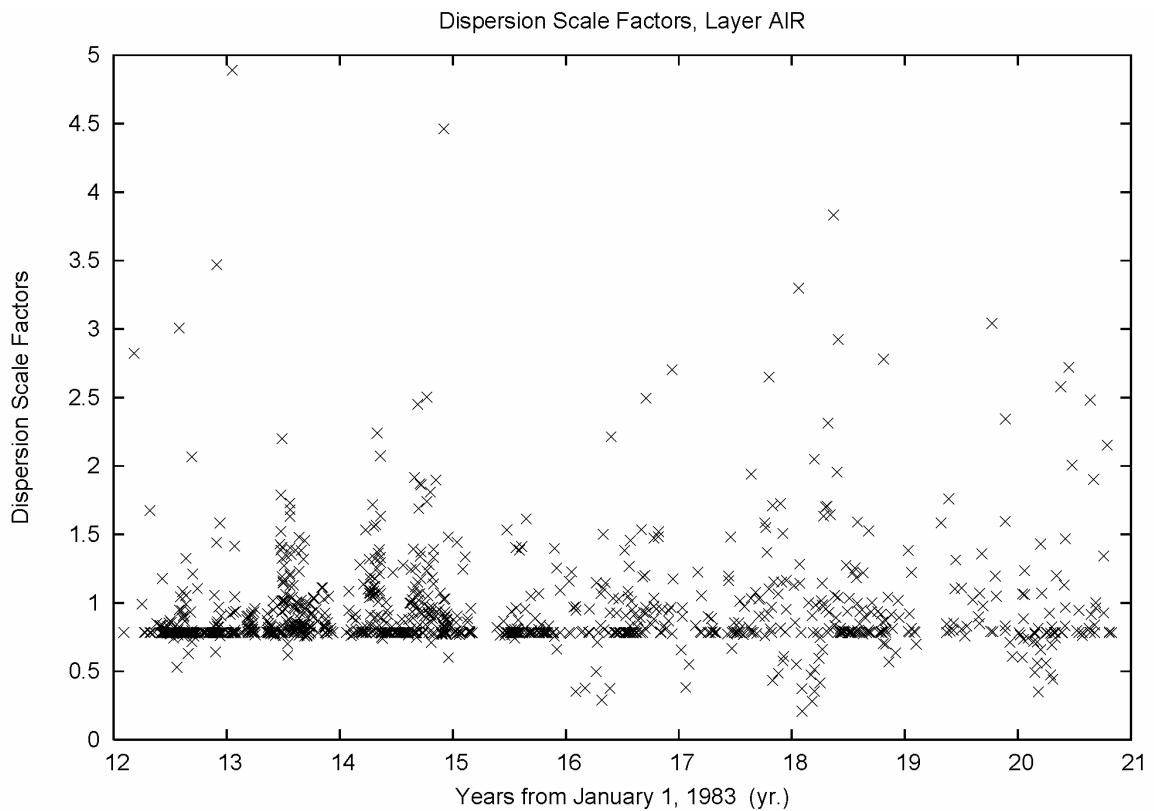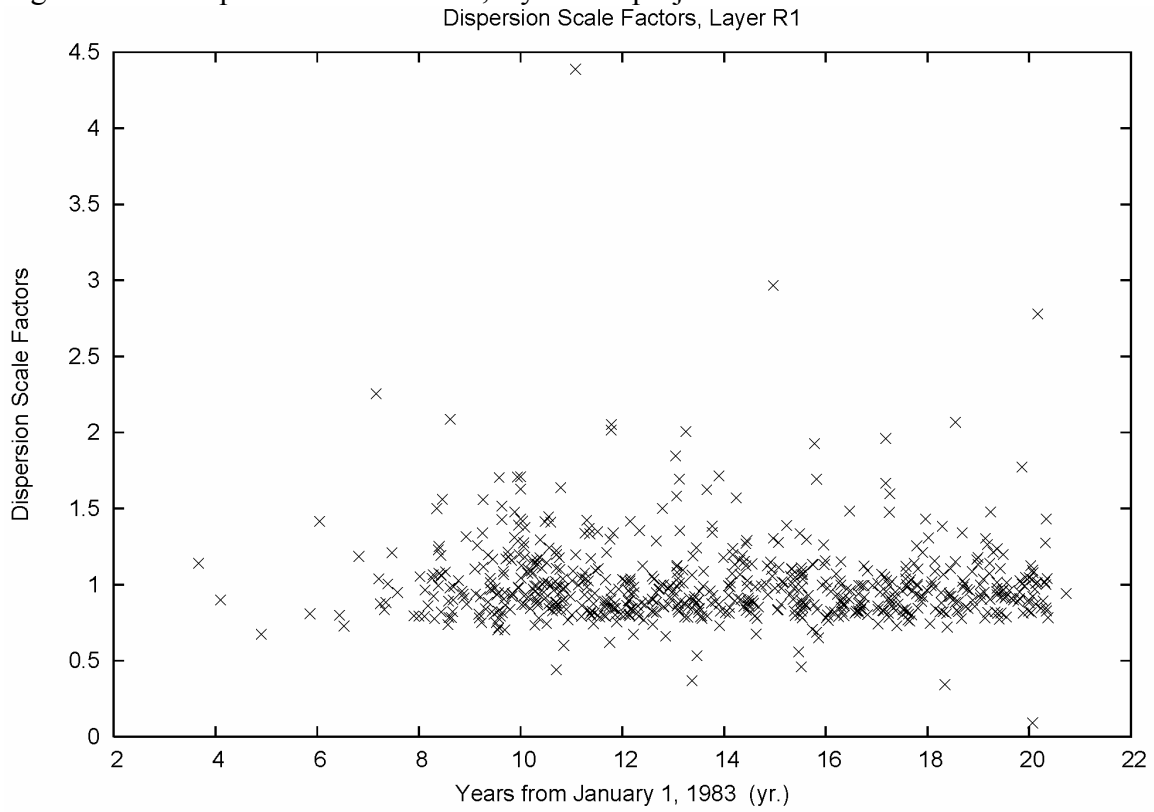Figure 32.7. Dispersion scale factors, layer AIR projects.

Dispersion Scale Factors, Layer R1

Figure 32.8. Dispersion scale factors, layer R1 projects.
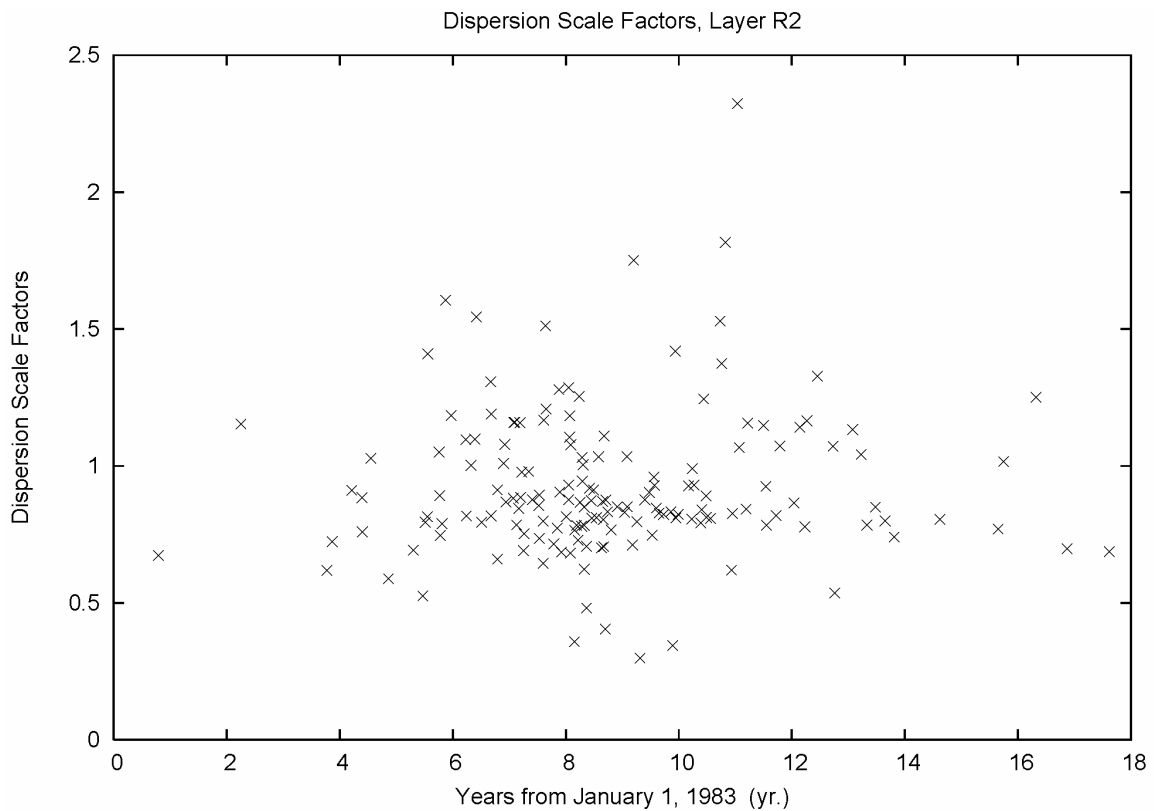

Dispersion Scale Factors, Layer R2

Figure 32.9. Dispersion scale factors, layer R2 projects.
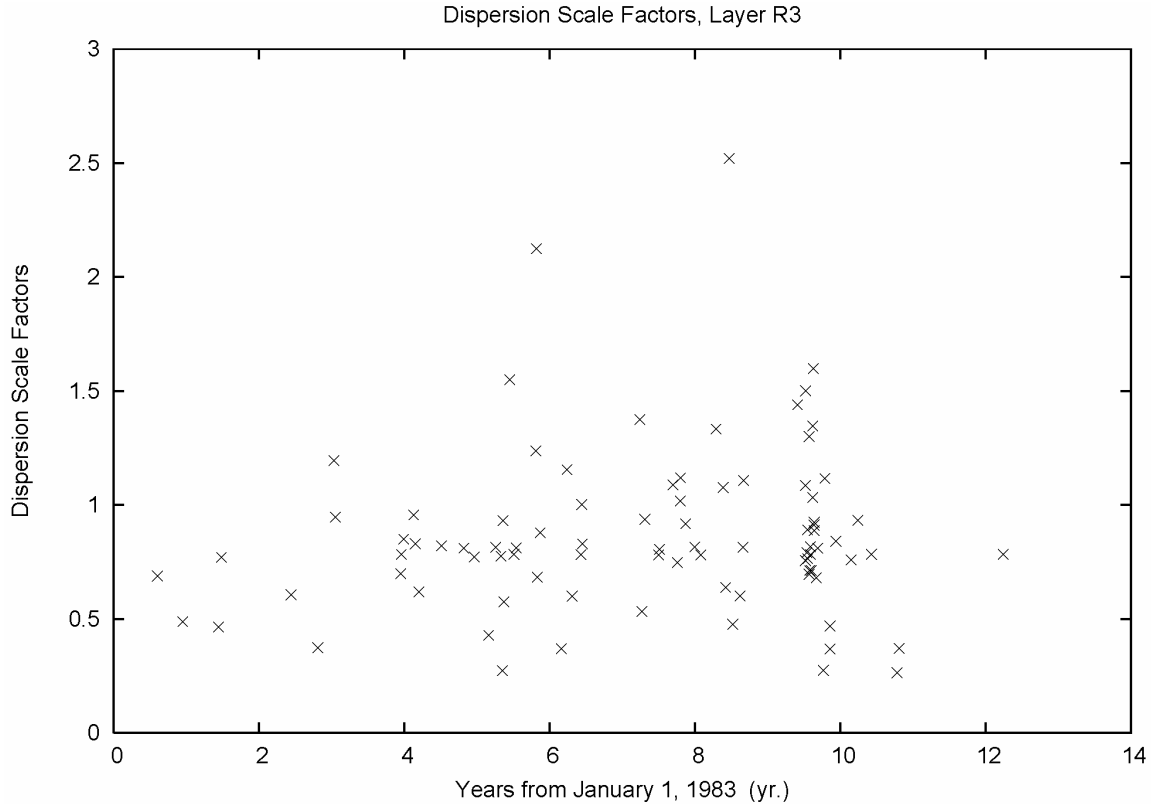
Figure 32.10. Dispersion scale factors, layer R3 projects.

Figure 32.2, showing the N2 layer, has a generally good cluster of points. But there are some distinct outliers. Those particular surveys should be inspected on both a standalone basis and on their residual differences and position shifts when brought into the network adjustment. The FAACORS layer, Figure 32.3, shows similar behavior. It should also be mentioned that rejection of standardized residual outliers should precede any project-level weight rescaling. The N3 layer, Figure 32.4, shows only one project outlier. The remaining projects are clustered, and are just coming in a little higher than 1.0. Note, also, that projects significantly below 1.0 should be weight rescaled, too. It is possible that outlier rejection in the course of the National free adjustment analysis greatly improved the fit of some remaining vectors within a given project. Figure 32.5, the N4 layer, has six large outliers and a few that are too small. Layer N5 (Figure 32.6) has a particularly large project dispersion scale factor that should be investigated.

Figure 32.7 plots the dispersion factors for the AIR layer. It is seen that this is the layer that contains the spur lines and figures discussed in Section 31. In addition to the horizontal lineation at 0.783319, significant scatter is seen in the remaining dispersion factors. However, that dispersion factor scatter may not be very meaningful if those remaining projects have few degrees of freedom or few connections to the network.

In the prior section a question was posed about withholding projects that only contained spur lines from the estimate of the variance of unit weight of a network

adjustment (the horizontal lineation of Figure 32.7). As a test, those projects that were assigned to the AIR layer, whose dispersion scale factor was 0.7833 +/- 0.01, and whose degrees of freedom were exactly integer (within a +/- 0.1 tolerance) were identified. Base on these criteria, 512 projects containing 6210 vectors were extracted. This collection of projects had an aggregate dispersion factor of 0.7836. When this set of projects was withheld from the total dispersion estimate, Equation 30-5, the estimate increased by 0.3%, from 0.99982 to 1.00303. In short, while the spur projects are numerous, they don't carry enough vectors to greatly impact the network variance of unit weight.

Resuming the inspection of the scatter plots of the project dispersion scale factors, Figure 32.8 portrays the R1 layer. This marks a transition from the "national" projects to "regional" projects. Generally, these are User Densification Network projects of First Order or lower order surveys. In Figure 32.8, project factor scatter is seen. But the distribution also has a clustering around the 0.78 line. The survey connections to the network are present, but are not strong in some cases. Fewer projects are present in the R2 layer of Figure 32.9, but they also show a bit of clustering about the 0.78 line. And, the R3 layer, Figure 32.10, shows the same behavior.

In summary of the layer analysis, the scatter and large magnitudes of the FAACORS layer are troublesome. This is particularly so, given that those surveys looked very good at the project level. But, when these projects were joined into the network, the estimated dispersions could jump 300 to 400%. The N4 layer has some distinct weight outliers, perhaps they are due to observation residual outliers. The N3 layer has no specific issue beyond a pair of outliers (high and low).

Next, the remaining 545 projects that did not get a layer assignment are depicted in Figure 38.11 as an unassigned layer. (Refer to file p-0.txt in the Electronic Support Material.) These would be projects that were processed more recently, as well as a category of projects in California. As seen from the figure, the "recent" project cluster is evident, and the tail would be mostly California projects. Because of the special treatment of California projects, these were not passed through the pre-adjustment horizontal and vertical standard deviation factor scaling process. This decision will be investigated in Section 33.
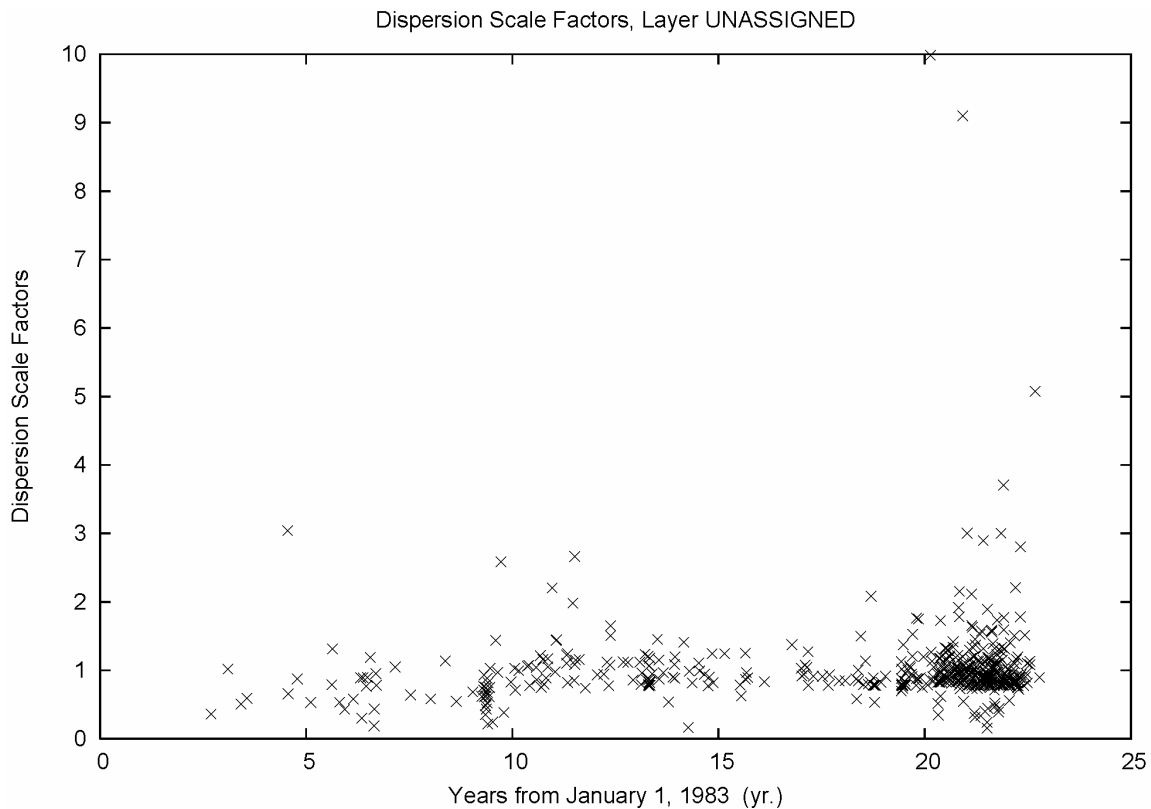
Figure 32.11. Dispersion scale factors, unassigned projects.

There are two subsets of the 545 unassigned projects; those where pre-adjustment horizontal and vertical standard deviation factor scaling was still performed, and 243 unscaled projects. (Refer to files p-sc.txt and p-un.txt, respectively, in the Electronic Support Material.) Recall, the unscaled projects had a combined 1.77 dispersion scale factor, and needed deeper study. Analysis shows, however, that eight of the 243 unscaled projects were not, in fact, assigned to the California Helmert blocks. (Refer to p-nc.txt in the Electronic Support Material.) Inspection of the 8 non-California unscaled projects found that project GPS1751 in Wisconsin had 205 vectors with a large variance sum. This project has a dispersion scale factor of 9.98, and can be seen at the very top of Figure 32.11. It is highly likely that this project never got scaled by the variance of unit weight, and carries the original, grossly overoptimistic weight estimates assigned by the GPS vector reduction software. The influence of these weights is such that this single project inflated the standard deviations of unit weight of both the free and fixed National Readjustment by 4%. Project GPS1751 is plotted in Figure 32.12. While it is not expected that the extremely optimistic weights of GPS1751 inadvertently caused the excellent vertical network accuracy concentration in Southern Wisconsin seen in Figure 23.5, that possibility can not be ruled out. The other seven non-California unscaled projects are smaller in size and contribute less error. Nonetheless, they should be processed with horizontal and vertical component scaling.

Project GPS1751
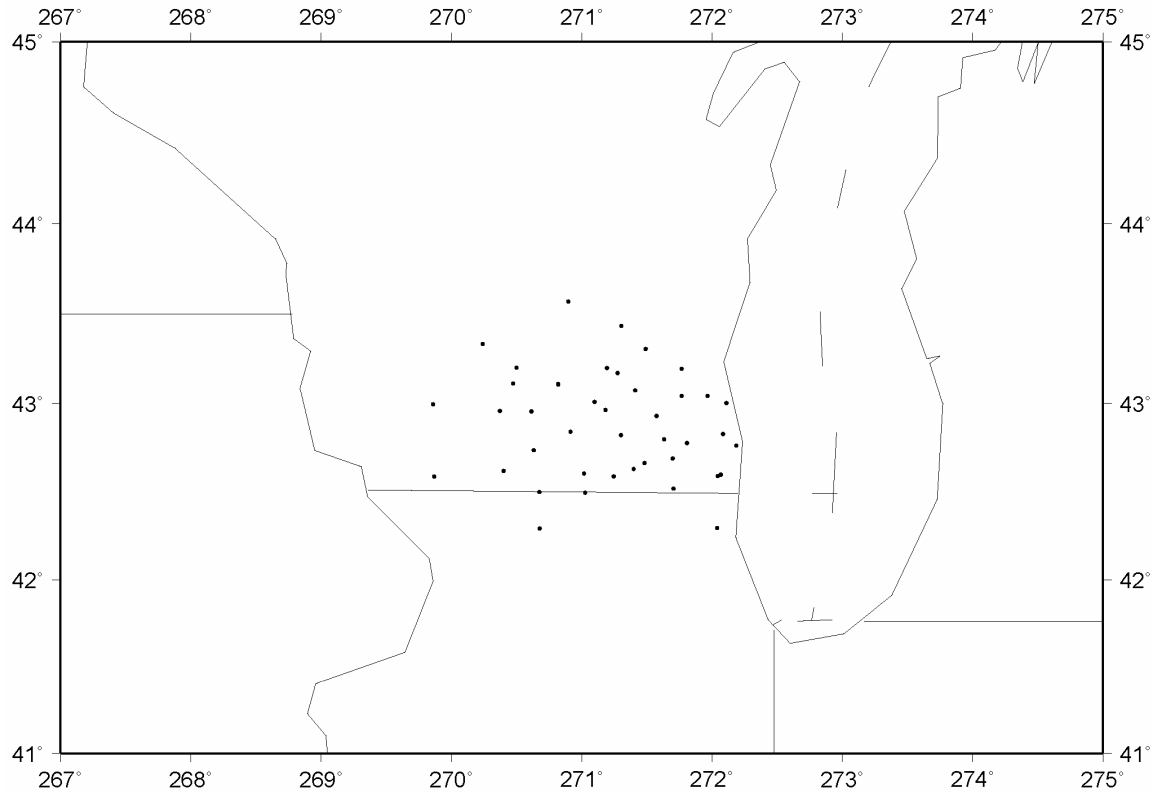
Figure 32.12. Project GPS1751 point distribution.

33. The unscaled California project dispersion factors

The 235 unscaled California projects are described as such because they did not pass through the pre-adjustment horizontal and vertical standard deviation factor scaling process of Section 15. Although not cross-checked in this report, it is believed that the projects did receive the customary scaling by the project standard deviation of unit weight. For this reason, the relative weights of the horizontal and vertical components of the GPS vectors, as well as the resulting horizontal-vertical magnitudes of network and local accuracies in California, are suspect. Recall that in Section 15 it was found that the horizontal standard deviations from simple project scaling were too optimistic relative to the vertical standard deviations by 50%.

It must also be mentioned that the California projects were passed through a separate weight rescaling program, `calwt4.f` (Pursell *et al.* 2008). However, the program did not make any special provisions for horizontal and vertical components. This is evident in a `calwt4.f` source code fragment reproduced in Table 33.1.

Table 33.1 – Source Code of California Project Reweighting, Fragment

```
distkm = 1.d-3 * dsqrt(dx*dx + dy*dy + dz*dz)
shtdp = 3.6d0 + 0.053d0*distkm
dt = dabs(epoch - dyear)
sx = dsqrt(sigx*sigx + shtdp*shtdp*dt*dt)
sy = dsqrt(sigy*sigy + shtdp*shtdp*dt*dt)
sz = dsqrt(sigz*sigz + shtdp*shtdp*dt*dt)
```

To partially understand the absence of absence of horizontal and vertical rescaling (Section 15) for the California projects, it is important to know that, although the estimation of the pre-adjustment horizontal and vertical standard deviation factors proceeded to the data submission cut-off date, the factors were not introduced into the NSRS 2007 adjustment until the last iteration (iteration 7) of the free adjustment (Pursell *et al*. 2008). (Yes, this means that the outlier rejection process occurred *before* the final weights were introduced.) In the earlier analysis, large residuals were seen on the older California GPS vectors, even though they had passed through HTDP. Since HTDP is a velocity field model, it is subject to error. And this error would grow for the older vectors being brought up to the 2007.0 computation epoch. This is seen in the code fragment above, where original standard deviations in *X,Y,Z*, denoted sigx, sigy, sigz, are augmented by model error to obtain updated standard deviations denoted sx, sy, sz.

If the weight-updated California projects were then passed through the pre-adjustment horizontal and vertical standard deviation factor estimation process, that process would have undone the time-dependent character of the project weights. But, this raises a question regarding the relative horizontal-vertical weights. On one hand, calwt4.f was never represented as a substitute for establishing distinct horizontal and vertical factors. On the other hand, HTDP only applies horizontal velocity corrections, whereas the code fragment is applying model error in all three components. Some provision should have been made for the distinction between horizontal and vertical in the fragment above (Table 33.1).

Given the three-dimensional weight updating that was applied in the presence of HTDP horizontal model error, we can not expect the project dispersion scale factors to reproduce the horizontal-to-vertical ratios found in Section 15. To analyze the end result, the three-dimensional project dispersion scale factors for the unscaled California projects are histogrammed in Figure 33.1. (Refer to p-ca.txt in the Electronic Support Material.)
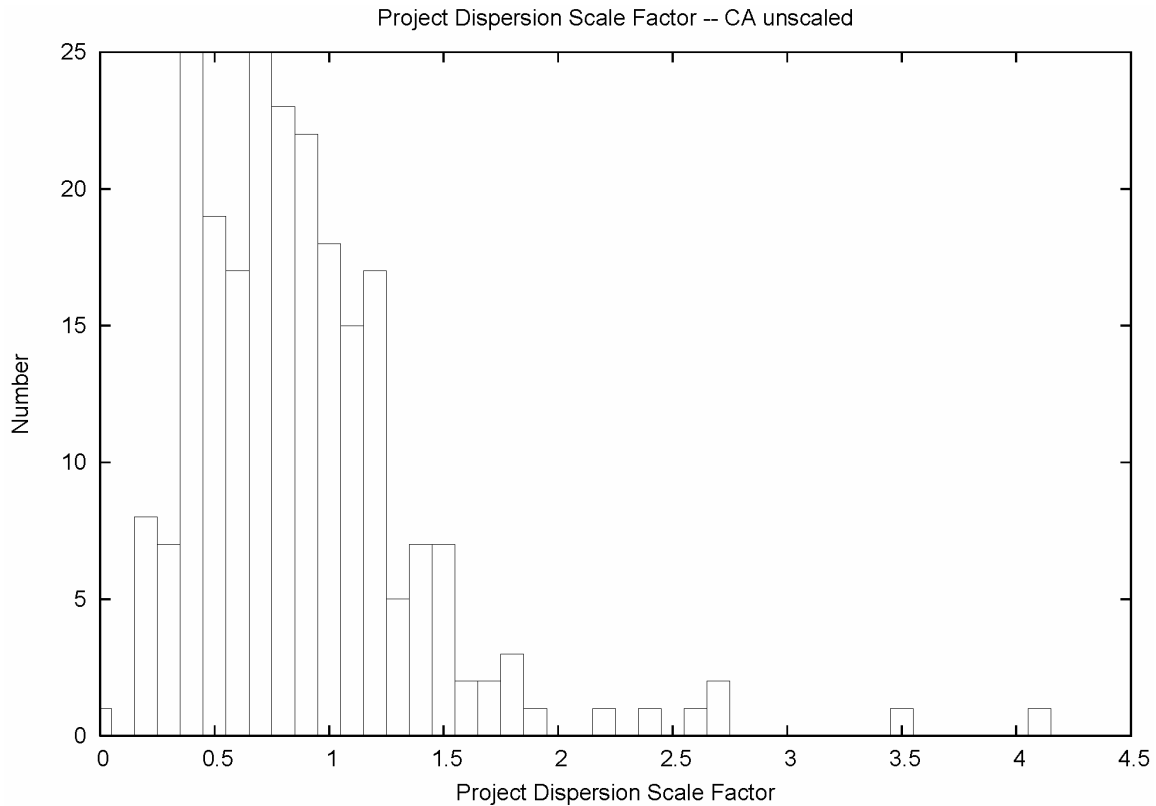
Figure 33.1. Unscaled California project dispersion factors.

Figure 33.1 is analogous to Figures 30.1-30.3 for the entire National Readjustment. Despite the similarity in shape, there is a distinct skew to the left. Note the two peaks in 0.4 and 0.7 bins. It is not obvious they are due to the behavior of spur line and spur figure projects.

Next, the horizontal and vertical project dispersion scale factors, d_h and d_v, are histogrammed in Figures 33.2 and 33.3, respectively. The horizontal dispersion factors show much more scatter than the vertical. And, the horizontal standard deviations for the unscaled California projects are too pessimistic in general. That is, one should multiply the horizontal network and local accuracies by about 0.7 in California. The tighter distribution of the vertical dispersion factors shows an even greater effect. One should multiply the vertical network and local accuracies by about 0.35 in California.

Figure 33.2. Unscaled California project horizontal dispersion factors.

Figure 33.3. Unscaled California project vertical dispersion factors.

Next, to provide comparison to Figure 15.3, ratios were computed for each horizontal/vertical dispersion scale factor for the unscaled California projects. Th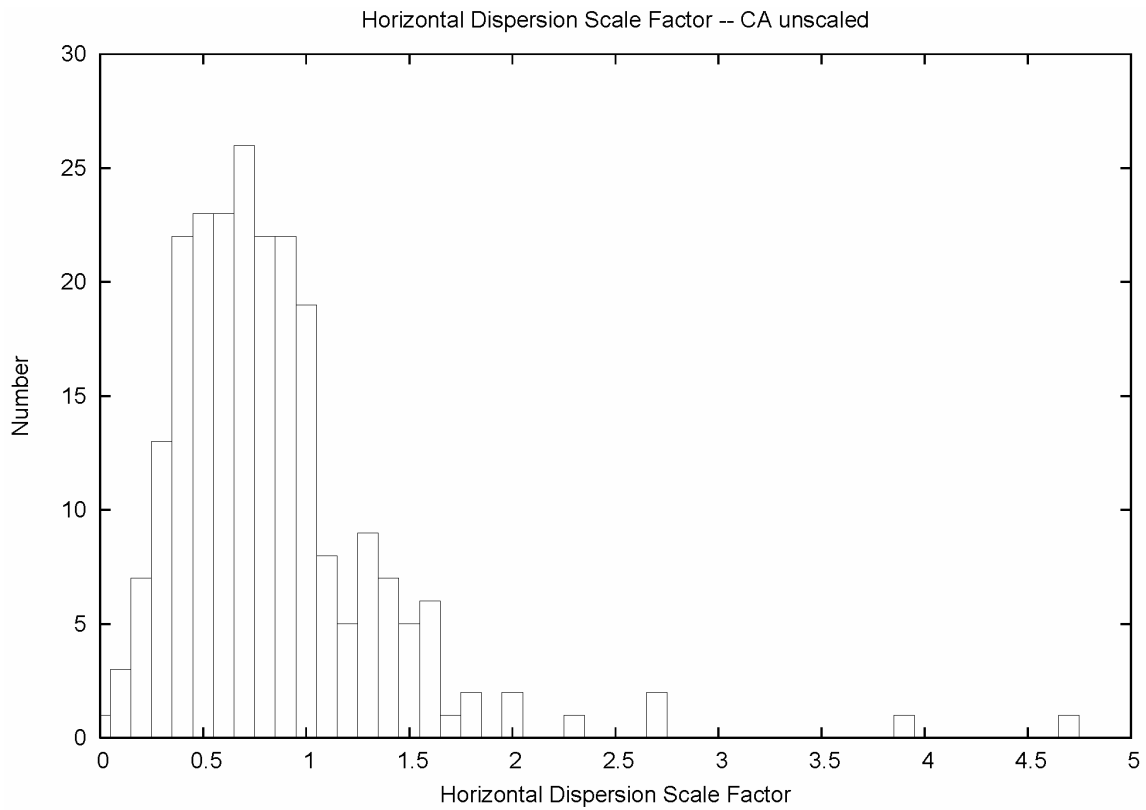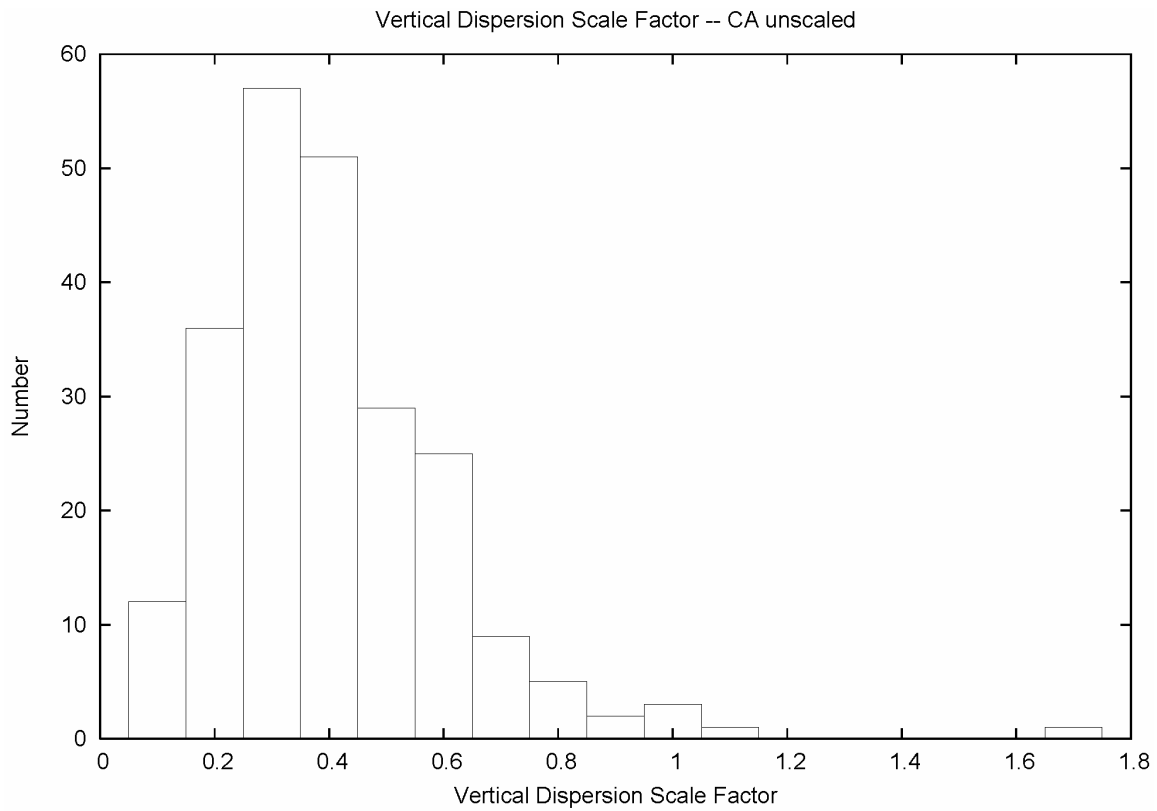ese are histogrammed in Figure 33.4. And, the percentiles are collected into Table 33.2. (Refer to propullca.txt in the Electronic Support Material.)
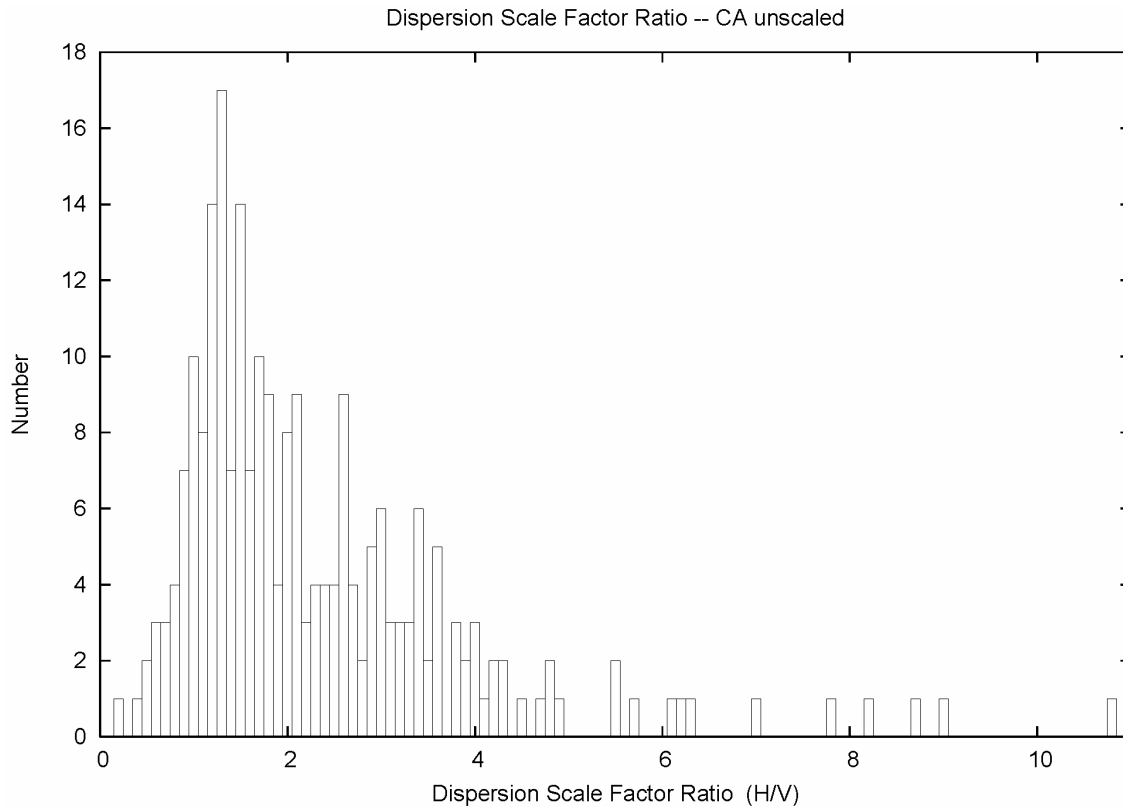
Figure 33.4. Unscaled California project horizontal/vertical dispersion factor ratios.

Table 33.2 – Percentiles of Unscaled California Hor./Vert. Dispersion Factor Ratios

Percentile	Ratio
50%	1.83
68%	2.59
90%	4.01
95%	4.92
99%	8.73
99.9%	10.84

The figures above show that the long tail to the right in the ratio distribution of Figure 33.4 is related to the horizontal tail of Figure 33.2, but is elongated due to the generally low magnitudes of the vertical dispersion scale factors of Figure 33.3. The median ratio is 1.83. That is, the horizontal standard deviations from treatment of California were too optimistic relative to the vertical standard deviations by 83%. This is in contrast to the 1.5 ratio generally obtained in Section 15. But, again, it must be remembered from Figures 33.2 and 33.3 that both the horizontal and vertical standard

116

deviations in California are too pessimistic. The pessimism of the height component weights of the California projects may be a factor in why a number of the California Height Modernization points (Figure 23.2) did not appear in the 1 cm vertical network accuracy plot (Figure 23.1).

The dispersion scale factors for the California unscaled projects can be inspected in time. This provides a check on the coefficients in the code fragment of Table 33.1. The temporal distribution of the three-dimensional project dispersion factors for the unscaled California projects is plotted in Figure 33.5.
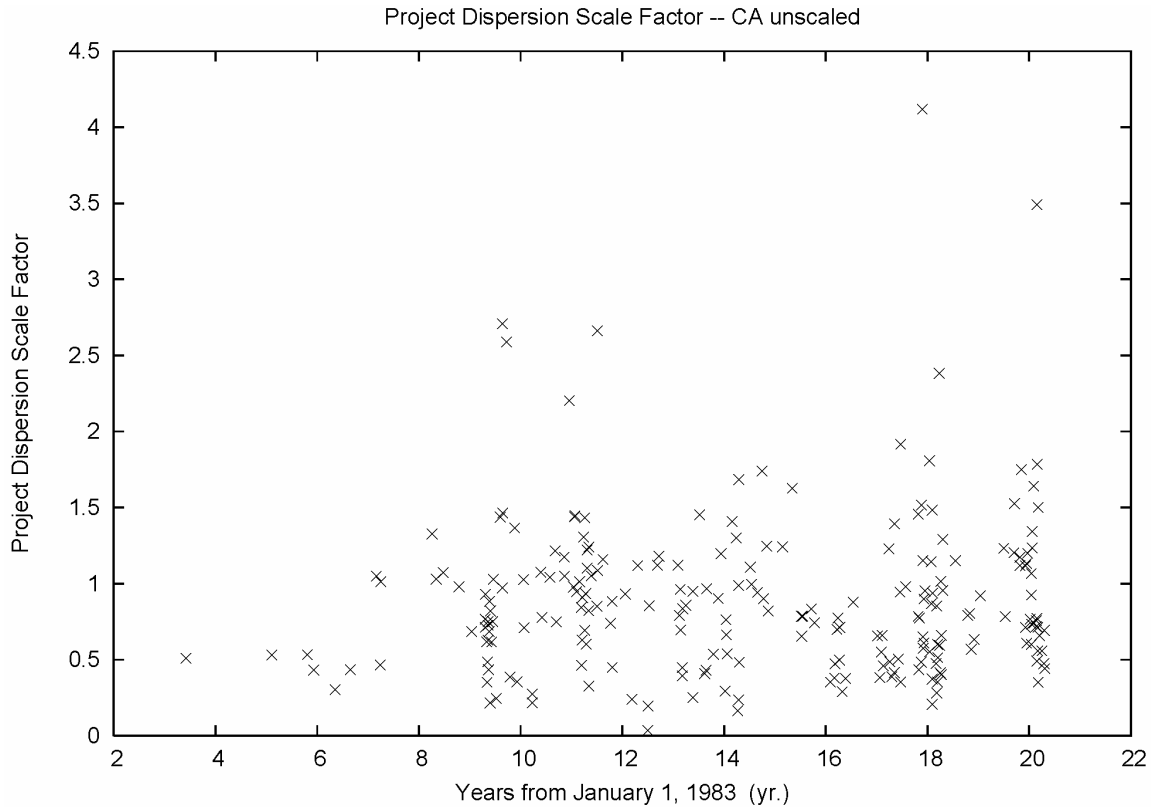
Figure 33.5. Temporal distribution of unscaled California project dispersion factors.

Although arguable, Figure 33.5 does give an impression of smaller factors on the left and larger factors on the right. Such an interpretation would indicate that the code fragment in Table 33.1 excessively deweighted older projects, and that the weight model coefficients could be reduced.

34. CORS fixed control

After passing through the rejection and data editing processes that lead to the final free adjustment, the vectors were then fixed to a set of NAD 83 CORS coordinates. Briefly recapitulating Pursell *et al*. (2008) and National Geodetic Survey (2007),

1. In California, the CORS coordinates at the 2007.0 epoch were obtained from the California Spatial Reference Center (CSRC) on 1/18/2007 from modeled position time series up to 12/28/2006.

2. In Arizona, Nevada, Oregon, and Washington, the CORS coordinate at the 2007.0 epoch were obtained by applying the HTDP 2.9 models.

3. In Alaska, the CORS coordinates at the 2003.0 epoch were fixed.

4. For the remainder of the country, the CORS coordinates at the 2002.0 epoch were fixed.

Figure 34.1 displays the CORS fixed control in the NSRS 2007 National Readjustment in the conterminous United States. (Refer to allcors23d.txt and allcors23nv4.txt in the Electronic Support Material.) Figures for CORS fixed control in Alaska and the Caribbean are in the Appendix.
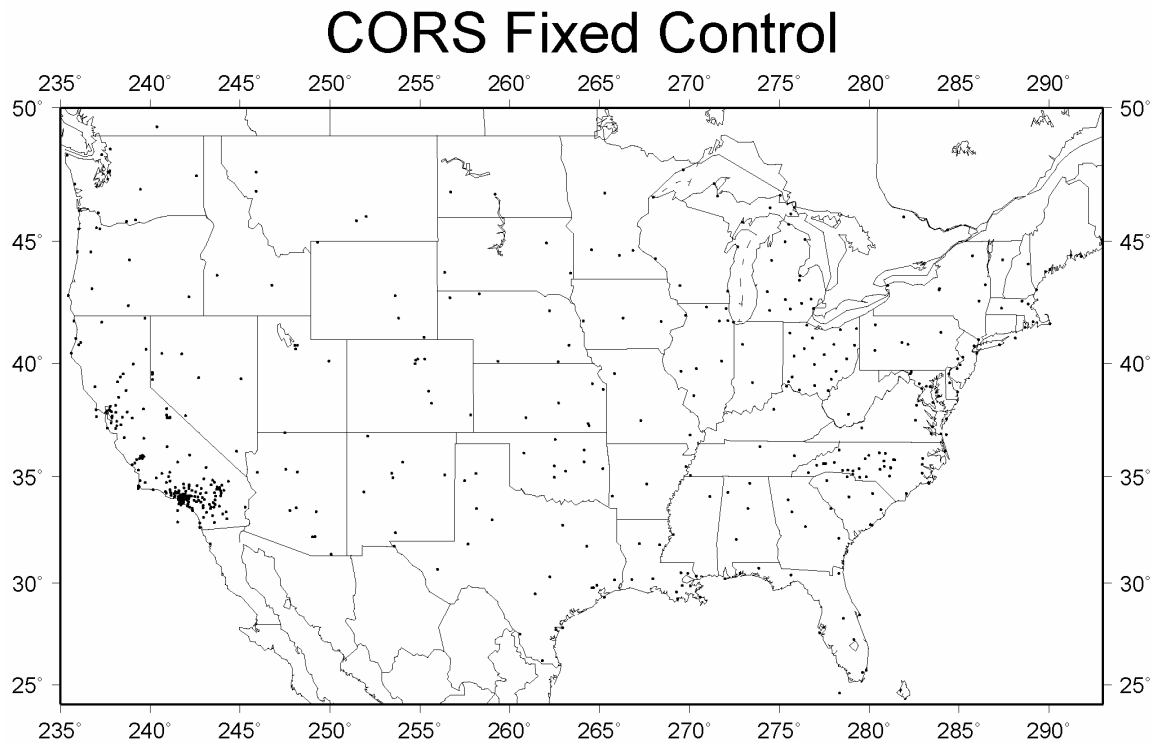
Figure 34.1. CORS fixed control, conterminous U.S.

In the course of analysis of the fixed adjustment, a fraction of the CORS was converted from a fixed status to a weighted status. Further, for these CORS stations, this was done independently for the horizontal and vertical components. Thus, as described in Table 1.1, 673 CORS were fixed in all three dimensions. Five CORS were fixed horizontally, and the vertical had a weight. Seven CORS were weighted in all three components. Three CORS (DF7065, AI9604, AH7473) were never weighted at all due to

clerical error. Figure 34.1 portrays those CORS that were fixed in either two or three dimensions.

When considering the sources of the NSRS 2007 CORS coordinates within the conterminous United States, one notes that CSRC CORS horizontal and vertical velocities are used to establish the CORS coordinates within California; that HTDP model horizontal velocities, only, established the CORS coordinates with the other motion states (Arizona, Nevada, Oregon, and Washington); and that the remainder of the country is considered stationary even if non-zero CORS velocities were available.

CORS velocities were computed from adjusted CORS data in March 2002 (Soler and Snay 2004). For those CORS installed since that time, CORS velocities are obtained with the HTDP model. Note that while a newer CORS velocity solution using data through 2003 is found in Snay *et al.* (2007), that solution was not operationally promulgated (Snay, private communication, 2007).

The CORS coordinate set used as fixed control was in the NAD 83 frame. As of March 2002, the NAD 83 set was identical to the ITRF set (Soler and Snay 2004), subject to a reference frame transformation. However, the CORS coordinates expressed in the NAD 83 frame are updated when exceeding a 2 cm horizontal, 4 cm vertical tolerance. This is in contrast to a 1 cm horizontal, 2 cm vertical tolerance established for the CORS coordinates in the ITRF frame. Note, this does not mean that the NAD 83 frame CORS coordinates are necessarily inaccurate at a 2 cm - 4 cm level.

There is no technical impediment to the transformation of the existing CORS coordinate and velocity data set in the ITRF00, epoch 1997.0 frame (with the tighter tolerances) into an NAD 83, epoch 2007.0 frame. Of course, one would update, operationalize, and publish any such NAD 83 CORS coordinates, epoch 2007.0, as a natural function of the NSRS 2007 National Readjustment. However, this was not done.

Unfortunately, the existence of the CORS coordinate tolerances, either ITRF or NAD 83, does not mean that the published CORS coordinates are actually maintained at those tolerances. As described later in this report (Section 41), the cases where CORS coordinate tolerances are exceeded have caused users to recommend that one manually correct OPUS runs to account for the CORS coordinate departures.

As an example of existing CORS coordinate departures, the 60 day time series for STKR is reproduced in Figure 34.2. The 60 day time series are an automated product found on National Geodetic Survey web pages. One notes the 1.35 cm horizontal departure exceeds the 1 cm horizontal tolerance for an ITRF00 position. And, the -3.28 cm vertical departure exceeds the 2 cm vertical tolerance. This is not a recent development. Figure 32.3 reproduces the 60 day time series for STKR obtained on February 21, 2007. While the 0.9957 cm horizontal departure does (barely) meet the 1 cm horizontal tolerance, the -2.85 cm vertical departure exceeded the 2 cm vertical tolerance back in early 2007. It is expected that the CORS coordinates for STKR will be updated by the time this report is published.

STKR: Daily minus Published ITRF00 Position

N(cm) = 0.93 (+−0.18) E(cm) = 0.98 (+−0.32) U(cm) = −3.28 (+−1.03)
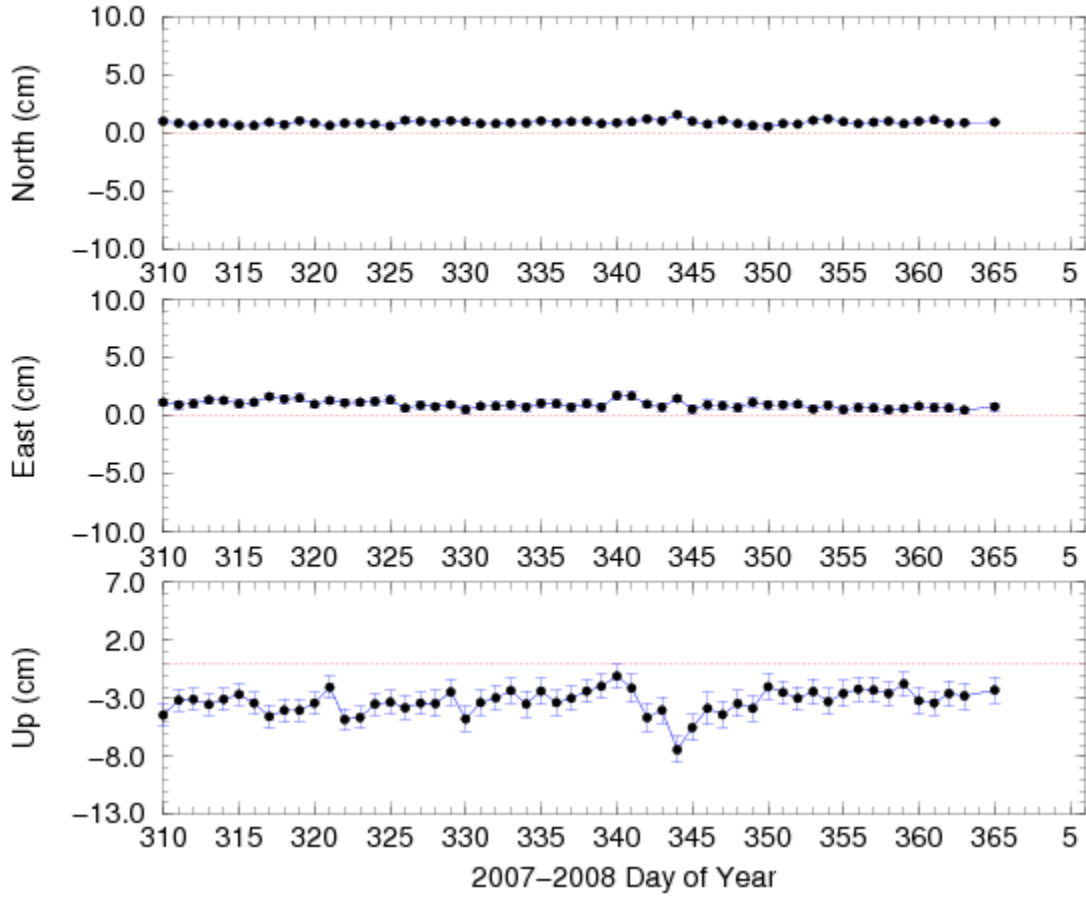
Figure 34.2. STKR, Ohio, 60 day time series, January 10, 2008.

STKR: Daily minus Published ITRF00 Position

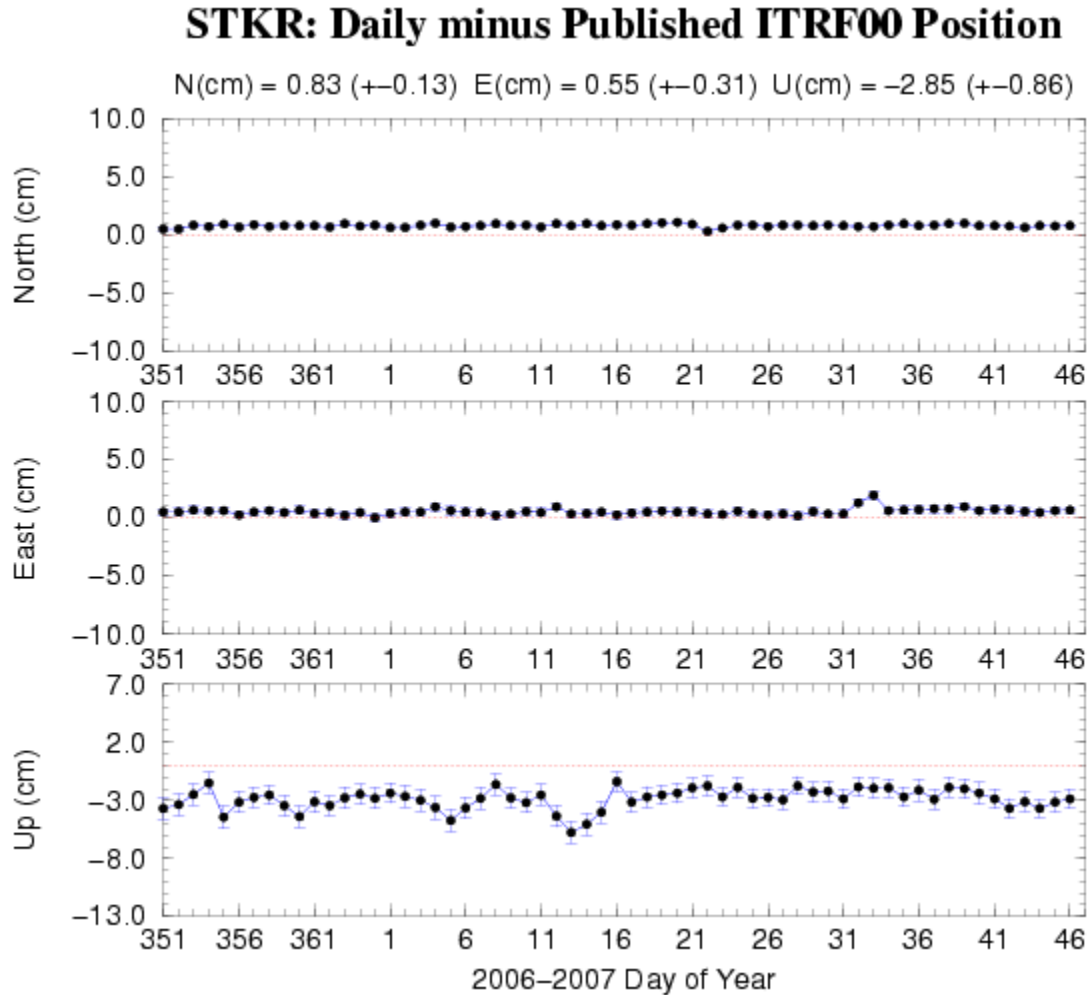N(cm) = 0.83 (+−0.13) E(cm) = 0.55 (+−0.31) U(cm) = −2.85 (+−0.86)

Figure 34.3. STKR, Ohio, 60 day time series, February 21, 2007.

In closing this section, it can be seen that the quality of the CORS fixed control used in the NSRS 2007 National Readjustment is mixed. The situation is not completely bleak. Inspection of temporal distribution of the GPS vectors in Figures 4.4 and 4.5 indicate that over half of the GPS vectors are within a +/- 5 year window about the 2002.0 epoch of the last published (March 2002) CORS sets. And, when a new CORS is emplaced, the NAD 83 coordinate is identical to the ITRF, subject to the reference frame transformation. Nonetheless, the presence of displacements such as those above makes analysis difficult.

35. CORS antenna displacements, 2002.0-2007.0

With the exception of California, CORS coordinate velocities were not used in the update of the coordinate set to 2007.0. To understand their potential effect, the CORS NAD 83 velocities were transformed into displacements over a 5 year interval. Five years was selected since over half the NSRS 2007 vectors are within a +/- 5 year window about the CORS NAD 83 2002.0 epoch (Figures 4.4 and 4.5). (Refer to cvmerge1.txt in the Electronic Support Material.) The CORS horizontal and vertical antenna

displacements (that are non-zero) are plotted as vectors in Figure 35.1 and 35.2, respectively.

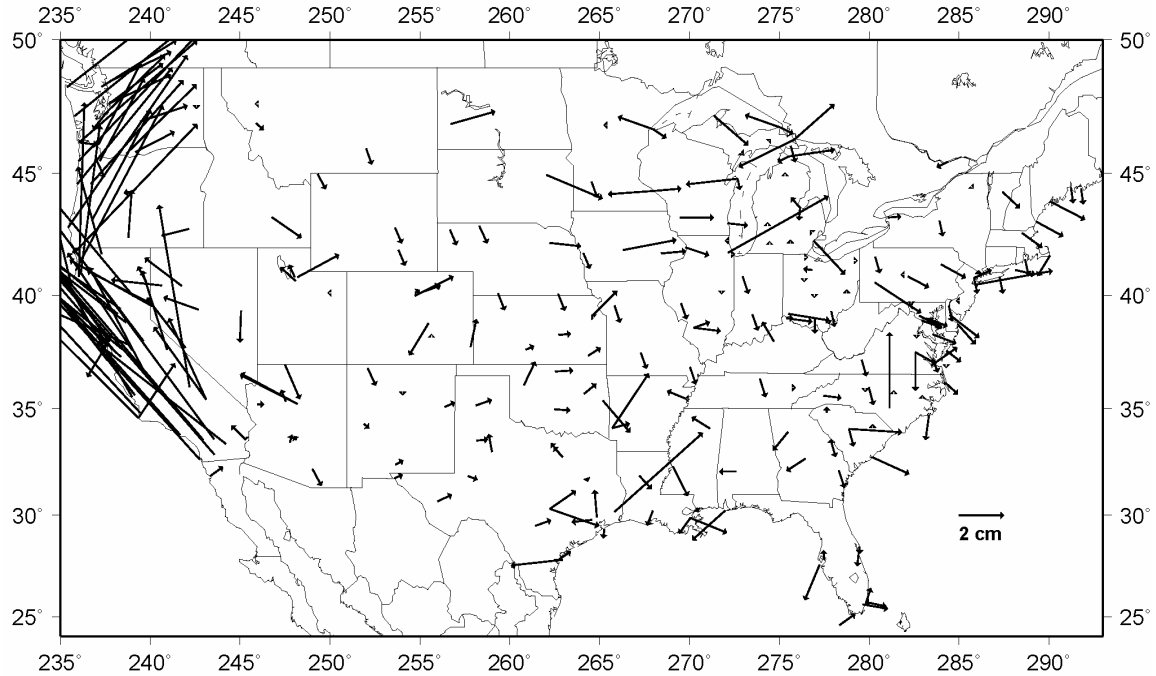## Antenna Displacements (5 years)

Figure 35.1. CORS horizontal antenna displacements, NAD 83, 2002.0-2007.0.
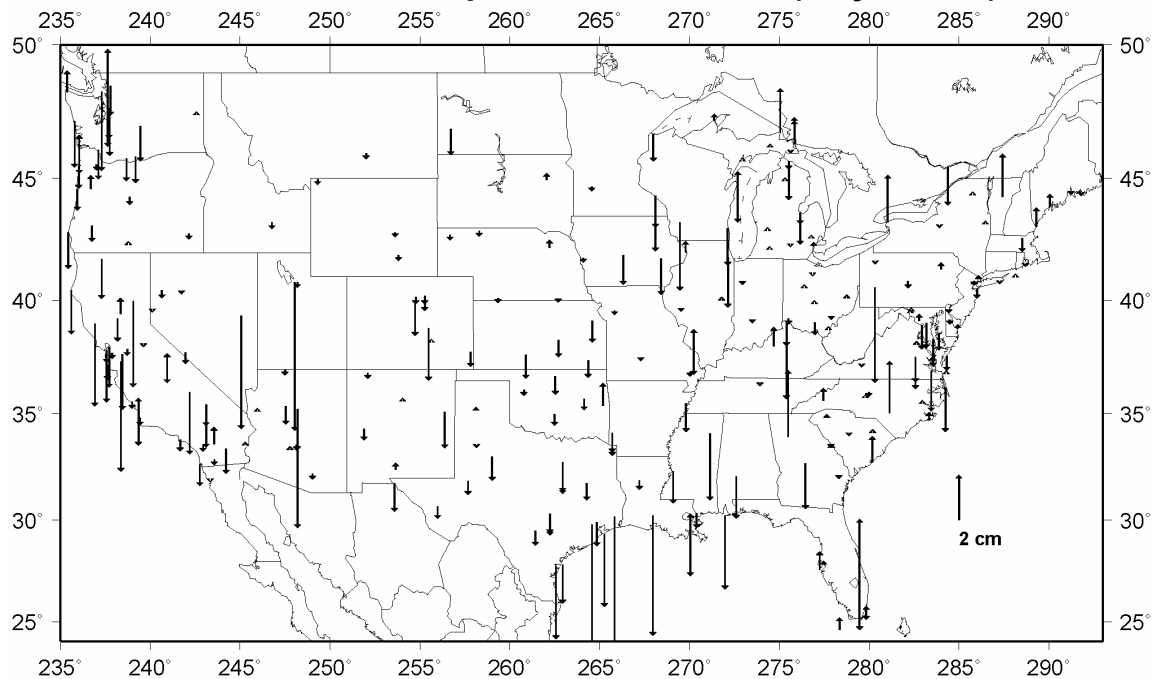
Antenna Displacements (5 years)

Figure 35.2. CORS vertical antenna displacements, NAD 83, 2002.0-2007.0.

It must be emphasized that the displacements in Figures 35.1 and 35.2 portray CORS antenna motion, not necessarily crustal motion. This distinction is necessary. CORS antennae have a variety of mounts; from steel girders and deep drilled pillars to building roofs and towers. While effort is made to insure detected motion is not local to the antenna, cases of nearby vectors with distinctly different displacements are seen in Figures 35.1 and 35.2.

Irrespective of whether the source of CORS antenna displacement is crustal motion, local soil mechanics, or antenna mount issues, any CORS secular motion must be considered when fixing CORS coordinates. This implies, not only the update of CORS coordinates with CORS velocities to the computation epoch, but also the update of the GPS vectors with CORS velocities to the computation epoch. The former update is claimed as unnecessary by assertion of a computation epoch of 2002.0 for non-motion states. The latter update was not performed for the bulk of the United States in the readjustment. Assertion of the computation epoch for NSRS 2007 as 2002.0 for non-motion states, while using a 2007 datum tag will cause confusion without explicit addition of an epoch. In addition, OPUS processing, which uses CORS velocities, is inconsistent with the NAD 83(NSRS2007) computational procedure.

Figure 35.1 certainly shows crustal motion in the Western states of the United States. Figure 35.2 shows subsidence in the Gulf Coast, as well as in spots throughout the conterminous United States. The vertical displacements are difficult to interpret, since one may be susceptible to soil mechanics and antenna mount problems. Kaula (1987) points out that vertical control requirements for subsidence detection are difficult to formulate, since there is no limit to the accuracy (when formulated by slope changes and length scales) that could be utilized. Thus, large differences in vertical displacement at nearby points could be real – a vertical motion field can have significant short length scale structure.

The displacements in Figures 35.1 and 35.2 do not have error estimates. This further complicates any interpretation. The underlying CORS velocities may be derived from data sets that were shorter than the 5 year interval that is portrayed. In such cases, one will get better results by not updating CORS coordinates or GPS vectors with suspect CORS velocities. The solution, of course, is compute CORS velocities with as much recent data as possible.

36. HTDP 2.9 model displacements, 2002.0-2007.0

Since HTDP 2.9 (Snay 1999) was used for GPS vector correction, as well as a surrogate for the CORS velocities, it is worthwhile to inspect its behavior over a 5 year interval. The horizontal and vertical position displacements (that are non-zero) at the CORS fixed control points are plotted as vectors in Figure 36.1 and 36.2, respectively. (Refer to corsdel5y.txt in the Electronic Support Material.) Note that the time interval includes the dislocations of the M6.5 San Simeon earthquake of December 2003 and the M6.0 Parkfield earthquake of September 2004. The absence of vectors in Figure 36.2

serves as a reminder that HTDP is a set of horizontal models, and that no vertical models are present.
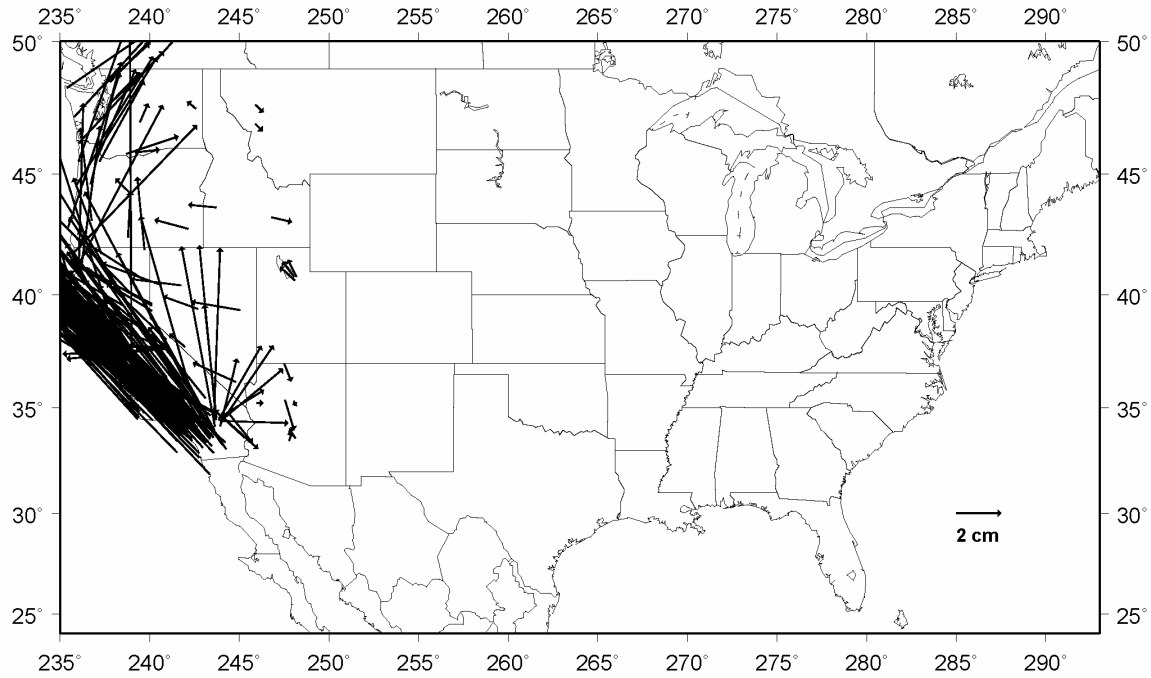
HTDP 2.9 (5 years)

Figure 36.1. HTDP model horizontal displacements at CORS, 2002.0-2007.0.
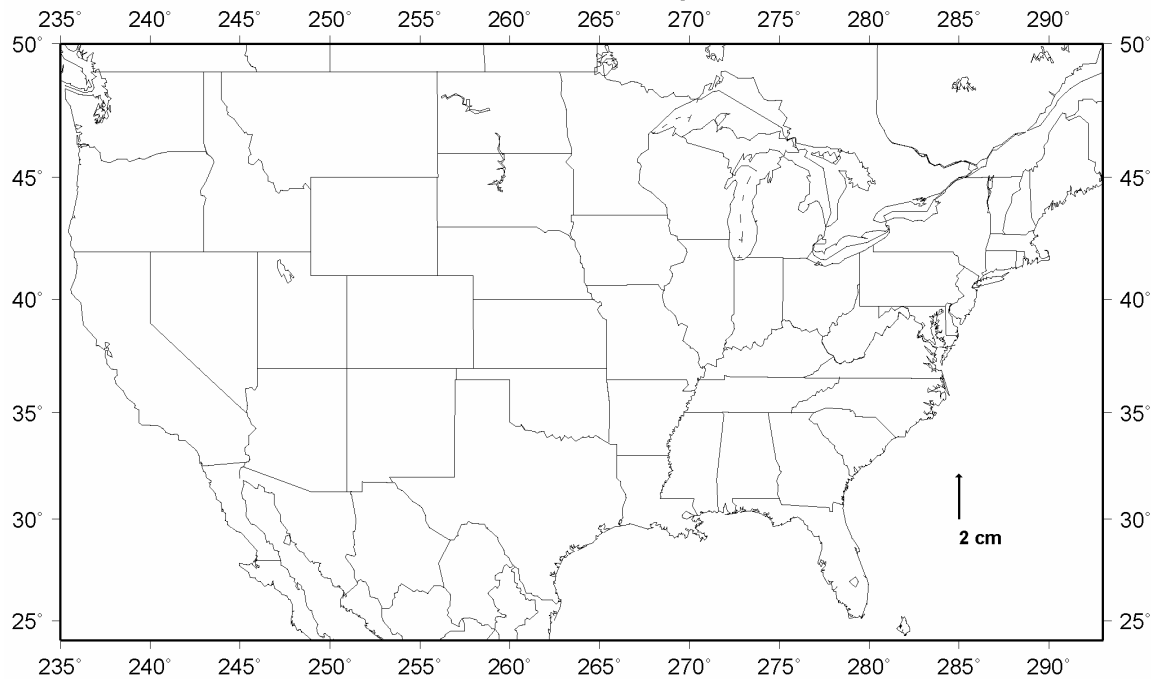
HTDP 2.9 (5 years)

Figure 36.2. HTDP model vertical displacements at CORS, 2002.0-2007.0.

The absence of vectors in the bulk of the conterminous United States (Figure 36.1) illustrates the restricted nature of the horizontal motion models in HTDP. This serves to crystallize the question, "Is there significant horizontal crustal motion in the majority of the United States?" And, "significant" could be interpreted in light of the median vector lengths (31 km) and network accuracy (1 cm) of NSRS 2007. The answer may well be "no" for many applications, but such a study should be conducted. In absence of such an NGS study, one could implement the spatially averaged residual velocity field in Figure 15 of Calais *et al.* (2006).

As a fine point in the NSRS 2007 data processing, there was no guarantee that all vectors involving points in crustal motion states were processed through HTDP. This is because HTDP was applied at the Helmert block level. And, projects as a whole were assigned to Helmert blocks (Pursell *el al.* 2008). But individual vectors in a project can span state boundaries, and even be wholly contained in an adjacent state. Hence, vectors can be missed. The simplest remedy is to process all Helmert blocks through HTDP.

37. CORS-HTDP displacement differences, 2002.0-2007.0

Since HTDP was used as a surrogate for CORS velocities in establishing the CORS fixed control for 2007.0, it is natural to look at the CORS – HTDP differences in the displacements over 2002.0 to 2007.0 for those CORS that have non-zero velocities. (Refer to cvlhtdp2v.txt in the Electronic Support Material.) The horizontal displacement differences are plotted in Figure 37.1, and the vertical displacement differences are plotted in Figure 37.2
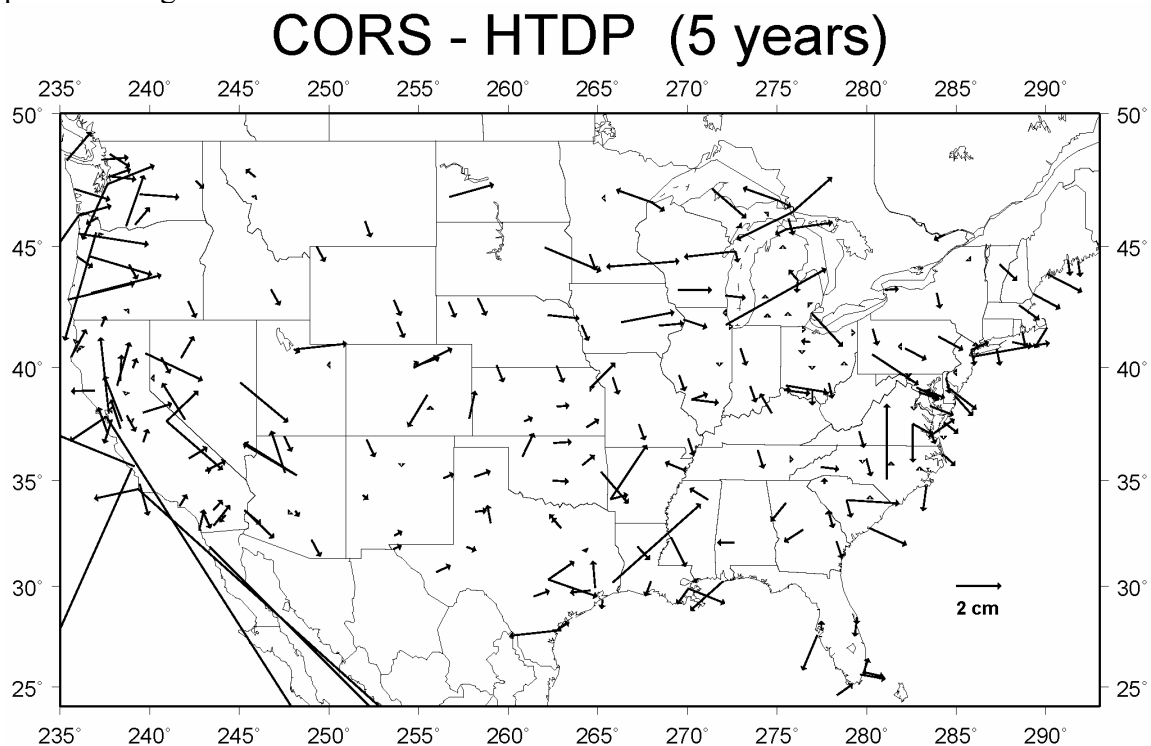

Figure 37.1. CORS-HTDP horizontal displacement differences, 2002.0-2007.0.
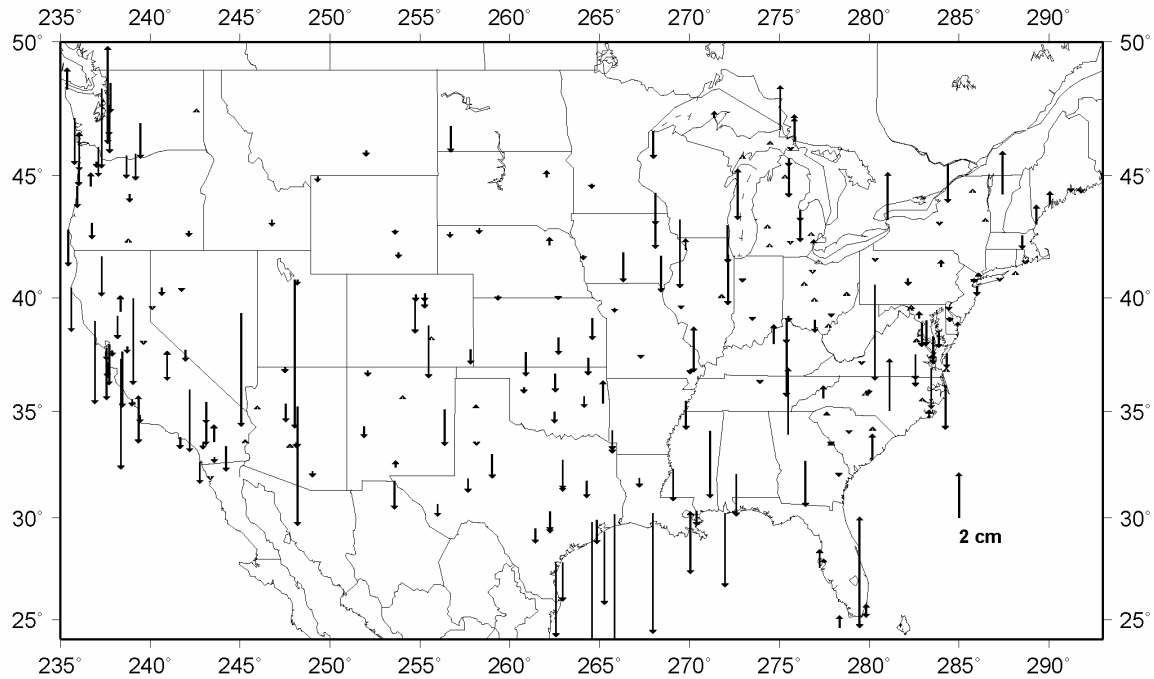
CORS - HTDP (5 years)

Figure 37.2. CORS-HTDP vertical displacement differences, 2002.0-2007.0.

Figure 37.1 contains few surprises. One merely sees the repetition of the CORS displacement plot (Figure 35.1) over the non-motion states, and the general removal of the tectonic displacement of the Pacific plate. However, there is a surprise in the presence of a number of sizable displacements along the West Coast. These are points with large differences in the two velocity fields. It is most notable in the Pacific Northwest. Also, recall that CSRC-derived CORS coordinates were used in California.

Figure 37.2 contains no surprises at all. Since HTDP is solely horizontal, nothing acts as a surrogate for the CORS vertical displacements.

The creation of Figures 37.1 and 37.2 was performed for those CORS points with non-zero velocities. However, certain CORS points had zero velocities and non-zero displacements modeled by HTDP. These displacements are plotted in Figure 37.3 in the sense of CORS - HTDP. Thus, they will reflect the HTDP model, but with an opposite sign (since the CORS is zero displacement). (Refer to cvlhtdp20.txt in the Electronic Support Material.) The large vectors in California are not immediately troublesome, since CSRC-derived CORS coordinates were used in California, but they should be investigated.
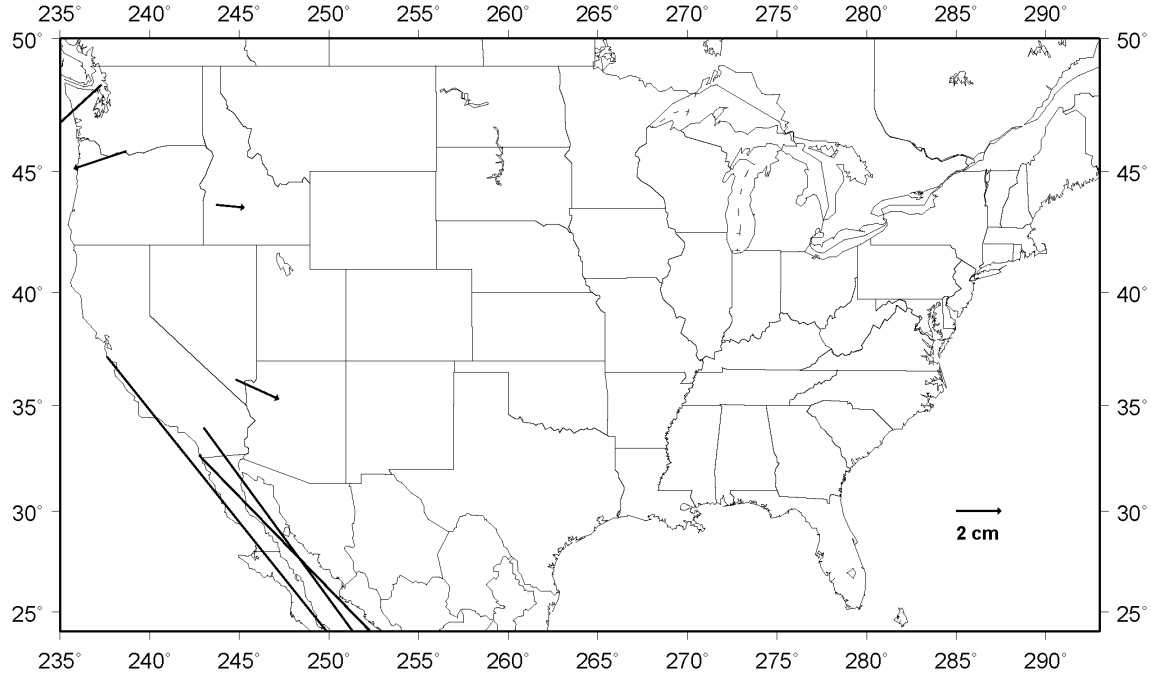
Figure 37.3. CORS-HTDP horizontal displacement differences, no CORS velocity.

As a final point in interpreting the plots in this section, it should be recalled that the CORS coordinates in California were obtained from CRSC. As such, the data spans for those CORS coordinates would be much longer, and the associated CORS velocities would be more accurate than the NGS data base values depicted above.

Distinct from the source of the California CORS coordinates, questions regarding the validity of the HTDP horizontal velocity models (and absence of vertical velocity) would still pertain in the comparisons. The pictures above depict discontinuities between CORS and HTDP velocities that would affect OPUS solutions in California as well as the NSRS 2007 adjustment in the Western U. S.

38. Residual differences due to CORS fixed control

This set of plots expresses the direct impact of applying the CORS fixed control. All the free adjustment residuals were differenced against their fixed adjustment counterparts. For those residual difference absolute values exceeding a given display tolerance, the vector midpoints are plotted. (Refer to alldres.txt in the Electronic Support Material.) Figure 38.1 displays those horizontal residuals that changed by more than 2 cm between the free and the fixed adjustment. Note that 2 cm represents the horizontal tolerance specified for the CORS NAD 83 coordinates.

Delta Horizontal Residuals, 2 cm
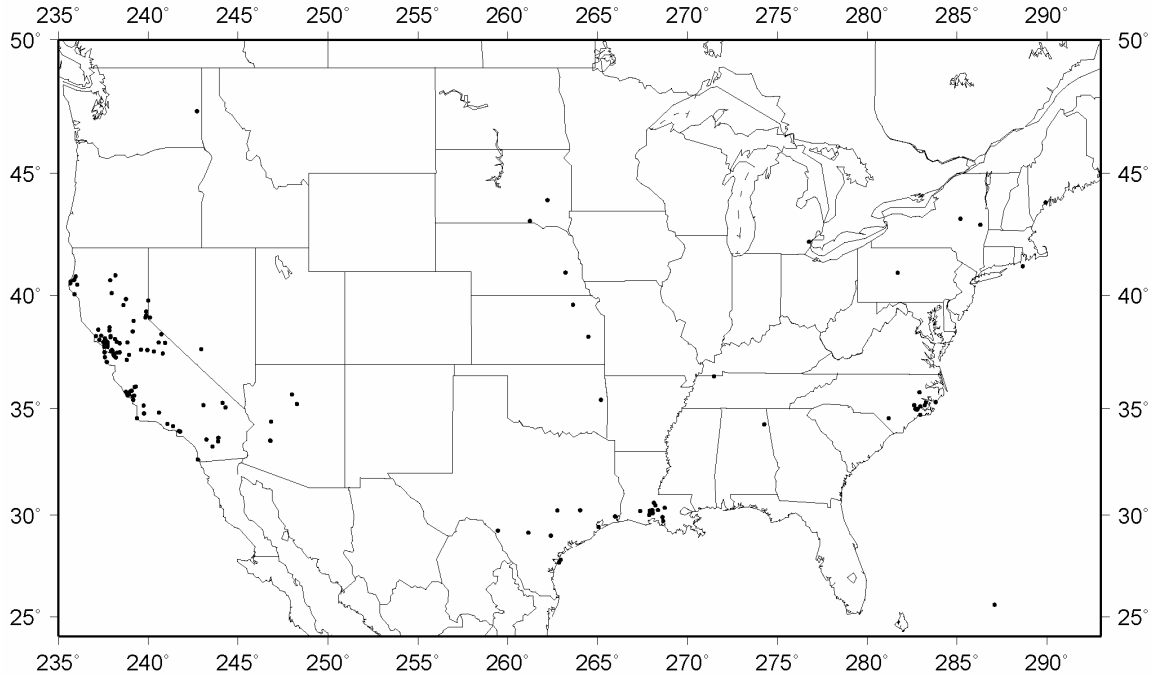
Figure 38.1. Midpoints of distance residual differences, fixed-free, exceeding 2 cm.

Figure 38.1 shows 386 vector midpoints that changed horizontally by more than 2 cm between the free and fixed adjustment. This is a very small number of points from the 283,691 residual differences. One notes they are primarily located in California, with secondary concentrations in Louisiana and North Carolina. Systematic error in the treatment of crustal motion (either due to the CORS point or the GPS vector) is the suspected cause for the California points. Be aware, however, that the points represent vector midpoints, and the actual vector endpoints could be some distance away.

The display tolerance for the horizontal differences is halved to 1 cm in Figure 38.2. This figure shows 2633 vectors. Note that this represents 0.928% of the total set of vector differences. Note, also, that 1 cm represents the median horizontal network accuracy of NSRS 2007.

Delta Horizontal Residuals, 1 cm

Figure 38.2. Midpoints of distance residual differences, fixed-free, exeeding 1 cm.

The additional points plotted in Figure 38.2 show a need for harmonization of the California CORS coordinate set at the GPS vectors of NSRS 2007. An improved HTDP model for California would be the likely solution. The clusters of points at other urban locations indicate a need to either accommodate the CORS antenna displacement, or inspect the CORS 60 day series for possible coordinate departures. The distribution of midpoints in Northern Georgia is curious. They are near Atlanta, but do not form a tight cluster. In general, when comparing Figure 38.2 and Figure 37.1, one notices occasional, incidental coincidence, but no major correlation except for California.

Next the midpoints of the vertical residual that changed by more than 4 cm between the free and the fixed adjustment are plotted in Figure 38.3. Note that 4 cm represents the vertical tolerance specified for the CORS NAD 83 coordinates.

129

Delta Vertical Residuals, 4 cm
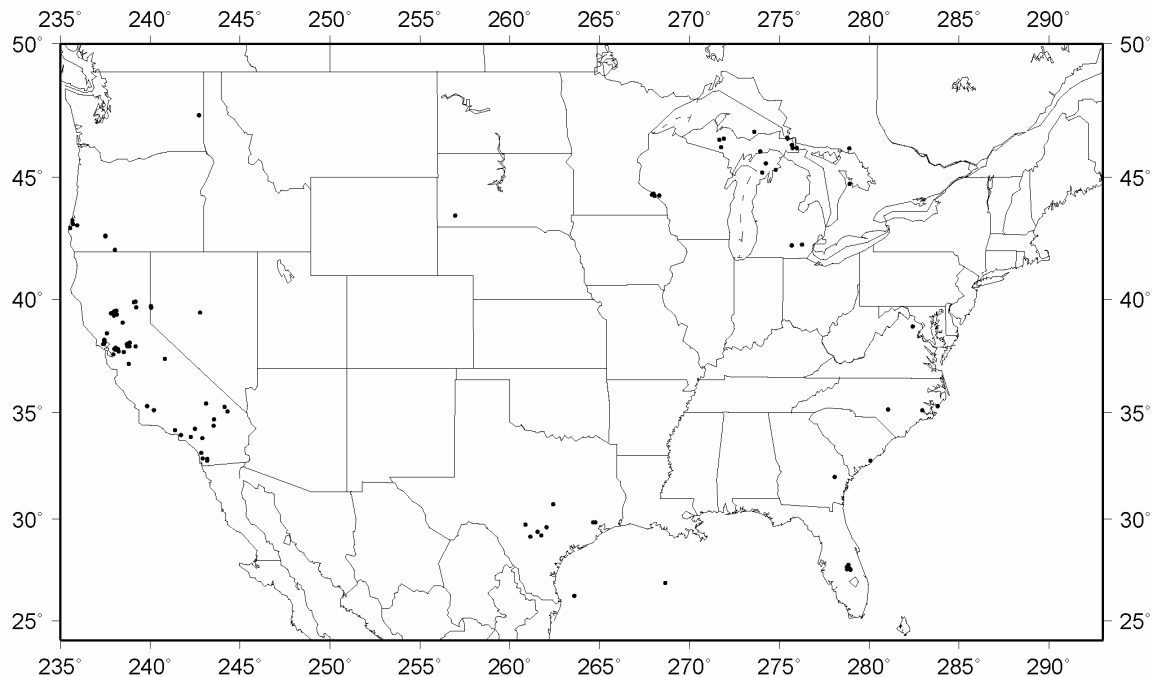
Figure 38.3. Midpoints of height residual differences, fixed-free, exeeding 4 cm.

Figure 38.3 shows 203 vector midpoints. Those points in the Gulf of Mexico serve to remind that midpoints are plotted, and that the endpoints may be quite far away. The vertical differences are harder to interpret, since vertical velocity can have short wavelength structure (Kaula 1987). Some correlation is present between Figure 38.3 and Figure 37.2. Note the coast of Oregon, North Central California, and Northern Michigan. This indicates the need to incorporate CORS vertical velocities in the constraints as well as in the GPS vector corrections.

The display tolerance for the vertical differences is now halved to 2 cm in Figure 38.4. This figure portrays 1387 vectors. This is only 0.489% of the total set of vector differences. Note, also, that 2 cm represents the median vertical network accuracy of NSRS 2007.

Delta Vertical Residuals, 2 cm
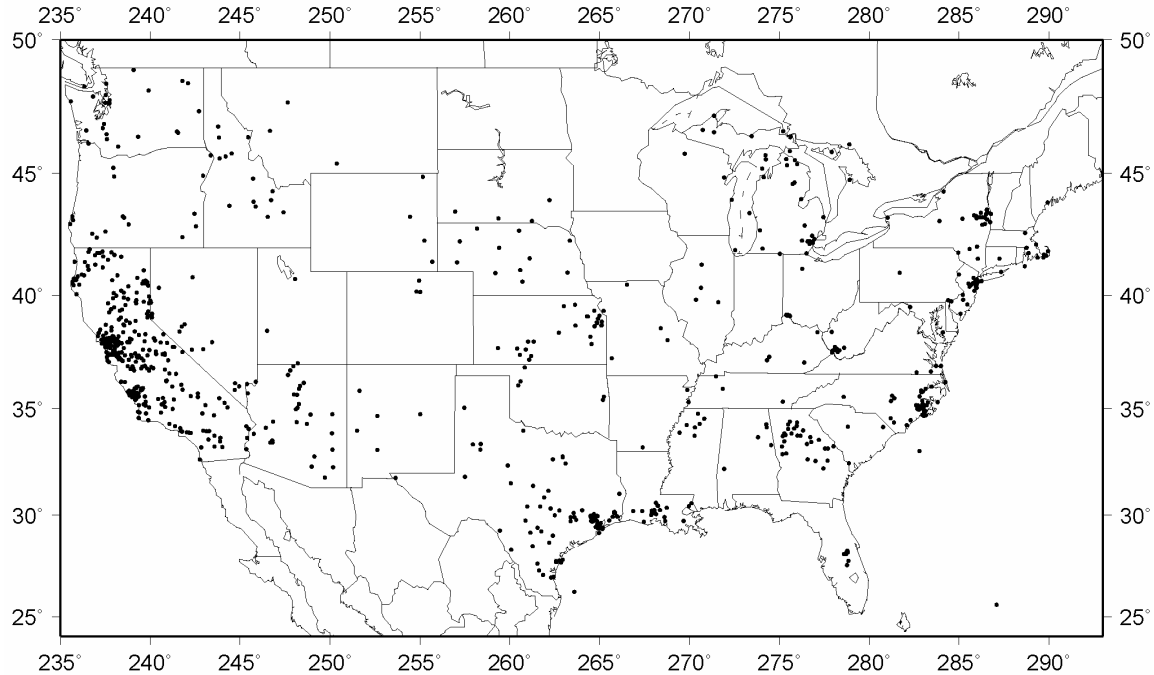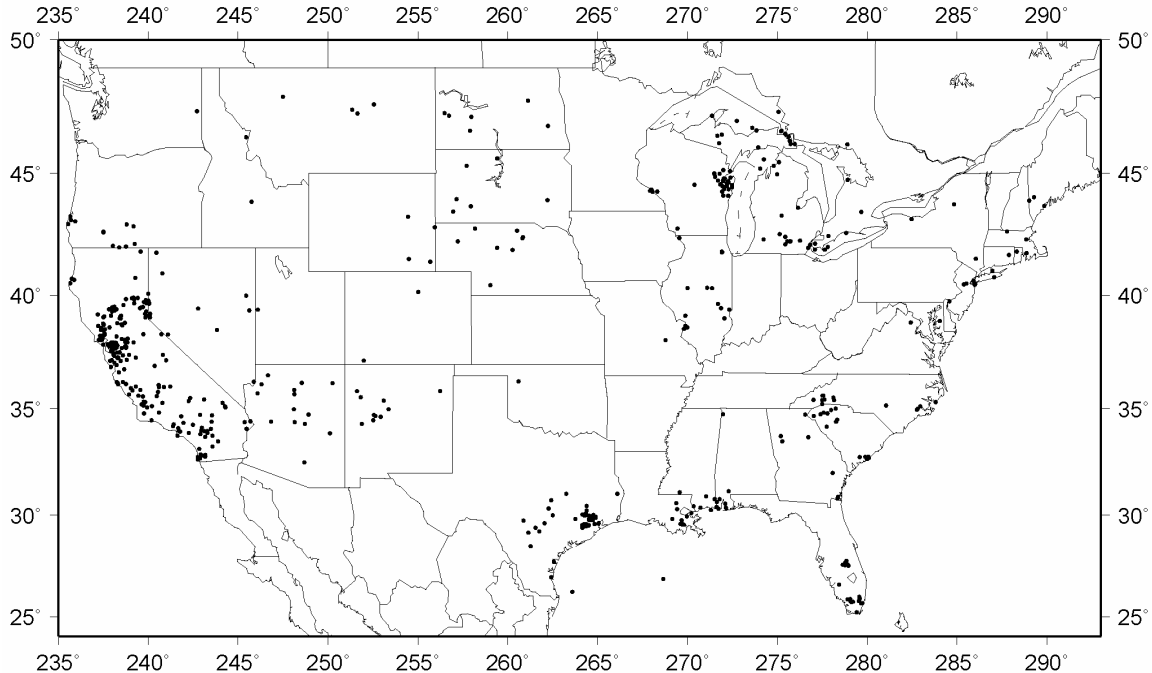

Figure 38.4. Midpoints of height residual differences, fixed-free, exeeding 2 cm.

Figure 38.4 does show evidence of vertical motion unaccommodated by the CORS and/or GPS vector correction. Houston/Galveston is very evident now, along with a string of midpoints along the Louisiana-Mississippi coast. A string of midpoints are now present in Northern Michigan near Sault Ste Marie. The concentration near Green Bay (East Wisconsin) may be due to vertical CORS NAD 83 coordinate departure(s) (although the vertical NAD 83 tolerance is 4 cm).

The NSRS 2007 variance of unit weight will be addressed in detail in the next section (Section 39). However, some comments can be made regarding the increase of the variance of unit weight between the free and fixed adjustment. The variance increased from 1.63 to 1.89, which is too large when adding 2055 constraints to 650,000 degrees of freedom. But the weighted variance sums tell a story. The expected variance sum should approach the degrees of freedom, or about 650,000. The free adjustment variance sum came in at 1056077.7; that is, about 400,000 too high in residual errors and weighting issues. The fixed adjustment variance sum was 1229874.4; which was another 174,000 in residual errors. But, that amount is only 30% of the excessive error seen in the NSRS 2007 fixed adjustment. (Which, in turn, was passed through to the accuracy estimates by means of the *a posteriori* protocol). When deciding where to spend NGS analytic resources, consider outlier clearing and project weight analysis. This will reduce the "tails" seen in many of the figures in this report. The free adjustment contains 2/3 of the excessive error.

That said, there is no substitute for the best possible CORS coordinates in the NAD 83 frame, the best possible CORS velocity estimates, and GPS vector correction

software that operates in three-dimensions and can distinguish between a crustal motion layer (vectors between monumented points) and a CORS motion layer (vectors to and from a CORS).

It is realized that the excellent median network accuracies of 1 cm horizontal and 2 cm vertical reported in Section 20 were a surprise. The comparatively small number of residual differences seen in Figures 38.1-38.4 suggests the GPS network is, in general, delivering this accuracy. Systematic departures follow patterns linked with crustal motion, subsidence, and, perhaps, Glacial Isostatic Adjustment (GIA).

39. The NSRS 2007 variance of unit weight

Certain remarks must be made regarding the free and fixed adjustment variance and standard deviations of unit weight. The core comment is that they are too large.

Table 39.1 reproduces the *a posteriori* statistics for the free and fixed adjustment extracted from Table 1.1.

Table 39.1 – Extract of key statistics of the NAD 83(NSRS2007) National Readjustment

```
Free Adjustment
647997 degrees of freedom, approximate
1056077.7 variance sum (vᵗPv)
1.629757 variance of unit weight
1.276619 standard deviation of unit weight

Fixed Adjustment
650049 degrees of freedom, approximate
1229874.4 variance sum (vᵗPv)
1.8919718 variance of unit weight
1.375490 standard deviation of unit weight
```

What may not be appreciated is that the uncertainty of an *a posteriori* variance of unit weight *decreases* as the degrees of freedom in an adjustment increase. And, NSRS 2007 has very many degrees of freedom. This makes any departure from an expected value of 1.0 particularly noticeable.

Dixon and Massey (1969) is used as a reference, although any introductory mathematical statistics book will serve. By theory, the variance sum, $v^t \mathbf{D}_o^{-1} v$ is distributed as chi-squared, χ^2. The variance of χ^2 is $2df$, where df is the degrees of freedom, and the dispersion of χ^2 is $(2df)^{1/2}$. In other words, $v^t \mathbf{D}_o^{-1} v$ slowly increases as the degrees of freedom increases. But, the *a posteriori* variance of unit weight is χ^2/df. And, so, the dispersion of the *a posteriori* variance of unit is $(2/df)^{1/2}$. The uncertainty of the *a posteriori* variance of unit weight gets smaller as the degrees of freedom increase.

This behavior is seen in Table A-6b "Percentiles of the χ^2/df distributions", on pages 466-467 of Dixon and Massey (1969). By use of the approximation for χ^2 for large degrees of freedom (pg. 465):

$$\chi^2 = df \left(1 - 2/(9\ df) + Z\left(2/(9\ df)\right)^{1/2}\right)^3 \qquad\qquad (39\text{-}1)$$

where Z is a normal deviate at some selected critical value, α, one may compute the critical value for an *a posteriori* variance of unit weight with any large number of degrees of freedom. This was done in a small program, with results shown in Table 39.2.

Table 39.2 – Critical values of variances of unit weight

Degrees of Freedom	Alpha (one-tailed)	Critical value of χ^2/df
1	0.9995	12.12
10	0.9995	3.14
100	0.9995	1.53
1000	0.9995	1.15
10000	0.9995	1.05
100000	0.9995	1.0148
650000	0.9995	1.0058
650000	0.999999	1.0084
650000	0.999999999999	1.0124

Table 39.2 demonstrates that when one has 650,000 degrees of freedom, then one only expects random change to generate a variance of unit weight greater than 1.0058 about 1 in 2000 times. Further, a variance of 1.0124 would only occur once in 10^{12} times. For example, 10^{12} represents the number of seconds in about 31,688 years. Clearly, the *a posteriori* variance of unit weight of 1.8919718 is excessive at an astronomical level.

Reasons for excessive variances of unit weight are numerous (Uotila 1975 and Mikhail 1976), collected in Table 39.3.

Table 39.3 – Reasons for Excessive Variance of Unit Weight

> Incorrect/incomplete mathematical model
>> Systematic errors
>> Neglected influences
>> Miscalibration
>> Invalid conditions imposed
> Computational error
>> Software "bugs"
>> Incomplete data processing procedures
> Data problems
>> Insufficient data cleaning and outliers
>> Blunders
> Incorrect *a priori* covariance matrix of observations, $\mathbf{D}_o$
> Excessive non-linearity

It is believed that data cleaning is a major contributor to the "tails" of many of the distributions plotted in this report. Outliers not only had a direct effect, but also lead to assignment of pessimistic weights of projects as a whole in the pre-adjustment project

assessments (Section 15). Certain projects did not get horizontal and vertical weight scaling. And, shortcomings or absence of crustal motion models for GPS vectors and CORS fixed coordinates certainly contribute to the final variance of unit weight.

It is probably not realistic to hope to achieve a variance of unit weight within likely statistical limits for heterogeneous data sets of the magnitude of the NSRS 2007. But the character of the various issues uncovered in this report suggest that a substantial reduction in the weighted variance sum excess could be possible if additional data cleansing and project weight analysis were performed.

40. Systematic Errors

This section briefly discusses the variety of systematic errors that can occur in GPS positioning. It is assumed that standard practice is applied regarding utilization of dual frequency receivers, antenna phase center variation models, precise orbits, and troposphere self-calibration.

It must be recalled that the vectors in the NSRS 2007 date back as far as 1983. At that time, geodetic positioning with GPS was an adventure. For example, GPS only reached Initial Operational Capability (IOC) on December 8, 1993. GPS geodetic receivers were evolving, and early precise orbits were much less accurate than they are today.

GPS vector reduction software was also in an embryonic state. Second generation codes, such as the NGS package OMNI, relied on manual editing of carrier phase cycle slips, as well as a manual process for ambiguity resolution. Later tools that automated the cycle slip repair process were rudimentary and underwent considerable evolution. The LAMBDA method of ambiguity resolution was first announced in 1993 (Teunissen 1993) and took some time to become widespread. The notion of validation of ambiguity resolution did not exist. Needless to say, edits and fixed ambiguities were not always correct in early vector processing. This introduced systematic or non-Gaussian errors into early GPS vector data.

GPS vector reduction software errors, themselves, also have a potential for introducing systematic errors. For example, `page4`, the principal NGS software for GPS vector reduction, had the wrong sign applied to the L1-L2 phase center offset. This bug was isolated and corrected January 31, 1996. The maximum effects would be on mixed antenna types and long baselines. The effect could reach several centimeters in ellipsoidal height due to bias absorption in the unconstrained tropospheric model parameter.

On occasion, incorrect starting coordinates are identified as potential source of systematic error. As shown in the Table 7.6 results in Remondi (1984), geocentric positions must be known at the 1 to 2 meter level to perform 10^{-7} relative positioning. While incorrect starting coordinates may have been an error source in the earliest GPS

surveys, those projects were generally dropped from the NSRS. This result, by the way, confirms the "rule of thumb" of Bauersima (1983):

$$\mathrm{d}b/b = \mathrm{d}r/r \tag{40-1}$$

where b is baseline length, $\mathrm{d}b$ is error propagated into the baseline, $\mathrm{d}r$ is orbit error, and r is nominal distance to the satellite (20,000,000 m for GPS).

Orbit error is related to starting coordinate error as a source of systematic error. It will generally tend to follow Bauersima's rule above (Equation 40-1), but one should not expect GPS orbit error to be common from one satellite to the next. IGS orbit error was about 15 cm in the early 1990's, and is now approaching 1 cm error. Prevalence of IGS precise orbits is undoubtedly one factor in the improved network accuracies plotted in time in Figures 22.1-22.6. It is likely that orbit error will be a significant error source for very long, old vectors. This will occur directly, through error propagation, and indirectly, by causing incorrect edits and fixed ambiguities.

While not a systematic error, *per se*, certain GPS reduction softwares do not issue the intervector correlation elements. As described in Section 8, current NGS operating procedures recognize this omission and only allow those softwares to be used for vector reduction of First Order (and lower) GPS projects. Rigorous processing of session data is recommended.

In closing this section, it must be remarked that the same GPS satellites, often the same GPS receivers and antennas, the same ionosphere, and the same troposphere, the same GPS orbits, frequently the same double-difference phase processing, and, in numerous cases, the same processing software is used to establish the CORS and the project vector computation. Thus, one should not expect dramatically different results between GPS phase data collected continuously at static sites, and GPS phase data collected in hour (or multi-hour) chunks at static sites. Provided one collects enough phase data to effectively reduce multipath error, identify and edit cycle slips, and resolve and validate the integer ambiguities, then one is left with a noise floor inherent to GPS technology. In retrospect, there should be little surprise that the bulk of the recent campaign-style GPS data displays accuracies comparable to continuous-style GPS.

41. Stakeholders

The scope of work defined for the analysis of the NAD 83(NSRS2007) National Readjustment included validation of the network and local accuracies with specific attention to addressing the concerns of stakeholders. This provision was included to insure the analysis investigated specific topics regarding the local accuracies. However, the author's data collection was broad, and included interviews as well as digital sources. The material in this section is not the opinion of the author. It is a communication of stakeholder concerns gathered during the analysis. The author found that user concerns were much more extensive than the topic of network and local accuracies.

The local accuracies expressed in the adjustment outputs and the *92* relative error records, described in Pursell *et al*. (2008), are complete. Those outputs arrange the local accuracies in an alphabetically ascending Point ID (PID) order. Thus, to consider local accuracy reciprocal relations, both the standpoint and the forepoint must be examined. A special test run (November 2007) of the NGS data sheet software validated complete reporting operation. As a footnote, it was found that the adjustment software incorrectly issued local accuracies for points that were only related through a rejected observation.

The magnitudes of the local accuracies relative to the network accuracies are generally valid. This concern is addressed in the diagnostic tests of the local accuracies performed in Section 29. Analysis did uncover that 0.2% of the 368158 local accuracies displayed a negative correlation. These few cases were related to the "rejection by downweighting" mechanic used in the NSRS 2007 adjustment software.

Because of the relational character of local accuracies, one may see very large and very small values in a local accuracy list at a given station. These would reflect very loose and very precise measurements to or from that given station. For this reason the FGDC specifies an approximate average to characterize local accuracy at a point (FGDC 1998, Part 1). An estimator of central tendency that is robust against outliers is the median (50% percentile). This offers a mechanism for implementing the approximate average. Regarding the expression of horizontal accuracies, both network and local, the introductory material in Section 20 details their computation from propagated error values by Leenhouts (1985).

Except for the foregoing and an issue discussed later in this section, it is found that the bulk of stakeholder concerns were not related to validity of the National Readjustment. Certain recurrent themes appear. Multiple "views" of geodetic data are desired, not limited to the standard datasheet or traditional retrieval options. (However, the standard datasheet must be retained as an option for legacy applications.) Expanded documentation is desired on all the datasheet content. While the term "User Guide" has never appeared explicitly, it summons the collective notion of providing greater detail. And, there is very broad desire for additional material on how to use network and local accuracies. As one example of collected input of user concerns, see Government Programs Committee (2007).

A series of user concerns related to the validity of the National Readjustment, the operation of OPUS, and the CORS coordinates are best summarized in this sentence. Users want interoperability between the active control points and the monumented control points.

"In Lawton, we are a long ways from abandoning physical monuments."

"I think putting out a readjustment without the very best initial epoch coordinates and velocities possible for the CORS is a very bad mistake."

"Personally I think they have more work to do to get the adjustment done right. . . . . I think this was a bit political and the rush to release was to coincide with the 200th anniversary for PR sake."

"It is a real bummer to me that the CORS coordinates were not first re-adjusted prior to the new NSRS 2007 readjustment. Why did they even bother?"

"This is starting to PMO!"

- - Excerpts from the Point of Beginning (POB) "Strictly Surveying" Message Board
www.i-boards.com/bnp/pob/

The analysis presented in Sections 34 through 38 portray the interaction of the CORS fixed control and the NSRS 2007 GPS vectors. It is seen that there is general agreement between the active and monumented points as a whole. However the residual midpoint concentrations seen in the figures of Section 38 are not solely random. They are reflecting inconsistent modeled motion (or unmodeled motion) between the CORS and the GPS vectors, as well as probable instances of CORS coordinate departures (as shown in Figures 34.2 and 34.3).

The residual midpoint concentrations of Section 38 are few when compared to the overall number of GPS vectors. Nonetheless, whenever coordinate mismatches occur, user frustration follows. The user quote, *"This is starting to PMO!"*, was in reference to the CORS coordinates being "...outside of their own SPEC" when used by OPUS. The situation is such that users routinely recommend that one should manually correct OPUS runs by 60 day time series to account for the CORS coordinate departures. This highlights that users also want interoperability among the active control points as well as between active and monumented points.

As of this writing there is only one specific instance of an NSRS 2007 mismatch detailed on the POB message board. QD1782 (PRINEVILLE) is felt to be wrong. The user feeling is that there is a velocity issue associated with this point in Oregon. Naturally, NGS response will need to consider the CORS coordinates, velocities, the HTDP model in the region, and the GPS vectors and surveys that established that point.

By contrast, multiple instances are cited where NSRS 2007 "fits". One user quotes 0.01 foot horizontal and 0.02 foot vertical for multiple points. Other cases, where the matches are less impressive, are within the position error quantities currently present on the datasheets.

While the POB forum may be considered as *avant-garde* to the survey community as a whole, they are demonstrating the spread of geodetic GPS technology and expertise,

and an increase in the ranks of geodesy stakeholders. This spread was anticipated, and was the chief motivation to construct geodetic standards that were founded on externally verifiable, numerical measures in place of the old "cookbook" methods. This enables the community to evaluate their own work, rather than depend on government "quality control". The POB forums show that geodetic survey work can be checked more easily than ever before.

CONCLUSIONS

The NSRS 2007 free adjustment contains multiple components. This created a rank defect solution. The free adjustment used rejected GPS vectors, included by a "rejection by downweighting" mechanic, to resolve the rank defects. This situation did not issue a numerical singularity or warning flags, and was not detected at the time of the free adjustment. The rank defects involved 235 points. While unfortunate, the presence of multiple components did not hamper residual inspection and analysis. However, free adjustment coordinates and standard deviations must be used with caution. The CORS constraints of the fixed adjustment *did* resolve all of the rank defects.

Exploratory analysis of the GPS network shows the annual rate of installation of new survey points has fallen in recent years. However, the submission rate of GPS vectors has remained generally uniform, indicating more reobservations have been taken recently. While GPS vectors can exceed 5000 km in length, the median length is 31 km. This shows the GPS network has a much more local character than generally believed.

Summary statistics indicate the bulk of the GPS vectors in the NGS data base do not have correlation information between vectors. This is due to NGS accepting lower order surveys reduced with software packages that did not issue rigorous intervector correlation elements. This introduces a degree of approximation in formal error statistics, and calls into question the utility of certain proposed error propagation procedures.

Aside from crustal motion behaviors, typical regional shifts between the old and new NAD 83 coordinates are just a few cm. This is well below the 5 cm criterion that was followed during earlier NGS statewide readjustment efforts. Of note, very little vertical coordinate shift was found in the Pacific Northwest region of the United States.

Residuals of up to 35 cm in magnitude were retained in the National Readjustment. The residual distributions show the use of a 5 cm inspection tolerance during the free adjustment solutions. However, the accuracies and magnitudes of the residuals indicate that a tighter rejection tolerance would have been appropriate. The residual distributions have very long tails. Little difference is seen between the free and fixed residual summary statistics. The rejection process did not consider standardized residuals. The outliers had impact on all the *a posteriori* statistics.

Analysis of the height standardized residuals shows them to be remarkably small as a group. This suggests that the presence of sizable residuals caused the project weight

scaling procedures to assign larger standard deviation factors to all observations in troublesome projects. This in turn, would tend to underestimate sets of standardized residuals. It is believed that insufficient outlier rejection lead to large factors applied to project dispersions. This effect is intensified slightly in the fixed adjustment.

The pre-adjustment weight scaling effort, which established distinct horizontal and vertical standard deviation factors for each project, was successful. It is seen that the horizontal standard deviations were too optimistic relative to the vertical standard deviations by 50%, when considering simple project scaling by the standard deviation of unit weight. With the exception of a category of unscaled projects, the *a priori* weights were rather good, and suffered only from insufficient outlier rejections and from estimation in very tiny projects.

The coordinate latitude and longitude standard deviations have extremely long tails. These are, in all likelihood, induced by large project scaling factors that were driven by unrejected outliers. Surprisingly, a bimodal structure was seen in the height standard deviations. The horizontal standard deviations show a general absence of correlation. The horizontal coordinate error ellipses are near circular, with a ratio of semiminor to semimajor axis of 0.8. This result validates the choice of a single number to represent FGDC horizontal network accuracy. It is seen that the orientation of the semimajor axes tend to be North-South. This is attributed to the inclination of the GPS satellites, which generate a "hole" in sky coverage about the poles.

Network accuracies are 95% statistics, and were computed for all the network points. The median network accuracies for the NSRS 2007 National Readjustment are 1.03 cm horizontal and 1.84 cm vertical. The network accuracy distributions contain long tails. Even with the tails, the network accuracies seldom exceed 4 cm horizontal and 8 cm vertical. Color plots of the network accuracies show considerable spatial variation across the country.

Temporal plots of network accuracies show trends of improving accuracy. This is evident since 2000 for the horizontal accuracies and since 1996 for the vertical accuracies. It is seen that the improvement in vertical network accuracy has been continual through to 2006. A general correlation of high accuracy vertical and Height Modernization points was confirmed. However, the bimodal distribution of points was not solely due to Height Modernization. The best vertical network accuracy quality is found in the surveys of Minnesota and Southern Wisconsin.

Relative position standard deviation distributions are somewhat smaller in magnitude than the coordinate standard deviation distributions. The relative position horizontal error ellipses show near-circularity and a general orientation to the North. The relative position statistics show a greater uniformity than was expected given the heterogeneous nature of the geodetic surveys comprising the NSRS.

Local accuracies are 95% statistics, and are computed between connected points. The median local accuracies for the NSRS 2007 National Readjustment are 0.78 cm

horizontal and 1.55 cm vertical. The local accuracy distributions also contain long tails. No evidence of proportional error behavior was found in the local accuracies. This validates the choice of length-free accuracy measures in the FGDC.

The computations and treatments of local accuracies are satisfactory, with the exception of the influence of the "rejection by downweighting" mechanic. Analysis finds that the magnitudes of individual local accuracies do, indeed, correspond to their parent network accuracies. Data sheet retrieval software was tested and found to function correctly. It is seen that a large number of measured point relations do not have a high correlation. This coincides with the uniformity of the relative position statistics noted above. The absence of high correlations also validates a number of aspects of the FGDC network and local accuracy computation procedure specified for geodetic surveys.

Analysis of variance (ANOVA) was conducted by computing dispersion scale factors by means of IAUE estimators. Comparison of factors for the horizontal and vertical components of the NSRS 2007 indicates the vertical component of the standard deviations of the observations could be tightened by an additional 14%. This small correction confirms the general validity of the NSRS 2007 weights and that the vertical network accuracies are, indeed, generally twice as large as the horizontal network accuracies.

The ANOVA also recognized the heterogeneous nature of the NSRS. Accuracy layers were defined based on earlier GPS survey categories, and dispersion scale factors were accumulated for these layers. The FAACORS layer, consisting of 100 FAA projects with CORS ties, had 23% excess error. This was surprising given the generally tight closures seen in analysis at the project level. The old A and B order projects were less surprising with 11% excess error. Issues such as incorrectly edited cycle slips and ambiguity resolutions are likely contributors to error in those projects.

The AIR layer comprises 1273 FAA detail surveys. ANOVA statistics clearly show the presence of pendant lines and figures that do not interconnect the network. Analysis indicates that, while the spur projects are numerous, they don't carry enough vectors to bias estimation of the network variance of unit weight for the interconnected surveys.

A category of projects (UNSCALED) did not get pre-adjustment horizontal and vertical standard deviation factors. This category has 77% excess error. The bulk of this error could be traced to a single project, GPS1751. This project, alone, inflated the standard deviations of both the free and fixed National Readjustment by 4%.

Most of the UNSCALED project layer was surveys in California. The special weight rescaling program, calwt4, did not adequately substitute for horizontal and vertical reweighting. One should multiply the horizontal network and local accuracies by about 0.7, and multiply the vertical network and local accuracies by about 0.35 in California. Temporal analysis also indicates excessive deweighting of the older projects.

CORS fixed control was obtained by applying a horizontal motion model instead of CORS three-dimensional velocity estimates. Further, the CORS fixed control was pulled from an NAD 83 coordinate set that was theoretically maintained at a 2 cm horizontal and 4 cm vertical accuracy tolerance. There was no technical impediment to the transformation of the existing CORS coordinate and velocity data set in the ITRF00, epoch 1997.0 frame (with tighter tolerances) into an NAD 83, epoch 2007.0 frame. The situation is alleviated somewhat by the use of CSRC as a source for NAD 83 2007.0 coordinates in California.

The quality of the CORS fixed control coordinates used in the NSRS 2007 National Readjustment is mixed. CORS coordinates are not regularly maintained at their theoretical tolerances (e.g. STKR). The last promulgated CORS solution extended only to the 2002.0 epoch. When new CORS are emplaced, the CORS velocities are obtained through the horizontal motion model, which only covers the Western United States. On a positive note, when a new CORS is emplaced, the NAD 83 coordinate is identical to the ITRF, subject to the reference frame transformation. And, over half of the NSRS GPS vectors are within a +/- 5 year window about the 2002.0 epoch of the last published CORS sets.

The addition of the CORS fixed control caused a relative tightening of the standard deviations from those of the free adjustment. However, error between the GPS network and the GPS CORS fixed control inflated the fixed adjustment *a posteriori* variance of unit weight to such an extent that any strengthening through fixing was lost.

Tabulation of the changes in residuals between the free and fixed adjustment shows that 2633 vectors, only 0.928% of the total set, exceed a 1 cm horizontal tolerance. And, 1387 vector differences, only 0.489% of the total set, exceed a 2 cm vertical tolerance. This demonstrates general agreement between the active and monumented points as a whole, despite the issues described above. The large residual changes show clusters that indicate CORS coordinate discontinuities as well as inconsistent modeled motion (or unmodeled motion) between the CORS and the GPS vectors.

The *a posteriori* variance of unit weight of 1.8919718 is excessive given the large number of degrees of freedom. The findings above suggest that a substantial reduction in the weighted variance sum excess is possible if additional data cleansing and project weight analysis were performed. It is seen that the free adjustment contains 2/3 of the excessive error. Updating the CORS fixed coordinates is not the sole remedy.

Stakeholders have had generally good experiences with the National Readjustment. Any lack of adoption has been due more to user satisfaction with the prior NAD 83 coordinate set. There are misgivings about NSRS 2007 regarding the treatment of the CORS fixed control. There is interest in how the NSRS network relates to the CORS. And, users want more descriptive material on the use and behaviors of network and local accuracies. It is clear that the users want interoperability between the active control points and the monumented control points. They also want interoperability among the active control points themselves. As cited above, CORS coordinates are not

regularly maintained at their theoretical tolerances. This is a source of stakeholder dissatisfaction.

In summary, NSRS 2007 vectors generally possessed very small residuals. By use of pre-adjustment weight scaling and *a posteriori* statistics, this lead to network accuracies with median values of about 1 cm horizontal and 2 cm vertical. Analysis of the residuals show insufficient outlier rejection and the potential need to reweight four categories of projects. These problems lead to long tails in statistical distributions and inflation of the *a posteriori* statistics. The sources and treatments of the NAD 83 CORS coordinate constraints are also a secondary factor in the *a posteriori* inflation. However, comparisons show that under 1% of the residuals change horizontally by 1 cm or more between the free and fixed adjustments. By this we may conclude that there is very good correspondence between the fixed control and the NSRS 2007 network.

RECOMMENDATIONS

These recommendations are the opinion of the author. The author was contracted to provide an independent assessment of the National Readjustment; an activity that was successfully discharged with the submission of this report. These recommendations do not represent National Geodetic Survey policy. (The author retired from the position of Chief Geodesist of the National Geodetic Survey in 2004.)

The recommendations are grouped by topics, but are not prioritized. Some recommendations require little resource outlay, and others will involve some manpower commitment. The author was instructed to consider all options in the recommendations.

However, there is some dependency ("threads", if you will) among the recommendations. The fact that the author was contracted to perform the analysis of the NSRS 2007 National Readjustment presupposes future readjustment of the monumented network was a viable option. It also suggests there are no plans to abandon NGS support of the monumented network for delivery of geodetic control in the near future. The recommendations are made in this context. (These are inferences of the author and should not be taken as NGS policy.)

I recommend publication of local accuracies in the data sheets. The magnitudes of the local accuracies are correct; both as aggregates (Table 29.1) and when considered individually (see Section 29 figures). Despite the number of local accuracies that form the spikes seen in Figures 29.1 and 29.3, the tails to the left of the spikes represent positive correlations -- correlations that can be judged non-negligible. A logic error in the September 2007 version of the data sheet program caused incomplete retrieval of the local accuracies. This bug was fixed at an early stage. The core local accuracy files loaded in the Integrated Data Base (IDB) are complete.

I recommend display of the median local accuracy in the data sheets. As noted in Section 41, FGDC specifies an approximate average to characterize local accuracy at a

point (FGDC 1998, Part 1). An estimator of central tendency that is robust against outliers is the median (50% percentile). I recommend this mechanism for implementing the approximate average.

I recommend publication of the true horizontal accuracy value for both the network horizontal accuracy and the local horizontal accuracy by means of Leenhouts (1985). This is in contrast to the current expression of the 1.96 sigma levels of the latitude and longitude standard deviations in the data sheet. A horizontal accuracy is a single number. As discussed in Section 20, the horizontal network accuracy is the radius of a circle of uncertainty, such that the reported coordinate is within the radius 95% of the time (FGDC 1998, Part 1, pg. 1-5). Use of a radial metric does *not* presuppose an underlying circular error distribution. Leenhouts (1985) provides a simple cubic equation that relates error ellipse components to the radius of the error circle.

I recommend true and complete rejection of GPS vectors flagged as "rejected" in *all* current and future NGS GPS vector adjustment software (including web-based applications). I make this recommendation irrespective of any future NGS National Readjustment. And, I recommend that true and complete rejection of GPS vectors be considered "best practice" in vector adjustment codes. This means that a rejected vector will not be used to form an observation equation, nor be accumulated into the normal equations. To assist in problem diagnosis, rejected vector misclosures should be reported in the adjustment software postprocessor modules. Further, the user must have complete freedom to reject and unreject vectors at the data input level, without any requirement to perform new data base retrievals, or to run specialized "rejected vector" applications (e.g. `shrink4`). This means that survey sessions of correlated vectors that contain one or more rejections will need to be internally re-indexed over unrejected vectors within a vector adjustment application. Corollary recommendations are that rejected vectors not be used in connectivity analysis, nor be considered when issuing local accuracies.

The rationale leading to the recommendation above is long and distressing. The "rejection by downweighting" mechanic masked the rank-defect solution of the free adjustment, and, to this day, has prevented identification of the number of components in the free network, the true number of degrees of freedom, and the actual *a posteriori* variance and standard deviation of unit weight in both the free and fixed adjustments (Section 1). Further, evaluation of the 26 cases of 10 cm weighted constraints of the CORS control is hampered by the uncertainty in obtaining the true fractional degrees of freedom of the fixed adjustment due to the "rejection by downweighting" mechanic. It was identified as the cause for different counts of vector components in delta *X,Y,Z* (and also in delta *N,E,U*), and differences in reported degrees of freedom sums. The software used for the readjustment (unlike program ADJUST) did a single accounting of connectivity for both normal equation organization and the generation of various reports and data products. Thus, summary counts indicated stations were connected when they were not, and local accuracies were issued over lines whose sole relation was rejected (Section 24). In addition, detailed investigation of instances of local accuracies that failed a size ratio test (negative correlation) found that the offending lines either had a rejected observation between them, or the line endpoints were participants in a correlated

GPS session that contained a rejected observation within it (Section 26). I made the best choice given the available information when I implemented "rejection by downweighting" inside program ADJUST (Milbert and Kass 1987). However, given what I know now, and given the potential pitfalls in "rejection by downweighting" implementation, I recommend true and complete rejection.

I recommend that *all* current and future NGS GPS vector adjustment software (including web-based applications) allow the user complete freedom to reject and unreject observations, and to reject and unreject stations participating in an adjustment. Such observation and station rejections should not require new data base retrievals, or the running of indexing applications. This means that codes should perform completely internal indexing, and never treat other values (such as Station Serial Numbers, SSNs) as direct index numbers. This does imply the addition of some type of special station rejection flag in the *80 Blue-Book record, or the creation of station rejection records in the AFILE of program ADJUST. This recommendation is based on conversations and review of Observation and Analysis Division practices (Section 7). I believe adjustment software should never be an impediment to the easy elimination (or restoration) of problematic observations or of problematic stations.

I recommend that more outliers be rejected. I recommend that rejections be performed not only on residual magnitude, but predominately on the magnitude of the normalized residual. I recommend consideration of values around 4 cm and 3 to 4 sigma as "hard" limits, and that these be imposed even if no-check and singular stations develop. I recommend an active effort to evaluate the monumented NSRS network, and to reobserve those lines and stations judged necessary to meet the NGS mission. The NGS reorganization considered in-depth analysis of the NSRS as a priority, and placed the responsibility for such analysis, along with survey design functions, in the Spatial Reference Systems Division. In cases of tiny residuals, remedy of excessive normalized residuals should be through appropriate reweighting at the observation or project level.

In conjunction with the outlier rejection, I recommend special attention to outliers be given to the extremely large (and extremely small) project dispersion scale factors computed in the ANOVA of Section 32. These extrema may be caused by outliers and/or incorrect weights, and may be caused by CORS coordinate discrepancies. Recall, the departures from 1.0 in the Section 32 ANOVA reflect changes in the residuals between the stand-alone projects and the projects adjusted together as a network. While all extrema should be considered (e.g. the N2 layer), special care should be taken with the FAACORS, N3, N4, and UNSCALED layers of the network.

I conditionally recommend an in-depth study of the large project dispersion scale factors that arose in the FAACORS layer of the ANOVA analysis. The condition is if the outlier rejection and project weight rescaling does not remedy the 23% error excess seen in Table 32.2. This error excess was a surprise, given that those projects were felt to be particularly good. There is some error effect that is occurring between the individual projects, and the projects combined into the network. The excess errors in the N3 and N4 layers are likely related to old projects with incomplete cycle slip editing and incorrect

ambiguity resolution. Outlier rejection (or reprocessing) will likely help those layers. Also, consider adoption of a length criterion for rejection of very long, very old vectors. As seen in Equation 40-1, orbit error propagation is proportional to GPS vector length, and the old IGS orbits were much less accurate than they are today.

I recommend that the eight no-check projects be investigated, and that redundant measurements be performed and added to them. Refer to no-check-projects.txt and proid3.txt in the Electronic Support Material.

I recommend that project GPS1751 be rescaled in both horizontal and vertical (Figure 32.12). I recommend that all the unassigned projects (Section 32) be given pre-adjustment standard deviation factors in horizontal and vertical (Section 15). This recommendation would undo the temporal reweighting performed for California (Section 33). I recommend that the temporal reweighting be re-calibrated using the project dispersion scale factors, that the temporal reweighting be distinct for horizontal and vertical, and that the temporal reweighting be applied as a controllable option within the network adjustment program. Rationale for correct project weights is found in Sections 32 and 33. And, misweighting is a likely cause of the larger network accuracies seen in California in Figures 21.1 and 21.2, as well as the absence of certain California Height Modernization projects in the 1 cm vertical network accuracy plot in Figure 23.1.

I recommend that projects be rescaled with newly-computed standard deviation factors in horizontal and vertical (Section 15) as part of the outlier rejection process. In fact, I recommend that this procedure be applied retroactively. As outliers were rejected throughout the NSRS 2007 free adjustment analysis process, new estimates of the project standard deviation factors could have been produced. However, this was not done. Note that some of the low extrema seen in the dispersion scale factors plotted in Section 32 could be due to pessimistic pre-adjustment weights that were driven by outliers and that were later rejected. Note, also, that while the pre-adjustment factors were applied very late in the free adjustment process (Pursell *et al*. 2008), they were not updated prior to application.

I recommend the NGS web page on the NSRS 2007 statistics at: www.ngs.noaa.gov/NationalReadjustment/StatusReports/Statistics.final/readjustment%20 statistics%20final.html be revised to indicate that the "Total" statistics are *a posteriori* variance of unit weight estimates, whereas the Helmert block "Variance" estimates are established from *a posteriori* residual statistics (distinct from the variance of unit weight estimates). This problem also exists in the Version 4 draft of (Pursell *et al*. 2008). As discussed in Section 30, the organization of that material causes a comparison of unlike quantities ("apples to oranges").

I recommend that the adjustment software used for the readjustment has a simple, user-friendly method for generation of ANOVA statistics at the project level. I also recommend the output of such ANOVA statistics be user-friendly and immediately usable in network analysis through inclusion of project names. This recommendation is

based on my personal experience, and will become evident when further computations of project dispersion scale factors is performed.

I recommend some form of pooling of statistics for the "non-network" projects (spur lines and figures) seen in the AIR layer (Sections 31 and 32) for project horizontal and vertical standard deviation factor computations. Some projects consist of as few as two vectors establishing one new point. An estimate of horizontal and vertical standard deviation for such a "project" will not be very reliable. Note that aggregation of such projects will not change coordinate solutions, or the fact that they are comprised of spur lines and figures. The objective is to get better estimates of observation dispersion. A corollary recommendation is that pooling be performed for all the ANOVA layers.

I recommend that the 26 CORS components that were weighted be allowed to float. Since the parameterization of the adjustment software doesn't cleanly allow local geodetic horizon component fixing/floating, I recommend component floating be implemented as 10 meter standard deviations. This element was not detailed in this report since independent analysis was hampered by the uncertainty in the fractional degrees of freedom induced by the "rejection by downweighting" mechanic (Section 1). No rationale for the use of 10 cm weights is provided in (Pursell *et al*. 2008). It is noted, for example, that the CORS AB6289 takes a 17 cm height shift under a 10 cm weighted constraint. One wonders what the shift would be when unconstrained. A corollary recommendation is that the floated components should be tabulated and analysis of potential causes be listed. Another corollary recommendation is that the standard deviations of the adjusted coordinates should be carefully monitored as the problematic CORS coordinates are floated to insure that no inadvertent rank defects arise.

I recommend regeneration of the chloroplethic maps of coordinate shifts, such as found on www.ngs.noaa.gov/NationalReadjustment/, by computing median coordinate shifts as a robust estimator. While not detailed in this report, stakeholder input has noted that average shifts are biased by outliers. Inspection of the thinned coordinate shifts in Figures 6.1 and 6.2 shows that coordinate shift outliers do, indeed, occur.

I recommend inspection of QD1782 (PRINEVILLE) for validity. This analysis should consider CORS coordinates, velocities, the HTDP model, and the GPS vectors and surveys that established that point (Section 41).

I recommend the transformation of the existing CORS coordinate and velocity data set in the ITRF00, epoch 1997.0 frame (with its tighter tolerances) into an NAD 83 frame of appropriate epoch to support a National Readjustment. I recommend the updating, operationalization, and publication any such NAD 83 CORS coordinates as a natural function of a National Readjustment.

I recommend that positional discrepancies of CORS be inspected and updated daily through automatic procedures as a fundamental component of the NGS mission to deliver the NSRS to the public. I make this recommendation irrespective of any future NGS National Readjustment. Adequate software should be in place to make reading the

daily discrepancy summary report as routine and easy as reading an e-mail in the morning. And, software should be in place to make CORS coordinate updating based on the discrepancies equally easy. Of course, such software would screen the CORS time series in a robust fashion to prevent updates due to a recent outlier. The presence of CORS coordinate discrepancies, as depicted in 34.2 and 34.3, is a likely source for some of the residual differences between the free and fixed adjustment shown in Section 38, as well as a source for the inflation of the variance of unit weight (Section 39). This inflation, in turn, lead to an increase in magnitude (Section 19) of the network and local accuracies of the NSRS 2007 National Readjustment. The stakeholder perspectives in Section 41 touch on confidence in the readjustment, as well as the use of OPUS to compute coordinates, as coordinate discrepancy issues. Finally, in my opinion, the National Geodetic Survey, and, indeed, any government agency, should implement the policies it articulates, including those involving positional tolerances. As related items, I recommend a substantial reduction in the CORS positional tolerance, and I recommend elimination of separate tolerances for the ITRF and NAD 83 frames. As a corollary result of this latter recommendation, sufficient updated NAD 83 coordinates should result that a wholesale update of the NAD 83 coordinate set seems indicated.

I conditionally recommend another National Readjustment of the NSRS in the near future. The two conditions for readjustment are that outliers be remedied, particularly through use of standardized residuals, and that project weights be additionally rescaled as indicated through subsequent ANOVA results. The outliers and project weights lead to the very long tails in the network and local accuracies. I do not recommend a National Readjustment based solely on the inclusion of an alternative CORS data set (*e.g.* an "ITRF adjustment"). Inspection of the a posteriori variances of unit weight between the free and fixed adjustments in Section 38 indicates that the free adjustment contains 2/3 of the excessive error. (This does not mean that the current NSRS 2007 CORS coordinate set should be retained. Other recommendations cover that topic.) I do not anticipate a significant change in the coordinates from a new readjustment as a whole. I do expect problematic points to be dropped or isolated from their valid neighbors, the distributional tails to shrink considerably, the *a posteriori* variances to reduce, and tighter network and local accuracies to result. As a personal remark, NSRS 2007 was the first attempt by NGS to publish both a new coordinate set and calibrated error estimates. It did this very well, and it can be improved.

In conjunction with the prior three recommendations, I recommend that the treatment of the CORS fixed coordinates and GPS vectors insure that the procedures for a future readjustment and a future OPUS computation are consistent. As seen in the readjustment procedure outlined in Section 34, and in the discussion in Section 35, OPUS processing is inconsistent with the NAD 83(NSRS2007) computational procedure. Stakeholder desire for active and monumented control point interoperability makes this recommendation for consistency a worthy goal. A corollary recommendation is that the level of consistency be numerically quantified for the stakeholders.

I recommend the creation of a three dimensional time-dependent processing program along the lines of HTDP. I make this recommendation irrespective of any future

NGS National Readjustment. This notional program should cover all of the conterminous United States. And, the program should carry two velocity "layers"; one for the Earth's crust, and one for the motion of CORS antennas. NGS study may determine its own customized velocity field, or it may implement the spatially averaged residual velocity field in Figure 15 of Calais *et al*. (2006). The figures in Section 37 display disagreements between CORS velocities and model velocities that sometimes exceed the network accuracies. Further, a fundamental theme of the stakeholder input of Section 41 was the need for interoperability between the active control points and the monumented control points. Such interoperability often requires time-dependent positioning support.

I recommend investigation of the CORS-HTDP displacements seen in Figures 37.1 and 37.3. While CSRC-derived coordinates were used in California, the displacements would be an issue for OPUS operation and its relationship to the monumented network. I also suggest intercomparisons of California CORS, NGS CORS, and HTDP velocity fields for insights on model behaviors and possible improvements.

I recommend a new solution of CORS velocities for the United States in the near future. I make this recommendation irrespective of any future NGS National Readjustment. The current CORS velocity/coordinate set was computed in March 2002 from data through 2002.0. The newer CORS velocity solution using data through 2003 was not operationally promulgated (Section 34). While new software is under prototype testing, CORS velocity solutions have halted for some time. When a CORS velocity is required, the horizontal velocity (alone) is modeled from HTDP. A gap has arisen between requirements and capability. The situation is such that CSRC was the source for CORS coordinate control in California. CORS are a fundamental component of the NSRS. I feel NGS should maintain an ongoing capability for regular computation of new and updated CORS coordinates and velocities. I feel that development work of prototype software, whatever the project, should not disable an operational capability. Remedy of the situation might require technology transfer from CSRC.

I recommend that a publicly available list of the PID and CORS 4-character identifiers, both current and historical, for all National, California, Cooperative, and IGS CORS, be created and maintained. It is understood that such relations are not one-to-one, and the list presentation should accommodate this fact. It is understood that NGS practice is to "hide" details of superseded points. It took inordinate effort to compile such a list for the NSRS 2007 CORS coordinates, and inordinate effort by the author to reproduce such a list after the National Readjustment. Further, resources not available to the public were needed to complete the effort. While only for individual stations, the "bilingual" character of Site Code/PID translation at: csrc.ucsd.edu/cgi-bin/checkCaSiteCodePid.cgi is a model to be considered. On a related note, I recommend that if a PID is a National, California, Cooperative, or IGS CORS, that there is a distinct note on the data sheet; preferably near the network accuracies.

I recommend further study of the Height Modernization category of projects in the NSRS 2007. While the vertical network accuracies in Table 23.1 were markedly

better than for the network as a whole (Table 20.1), the Height Modernization distributions still possess sizable tails. The survey design and data reduction issues that relate to these tails may be a fruitful avenue to explore regarding what situations to avoid.

I recommend an analysis of those cases where the standard deviation in height is less than the associated latitude or longitude standard deviations at a point. Such cases are seen to occur in Figures 18.2 and 18.3. While they may be driven by statistical fluctuations in the pre-adjustment project standard deviation factor estimation process (Chapter 15), there could be some other subtle mechanism at work. Any factor that leads to improved heights is worthy of pursuit.

I recommend that NGS develop an error model for GPS geodetic positioning that is accurate. Ideally, such a model would be usable not only by NGS, but by all GNSS vector computation packages. The current method of scaling the double-difference normal equation inverse by an RMS of fit is far too optimistic. The unfortunate experience with GPS1751 (Figures 32.11 and 32.12), not to mention the need to develop distinct estimates of pre-adjustment horizontal and vertical standard deviation factors for all the projects (Chapter 15), illustrates this point. Any desire to expand the operation of OPUS should be coupled with an equivalent desire to obtain realistic error estimates from OPUS. My recommendation that OPUS use three CORS stations was to provide a level of validation of the ambiguity resolution process, and not to substitute for improved error modeling. The redundancy present in the NSRS 2007 network enabled project standard deviation calibrations and sophisticated ANOVA analysis. OPUS doesn't possess this advantage. This is a challenge for NGS.

As a remaining set of items, consider addition of vector lengths to the individual local accuracy list on the data sheet. Consider an alphabetic sort by PID on the individual local accuracy list. Consider the best location for placement of a long local accuracy list. Consider suppressing local accuracy listings for all CORS, since local accuracies from a CORS are, generally, network accuracies. Consider review of all projects that had 1.0,1.0 pre-adjustment standard deviation scale factors. Consider running HTDP for all the projects in the NSRS 2007. This will insure that vectors which span motion and non-motion states, and which get collected into a non-motion state Helmert block, will still get a velocity correction.

In closing these recommendations I wish to take the opportunity to salute the National Geodetic Survey; who, on their own initiative, invited a detailed inspection of their work, and provided total support for that inspection. In return, I could do no less than give my very best effort in this analysis.

ACKNOWLEDGEMENTS

REFERENCES

Amiri-Simkooei, A., 2007: Least-squares variance component estimation theory and GPS applications. *Publications on Geodesy 64*, NCG, Netherlands Geodetic Commission, Delft, Netherlands, March 2007, 208 pp.

Bauersima, I., 1983: NAVSTAR/Global Positioning Systems (GPS), II, *Mitteilungen der Satellitenbeobachtungsstation Zimmerwald, Nr. 10,* University of Berne, Switzerland.

Blewitt, G., 1989: Carrier phase ambiguity resolution for the Global Positioning System applied to geodetic baselines up to 2000 km. *J. Geophys. Res.*, 94(B8), August 10, 1989, 10187-10203.

Bossler, J. D. and R. H. Hanson, 1980: Application of special variance estimators for geodesy. *NOAA Technical Report NOS 84 NGS 15*, National Geodetic Survey, NOAA, Silver Spring, MD, February 1980, 8 pp.

Calais, E., J. Y. Han, C. DeMets, and J. M. Nocquet, 2006: Deformation of the North American plate interior from a decade of continuous GPS measurements, *J. Geophys. Res.*, 111, B06402, doi:10.1029/2005JB004253.

Dixon, W. J. and F. J. Massey, 1969: *Introduction to Statistical Analysis, Third Ed*. McGraw-Hill Book Co., New York, 638 pp.

El-Hakim, S. F., 1981: A practical study of gross-error detection in bundle adjustment. *The Canadian Surveyor*, 35(4), 373-386.

Federal Geodetic Control Subcommittee, 1988: *Geometric Geodesy Accuracy Standards and Specifications for Using GPS Relative Positioning Techniques (Draft)*. National Geodetic Survey, NOAA, Silver Spring, MD, corrected, August 1, 1989.

Federal Geodetic Control Subcommittee, 1995: *Standards for Geodetic Control Networks (Draft)*. National Geodetic Survey, NOAA, Silver Spring, MD, May 23, 1995.

Federal Geographic Data Committee, 1998: *Geospatial Positioning Accuracy Standards, Part 1: Reporting Methodology*. FGDC-STD-007.1-1998. Web page at: www.fgdc.gov/standards/projects/FGDC-standards-projects/accuracy/part1/chapter1

Federal Geographic Data Committee, 1998: *Geospatial Positioning Accuracy Standards, Part 2: Standards for Geodetic Networks*. FGDC-STD-007.2-1998. Web page at: www.fgdc.gov/standards/projects/FGDC-standards-projects/accuracy/part2/chapter2

Förstner, W., 1979a: Konvergenzbeschleunigung bei der posteriori varianzschätzung. *Zeitschrift für Vermessungswesen*, 104(4), 149-156.

Förstner, W., 1979b: Ein verfahren zur schätzung von varianz - und kovarianzkomponenten. *Allgemeine Vermessungsnachrichten*, 86(11-12), 446-453.

Förstner, W., 1979c: On internal and external reliability of photogrammetric coordinates. Proceedings of the American Society of Photogrammetry. 45th Annual Meeting, March 18-24, 1979, Washington, D.C., pp. 294-305.

Geodetic Survey Division, 1996: Accuracy Standards for Positioning Version 1.0. Geomatics Canada, Natural Resources Canada, Ottawa, September 1996, 28 pp.

Government Programs Committee, 2007: National Geodetic Survey Datasheet Recommendations and Questionnaire Responses. Advisory document, September 17, 2007, American Association for Geodetic Surveying, Gaithersburg, MD, 16 pp.

Kaula, W. M., 1987: The need for vertical control. *Surveying and Mapping*, 47(1), March 1987, 57-64.

Leenhouts, P. P., 1985: On the computation of bi-normal radial error. *NAVIGATION: Journal of the Institute of Navigation*, 32(1), Spring 1985, 16-28.

Leick, A., 1995: *GPS Satellite Surveying, Second Ed.* John Wiley & Sons, Inc., New York, 560 pp.

Liebelt, P. B., 1967: *An Introduction to Optimal Estimation*. Addison-Wesley, Reading, Massachusetts, 273 pp.

Lucas, J. R., 1985: A variance component estimation method for sparse matrix applications. *NOAA Technical Report NOS 111 NGS 33*, National Geodetic Survey, NOAA, Silver Spring, MD, June 1985, 12 pp.

McKay, E. J., 2001: Positioning accuracy standards. Presentation to NC Society of Surveyors, New Bern, North Carolina, October 16, 2001, National Geodetic Survey, Silver Spring, Power Point presentation. Web page (Power Point) at: www.ngs.noaa.gov/PC_PROD/WorkShops/PPT/Standards-NewBern.ppt

Mikhail, E. M., 1976: *Observations and Least Squares*. IEP -- Dun-Donnelley, New York, 497 pp.

Milbert, D. G., 1985: A note on observation decorrelation, variances of residuals, and redundancy numbers. *Bulletin Geodesique*, 59, 71-80.

Milbert, D. G. and W. G., 1987: ADJUST: The horizontal observation adjustment program. *NOAA Technical Memorandum NOS NGS 47*, National Geodetic Survey, NOAA, Silver Spring, MD, September 1987, 53 pp.

Milbert, K. O. and D. G. Milbert, 1994: State readjustments at the National Geodetic
Survey. *Surv. Land Info. Sys.*, 54(4), 219-230.

Milbert, K. O., 2003: National Readjustment Plan. Internal document, National
Geodetic Survey, NOAA, Silver Spring, MD, October 2003, 16 pp.

National Geodetic Survey, 2007: Statement regarding control used for the NAD
83(NSRS2007). Web page (PDF document) at:
www.ngs.noaa.gov/NationalReadjustment/Library/Statement2%20regarding%20cont
rol%20used%20for%20the%20NAD%2083.pdf

Pursell, D. G., M. L. Vorhauer, M. Potterfield, C. R. Schwarz, and G. G. Edwards, 2008:
NAD 83(NSRS2007) National readjustment final report. *NOAA Professional Paper
NOS XXX*, National Geodetic Survey, NOAA, Silver Spring, MD, September 2007
V.4 draft.

Remondi, B. W., 1984: Using the Global Positioning System (GPS) phase observable for
relative geodesy: modeling, processing, and results. *Center for Space Research
Report, CSR-84-2*, May 1984, Ph.D. Dissertation, University of Texas at Austin,
available: National Geodetic Survey, NOAA, Silver Spring, MD, 360 pp.

Schwarz, C. R., 2005: The effects of unestimated parameters. *Surv. Land Info. Sys.*,
65(2), 89-90.

Smith, W. H. F., and P. Wessel, 1990: Gridding with continuous curvature splines in
tension. *Geophysics*, 55(3), 293-305.

Snay, R. A, 1999: Using the HTDP software to transform spatial coordinates across time
and between reference frames. *Surv. Land Info. Sys.*, 59(1), 15-25. Also, web page
at: www.ngs.noaa.gov/TOOLS/Htdp/Htdp.html

Snay, R. A., M. Cline, W. Dillinger, R. Foote, S. Hilla, W. Kass, J. Ray, J. Rohde, G.
Sella, T. Soler, 2007: Using Global Positioning System-derived crustal velocities to
estimate rates of absolute sea level change from North American tide gauge records.
J. Geophys. Res., 112, B04409, doi:10.1029/2006JB004606.

Soler, T., and R. A. Snay, 2004: Transforming positions and velocities between the
International Terrestrial Reference Frame of 2000 and North American Datum of
1983. *J. Surv. Eng.*, 130(2), May 2004, 49-55.

Teunissen, P. J. G., 1993: Least-squares estimation of the integer GPS ambiguities,
Invited lecture, Sect IV, Theory and Methodology, IAG General Meeting,
Beijing, August 1993.

Uotila, U. A., 1975: Statistical tests as guidelines in analyses of adjustment of control nets. *Surveying and Mapping*, 35(1), March 1975, 47-52.

Wessel, P. and W. H. F. Smith, 1995: New version of the Generic Mapping Tools released. *EOS Trans. Amer. Geophys. U*., 76(33), pp. 329.

Zilkoski, D. B., J. D. D'Onofrio, and S. J. Frakes, 1997: Guidelines for establishing GPS-derived ellipsoid heights (Standards: 2 cm and 5 cm), Version 4.3. *NOAA Technical Memorandum NOS NGS 58*, National Geodetic Survey, NOAA, Silver Spring, MD, November 1997, 23 pp.

About the Author

Dr. Dennis Milbert received his Bachelors degree in Physics from the University of Colorado, and his M.S. and Ph.D. degrees in Geodetic Science from The Ohio State University. He worked for over 29 years at the National Geodetic Survey (NGS) of the National Oceanic and Atmospheric Administration, where he was promoted to the position of Chief Geodesist. In his federal career he developed accuracy standards, adjustment software, gravity and geoid models, GPS kinematic surveys, and vertical datum transformations. Dr. Milbert served on numerous federal technical and policy working groups and he was an alternate representative to the Senior Steering Group of the Interagency GPS Executive Board. He served for eight years on the joint Editorial Board for Manuscripta Geodetica/Bulletin Geodesique and the Journal of Geodesy. Dr. Milbert is a recipient of the Kaarina and Weikko A. Heiskanen Award, the NOAA Administrator's Award, the Department of Commerce Bronze Medal, and two Department of Commerce Silver Medals. He is a member of the American Geophysical Union, the International Association of Geodesy, and the Institute of Navigation. Dr. Milbert retired from government service in 2004 and pursues research in various geodesy topics.

PLATES

Plate 1. Monumented points of NSRS 2007, Conterminous U. S.

Plate 2. Gridded horizontal network accuracies. White exceeds 5 cm.

Plate 3. Gridded vertical network accuracies. White exceeds 10 cm.

NSRS 2007

157
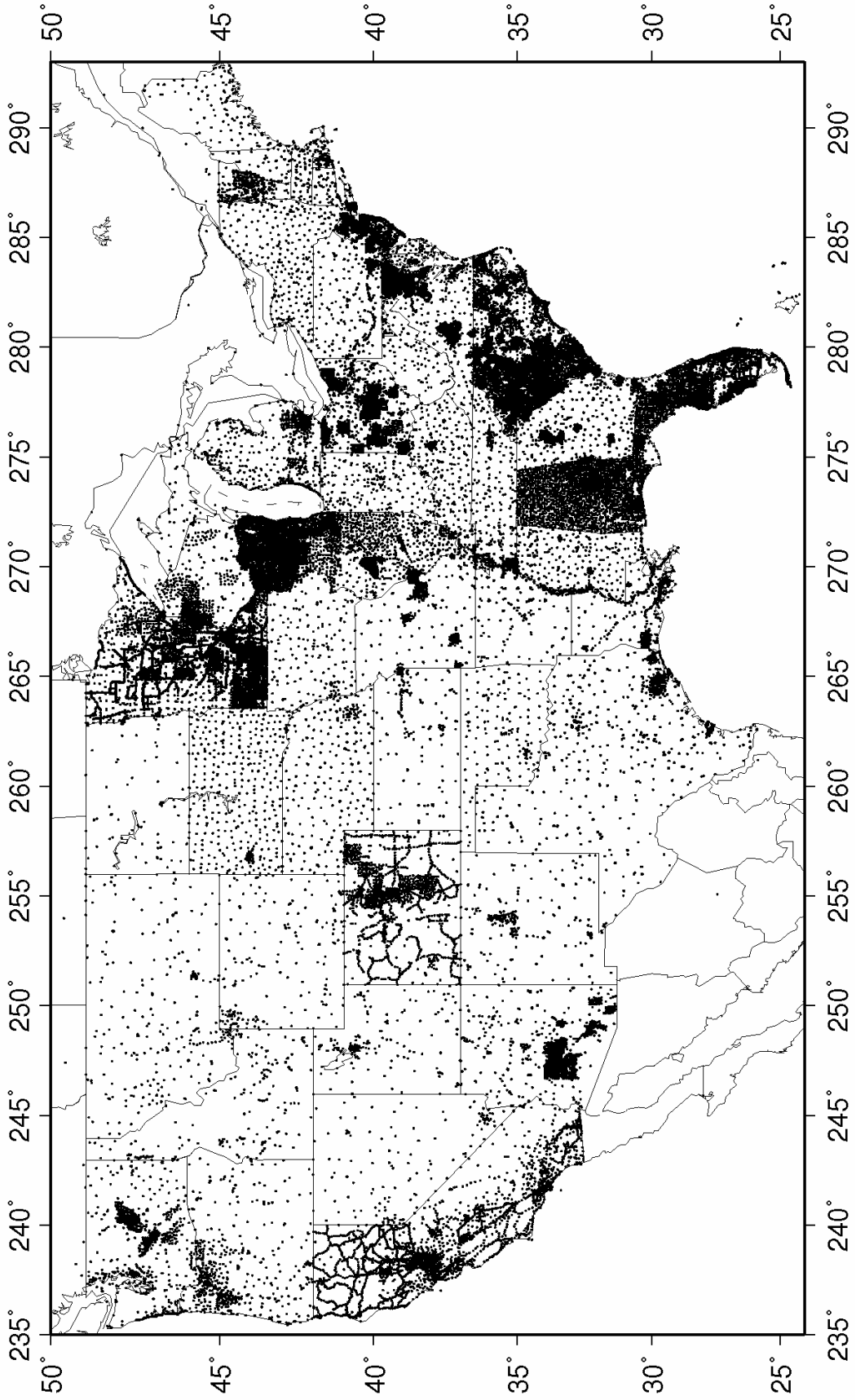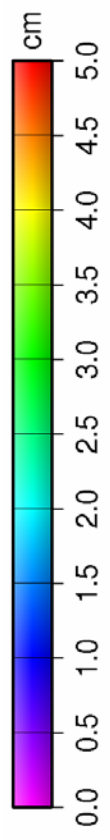
Horizontal Network Accuracies

Vertical Network Accuracies

159
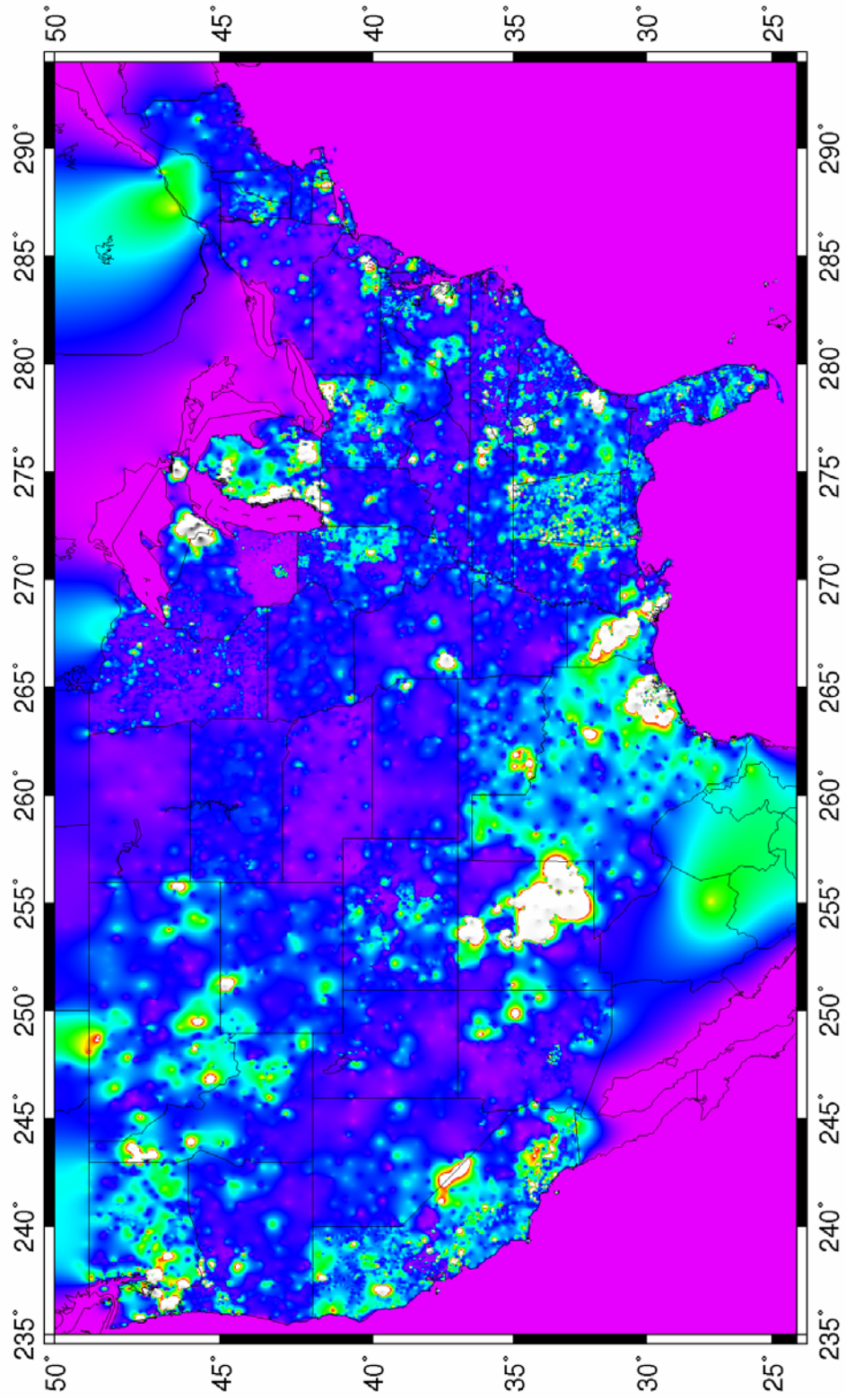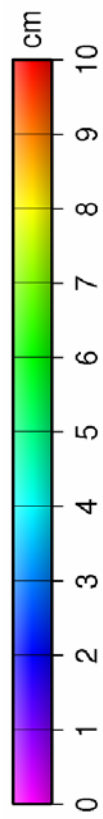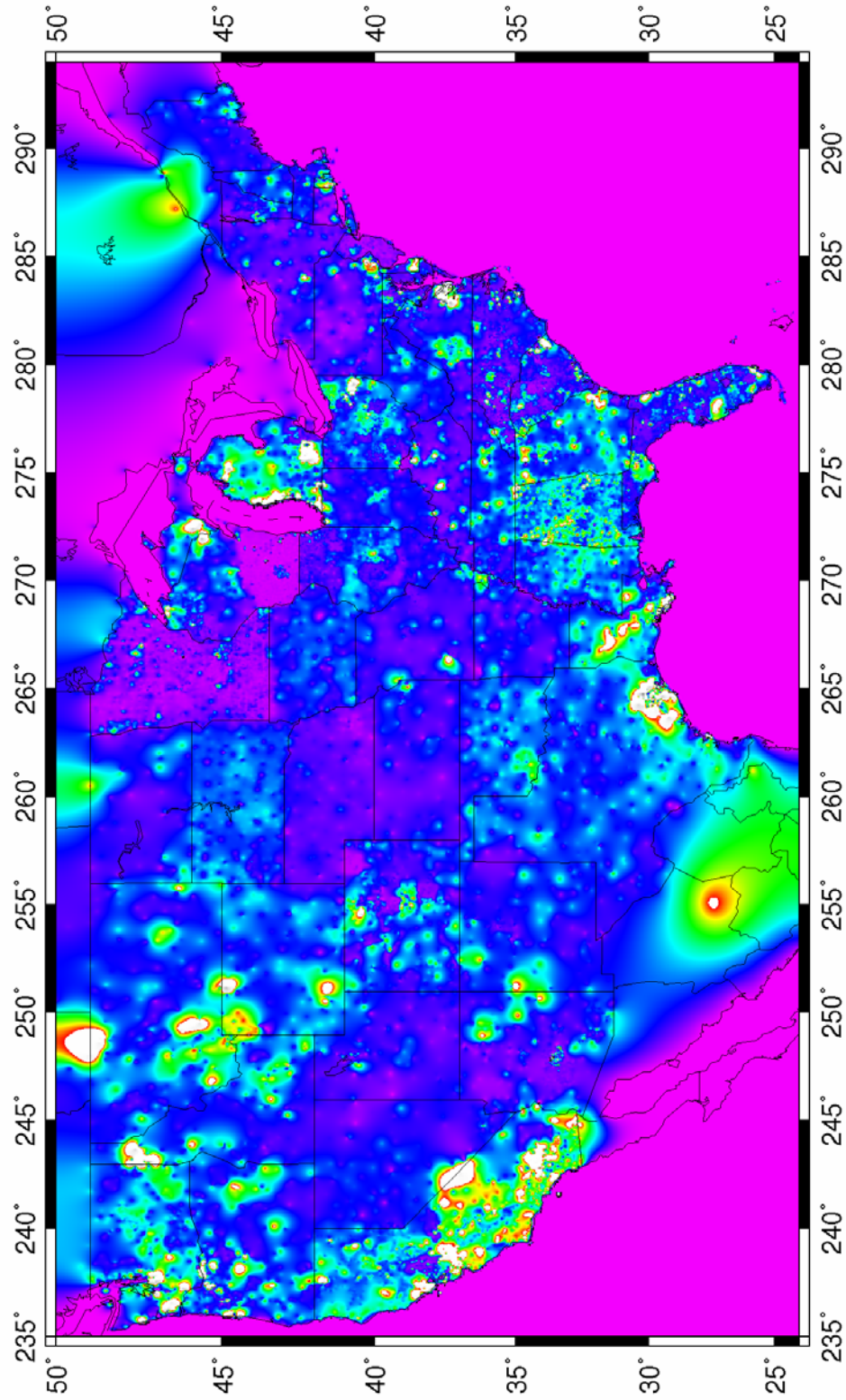
APPENDIX

NSRS 2007
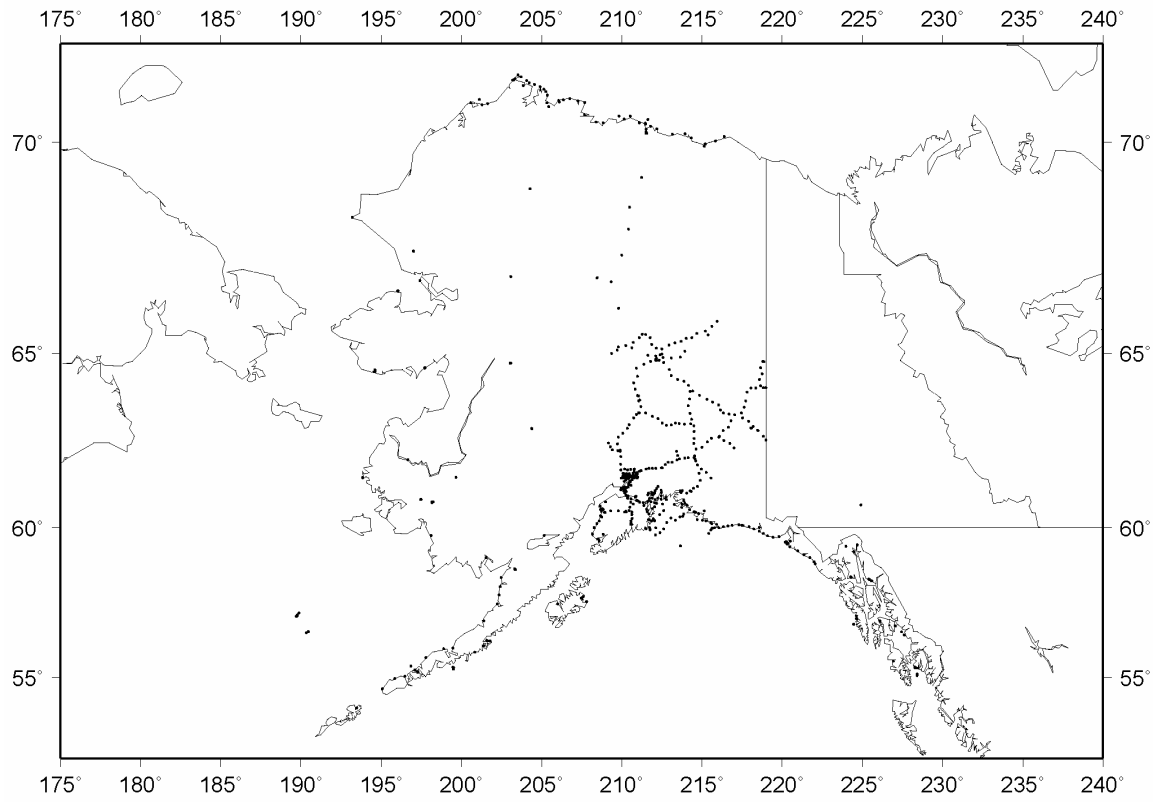
Figure A.3.2. Monumented points of NSRS 2007, Alaska.
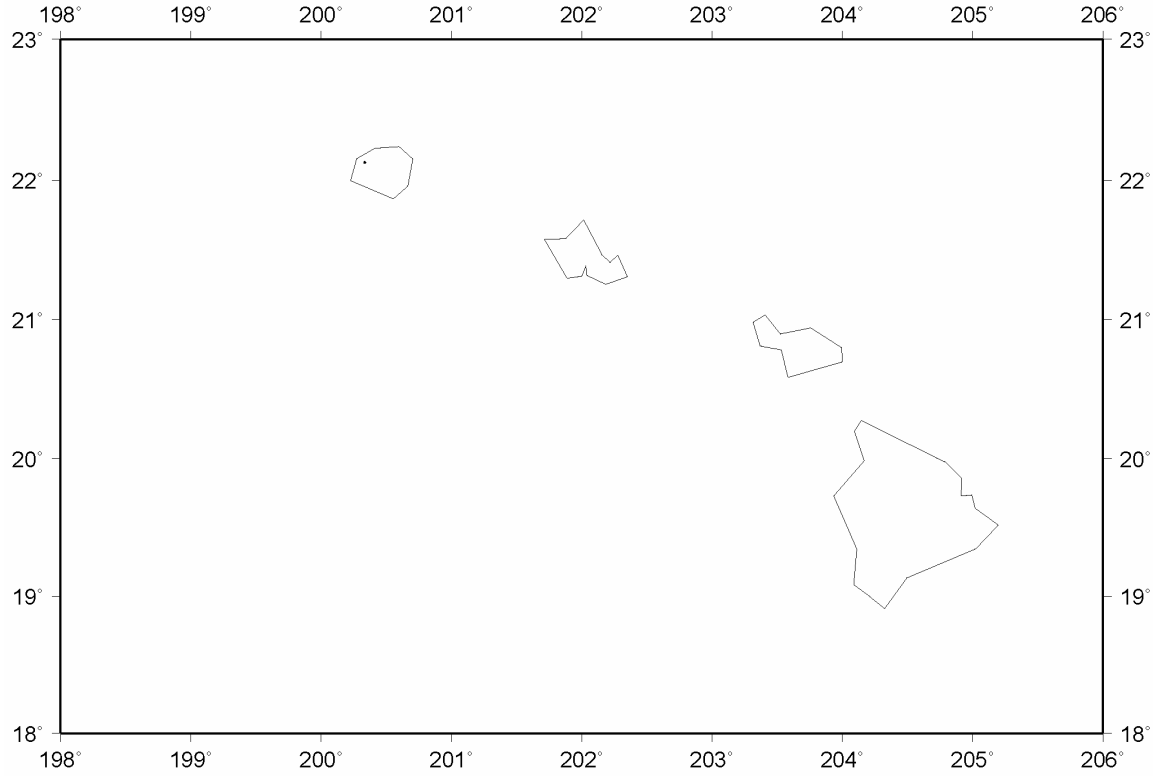
NSRS 2007

Figure A.3.3. Monumented points of NSRS 2007, Hawaii.

NSRS 2007
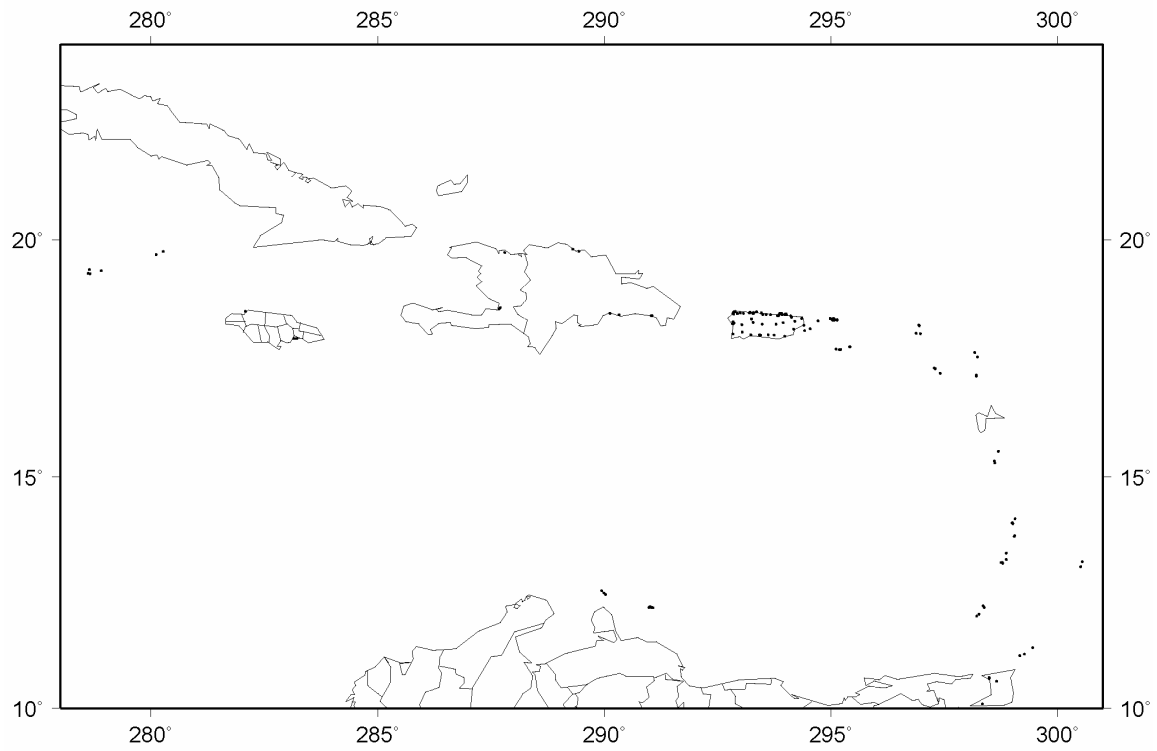
Figure A.3.4. Monumented points of NSRS 2007, Caribbean.

NSRS 2007 - Old NAD83
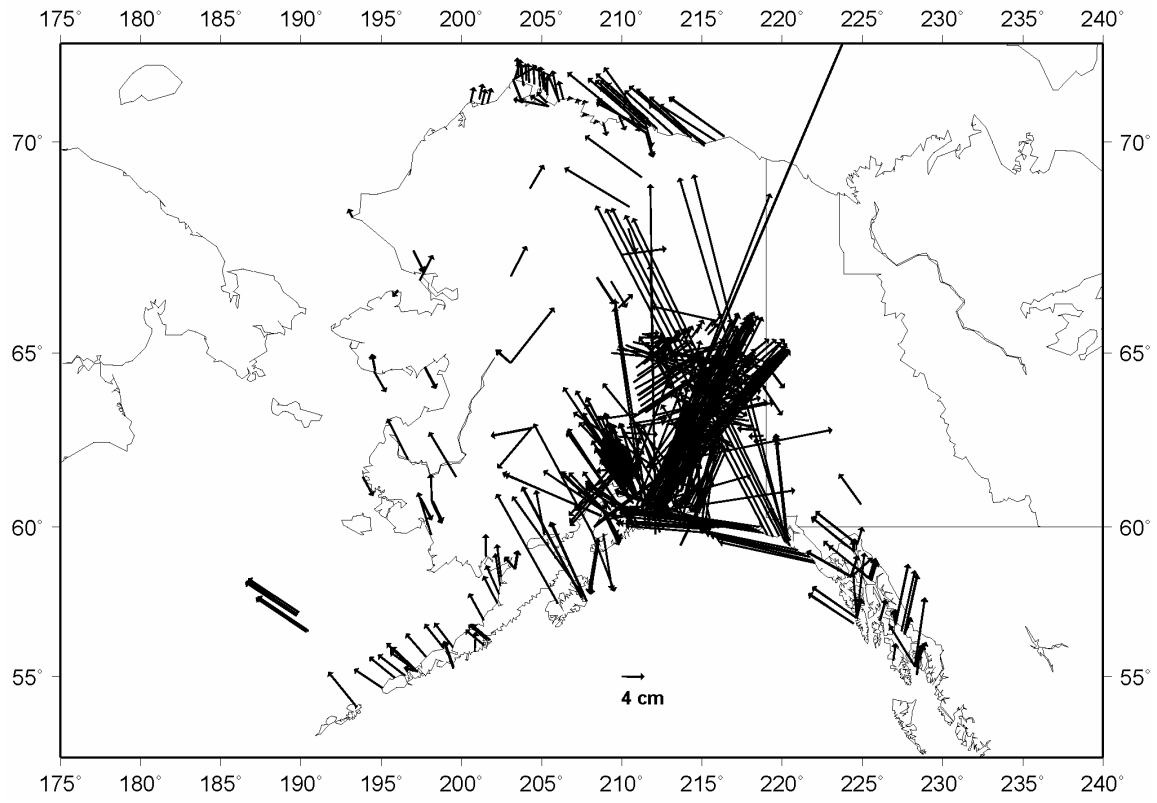
Figure A.6.4. Horizontal position shifts of NSRS 2007, Alaska.

NSRS 2007 - Old NAD83
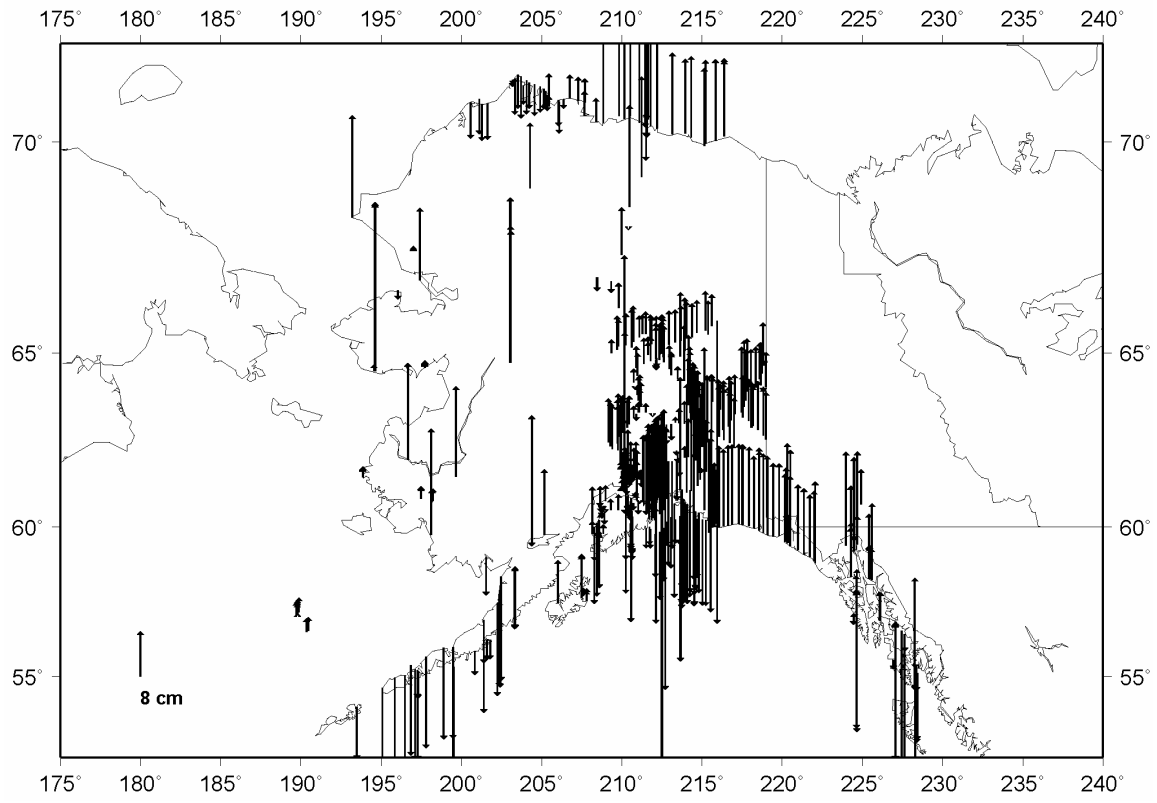
Figure A.6.5. Vertical position shifts of NSRS 2007, Alaska.
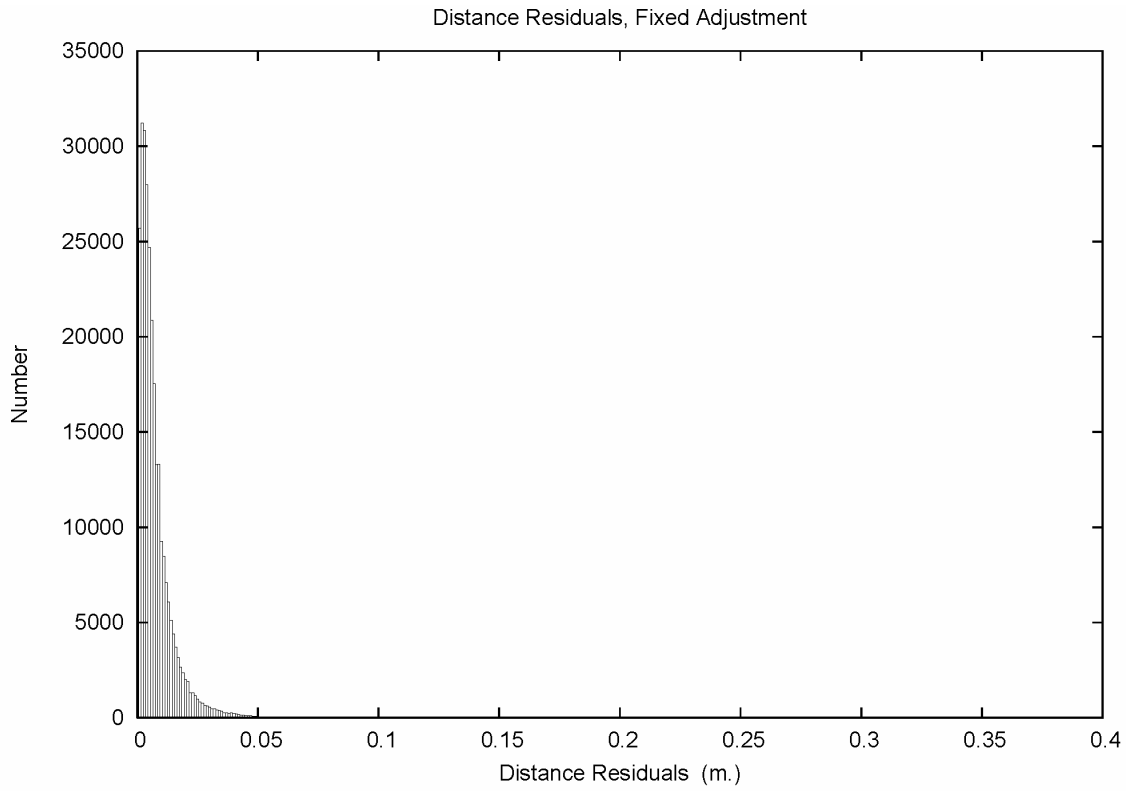
Figure A.14.1. Distance residuals, fixed adjustment.
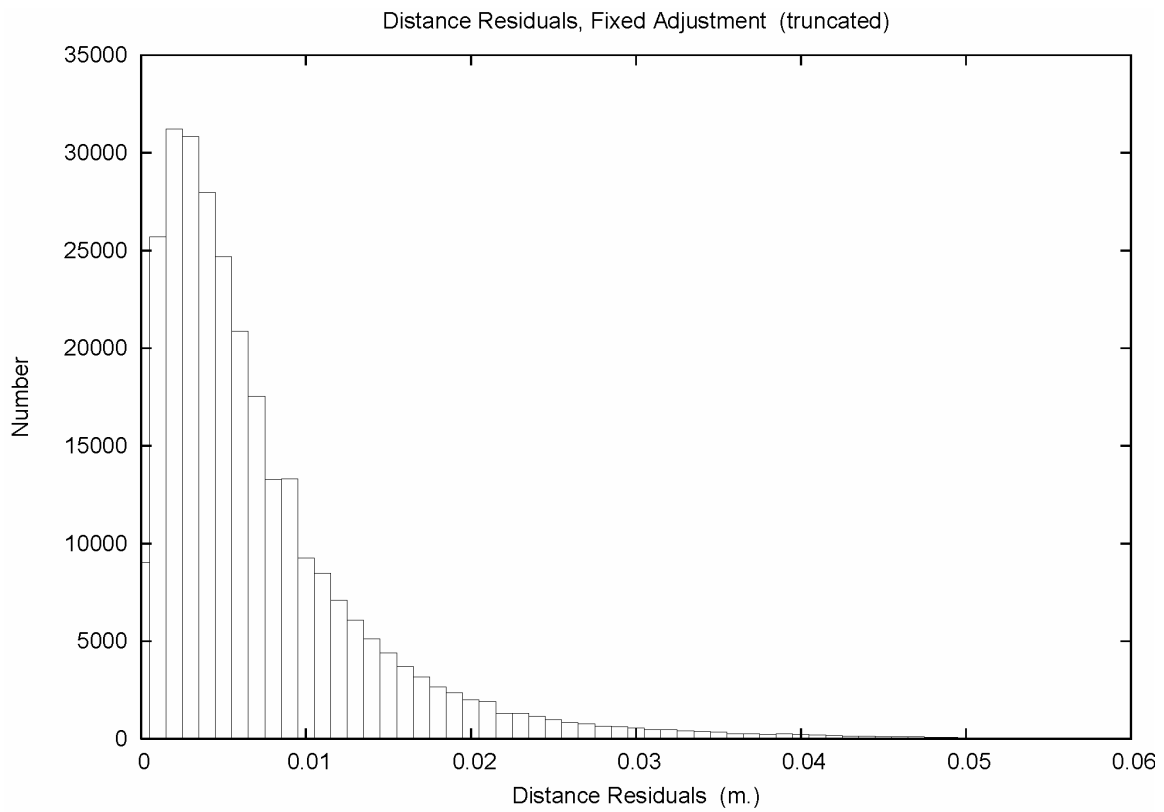
Figure A.14.2. Distance residuals, fixed adjustment, detail.
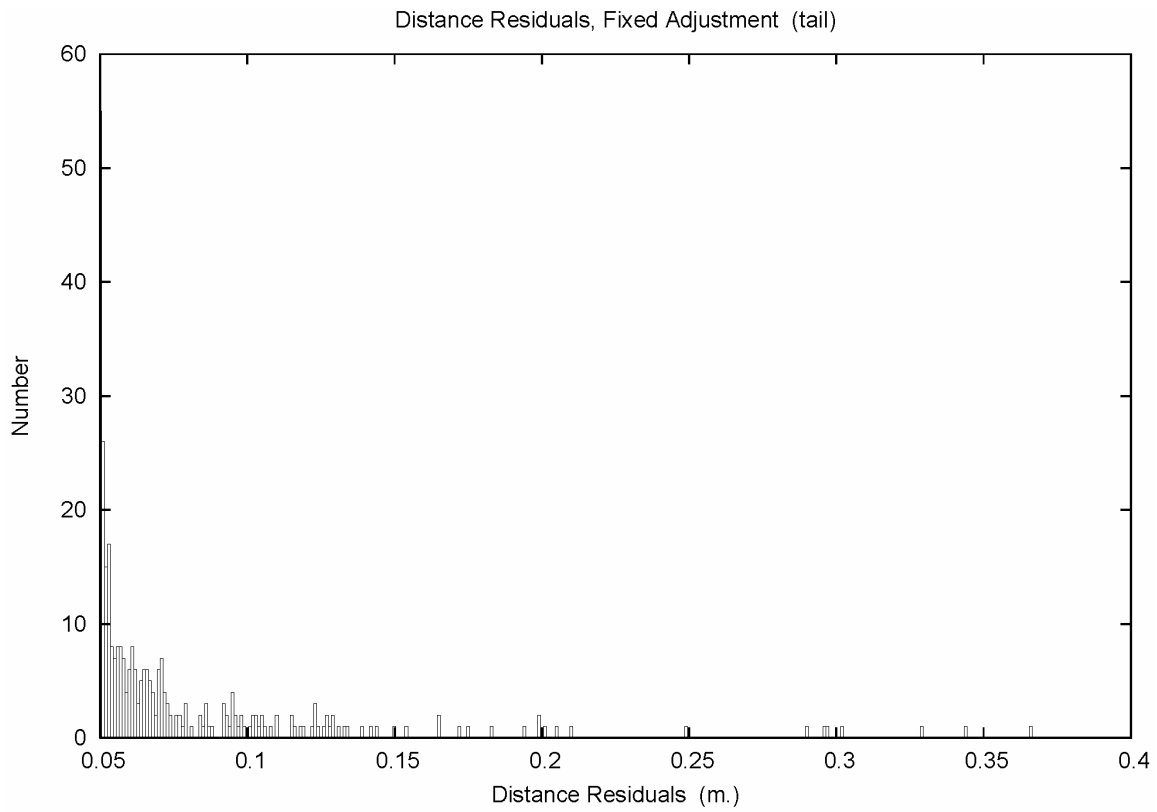
Figure A.14.3. Distance residuals, fixed adjustment, distribution tail.
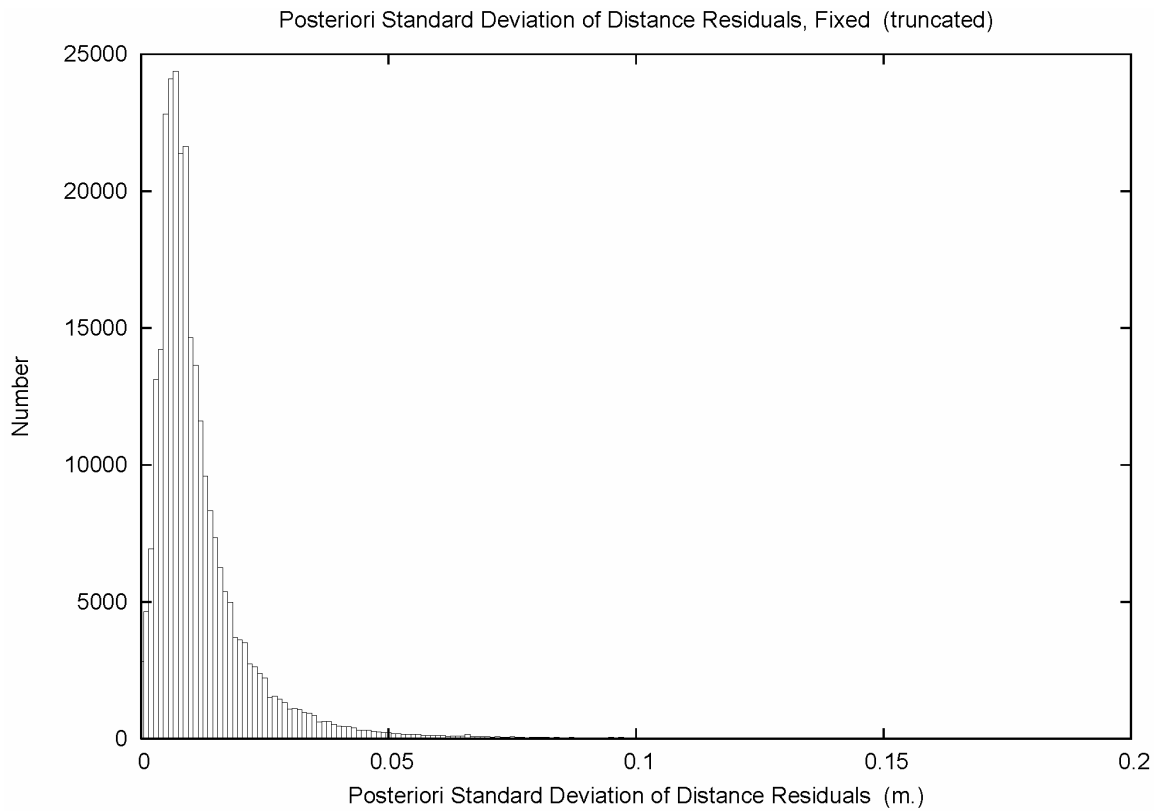
Figure A.14.4. Standard deviation of distance residuals, fixed adjustment.
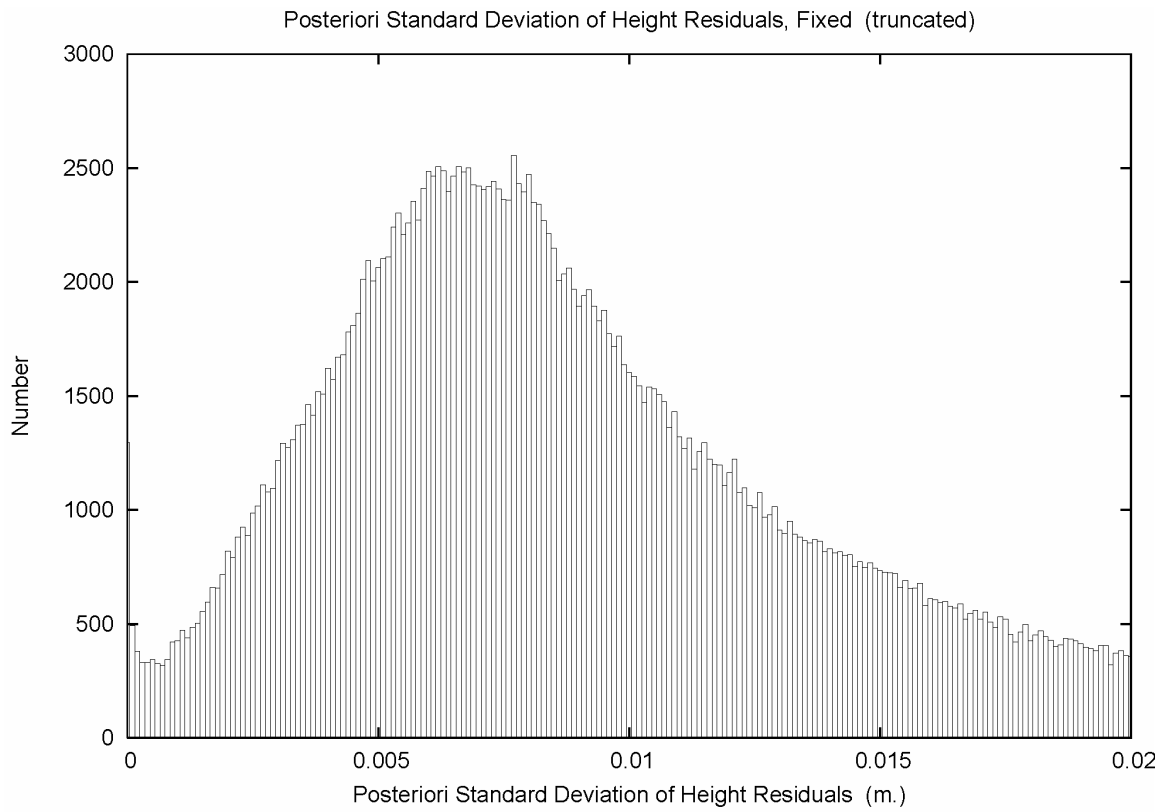
Figure A.14.5. Standard deviation of distance residuals, fixed adjustment, detail.
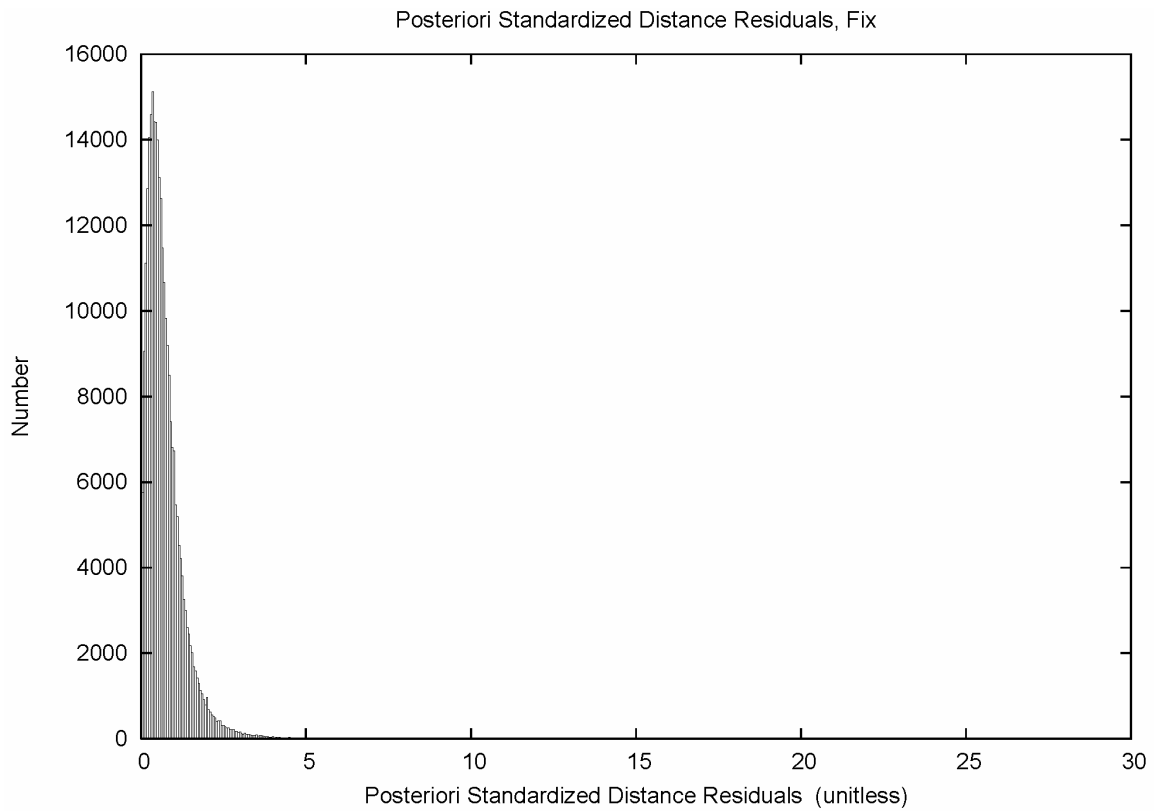
Figure A.14.6. Standardized distance residuals, fixed adjustment.
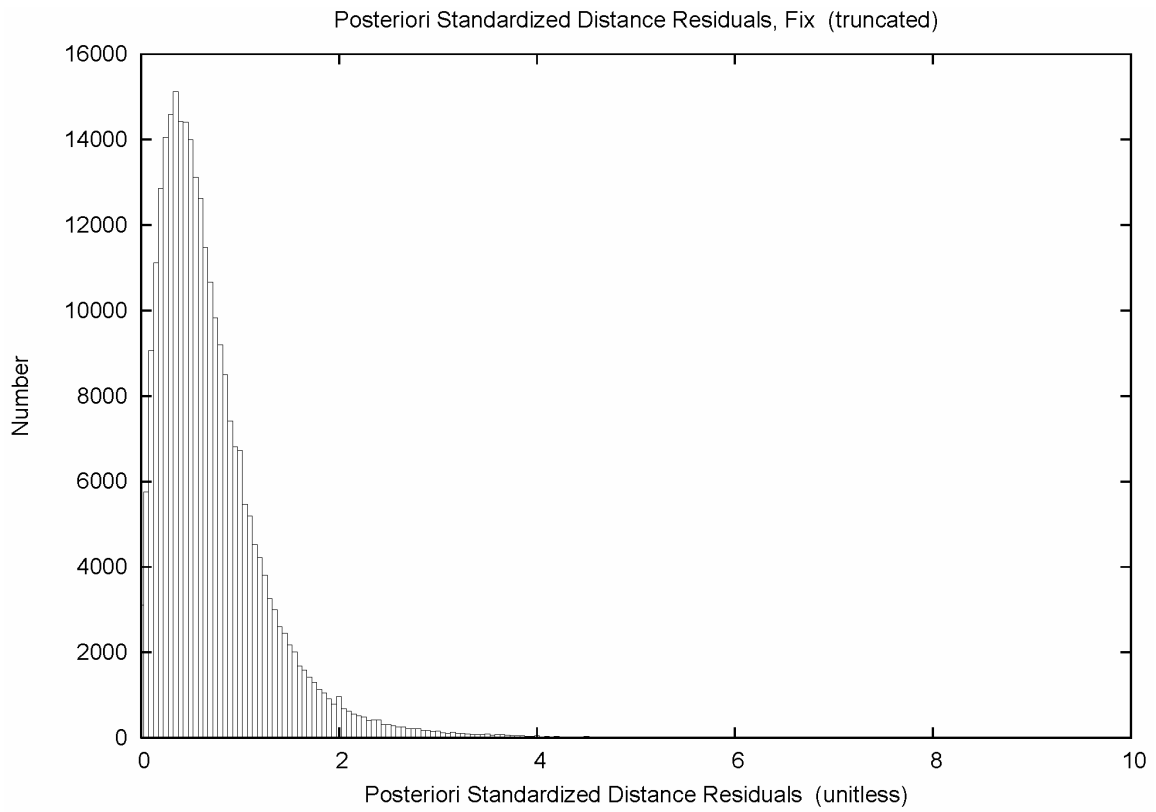
Figure A.14.7. Standardized distance residuals, fixed adjustment, detail.
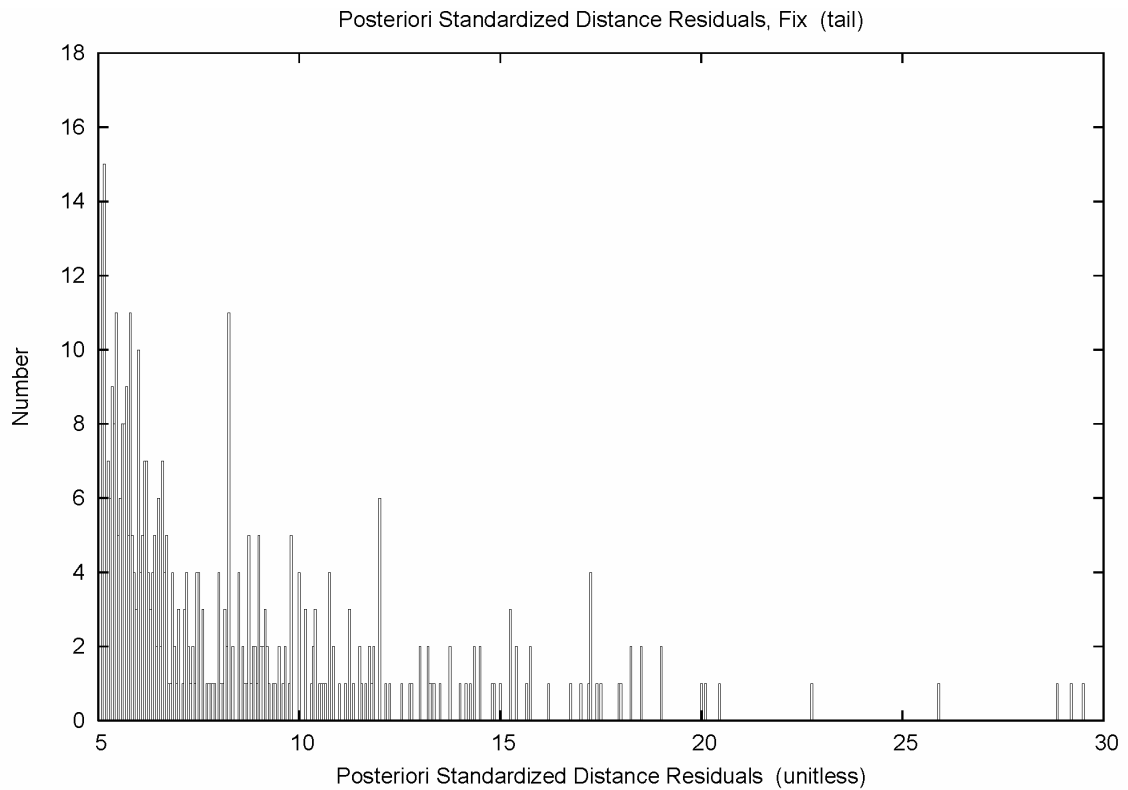
Figure A.14.8. Standardized distance residuals, fixed adjustment, distribution tail.
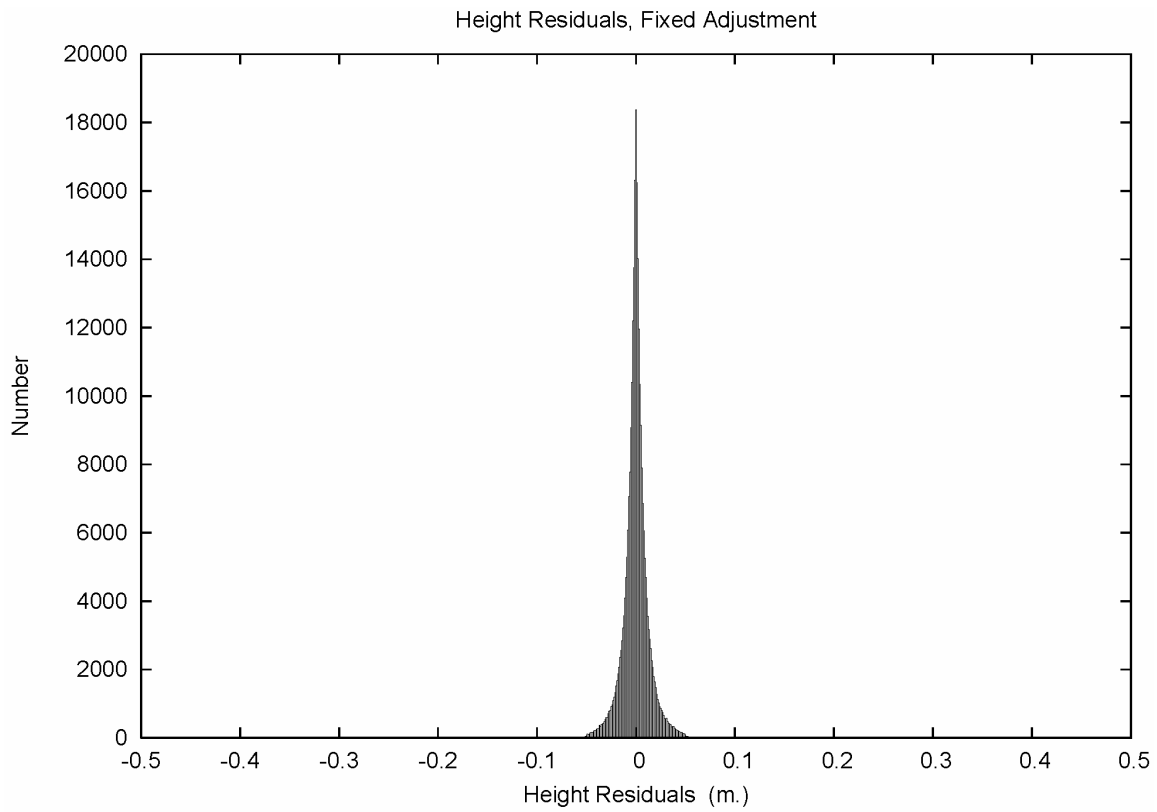
Figure A.14.9. Height residuals, fixed adjustment.
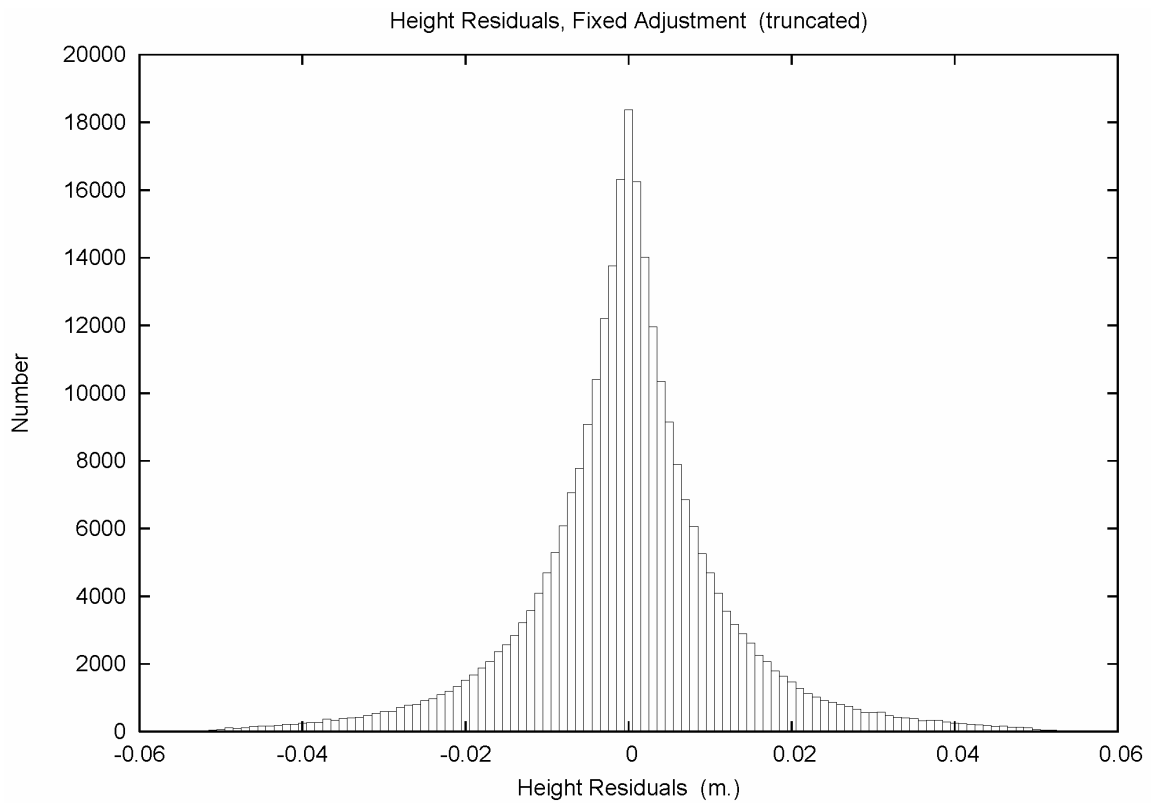
Figure A.14.10. Height residuals, fixed adjustment, detail.
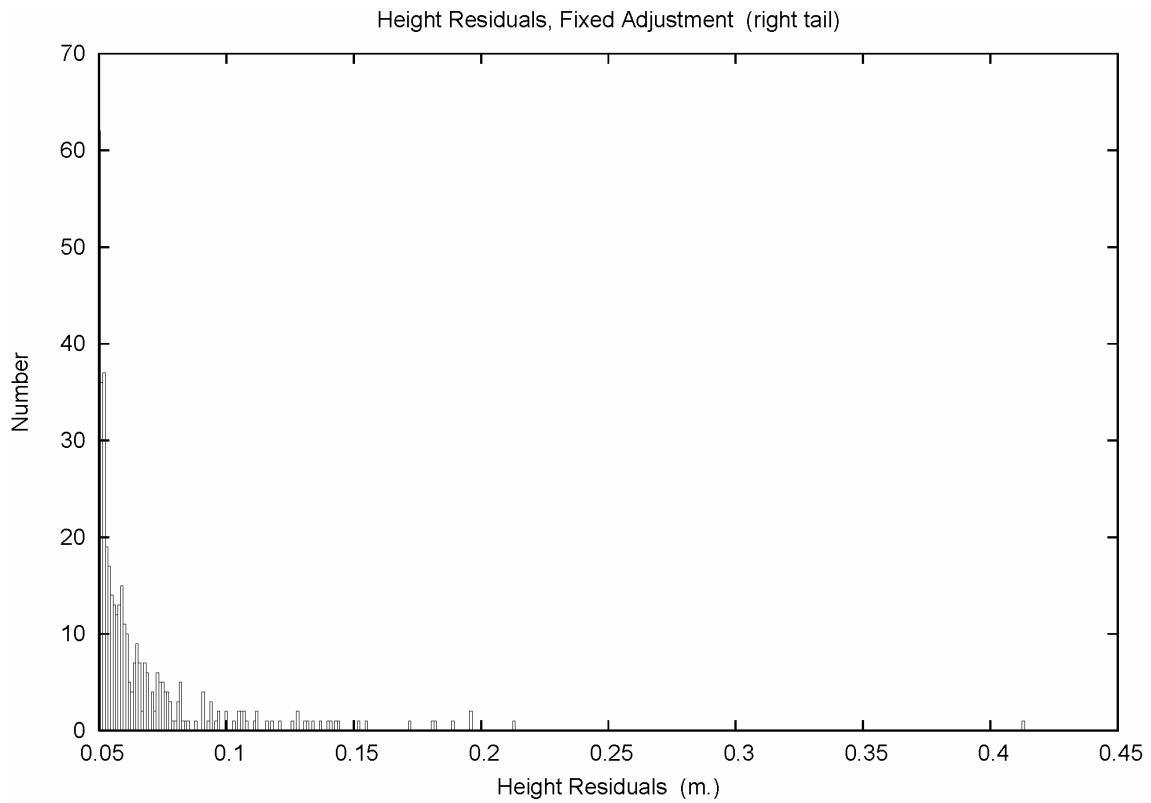
Figure A.14.11. Height residuals, fixed adjustment, right tail.
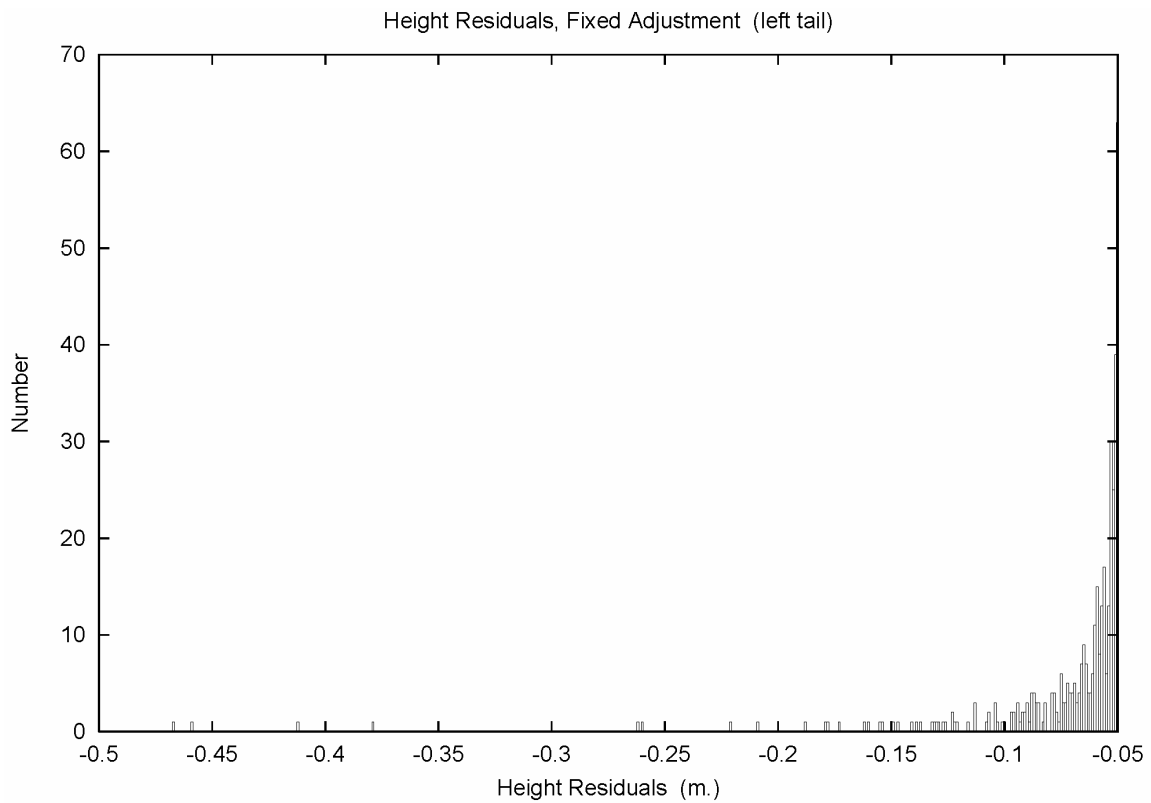
Figure A.14.12. Height residuals, fixed adjustment, left tail.
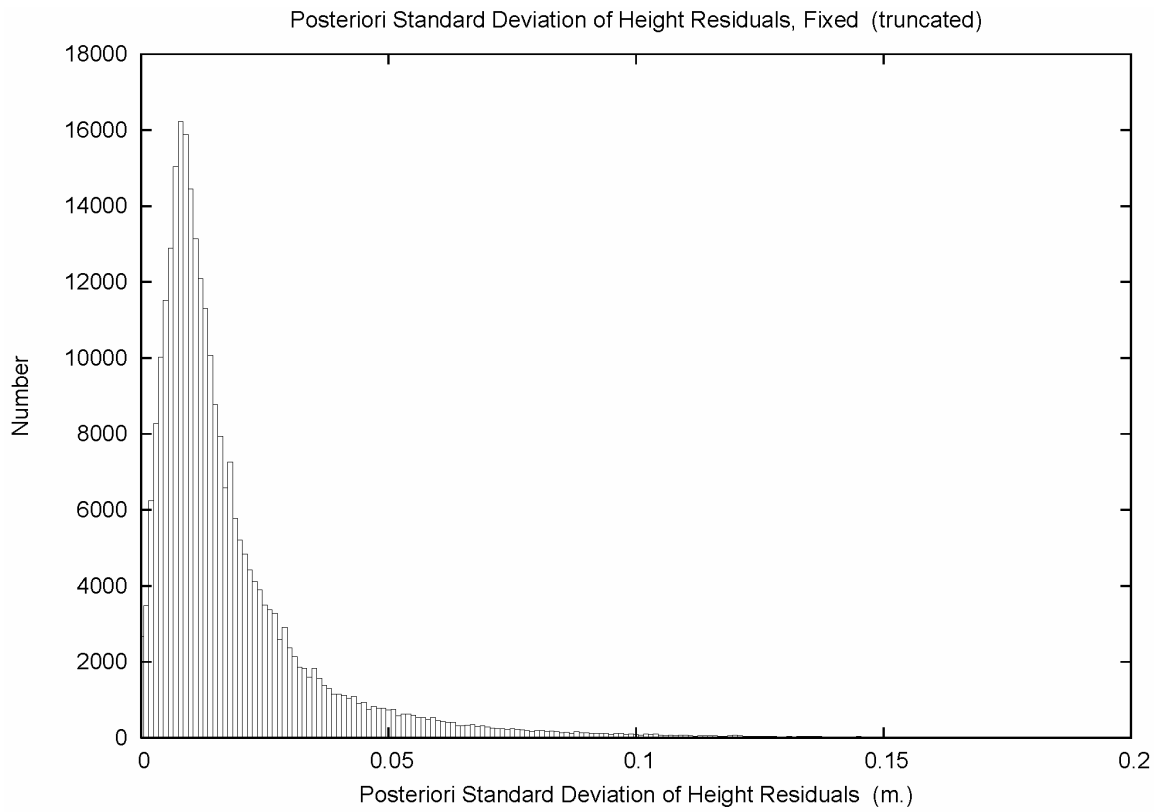
Figure A.14.13. Standard deviation of height residuals, fixed adjustment.
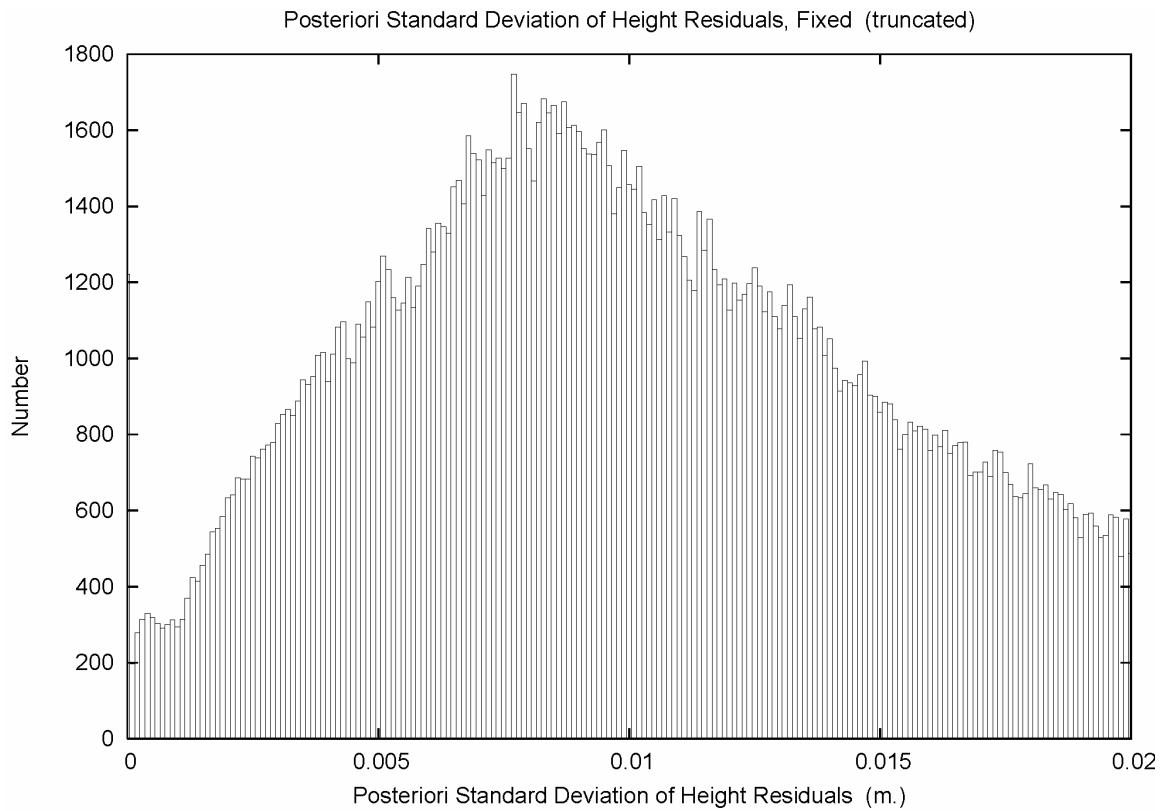
Figure A.14.14. Standard deviation of height residuals, fixed adjustment, detail.
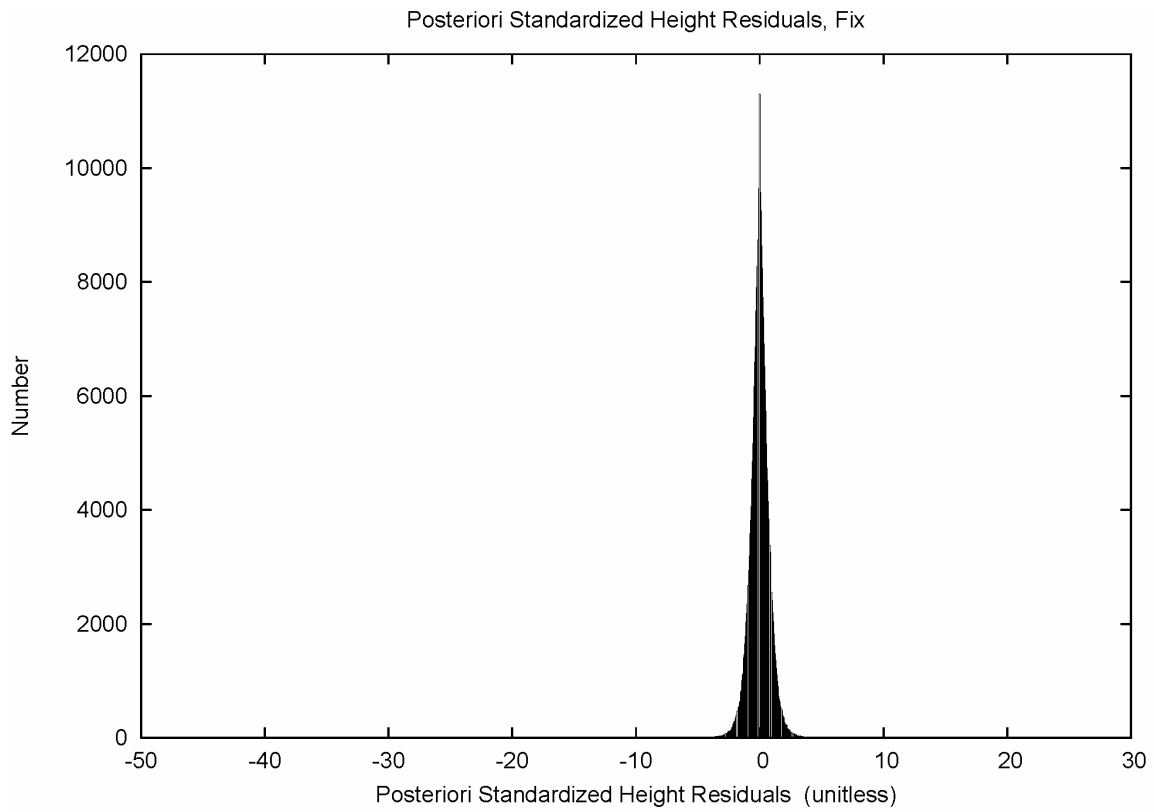
Figure A.14.15. Standardized height residuals, fixed adjustment.
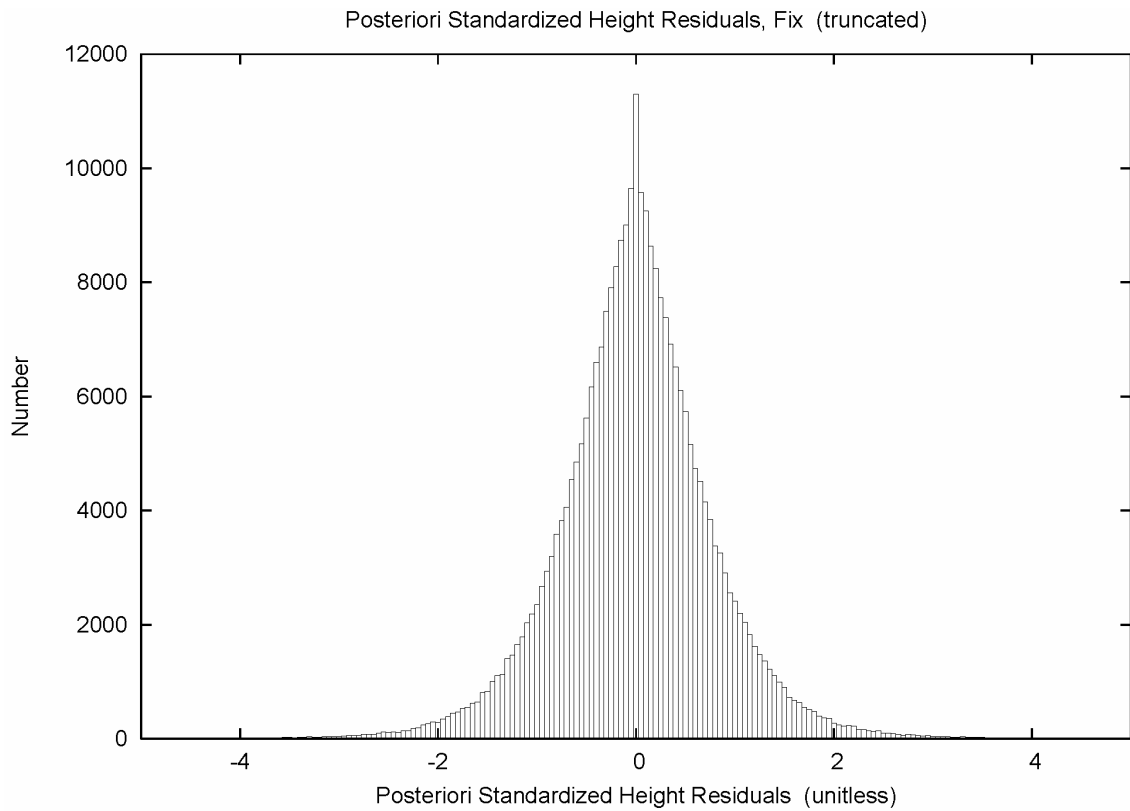
Figure A.14.16. Standardized height residuals, fixed adjustment, detail.
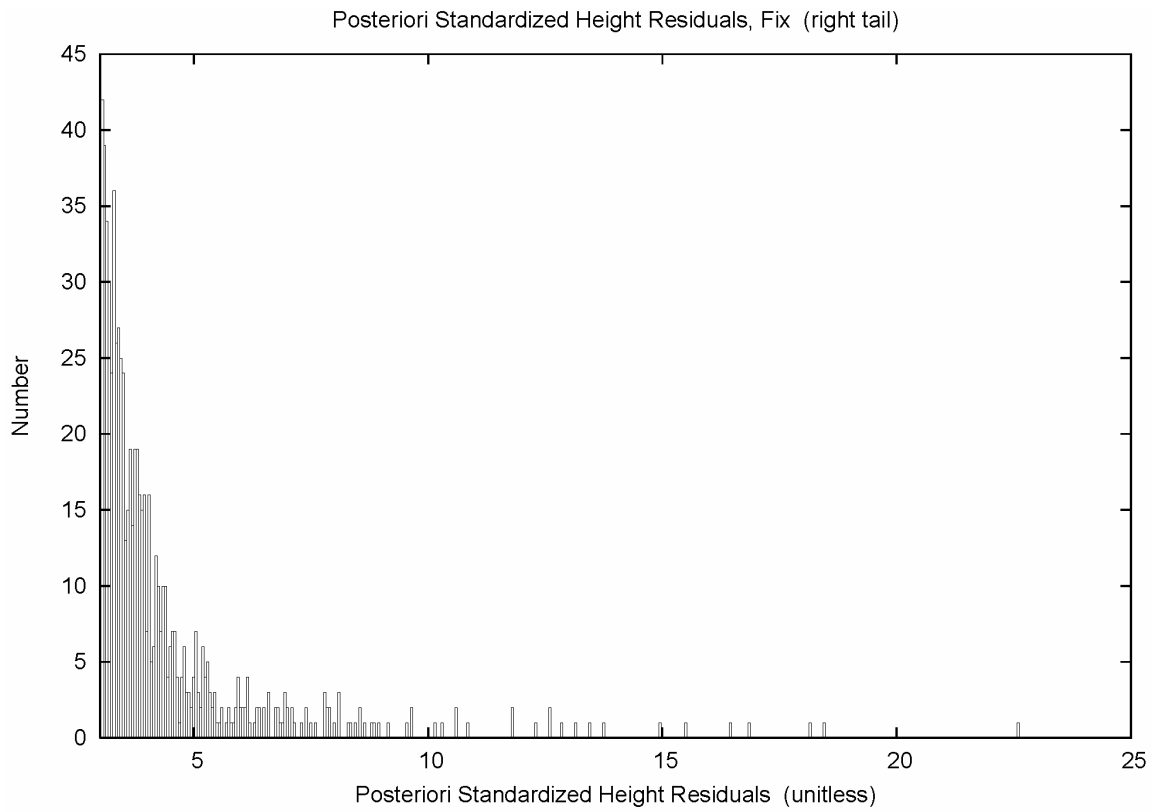
Figure A.14.17. Standardized height residuals, fixed adjustment, right tail.
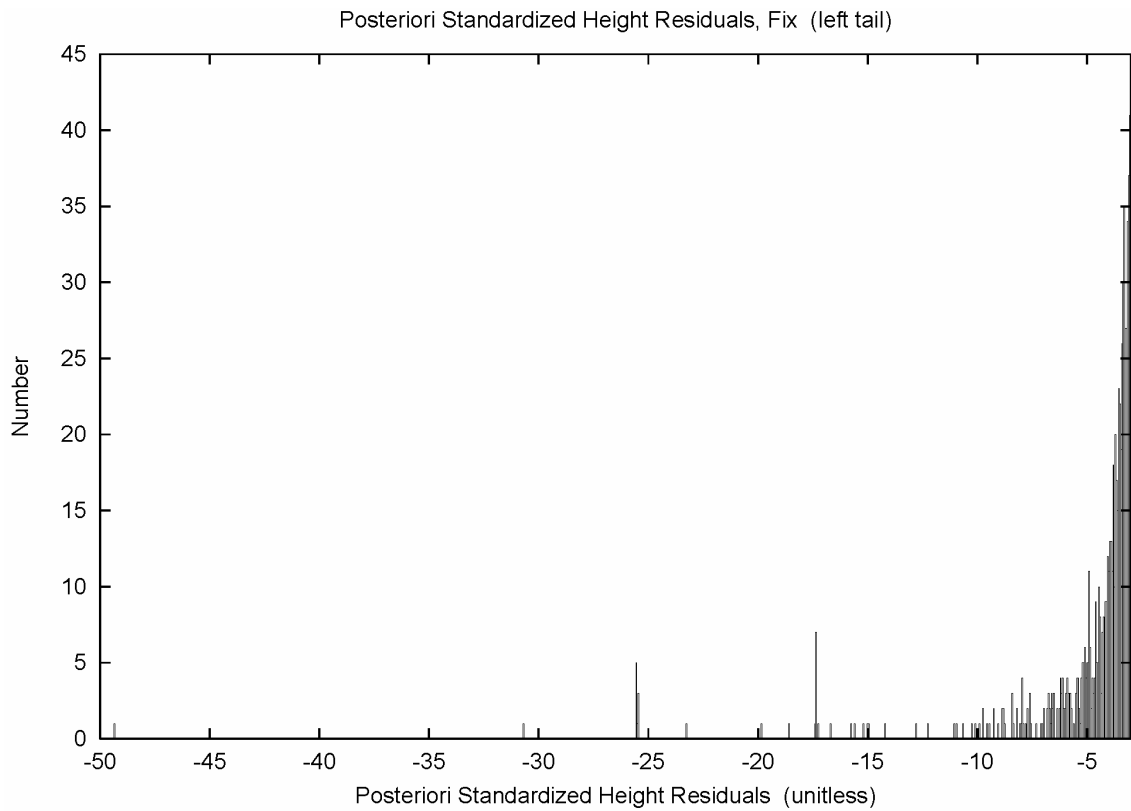
Figure A.14.18. Standardized height residuals, fixed adjustment, left tail.

A.25. Detail on artifact in azimuth of semimajor axis of horizontal error ellipses

As described in Section 25, slight peaks may be seen at +/- 45° of the histogram distribution of the semimajor axis of the horizontal relative error ellipses, Figure 25.3. In fact, this artifact can also be seen in Figure 17.3 for the horizontal position error ellipses.

If one plots the azimuths of Figure 25.3 with a 0.01° bin width, Figure A.25.4, one finds the 45° become quite pronounced.
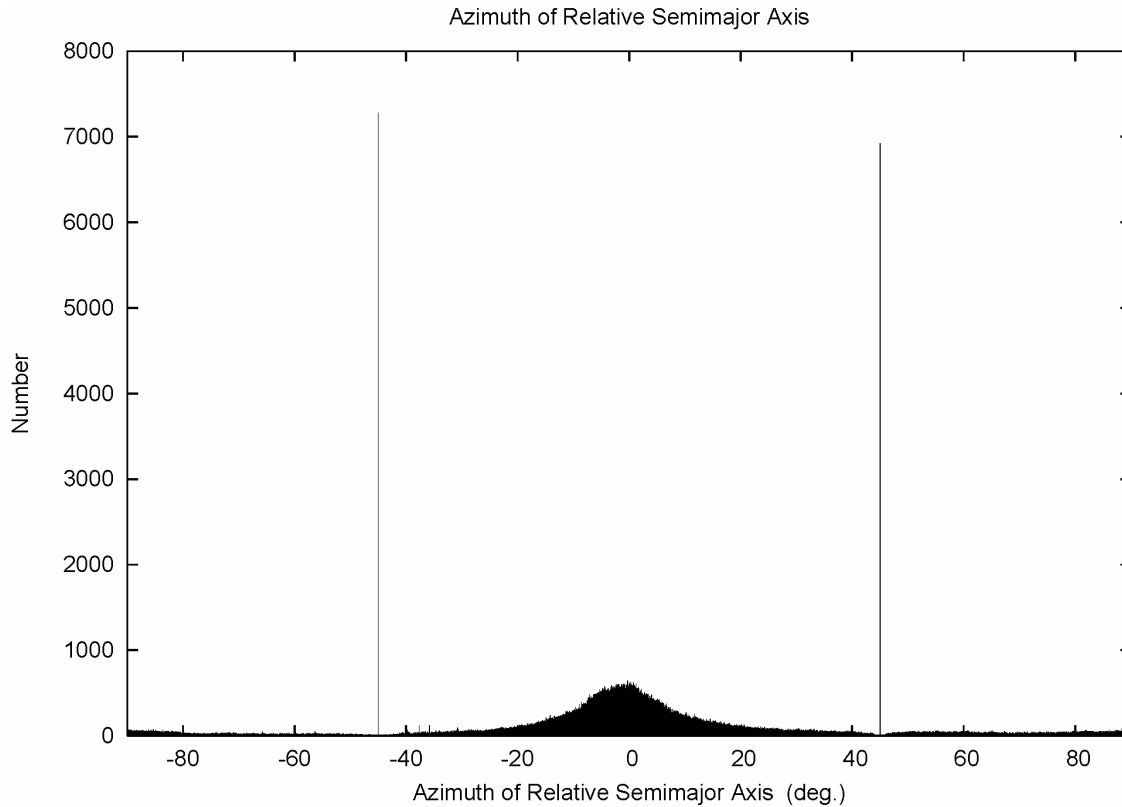
Figure A.25.4. Azimuth (rounding) of semimajor axis of horizontal relative error ellipse.

In addition, a detail view of the distribution, Figure A.25.5, shows that in addition to the +/- 45° spikes, there are an *absence* of values in the close vicinity of +/- 45°.
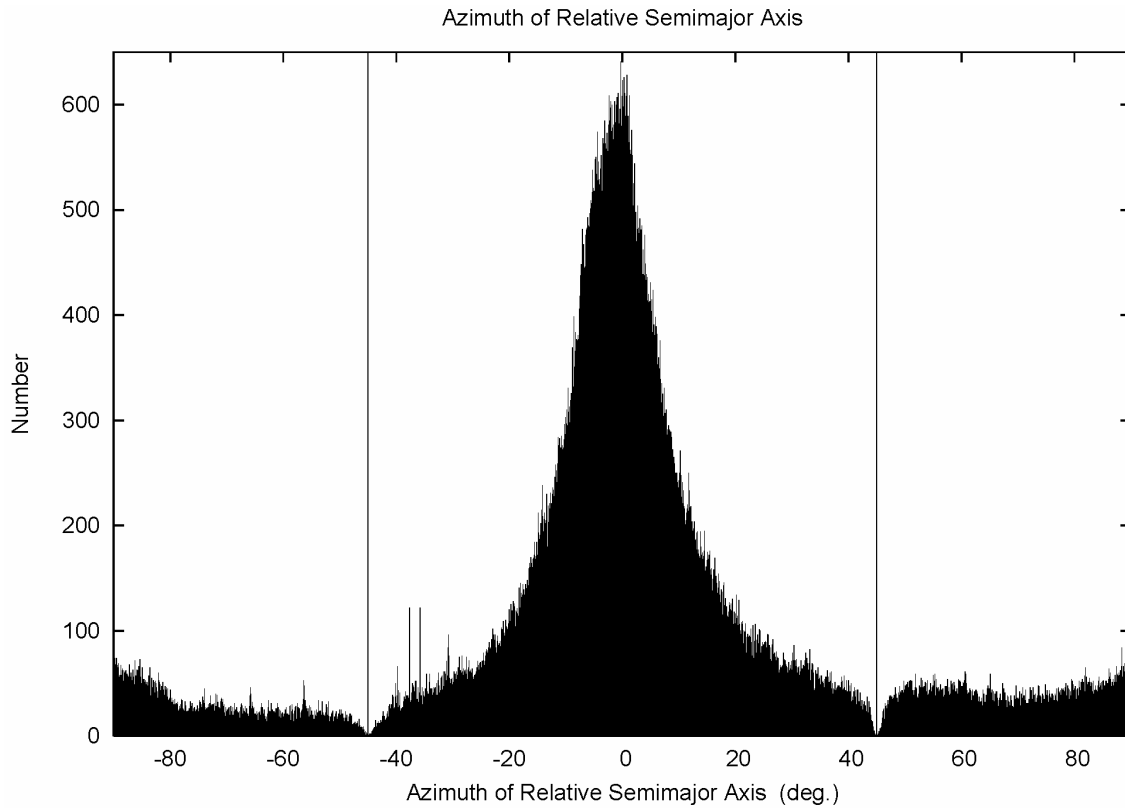
Figure A.25.5. Azimuth (rounding) of semimajor axis of horiz. rel. error ellipse, detail.

This behavior is due to the use of a fixed precision format for standard deviations of the latitude and longitude (and relative standard deviations) with a least count of 0.01 cm. Some error ellipses have *very* small magnitudes. And measures, such as azimuth, can only take on fewer values as the magnitudes approach the least count. For example, one may have a latitude standard deviation of 0.054 cm that is rounded to 0.05 cm in combination with a longitude standard deviation of 0.047 cm, which is also rounded to 0.05 cm. This leads to artifacts appearing in certain derived statistics caused by the rounding.

To confirm this description, a program was written to process the 226,673 unrejected, single-vector session, GPS vectors of the NSRS 2007 adjustment. Vector covariances were rotated into the local geodetic horizon system, and the horizontal vector relative semimajor axis azimuths were computed without any rounding whatsoever. These results are plotted in Figure A.25.6.
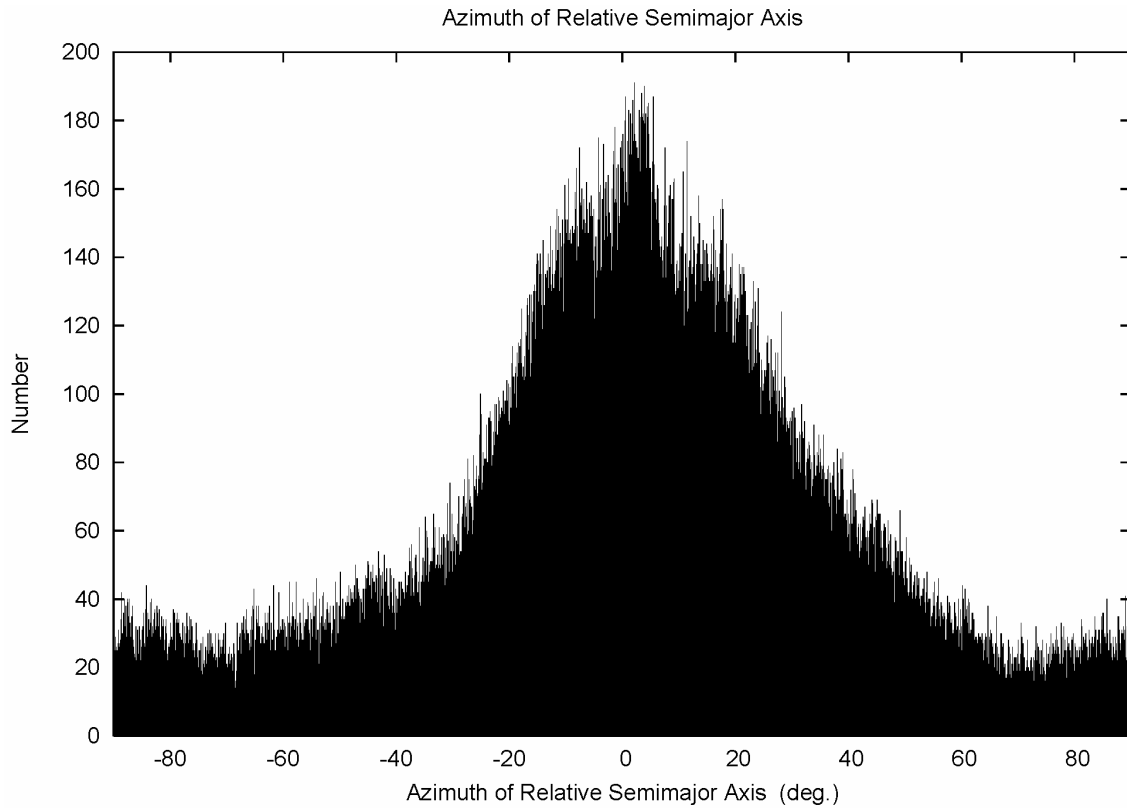
Figure A.25.6. Precise azimuth of semimajor axis, GPS vector horizontal error ellipses.

As expected, one sees a general centering about zero. The key feature is that there are no spikes at +/- 45°, nor is there any depletion of values in the near vicinities of +/- 45°.

Then, within that same program, a rounding process was imposed that duplicated the rounding that occurs when using an output file limited to a fixed precision. These results are displayed in Figure A.25.7. The figure confirms the spikes at +/- 45°, and the depletion of values in the near vicinities of +/- 45° are format rounding artifacts. (Refer to filt17.txt in the Electronic Support Material.)
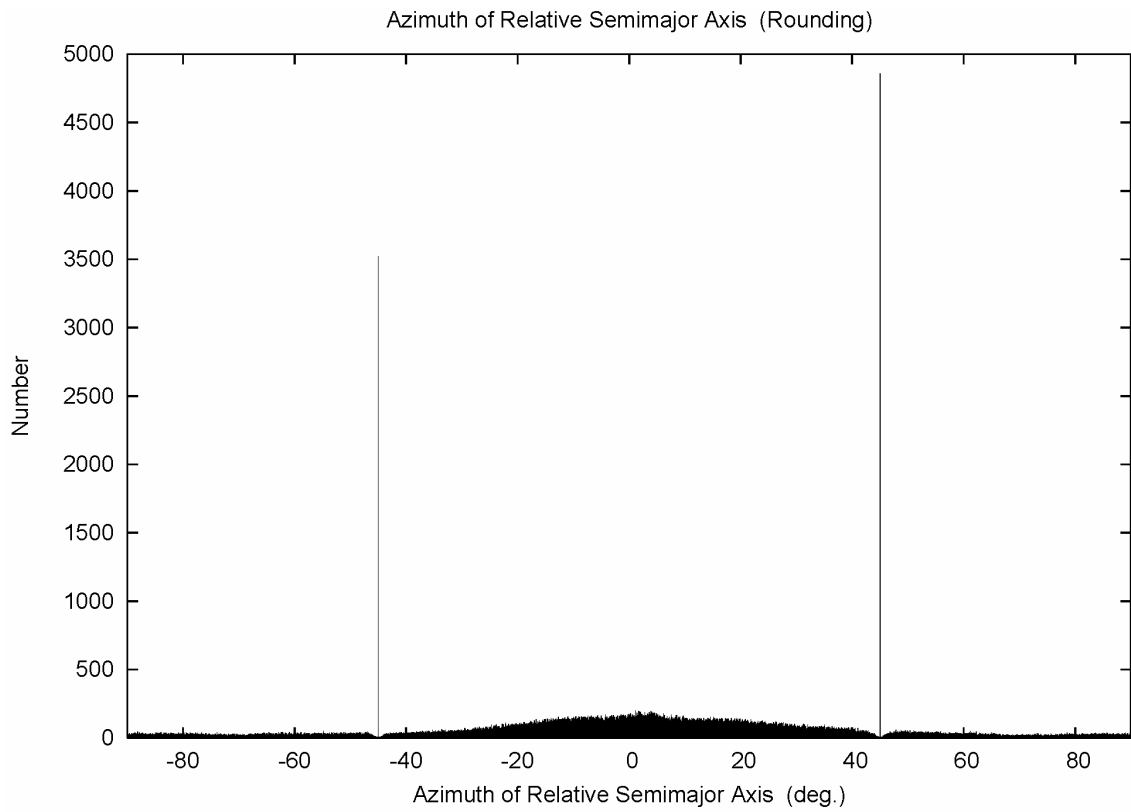
Figure A.25.7. Azimuth (rounding) of semimajor axis of GPS vector error ellipses.
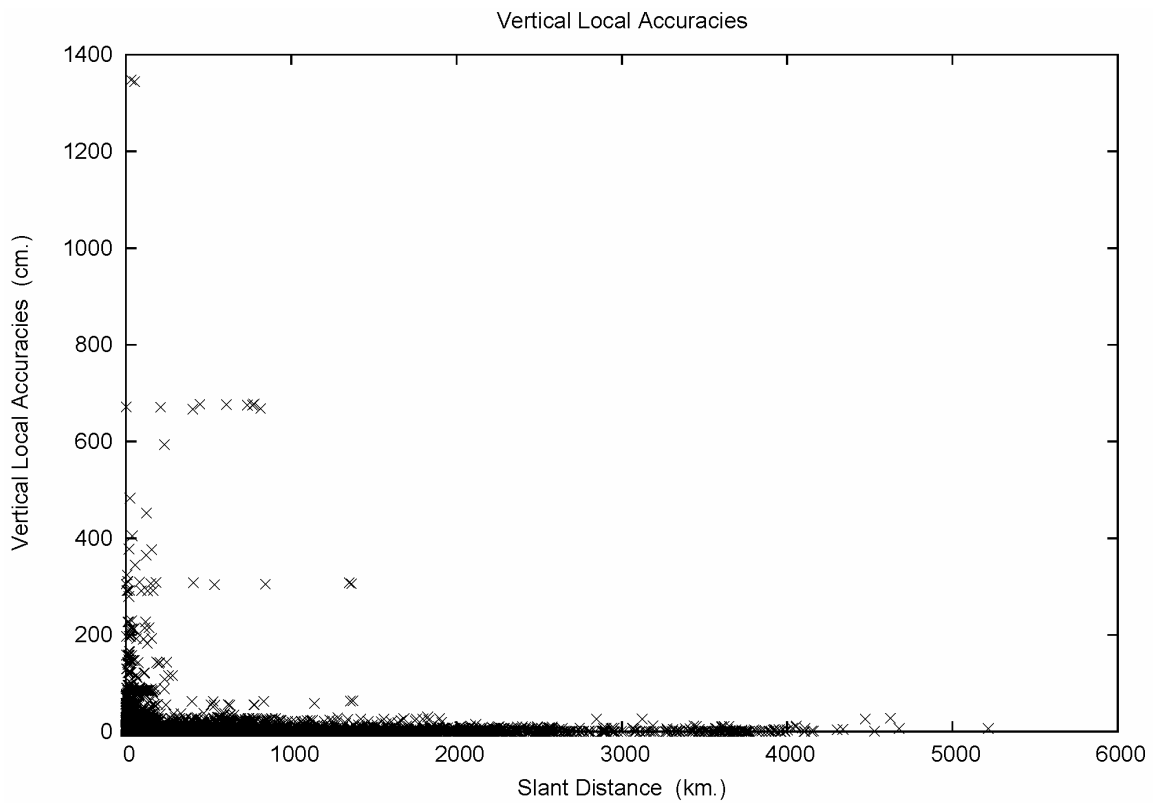
Figure A.28.6. Length distribution of vertical local accuracies.
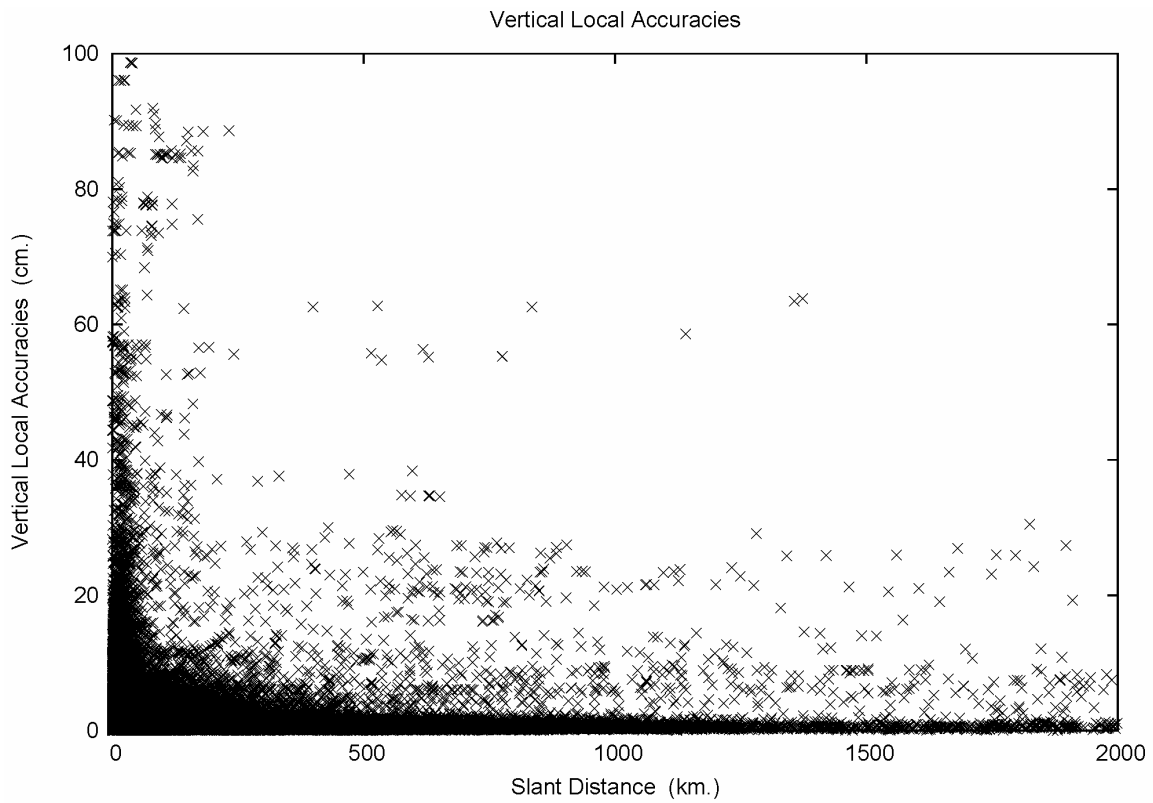
Figure A.28.7. Length distribution of vertical local accuracies, detail.
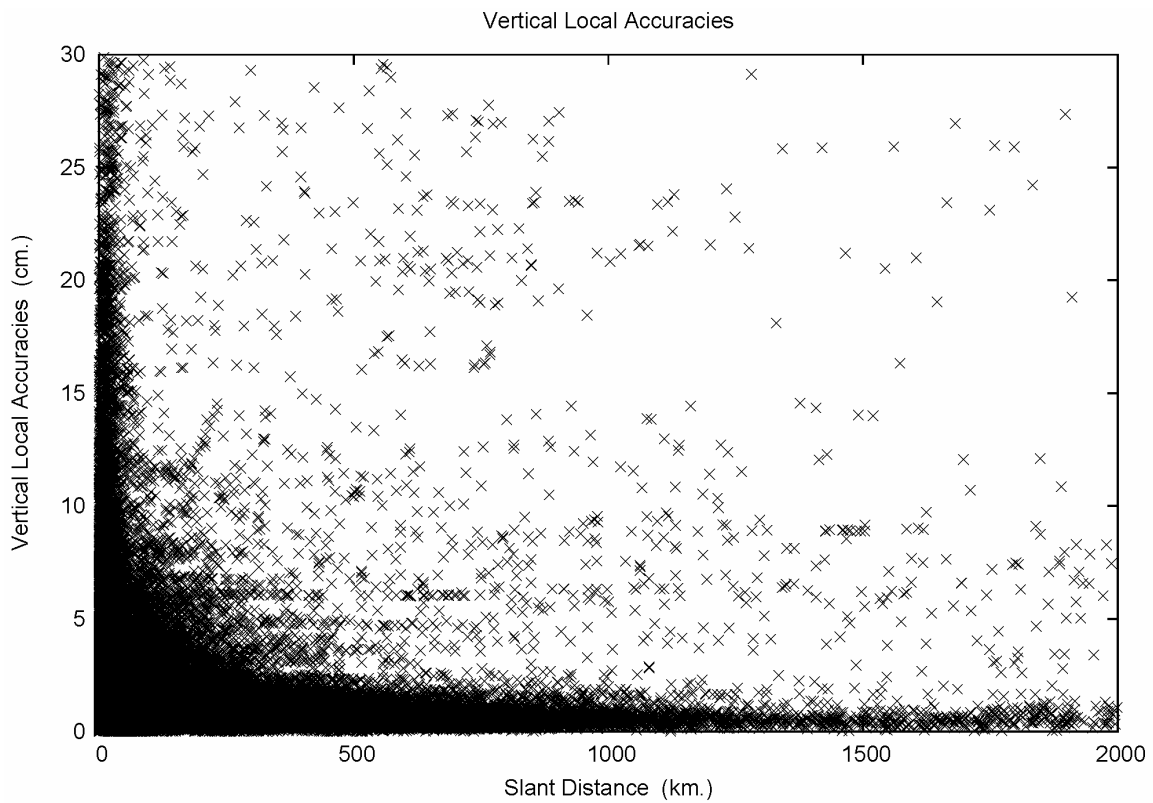
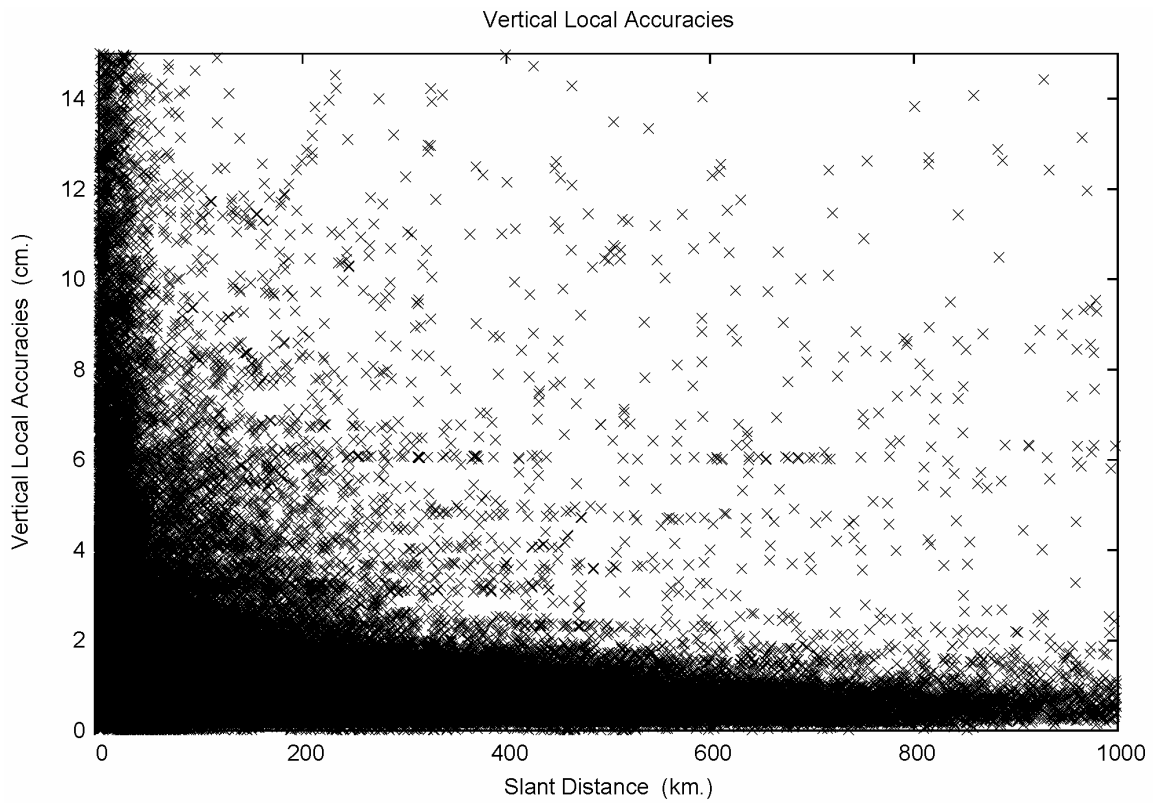Figure A.28.8. Length distribution of vertical local accuracies, detail 2.

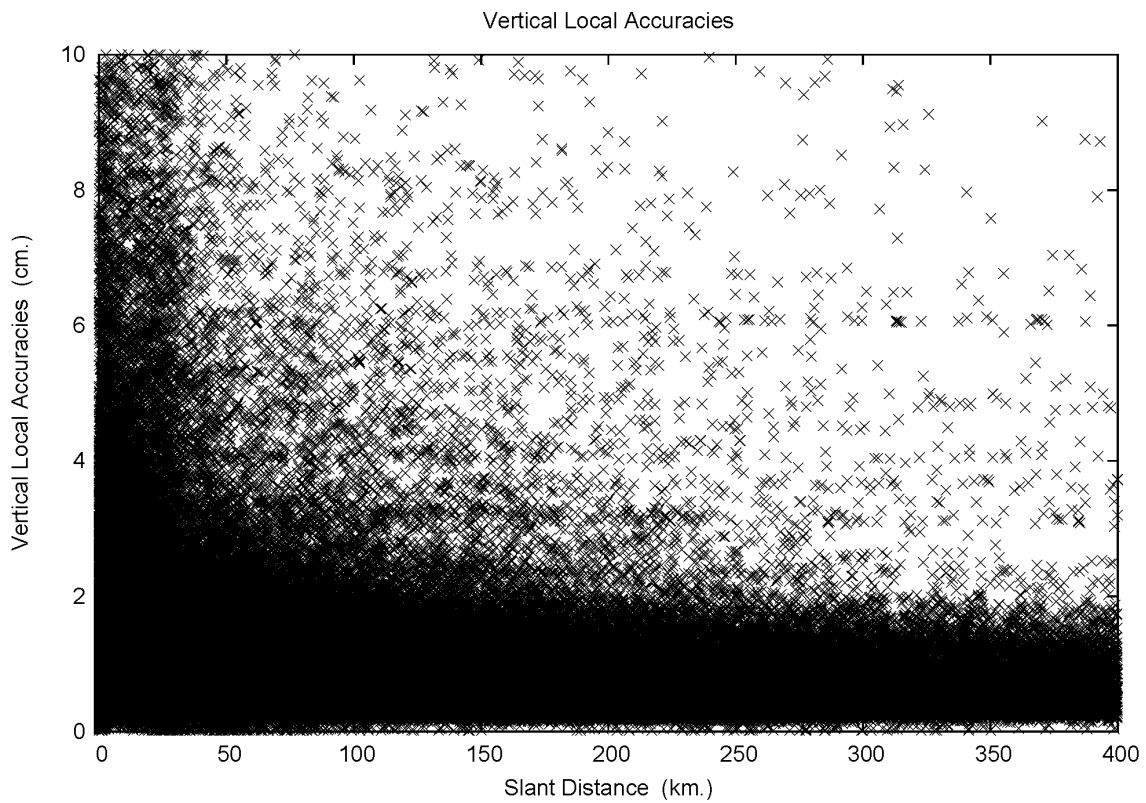Figure A.28.9. Length distribution of vertical local accuracies, detail 3.

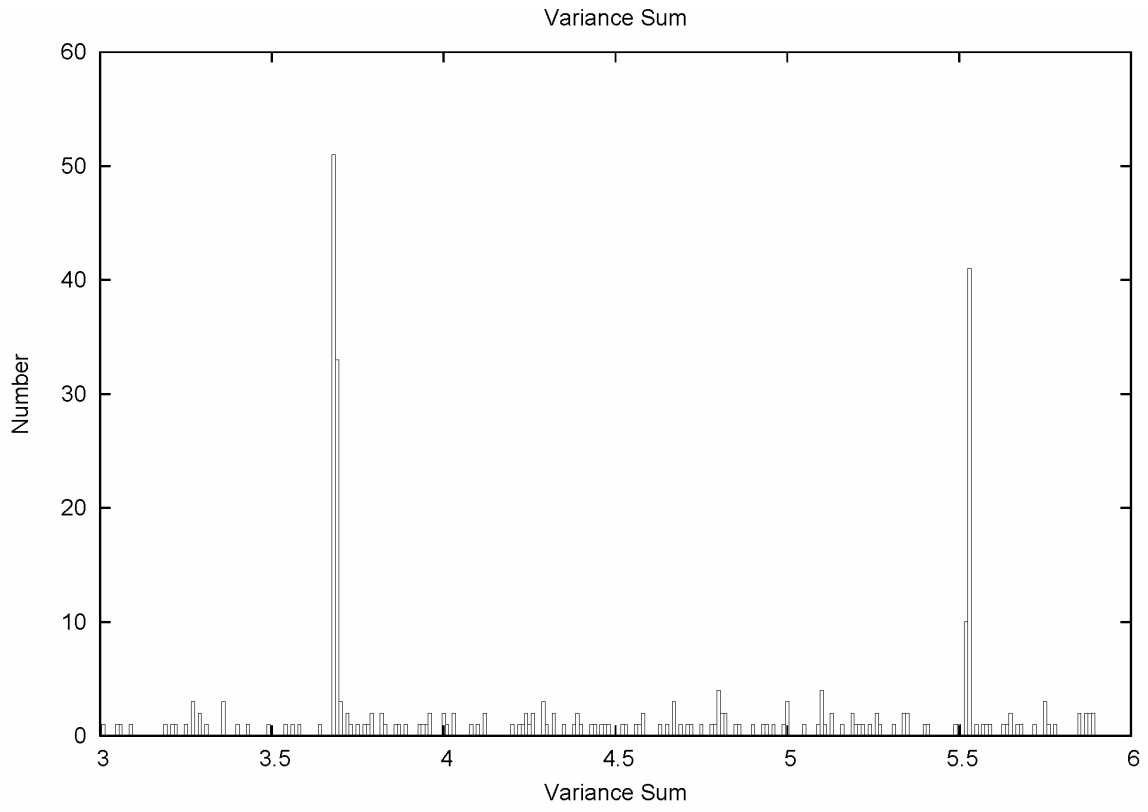Figure A.28.10. Length distribution of vertical local accuracies, detail 4.

Figure A.31.5. Irregular distribution of project variance sums, detail 2.
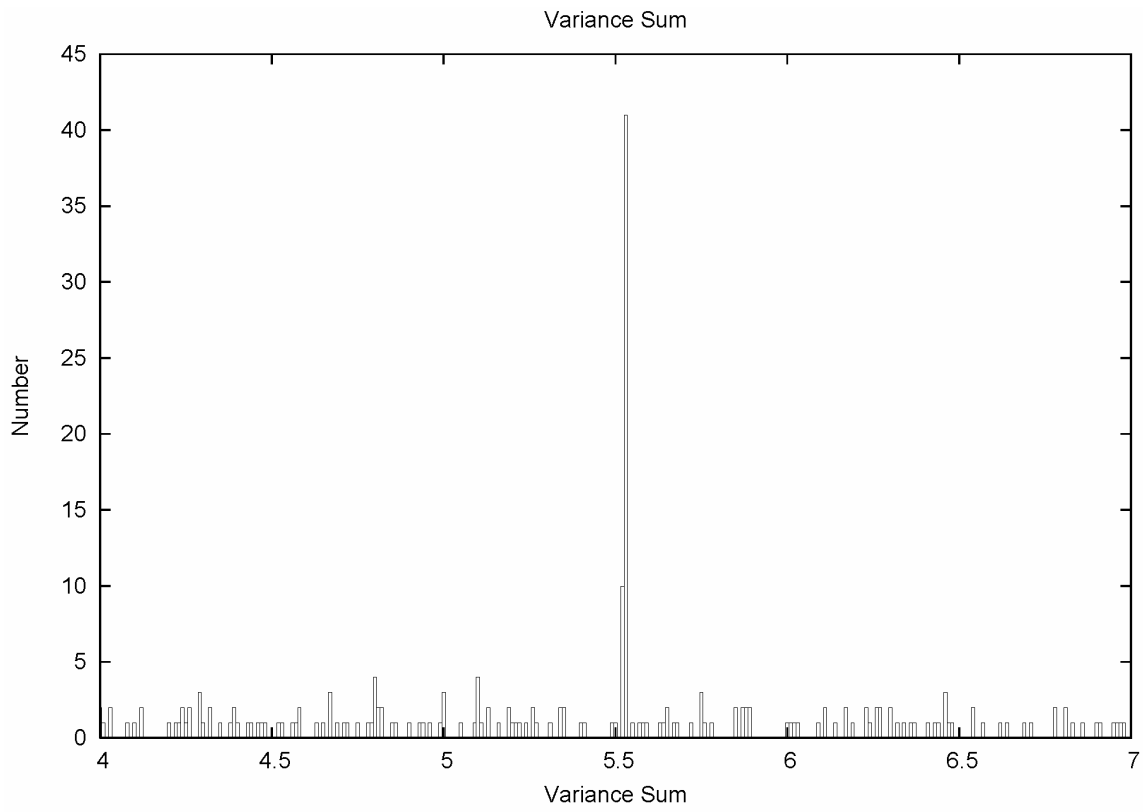
Figure A.31.6. Irregular distribution of project variance sums, detail 3.
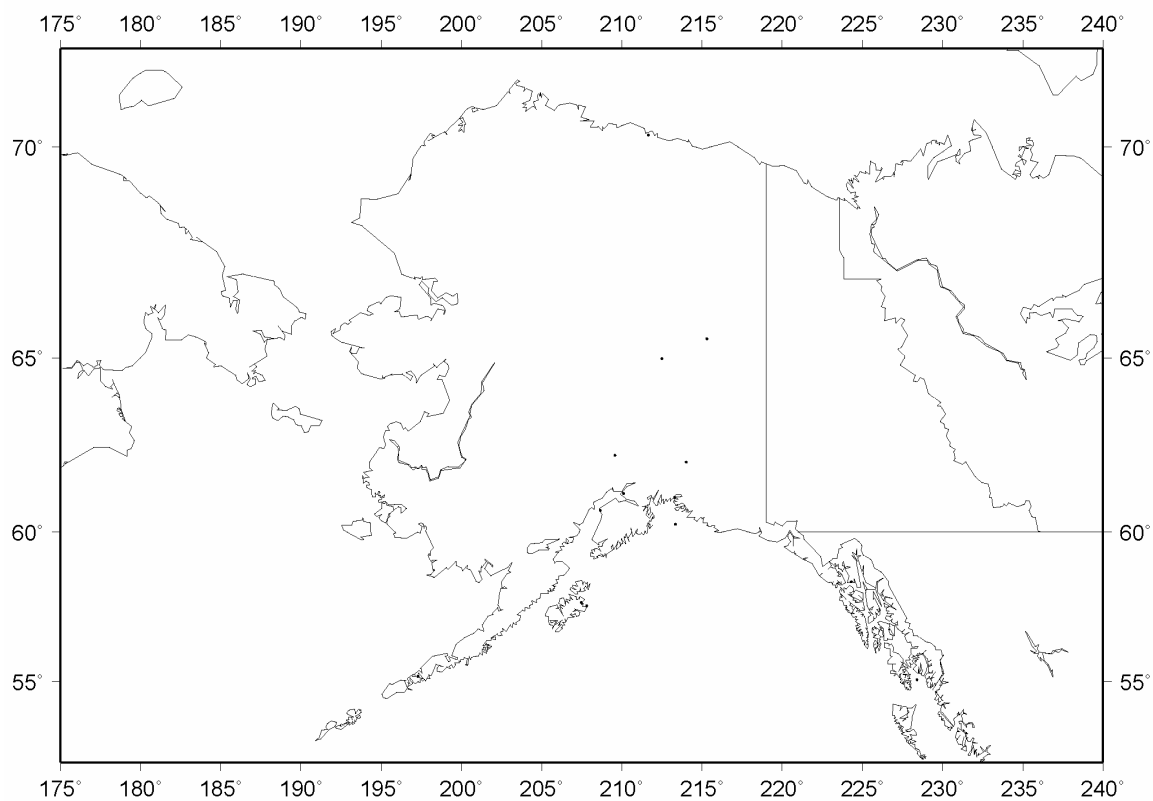
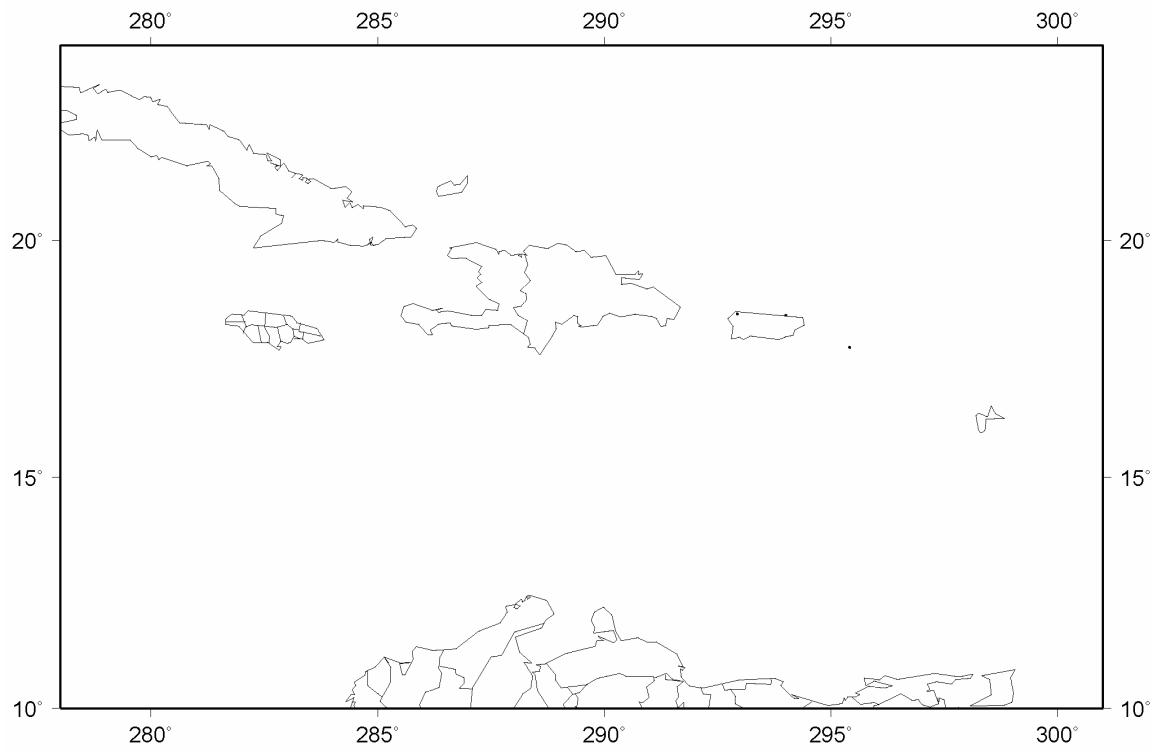# CORS Fixed Control

Figure A.34.2. CORS fixed control, Alaska.

CORS Fixed Control

Figure A.34.3. CORS fixed control, Caribbean.